2016

Development of biomarker-based proxies for paleo sea-ice reconstructions

Smik, Lukas

DEVELOPMENT OF BIOMARKER-BASED PROXIES FOR PALEO SEA-ICE RECONSTRUCTIONS

by

Lukas Smik

A thesis submitted to Plymouth University in partial fulfilment for the degree of:

DOCTOR OF PHILOSOPHY

Petroleum and Environmental Geochemistry Group

School of Geography, Earth and Environmental Sciences

Plymouth University

June 2016

This thesis is dedicated to my gorgeous wife Martina and our two darlings Oskar and Tereza.

Thank you!

All our dreams can come true if we have the courage to pursue them.

(Walt Disney)

Development of biomarker-based proxies for paleo sea-ice reconstructions

Lukas Smik

ABSTRACT

The analysis of the sea-ice diatom biomarker IP_{25} (a mono-unsaturated Highly Branched Isoprenoid (HBI) alkene) in Arctic marine sediments has previously been shown to provide a useful qualitative proxy measure for the past spring sea-ice occurrence. In the Southern Ocean the occurrence and variable abundance of a structurally similar di-unsaturated HBI (HBI diene II) has previously been proposed as a proxy measure of paleo sea-ice extent. However, the use of such biomarker proxies remains under development. In the current study, a number of additional palaeoceanographic developments of HBIs as sea-ice biomarkers in both polar regions has been undertaken. For the Arctic, an investigation into the combined analysis of IP_{25} and certain phytoplankton biomarkers has been conducted with the aim of providing more detailed and semi-quantitative descriptions of sea-ice conditions in the Barents Sea. In contrast, analysis of HBIs and other lipids within water column, surface sediment and sea-ice samples has been undertaken to provide further insights into the use of HBIs as proxies for Antarctic sea-ice.

Analysis of surface sediments from across the Barents Sea has shown that the relative abundances of IP_{25} and a tri-unsaturated HBI lipid (HBI triene IIIa) are characteristic of the overlying surface oceanographic conditions, most notably, the location of the seasonal sea-ice edge. A semi-quantitative approach, in the form of the PIP_{25} index, showed a good positive linear relationship between PIP_{25} indices and spring sea-ice concentration, with a particularly strong relationship found when using HBI triene IIIa ($P_{IIIa}IP_{25}$) as the open-water counterpart to IP_{25}. The quality of the linear fits were not especially dependent on the balance factor *c*, used in the PIP_{25} calculation, which may have important positive consequences for down-core sea-ice reconstruction, and when making comparisons between outcomes from different Arctic regions or climatic epochs. Further, a lower limit threshold for $P_{IIIa}IP_{25}$ (0.8) might represent a useful qualitative proxy for the past occurrence of summer sea-ice. The re-evaluation of biomarker data from three dated marine sequences in the Barents Sea suggests that the combined analysis of IP_{25} and HBI triene IIIa can provide information on temporal variations in the position of the maximum (winter) Arctic sea-ice extent, together with more quantitative sea-ice reconstructions.

In the Southern Ocean, the distributions of di- and tri-unsaturated HBIs (HBI diene II and HBI trienes IIIa and IIIb) in surface waters were shown to be extremely sensitive to the local sea-ice conditions, consistent with significant environmental control over their biosynthesis by sea-ice diatoms and open water phytoplankton, respectively. Within the water column, the apparent alteration to HBI and other lipid abundances was evident between the photic and benthic parts of the water column, which, along with additional local factors (e.g. polynya formation), may have important implications for paleo sea-ice reconstructions. The sedimentary occurrence and distribution of HBI diene II (termed here as $IPSO_{25}$) were consistent with the recent identification of the diatom *Berkeleya adeliensis* Medlin as a source of $IPSO_{25}$. The tendency for *B. adeliensis* to flourish in platelet ice, the formation of which is strongly associated with super-cooled freshwater inflow, means that sedimentary $IPSO_{25}$ may provide a potentially sensitive proxy indicator of landfast sea-ice influenced by meltwater discharge from nearby glaciers and ice shelves. Re-examination of some previous $IPSO_{25}$ down-core records supports this suggestion, although further down-core analysis is required to confirm this hypothesis. The similar sedimentary distribution relationship between phytoplankton-derived HBI trienes and $IPSO_{25}$, further indicates that the former may reflect production of these biomarkers by certain diatoms that flourish within the region of the retreating ice edge; however, the source identification of the HBI trienes is still needed to place this interpretation on a firmer footing.

Table of Contents

LIST OF FIGURES

LIST OF TABLES

ACKNOWLEDGEMENTS

It is a real pleasure to thank many people that made this thesis possible.

First and foremost I would like to say my most sincere and deepest thanks to my supervisors, Professor Simon Belt and Dr Thomas Brown for their extraordinary support, enthusiasm and constant encouragement during the entire course of my PhD. I feel very fortunate to have been able to work under their supervision and without their incredible guidance and patience I would not have been able to do it!

I am especially grateful for the support and friendship of Dr Patricia Cabedo-Sanz, who became my mentor at the beginning of this journey and has always been there willing to help and offer her advice with just about anything. Thank you Patri!

I would also like to say special thanks to Dr Claire Allen (British Antarctic Survey) and Dr Leanne Armand (Macquarie University, Sydney), for sharing hardly collected samples, useful information, but most importantly their knowledge and expertise with me, which have greatly contributed to this study.

My thanks also to Dr Jung-Hyun Kim, Dr Jong-Ku Gal (Hanyang University, Soul), Dr Rainer Gersonde (AWI, Germany), Dr Jochen Knies (NGU, Trondheim) and Dr Suzanne MacLachlan (Brittish Ocean Sediment Core Research Facility) for sharing sediment samples.

Thanks to Ms. Mairi Fenton (Britich Antarctic Survey) for collecting sea-ice samples and to Dr Kyle Taylor (Isoprime, UK) for stable isotope analysis.

I am also grateful to Mr Shaun Lewin for assistance with cartography.

I would also like to thank the technical staff of the School of Environmental Sciences (Plymouth University), Andrew Tonkin, Andy Arnold, Claire Williams, Rebecca Sharp and Ian Doidge for their expertise and assistance and to Dr. Paul Sutton for his constant technical support.

I acknowledge financial support for my research study from Plymouth University.

To everyone in the BGC group, thanks for your friendship and for making this a really great experience!

Very special thanks to Dr Ingrid Hallin, who undertook not an easy task of proof reading the lines of this thesis.

Most importantly, none of this would have been possible without the love and patience of my family. Thank you so much for all your support and encouragement during the good and bad times but especially in the past couple of weeks when I needed it most.

AUTHOR'S DECLARATION

At no time during the registration for the degree of Doctor of Philosophy has the author been registered for any other University award without prior agreement of the Graduate Committee.

Work submitted for this research degree at the Plymouth University has not formed part of any other degree either at Plymouth University or at another establishment.

This study was financed with the aid of a research studentship by Plymouth University.

A programme of advanced study was undertaken, with relevant scientific seminars and conferences attended, at which work was often presented.

Word count of main body of thesis: 36654

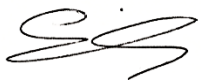

Signed . . . . . .

Lukas Smik

Date: June 2016

PUBLICATIONS

Belt, S.T., **Smik, L**., Brown T.A., Kim, J.-H., Rowland, S.J., Allen, C.S., Gal, J.-K., Shin, K.-H., Lee, J.I., Taylor, K.W.R., 2016. Source identification and distribution reveals the potential of the geochemical Antarctic sea ice proxy $IPSO_{25}$. Nature Communications 7, 12655

Cabedo-Sanz, P., **Smik, L**., Belt, S.T., 2016. On the stability of various highly branched isoprenoid (HBI) lipids in stored sediments and sediment extracts. Organic Geochemistry 97, 74-77

Smik, L., Belt, S.T., Lieser, J.L., Armand, L.K., Leventer, A., 2016. Distributions of highly branched isoprenoid alkenes and other algal lipids in surface waters from East Antarctica: further insights for biomarker-based paleo sea-ice reconstruction. Organic Geochemistry 95, 71-80

Smik, L., Cabedo-Sanz, P., Belt, S.T., 2016. Semi-quantitative estimates of paleo Arctic sea-ice concentration based on source-specific highly branched isoprenoid alkenes: A further development of the PIP_{25} index. Organic Geochemistry 92, 63-69.

Belt, S.T., Cabedo-Sanz, P, **Smik, L**., Navarro-Rodriguez, A., Berben, S.M. P., Knies, J. and Husum, K., 2015. Identification of paleo Arctic winter sea-ice limits and the marginal ice zone: Optimised biomarker-based reconstructions of late Quaternary Arctic sea-ice. Earth and Planetary Science Letters 431, 127-139.

PRESENTATIONS AND CONFERENCES ATTENDED

European Geosciences Union General Assembly 2016, Vienna, **Austria,** 17-22 April 2016. Poster presentation: “Development of source specific diatom lipids biomarkers as Antarctic Sea-ice proxies”.

NESSC Molecular Organic Biogeochemistry course 2015, Royal Netherlands Institute for Sea Research (NIOZ), Texel, **The Netherlands**, 2-6 November 2015. Oral presentation: “Variations in algal lipid distribution is seasonally sea-ice covered surface waters from East Antarctica”.

UK Arctic Science Conference 2015, Sheffield, **U.K.**, 16-18 September 2015. Poster presentation: "Identification of Paleo Arctic Winter Sea-ice Limits and the Marginal Ice Zone: Optimised Biomarker-based Reconstructions of Late Quaternary Arctic Sea-ice".

6th Annual Biogeochemistry Centre Conference, National Marine Aquarium, Plymouth, **U.K.**, 17 December 2014. Oral presentation: "An Assessment of Highly Branched Isoprenoid (HBI) Alkenes as Antarctic Sea-ice Proxies".

25th Annual Meeting of the British Organic Geochemical Society, Liverpool John Moores Univesity, Liverpool **U.K.**, 10-11 July 2014. Oral presentation: "A Spatial Assessment of a Di-unsaturated Highly Branched Isoprenoid (HBI) Alkene as an Antarctic Sea-ice Proxy".

3rd workshop of the PAGES Sea-ice Proxy (SIP) working group-Sea-ice proxy synthesis and data-model comparison, Alfred Wegener Institute (AWI), Bremerhaven, **Germany**, 23-25 June 2014. Poster presentation: "A Spatial Assessment of a Di-unsaturated Highly Branched Isoprenoid (HBI) Alkene as an Antarctic Sea-ice Proxy".

Winter School on Sea-ice Variability in the Arctic-Past and Present Conditions, The Arctic University of Norway, Tromsø, **Norway**, 30 March-4 April 2014. Poster presentation: "Analysis of the Sea-ice Biomarker IP_{25} in Marine Sediments from the Barents Sea".

5th Annual Biogeochemistry Centre Conference, Plymouth University, Plymouth, **U.K.**, 12 December 2013. Oral presentation: "It's Not an Ordinary Sediment!- suitability assessment of sediment material from Barrow Strait (Canadian Arctic) for use as reference sediment in analysis of biomarker proxy IP_{25}".

LIST OF COMMON ABBREVIATIONS

DCM-Dichloromethane
GC-Gas chromatography
GC-MS-Gas chromatography-mass spectrometry
HBI-Highly branched isoprenoid
IP_{25}-C_{25} highly branched isoprenoid monoene
MIZ-Marginal ice zone
NSIDC-National Snow and Ice Data Centre
NSL-Non saponifiable lipids
PIP_{25}-Ratio between IP_{25} and a phytoplankton biomarker
$P_{III}IP_{25}$-Ratio between IP_{25} and HBI triene IIIa
P_BIP_{25}-Ratio between IP_{25} and 24-methyl cholest-5,22-dien-3β-ol (brassicasterol)
POOZ-Permanently open ocean zone
RF-Response factor
SIM-Selective ion monitoring
SIZ-Seasonal ice zone
SpSIC-Spring sea ice concentration
SuSIC-Summer sea ice concentration
THE-Total hexane extract
TIC-Total ion current
TOE-Total organic extract
9-OHD-9-octylheptadec-8-ene

CHAPTER ONE

1 Introduction

This thesis describes the development of diatom specific biomarker lipids, named Highly Branched Isoprenoid (HBI) alkenes, as proxies for the past occurrence of sea-ice in the Arctic and the Antarctic. In recent years, the research interest in HBIs in the Arctic has expanded rapidly, particularly following the discovery of the highly selective sea-ice diatom biomarker IP_{25} (Belt et al., 2007) (Figure 1.1). Since then, the analysis of this biomarker has shown to be a useful approach to provide a qualitative measure of past occurrence of sea-ice in the Arctic. Furthermore, combined measurements of IP_{25} and phytoplankton biomarkers have been suggested to provide more semi-quantitative estimates of sea-ice concentration. In the Antarctic, a di-unsaturated HBI analogue to IP_{25} (not present in the Antarctic) has more recently been proposed as a useful proxy indicator of sea-ice. However, levels of research have not reached the same heights as seen for IP_{25} in the Arctic.

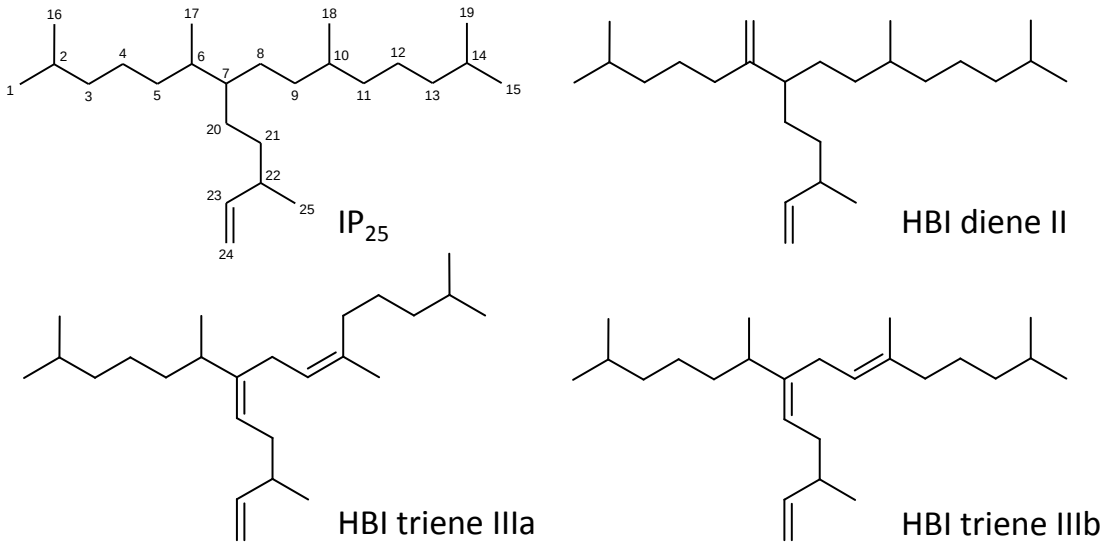

Figure 1.1: Molecular structures of C_{25} HBI alkenes; IP_{25}, HBI diene II and HBI trienes IIIa and IIIb. Carbon labelling is shown on the structure of IP_{25}.

Despite growing interest in both hemispheres, our understanding of HBIs in general is not complete. This provides the opportunity for further research, resulting in better understanding of the environmental significance of these unique biomarkers with respect to sea-ice conditions. This, in turn, allows for more informed paleo reconstructions to be conducted. With that view, the work presented in this thesis was set up to further develop our understanding of certain HBIs in the Arctic and Antarctic regions.

1.1 Sea-ice

Sea-ice is a critical component of the Earth's system with regard to global climate, its physical environment and the biosphere. It is one of the largest known biomes on Earth (Dieckmann and Hellmer, 2010), covering about 7% of the World Ocean, with remarkable seasonal variations seen in both hemispheres (Comiso, 2010).

In the climate system, sea-ice cover generally acts as an amplifier. First, it influences the energy budget at the surface of the Earth, because it reflects a significant part of the incoming solar radiation (albedo). Reflectivity of sea-ice (50-70%) greatly exceeds that of open water (6%), hence sea-ice limits the heat exchange between the ocean and the atmosphere (Maykut, 1978; Thomas and Dieckmann, 2010). Decreased sea-ice extent may thus have a positive feedback on climate change, through greater absorption of heat by exposed sea water (Armand and Leventer, 2010). Second, sea-ice plays an important role for physical oceanography, as its formation is accompanied by brine release and convection, thereby influencing the entrainment of water in the mixed layer and deep ocean ventilation (Killworth, 1983). Moreover, sea-ice constitutes a large freshwater reservoir, thus potentially playing a role in the thermohaline circulation (Dickson et al., 2007). Finally, sea-ice provides a unique and ecologically important habitat for a wide

variety of microorganisms (Arrigo et al., 2010; Horner et al., 1992) and polar marine mammals and birds (Tynan et al., 2010).

Sea-ice is also a highly dynamic component of the climate ocean system. Not only does the extent of sea-ice cover vary, but also its thickness and thus its volume. Therefore, the size of the sea-ice reservoir and its contribution to the freshwater budget may fluctuate considerably. The development of first year ice and the accumulation of multi-year ice that regulates the thickness, the drift pattern and the export of sea-ice towards low latitudes are all important processes. From these points of view, the polar configuration of land and ocean in the Northern and Southern Hemispheres are important as they account for very different sea-ice dynamics.

In the Southern Ocean, sea-ice experiences one of the most marked seasonal changes on the planet, expanding from a minimum of around $3x10^6$ km^2 in February , to a maximum of approximately $18x10^6$ km^2 in September (Arrigo et al., 1997) (Figure 1.2). Distribution of winter sea-ice in Antarctica is also relatively symmetric from a circumpolar perspective (Figure 1.2). The position of the maximum (winter) ice margin depends mainly upon the interplay between the northward advection of the newly formed ice by winds and melting of the ice edge in warmer waters (Pezza et al., 2012). In the spring, sea-ice retreats from its maximum extent (~55°S in the Atlantic and Indian Oceans, ~60°S in the Pacific Ocean) to the coast of the Antarctica, with little or no perennial ice being present around the continent (Ackley, 1981; Fetterer at al., 2002) (Figure 1.2). Some of the controls behind the formation of sea-ice include seasonal insolation, sea surface temperature, and the surface wind speed, which control the ice advection from the site of formation (Pezza et al., 2012).

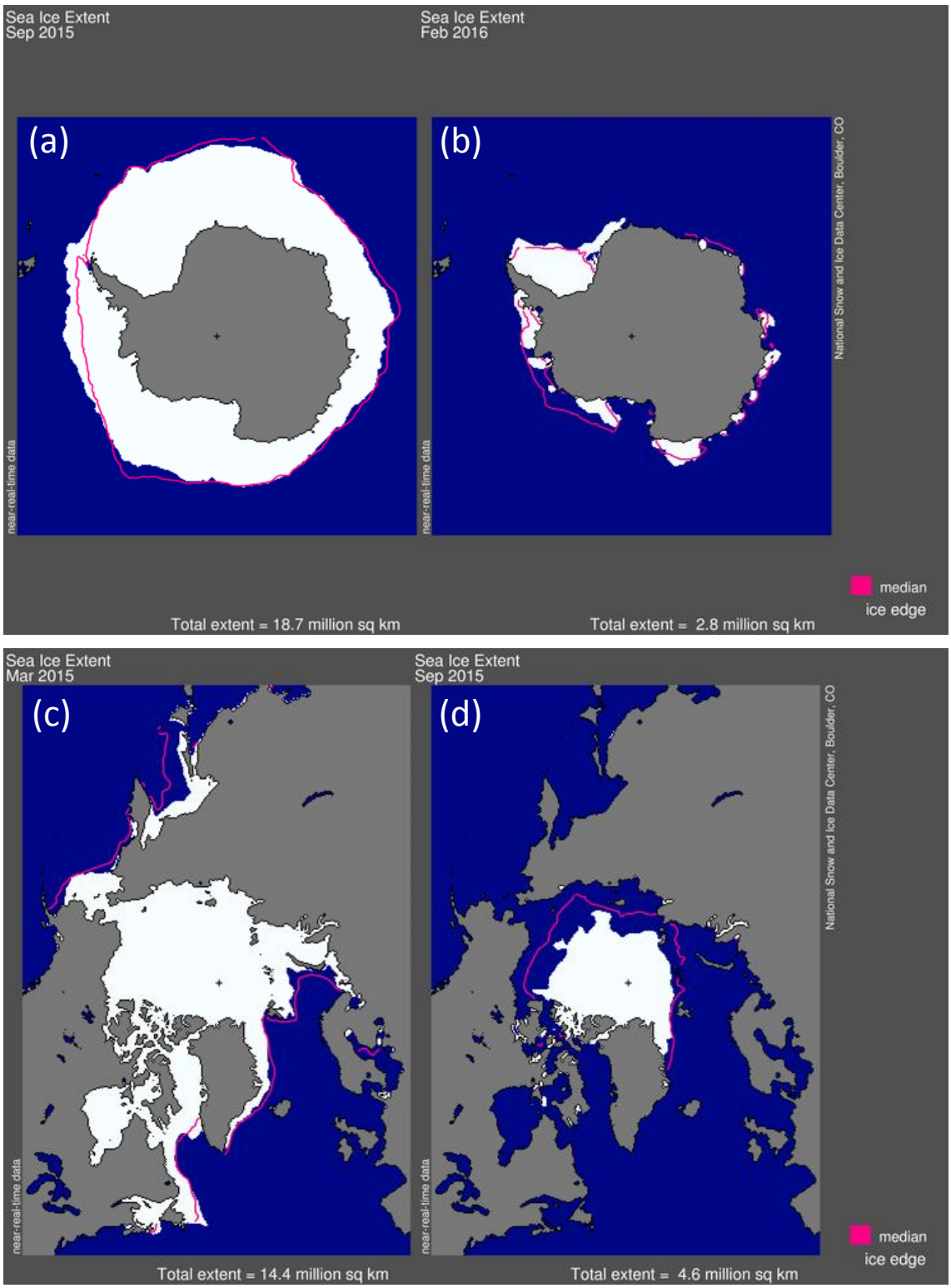

Figure 1.2: Maps showing seasonal sea-ice variation in the Antarctic (a, b) and the Arctic (c, d). Images courtesy of the National Snow and Ice Data Center (Fetterer et al., 2002).

In the Arctic, atmospheric and ocean circulations are characterised by variable patterns. The relative strengths of the Beaufort Gyre and Trans Polar Drift play an important role on variations in the residence time of sea-ice in the Arctic Ocean and in the freshwater

budget of the Arctic and Nordic Seas (e.g. Rigor et al., 2002; Stroeve et al., 2011). The relative strength of the Beaufort Gyre and Trans Polar Drift also results in asymmetrical distributions of seasonal sea-ice cover. Through the annual cycle, from winter (March) to summer (September, Figure 1.2), Arctic sea-ice cover ranges from a maximum of $15x10^6$ km^2 to a minimum of about $7x10^6$ km^2 (Fetterer at al., 2002). Whereas the seasonal amplitude in sea-ice extent is less than that of the Southern Hemisphere, the magnitude of the recent trend is significant.

Much of what is currently known about sea-ice extent comes from satellite observations. Dating back to the late 1970s, satellite passive-microwave imagery became an effective means of monitoring sea-ice conditions (Comiso et al., 2008). These satellite observations show substantial, accelerating retreat and thinning of, predominantly Arctic sea-ice cover over the last few decades (Comiso et al., 2008). For example, the total area of Arctic sea-ice fell to the record low (3.6 million km^2) during the summer of 2012 (Figure 1.3; Fetterer et al., 2002), when compared with the 34-year satellite record (Schiermeier, 2012).

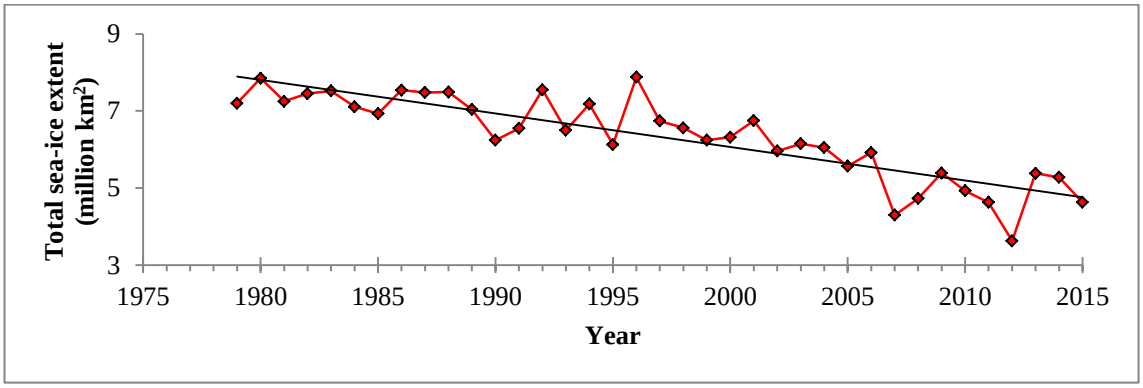

Figure 1.3: Average September (minimum) sea-ice extents for the period 1979-2015 in the Arctic. Data courtesy of National Snow and Ice Data Centre (Fetterer et al., 2002).

The possible implications and feedback mechanisms of the dramatic changes observed of Arctic sea-ice are not yet fully understood, however. For example, shrinking sea-ice cover has been associated with a 30% increase in net primary production by

phytoplankton within the Arctic Ocean between 1998 and 2012 (Arrigo and van Dijken, 2015), a change that is likely to have a major impact on marine ecosystems in the future (Arrigo et al., 2008; Wisz et al., 2015).

In contrast, Antarctic sea-ice extent has slightly increased (~1% per decade) over the last thirty years (Figure 1.4; Fetterer et al., 2002). Reaching a record high in 2014, Antarctic sea-ice extent exceeded 20 million km^2 for the first time since 1979 (Fetterer et al., 2002). Despite this overall increase, the regional variability is large (Parkinson and Cavalieri, 2012; Stammerjohn et al., 2012), with a strong pattern of decreasing ice coverage in the Bellingshausen/Amundsen Seas region and increasing ice coverage in the Ross and Weddell Sea region (Parkinson and Cavalieri, 2012). Furthermore, small but significant trends, both positive and negative depending on the longitudinal sector, are recognized for recent decades (Comiso and Nishio, 2008; Parkinson and Cavalieri, 2012). In any case, Antarctic sea-ice extent is consistently projected to decrease by the end of the 21st century (Arzel et al., 2006).

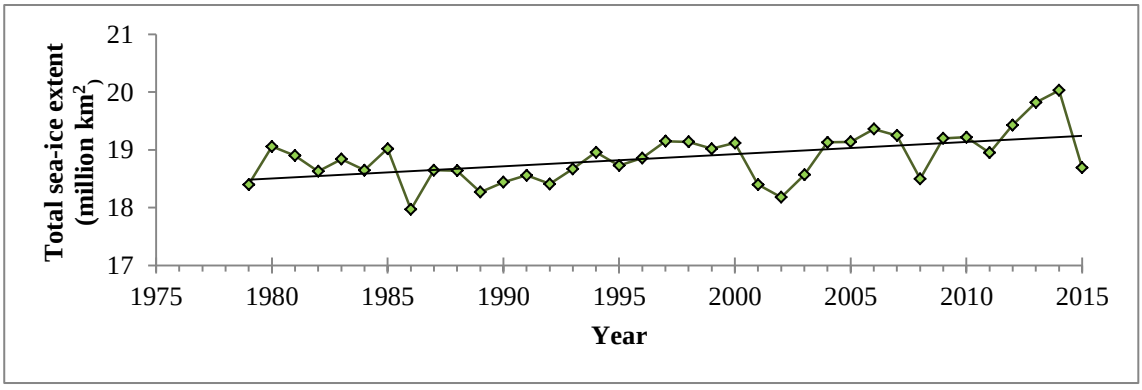

Figure 1.4: Average September (maximum) sea-ice extents for the period 1979-2015 in the Antarctic. Data courtesy of National Snow and Ice Data Centre (Fetterer et al., 2002).

Paleoceanographic reconstructions that include estimates of paleo sea-ice extent are, therefore, of great interest to researchers from a number of disciplines. These reconstructions are particularly significant as most models of global climate change predict that the polar regions will warm more rapidly than most of the rest of the planet

(Bi et al., 2001; Holland et al., 2006; Wang and Overland, 2009), with profound effects for the ice regime. These data provide much needed information for scientists, allowing them to develop a better and necessary understanding of the relationships between climate change and sea-ice, on much longer time scales than is available through recent satellite monitoring.

1.2 Marine proxies for paleoenvironmental reconstructions in the Arctic and the Antarctic

Paleo sea-ice reconstructions rely heavily on proxy-based methods, so the development and application of sea-ice proxies have also received considerable attention in recent years (de Vernal et al., 2013a; Polyak et al., 2010). A number of methods for palaeo sea-ice reconstructions are used, and include analysis of microscopic remains of marine organism in marine sediments. These biogenic proxies include microfossils such as diatoms (e.g. Crosta et al., 2004; Armand and Leventer, 2010; Gersonde et al., 2005; Justwan et al., 2008), dinoflagellate cysts (e.g. de Vernal et al., 2001, 2005), ostracods (Cronin et al., 2010) and foraminifera (e.g. Scott et al., 2009; Seidenkrantz, 2013). An additional group of proxies used for paleo reconstruction in both polar regions include organic biomarkers such as IP_{25} (e.g. Belt et al., 2007; Massé et al., 2011; Belt and Müller, 2013).

There are general differences in the value of various types of paleo sea-ice proxies used in the Northern and Southern hemisphere (Armand and Leventer, 2010). In the Northern hemisphere, quantitative analysis of dinocyst assemblages has been shown to be a relatively powerful tool, while in the Southern Ocean, diatom assemblages have been the most useful method (Armand and Leventer, 2010).

The following part of this chapter provides a general overview of the most common proxies used for reconstruction of ancient and modern environmental conditions in the Arctic and the Antarctic Ocean.

1.2.1 Dinoflagellates

Dinoflagellates belong to a group of microfossils named marine palynomorphs. They occur in most aquatic environments and constitute one of the main primary producers in marine environments (Stein, 2008). During their life cycle, some taxa produce highly resistant organic-walled cysts, providing generally good resistance to dissolution in the water column and sediments. As with other microorganisms living in the photic zone, the distribution of dinoflagellates is sensitive to changes in the upper water column, including fluctuations in sea surface temperature, salinity and sea-ice cover (Armand and Leventer, 2010). Dinoflagellate populations are relatively diverse (de Vernal et al., 2001, 2005), with changes in assemblage composition of new cysts (dinocysts) reflecting changes in surface water conditions (e.g. de Vernal et al., 2000, 2001; Levac et al., 2001; Mudie and Rochon, 2001; Solignac et al., 2006; Voronina et al., 2001). Reconstruction of surface ocean conditions through analysis of dinocysts, has been done mainly through application of modern analogue techniques and transfer functions (de Vernal et al., 2001, 2013c).

Although, widely used for paleo reconstructions (de Vernal et al., 2005, 2013b, 2013c; Matthiessen et al., 1997; Solignac et al., 2009; Voronina et al., 2001), a number of limitations exist when reconstructing quantitative palaeoceanographic conditions using dinocysts. Among those are morphological variations within taxa, sparse hydrological data and large inter-annual variations of temperature and salinity in surface Arctic waters (e.g. de Vernal et al., 2001).

1.2.2 Foraminifera

Planktonic or benthic in their mode of life, foraminifera are single-celled protists with shells made of calcium carbonate ($CaCO_3$) or agglutinated sediment particles, that are found in a wide range of marine environments (Gooday, 2003; Murray, 2002). Besides their use as palaeonvironmental proxies, they are of major importance for correlating and dating sediment cores (Stein, 2008). Regarding their use for palaeo sea-ice reconstructions, benthic foraminifera have been used as a palaeo sea-ice indicator (e.g. Jennings et al., 2002; Scott et al., 2009) and, although they give information on sea-ice cover variation, they are not considered direct proxies for sea-ice and their response to changing sea-ice conditions is not well understood (Seidenkrantz, 2013). In addition, studies based on planktonic foraminifera have also been used to reconstruct sea-ice cover in the Arctic (Sarnthein et al., 2003a).

1.2.3 Ostracods

Ostracods are small bivalve crustaceans that occur throughout the Arctic Ocean and are common in Quaternary Arctic sediments (Cronin et al., 1994; Taldenkova et al., 2005). Many species of ostracods are ecologically sensitive and restricted to particular oceanic conditions (Cronin et al., 1994, 1995; Jones et al., 1999). In a number of studies, ostracod assemblages have been used to reconstruct Arctic palaeoceanography (e.g. Cronin et al., 1994; Jones et al., 1999; Poirier et al., 2012; Taldenkova et al., 2005) and sea-ice history (e.g. Cronin et al., 2010, 2013).

1.2.4 Ice Rafted Debris (IRD)

Ice Rafted Debris (IRD) are components of sediments that have been transported by icebergs and/or sea-ice. While icebergs are able to transport material of all sizes, clay to silt size particles are generally carried by sea-ice (Pfirman et al., 1989). Such a distinction is, however, not always clear and hence, only a few studies have utilised fine grained IRD (>100 µm) as a proxy for sea-ice extent (e.g. Bond et al., 1997). However, IRD has been used successfully as a proxy for reconstructing paleoclimate conditions (e.g. Bond et al., 2001; Moros et al., 2004, 2006; Sarnthein et al., 2003b). Further, the composition of other particles in sediments, such as quartz (Bond et al., 2001; Eiríksson et al., 2000; Moros et al., 2006) or coal fragments (Bischof and Darby, 2000), can be related to movement of drift ice or icebergs (e.g. Andrews and Eberl, 2007).

1.2.5 Diatoms

Most widely used in the Southern Ocean, diatoms are aquatic, unicellular microscopic algae, which occur individually or in colonies. Diatoms have a cell wall (frustule) composed of silica and exhibit a wide range of forms (Crosta and Koç, 2007; Round et al., 1990). The distribution of diatoms in, for example, surface waters of the Southern Ocean, is controlled by a variety of environmental factors, including sea-ice. In particular, sea-ice plays an important role on diatom productivity and export in the Southern Ocean (Arrigo et al., 2010; Whitaker, 1982). As such, an association of certain diatom groups to sea-ice or the open ocean environment has formed the basis of several Antarctic paleo sea-ice reconstructions (Allen et al., 2005; Crosta et al., 1998; Gersonde and Zielinski, 2000).

The sea-ice-associated diatom species in the Southern Ocean, including *Fragilariopsis curta*, are confined to regions south of the Polar Front (Armand et al., 2005). There, sea-

ice-associated diatoms are dominant in the sea-ice zone (SIZ) and the marginal ice zone (MIZ) towards the Antarctic continent. Consequently, the open ocean zone north of the Polar Front, is dominated by open ocean diatom species, such as *Fragialaripsis kerguelensis* (Crosta et al., 2005).

The use of diatoms as paleoenvironmental indicators in the Antarctic region is strongly dependant on the preservation and identification of the diatom frustules within sediments (Allen et al., 2011; Crosta et al., 1998; Gersonde and Zielinski, 2000). Some of the diatoms associated with sea-ice are small and may be characterised by lightly silicified frustules which are prone to dissolution in the water column. However, even when dissolution is insignificant in the water column, poor preservation of these frustules within the sediment can make identification of the individual diatoms difficult, and potentially leads to inaccurate reconstructions. However, some sea-ice diatoms (e.g. *Fragilariopsis curta* and *Fragilariopsis cylindrus*), and some open water diatoms (e.g. *Thalassiosira antarctica* and *Fragilariopsis kerguelensis)* display better preservation tendencies, and are normally considered more suitable for sea-ice reconstructions (Leventer, 1998).

Their use in the northern high latitudes is more limited, however, mainly as a result of the more lightly silicified and more easily dissolved frustules found in the nutrient limited Arctic (Armand and Leventer, 2003).

Given some of the disadvantages of each of the proxies outlined so far, the development of additional and complementary proxies for Arctic and Antarctic paleo reconstructions constitutes a desirable objective in order to enhance our understanding of past sea-ice variability in both hemispheres.

1.3 Organic geochemical biomarkers

Molecular biomarkers are chemical signatures or fingerprints of the biota from which they are produced (Killops and Killops, 2009). They occur across all taxonomic levels and can be classified into general classes (e.g. lipids), smaller groupings (e.g. fatty acids, sterols) or individual representatives of these (e.g. cholesterol is a specific and commonly occurring example of a sterol). In addition, biomarkers may be either primary or secondary metabolites and their occurrence can either represent the general indicators of origin (e.g. long-chain *n*-alkanes from terrestrial plants) or be of a more source-specific nature (e.g. alkenones from unicellular eukaryotic haptophytes-coccolithophores). In recent decades, an increasing appreciation of the structures and sources of an individual and the groups of such chemicals has resulted in several biomarker-based applications in paleoclimatology (Eglinton and Eglinton, 2008). For example, the influence of temperature on the distribution of alkenones from the coccolithophore *Emiliana huxleyi* (Brassell et al., 1986) and glycerol dialkyl glycerol tetraethers (GDGTs) from Archaea (Kim et al., 2008; Schouten et al., 2002) have provided the basis for the $U^{K'}_{37}$ and TEX_{86} indices, used commonly for reconstructing past sea surface temperatures.

1.3.1 Highly Branched Isoprenoid (HBI) alkenes as source specific biomarkers from diatoms

Highly branched isoprenoid (HBI) alkenes are structurally unusual secondary metabolites produced by a relatively small number of marine and freshwater diatoms belonging to the *Haslea, Navicula*, *Pleurosigma*, *Rhizosolenia*, *Berkeleya and Pseudosolenia* genera (Belt et al., 1996; Brown et al., 2014a; Kaiser et al., 2016; Sinninghe Damsté et al., 2004; Volkman et al., 1994). HBIs occur with C_{20}, C_{25} and C_{30}

carbon skeletons and are widely distributed in marine sediments (Rowland and Robson, 1990). Over the past two decades, the sources and structures of several individual HBI lipid biomarkers have been reported, mainly following large-scale culturing of an individual diatom taxa and subsequent analysis of the purified extracts using a combination of Mass Spectrometric (MS) and Nuclear Magnetic Resonance (NMR) spectrometric methods (Belt et al., 1996, 2001a, 2001b; Sinninghe Damsté et al., 1999a, 1999b; Wraige et al., 1997). In particular, these investigations have enabled the number, position and stereochemistry of the double bonds to be determined. Despite advances in the source identifications and structural determinations, the functions or role(s) of HBIs in diatoms remains unknown. What is clear, however, is that the source-specific nature of HBIs makes them potentially useful biomarkers for paleoenvironmental studies.

One such biomarker, an HBI lipid, termed IP_{25} (Figure 1.1) has recently been proposed and used as a proxy for past sea-ice occurrence in the Arctic (Belt et al., 2007). Comprehensive studies on sea-ice, sediment trap and sediment samples from the Canadian High Arctic have demonstrated that IP_{25} can be used as a proxy for past sea-ice presence in the Arctic (Belt et al., 2007). Since the initial discovery of IP_{25} (Belt et al., 2007), analysis of this biomarker in sediments has formed the basis of a proxy measure for the past occurrence of Arctic sea-ice. This has been done either as an individual proxy or combined with other biomarkers, including those derived from open-water phytoplankton, and a number of paleo sea-ice reconstructions have appeared (Cabedo-Sanz et al., 2013; Knies et al., 2014; Massé et al., 2008; Méheust et al., 2016; Müller et al., 2009, 2012; Müller and Stein, 2014; Stein et al., 2016; Vare et al., 2009, 2010). Covering variable timescales, the success of these reconstructions was estimated through comparison with known sea-ice conditions, data derived from the other sea-ice proxy-based methods, other paleoclimate information, or a combination of these.

The presence (absence) of IP_{25} in Arctic marine sediments is especially sensitive to the past occurrence (absence) of sea-ice (Belt and Müller, 2013), while abundance variations are usually consistent with corresponding directional changes in sea-ice cover (Belt and Müller, 2013). Thus, for example, in the first analysis of surface sediments from across the Canadian Arctic (Belt et al., 2007), IP_{25} was identified in sediments from all locations of seasonal sea-ice cover, often as the most abundant HBI alkene. In contrast, IP_{25} was absent in sediments from regions of permanent ice cover, reflecting unsuitable conditions for sea-ice diatoms. Subsequently, Müller et al. (2011) analysed the biomarker composition of surface sediments from different regions of the continental margins of East Greenland and West Spitsbergen and compared the biomarker data with sea-ice concentrations derived from satellite observations and numerical modelling experiments. IP_{25} content in these surface sediments, presumed to represent recent decades of accumulation, showed a positive correlation with mean (spring) sea-ice concentrations derived from satellite data. In addition, reduced IP_{25} content was also determined at core sites of highest (near permanent) sea-ice coverage consistent with the early findings from the Canadian Arctic (Belt et al., 2007).

A further spatial account of sea-ice cover over the recent decades across the Barents Sea was carried out by Navarro-Rodriguez et al. (2013), who demonstrated a clear relationship between regions of known seasonal sea-ice cover and the occurrence of IP_{25}, although the linear correlations between IP_{25} data and sea-ice concentrations were poorer than those reported previously (Müller et al., 2011). In contrast, IP_{25} was absent from the majority of locations that have experienced ice-free conditions in recent decades, although, exceptionally, IP_{25} was present in a small number of sediments representing locations beyond the position of maximum sea-ice extent. For these latter sediments, it was hypothesized that the presence of IP_{25} represented allochthonous input,

likely as a result of sediment advection following initial deposition of IP_{25} in ice covered locations (Navarro-Rodriguez et al., 2013).

With their analysis of surface sediments from the Kara and Laptev Sea, Xiao et al. (2013) provided a valuable extension of the IP_{25} database of Arctic Ocean surface samples. The study area covered sites from the Ob, Lena and Yenisei estuaries, coastal and shelf areas, continental margins and regions of the central Arctic Ocean. Thus, the investigation by Xiao et al. (2013) focused on Arctic environments characterised by severe sea-ice coverage and enormous riverine freshwater supply. This provided a valuable inventory of information about the distribution of IP_{25} and other biomarkers related to complex sea surface conditions. The distribution patterns of IP_{25} and other marine and terrigenous biomarkers provided an essential insight into the impact that a significant river discharge and highly diverse sea-ice settings (permanent to seasonally ice-free conditions, fast ice, ice massifs, polynya conditions) can have on the primary productivity of ice algae and phytoplankton in such environmental systems. As in the study from Barents Sea (Navarro-Rodriguez et al., 2013), IP_{25} data did not correlate particularly well with sea-ice concentrations over recent decades, and this was suggested to be related to the complex sea-ice settings and the strong river discharge.

An expanded dataset of IP_{25} and phytoplankton biomarker abundances in surface sediments from the East Siberian Sea, the Chukchi Sea and Bering Sea, the NE and NW subpolar Pacific, and the NW Atlantic Ocean has been generated by Stoynova et al. (2013). Despite the occurrence of similar sea-ice conditions for parts of these regions, generally higher IP_{25} concentrations in the Atlantic sector were identified compared to those found in the Pacific, highlighting the need to consider the potential impacts of different environmental settings and sea-ice properties that govern IP_{25} and phytoplankton.

Most recently, the spatial analysis of $IP_{25,}$ has been extended for locations from the Central Arctic (Xiao et al., 2015). In line with year-round sea-ice cover that is present in the Central Arctic, IP_{25} was either absent or very low in abundance, although the latter observation might reflect the advection of the material to the Central Arctic locations from the MIZ, where IP_{25} is biosynthesised during the spring bloom (Brown et al., 2014b).

Therefore, it is clear that, across the Arctic, the selectivity of IP_{25} to seasonally ice-covered locations remains. This attribute makes IP_{25} a qualitative proxy of seasonal sea-ice, at least.

Despite its widespread occurrence in Arctic sea-ice, IP_{25} has never been reported in Antarctic sea-ice or sediments. The reason for this is not yet known, but probably reflects the absence of the specific diatom species responsible for production of IP_{25} (Brown et al., 2014b) (Figure 1.5). Alternatively, there may be (as yet) an unidentified environmental control influencing the biosynthetic mechanism responsible for production of IP_{25} that does not exist in the Antarctic.

Although IP_{25} has not, to date, been reported in the Antarctic environment, the presence of a structurally similar di-unsaturated HBI (HBI diene II; Figure 1.1) has been noted in a number of studies. For example, Nichols et al. (1988) reported a di-unsaturated HBI in mixed sea-ice diatom samples and Venkatesan (1988) showed that the same HBI was present in sediment horizons as old as 2.5 ky BP. Later, Johns et al. (1999) confirmed the identity of this HBI as HBI diene II, and the same as that produced in laboratory cultures of the temperate diatom *Haslea ostrearia*. This was done through mass spectrometric and gas chromatographic analyses of sediment samples from McMurdo Sound (East Antarctica). Further, Matsumoto et al. (1992) identified an HBI diene (probably HBI diene II) in sections of sediment cores from Lützow-Holm Bay and

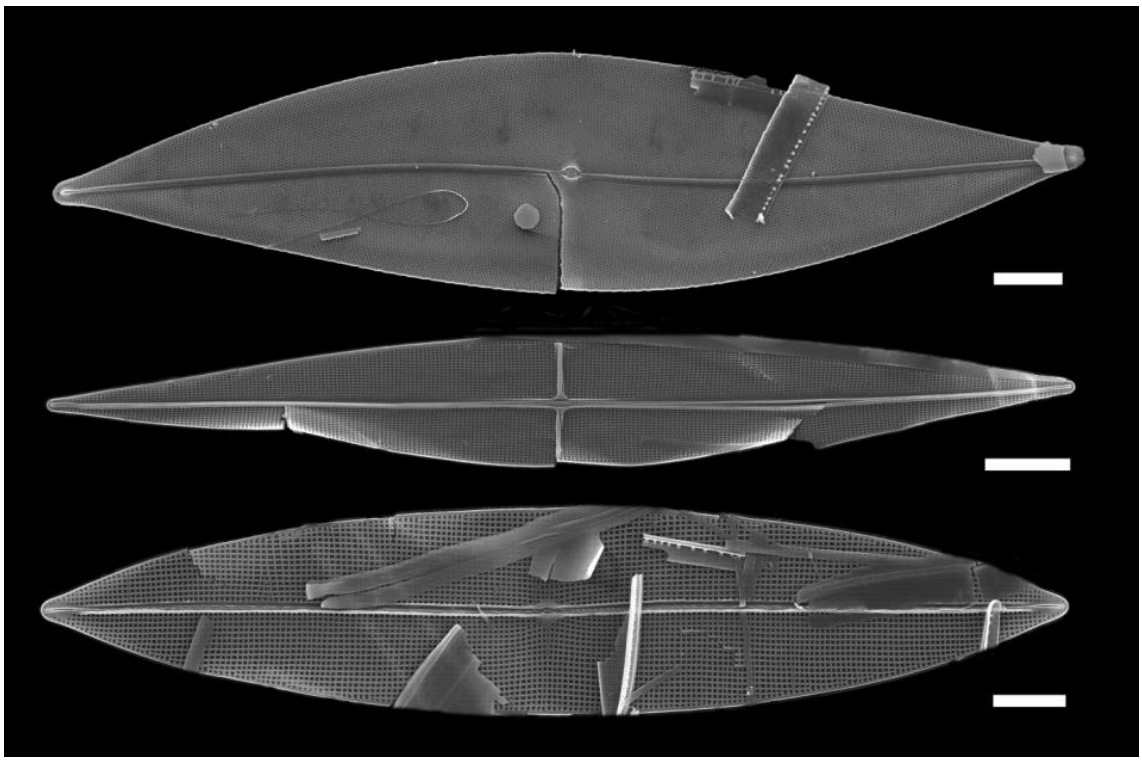

Figure 1.5: Scanning electron micrographs (SEM) of IP_{25}-producing diatom species: *Pleurosigma stuxbergi var. rhomboids* (upper), *Haslea crucigeroids* or *Haslea spicula* (middle) and *Haslea Kjelmanii* (top). Scale bar is 10 µm. Figure courtesy of Brown et al. (2014b).

suggested that it likely originated from sea-ice diatoms. More recently, Sinninghe Damsté et al. (2007) reported the presence of HBI diene II in anoxic sediments from Ellis Fjord in East Antarctica, with $\delta^{13}C$ values of -9.1 to -9.4‰ suggested as being consistent with a sea-ice diatom origin for this alkene.

Unlike IP_{25}, HBI diene II is not unique to an Antarctic environment. It is also present in the Arctic, being co-produced alongside IP_{25} by Arctic sea-ice diatoms (Brown et al., 2014b), and when quantified in sediments, shows a highly positive linear relationship with IP_{25} (Belt et al., 2010; Massé et al., 2008; Vare et al., 2009). Therefore, HBI diene II can also be used as a proxy for Arctic sea-ice. Moreover, in the absence of IP_{25}, HBI diene II has the potential to provide the basis for paleo sea-ice reconstruction for the Southern Ocean, although the development of this proxy is less advanced than that of IP_{25} for the Arctic.

To date, the only comprehensive investigation into the use of HBIs, and HBI diene II in particular, as sea-ice indicators in the Southern Ocean, comes from Massé et al. (2011). The authors showed that in nine sea-ice samples from two well separated regions of the Antarctic, HBI diene II occurred as the only major HBI isomer. Determination of the stable carbon isotopic composition of HBI diene II in the sea-ice samples produced average values of -8.5 and -5.7‰ for the sampling locations. These values were similar to those reported previously for HBI diene II in sediments from Ellis Fjord, Antarctica (-9.1 and -9.4‰, Sinninghe Damsté et al., 2007). Additionally, the $\delta^{13}C$ values were consistent with an origin from diatoms growing within sea-ice where CO_2 concentrations are often depleted, depending on the physical condition of the ice (Belt et al., 2008; Gibson et al., 1999; Kennedy et al., 2002).

Further in the study by Massé et al. (2011), an analysis of phytoplankton samples collected in Antarctic open waters during a summer algal bloom, showed the absence of HBI diene II. However, samples did contain a suite of tri- to penta unsaturated HBI isomers, with considerably lighter $\delta^{13}C$ values (-38 to -41‰) observed, indicative of a CO_2 replete environment. Further evidence of the sea-ice origin of HBI diene II was given by Massé et al. (2011) through surface sediment analysis. Although a number of HBI isomers were present, HBI diene II was shown to be especially evident at sites experiencing landfast ice for the majority of the year. At the only site where HBI diene II was absent in the sediment, satellite observations indicated year-round ice-free conditions. Interestingly, only trace amounts of tri-unsaturated HBI isomers were observed. The isotopic composition ($\delta^{13}C$) of HBI diene II was found to be -17.8±1.0‰, somewhat different to that found in the sea-ice samples ($\delta^{13}C$=-8.5 and -5.7‰). This was interpreted as HBI diene II in the Antarctic sediments being biosynthesised by sea-ice diatoms, both during periods of ice melt and during earlier phases, when maximum algal growth occurs and CO_2 supply becomes limited

(Gibson et al., 1999). Importantly, however, sedimentary $\delta^{13}C$ of HBI diene II was very different to that found for the polyunsaturated HBIs (-36.1 to -41.6‰), clearly indicating different environmental conditions/settings during the biosynthesis of HBI diene II compare to the other HBIs. Therefore, the presence of HBI diene II within Antarctic sea-ice, its absence from open-water phytoplankton assemblages, and its high $\delta^{13}C$ signature in a number of Antarctic locations, led Massé et al. (2011) to propose its presence in Antarctic sediments to be a useful proxy indicator for the contribution of organic matter derived from sea-ice diatoms.

Although the study by Massé et al. (2011) provided preliminary evidence of the biosynthesis of HBI diene II in sea-ice, on the whole, the sedimentary distribution of this biomarker for paleo reconstructions in Antarctica is limited to a small number of surface sediments and water column samples. Despite this, a number of sea-ice reconstruction studies based on the variable abundance of HBI diene II in Antarctic sediments have already begun to appear (Barbara et al., 2010, 2013, 2016; Campagne et al., 2015, 2016; Collins et al., 2013; Denis et al., 2010; Etourneau et al., 2013).

1.3.1.1 Coupling sea-ice biomarkers with phytoplankton biomarkers

In the Arctic, sedimentary measurements of IP_{25} have sometimes been accompanied by measurements of some sterols (brassicasterol), to provide complementary evidence of open-water conditions, especially for regions of seasonal sea-ice. Thus, for example, by analysing brassicasterol data during periods when IP_{25} was absent, Müller et al. (2009) showed that different climatic extremes could be distinguished, with the (additional) absence or low abundance of brassicasterol reflecting permanent sea-ice coverage and elevated brassicasterol content indicating predominantly ice-free conditions. Furthermore, the nature of intermediate paleo sea-ice conditions (e.g. seasonal ice

margin) could be determined from high (but variable) abundances of both IP_{25} and brassicasterol, reflecting beneficial environments for the growth of sea-ice diatoms and phytoplankton (Smith et al., 1985, 1987). Hence, by considering both IP_{25} and phytoplankton biomarkers, there is the potential to distinguish between ice-free and permanent sea-ice cover scenarios and also to provide additional information about primary productivity and the sea-ice conditions that strongly influence it (e.g. the presence of a marginal ice zone). The possibility of identifying paleo sea-ice margins is additionally significant since they denote areas of contrasting sea surface conditions that control atmospheric and oceanic interactions which, for example, influence continental ice-sheet dynamics. Application of this combinatory biomarker approach may, therefore, enable sea-ice margins to be located and this may inform large-scale climate modelling studies.

In an attempt to make the combinatory biomarker approach to sea-ice reconstruction more quantitative, Müller et al. (2011) combined IP_{25} and phytoplankton biomarker data obtained from surface sediments from the continental margins of East Greenland and West Spitsbergen to establish a novel index (PIP_{25}, Equation 1.1) that could potentially provide a more detailed assessment of sea-ice conditions that would be useful, in particular, for climate modellers.

Equation 1.1:

$$PIP_{25} = \frac{IP_{25}}{(IP_{25} + (phytoplankton\ biomarker * c))}$$

By calculating the ratio of IP_{25} to the combined IP_{25} and phytoplankton biomarker abundances, the PIP_{25} index integrates environmental information pertinent to both sea-ice diatoms and open water phytoplankton. However, Müller et al. (2011) noted the need to include a balance factor (*c*; Equation 1.1) to compensate for the distinctly higher

phytoplankton biomarker content compared to the relatively low IP_{25} concentrations within sediments from East Greenland and West Spitsbergen (Müller et al., 2011). It was also suggested that this term would likely have to be re-calculated for different regions of the Arctic Ocean. In addition, although the emphasis of the initial study was placed on using brassicasterol as a phytoplanktic indicator, Müller et al. (2011) stated that it should also be feasible to determine related PIP_{25} indices using other marine biomarkers derived from organisms living at the (ice-free) sea surface. In essence, relatively high IP_{25} and low phytoplankton biomarker abundances yield high PIP_{25} values consistent with frequent or extensive sea-ice cover, low IP_{25} content and relatively high phytoplankton biomarker concentrations result in low PIP_{25} values indicative of minimum sea-ice coverage, while intermediate PIP_{25} values imply marginal sea-ice or ice-edge conditions (Müller et al., 2011). In support of this model, Müller et al. (2011) found good linear correlations between satellite-derived spring sea-ice concentrations and PIP_{25} values obtained from analysis of surface sediments from the continental margins of East Greenland and West Svalbard, and suggested that this approach may be adopted for other study areas and for paleo sea-ice reconstructions. Indeed, Stoynova et al. (2013) adopted this method to show that PIP_{25} values derived from analysis of biomarkers in surface sediments from regions of the Arctic and subarctic Atlantic and Pacific also correlated well with satellite-derived sea-ice concentrations, although the correlations were better defined by logarithmic (PIP_{25}) relationships. In contrast, relatively poor correlations between near-surface PIP_{25} data and sea-ice concentrations have been observed for the Barents Sea (Navarro-Rodriguez et al., 2013) and the Kara & Laptev Seas (Xiao et al., 2013).

Despite this development, a number of factors still need to be better understood before the general applicability of the PIP_{25} approach can be established (Belt and Müller, 2013; Xiao et al., 2015). Some of these include identification of the most suitable open-

water (pelagic) biomarkers as counterparts to IP_{25} and the possible impacts of additional (non-marine) sources to the pelagic biomarker budget. For example, according to the original model presented by Müller et al. (2011), the phytoplankton marker should ideally provide a representative and consistent response to the proximal sea-ice conditions and have a selective marine origin. In practice, the most appropriate phytoplankton marker for PIP_{25}-based sea-ice concentration estimates has been shown to be strongly regionally dependent (Müller et al., 2011; Stoynova et al., 2013; Xiao et al., 2015), while some sterols may be derived from marine and non-marine sources (e.g. Huang and Meinschein, 1976; Volkman, 1986).

Additionally, the consequences of variability within the so-called balance factor used in the PIP_{25} calculation provide further caveats. The inclusion of the *c* term was originally introduced by Müller et al. (2011) to compensate for the generally significantly higher sedimentary concentrations of pelagic biomarkers compared to IP_{25}. In the absence of an established fixed value for *c* (global or regional), this balance factor is derived from the relative mean concentration of each biomarker within a suite of surface or down core sediments pertinent to the individual spatial or temporal study, respectively (Equation 1.1). However, this piecemeal mode of calculation can lead to problems in both cases. For down-core records, the magnitude of the *c* factor can be strongly dependent on the nature of the temporal window of the core being studied (e.g. ice-covered versus ice-free) or, indeed, of any sub-interval (Belt and Müller, 2013; Belt et al., 2015), with consequential impacts on PIP_{25}. As an example, relatively high PIP_{25} values, interpreted as reflecting extensive sea-ice cover, can be modified to low/medium values (low or occasional sea-ice) simply by extension of the temporal record to intervals that have higher IP_{25} content, as can frequently be the case when studying consecutive climatic epochs with contrasting sea-ice cover such as the Younger Dryas and the early Holocene (Müller et al., 2009; Cabedo-Sanz et al., 2013;

Müller and Stein, 2014; Belt et al., 2015). For spatial studies, the inclusion of substantial numbers of sediments from ice-free locations clearly impacts on the mean IP_{25} value, in particular, thus negatively influencing the *c* factor and, therefore, outcomes for regions of seasonal sea-ice cover. In addition, supplementing new biomarker data, either within surface sediment-based calibrations or for down-core records, requires continuous re-calculation of the *c* factor, which is not only cumbersome, but makes comparisons of datasets (or sub-sets) virtually impossible. Recently, Xiao et al. (2015) suggested that a global *c* factor, derived from biomarker data from a large number of sediments from different Arctic regions, might be more useful in these respects. In practice, however, significant regional differences in the *c* factor means that selection of the most suitable value remains problematic.

An additional limitation of the PIP_{25} approach arises when there are in-phase fluctuations of IP_{25} and phytoplankton biomarkers. For example, Müller et al. (2011) noted that coevally low (due to a permanent-like sea-ice cover) or high (due to marginal ice zone conditions) changes to individual biomarker content would result in similar PIP_{25} values, despite clear differences in sea-ice conditions. Indeed, this outcome has been observed for the PIP_{25} record of a sediment core from the West Spitsbergen slope, where the Late Holocene was characterized by short-term biomarker fluctuations interpreted as reflecting a rapidly advancing and retreating sea-ice margin. In this instance, Müller et al. (2012) suggested that environmental (i.e. sea-ice) reconstructions are based on the individual IP_{25} and phytoplankton biomarker records, instead of focusing on PIP_{25} values alone. Indeed, a recommendation when using the PIP_{25} index for carrying out paleo sea-ice reconstructions in the future is to interpret such data alongside those of the individual biomarker records in order to obtain a more balanced assessment.

Despite these limitations, PIP_{25}-derived estimates of (spring) sea-ice concentration are normally better than those based on IP_{25} alone, so further investigations into this type of approach are certainly worthwhile, and are therefore amongst the research objectives of the current project.

To date, a PIP_{25} style approach has not been developed or employed for the Antarctic. However, the relative abundances of HBI diene II in Antarctic paleo sea-ice reconstructions have generally been accompanied by measurement of another HBI isomer, HBI triene IIIa (Figure 1.1), believed to be derived from phytoplankton (Section 1.3.1). Indeed, the presence of HBI triene IIIa in a phytoplankton sample and its absence in sea-ice, along with its light isotopic signature within the Antarctic environment, led Massé et al. (2011) to propose, that a ratio of the concentrations of HBI diene II and HBI triene IIIa (II/IIIa) might reflect the relative contributions of sea-ice and phytoplankton derived organic matter to Antarctic sediments. To date, this represents the closest parallel to the PIP_{25} index employed for the Arctic. In any case, measurement of HBI diene II in Antarctic sediments has generally been used to provide proxy evidence of variability in past sea-ice extent for the Southern Ocean, while parallel quantification of HBI triene IIIa has been used to demonstrate open-water conditions and possibly changes in seasonality of Antarctic sea-ice (Collins et al. 2013). However, it is noted that research into HBIs as Antarctic sea-ice proxies is much less advanced than that of IP_{25} for the Arctic. Therefore, it is evident that further investigations of HBIs, within surface sediments and water column samples from wider locations in Antarctica, is needed in order to evaluate the general interpretations of individual and combined abundances of these biomarkers.

1.4 Specific aims of the current project

Overall, the main aim of this study was to improve biomarker-based methods for sea-ice reconstruction in both polar regions.

More specifically, in the Arctic, a research objective was to improve the application of the IP_{25} proxy for sea-ice reconstruction by examining further means of making them more quantitative or, at least, for improved definition of the sea-ice conditions. In particular, the use of a combined biomarker approach, by coupling IP_{25} with alternative phytoplankton biomarkers, was examined.

In the Southern Ocean, a considerable lack of information regarding the distribution of HBI biomarkers prompted the aim of improving our fundamental understanding of biomarker-based sea-ice reconstructions, through measurements of HBIs in sea-ice, water column and sediments.

The final aim of this project was to investigate, and identify, any common environmental relationships between the respective biomarkers in the Arctic and the Antarctic.

In order to achieve these aims, a number of investigations were carried out, which are presented and discussed in the following chapters:

Chapter 2: *Methodology.*

This chapter provides a description of the general laboratory and instrumental analytical procedures employed to obtain the data used to address the main aims of this research.

Chapter 3: (Results 1) *Optimised biomarker-based reconstruction of Arctic sea-ice margins and concentrations in the Barents Sea.*

This chapter describes the sedimentary analysis of IP_{25} (and other HBI biomarker) in surface sediments from the Barents Sea in order to provide a more detailed description of sea-ice conditions, including estimates of spring sea-ice concentrations.

Outcomes presented in Chapter 3 are part of the study published in Belt, S.T., Cabedo-Sanz, P, Smik, L., Navarro-Rodriguez, A., Berben, S.M. P., Knies, J. and Husum, K., 2015. Identification of paleo Arctic winter sea-ice limits and the marginal ice zone: Optimised biomarker-based reconstructions of late Quaternary Arctic sea-ice. Earth and Planetary Science Letters 431, 127-139, and in Smik, L., Cabedo-Sanz, P., Belt, S.T., 2016. Semi-quantitative estimates of paleo Arctic sea-ice concentration based on source-specific highly branched isoprenoid alkenes: A further development of the PIP_{25} index. Organic Geochemistry 92, 63-69.

Chapter 4: (Results 2) *Distribution of highly branched isoprenoid alkenes and other algal lipids in surface and water column waters from East Antarctica: further insight for biomarker-based paleo sea-ice reconstructions.*

This chapter describes the investigation into the distribution of various HBIs and other biomarkers in surface and water column waters from East Antarctica in order to investigate the sensitivity of various biomarkers to the overlaying environmental conditions.

Some of the outcomes presented in Chapter 4 are part of the study published in Smik, L., Belt, S.T., Lieser, J.L., Armand, L.K., Leventer, A., 2016. Distributions of highly branched isoprenoid alkenes and other algal lipids in surface waters from East Antarctica: further insights for biomarker-based paleo sea-ice reconstruction. Organic Geochemistry 95, 71-80.

Chapter 5: (Results 3) *Source, distribution and environmental significance of an organic geochemical proxy for Antarctic sea-ice: $IPSO_{25}$.*

This chapter describes the identification of the source responsible for biosynthesis of di-unsaturated HBI (HBI diene II), used as a sea-ice indicator in the Southern Ocean. Sedimentary distributions of this and other HBI biomarker found in large number of surface sediments are presented.

Some of the outcomes presented in Chapter 5 are part of the study published in Belt, S.T., Smik, L., Brown T.A., Kim, J.-H., Rowland, S.J., Allen, C.S., Gal, J.-K., Shin, K.-H., Lee, J.I., Taylor, K.W.R., 2016. Source identification and distribution reveals the potential of the geochemical Antarctic sea ice proxy $IPSO_{25}$. Nature Communications 7, 12655.

Chapter 6: *Conclusions and future work.*

This chapter summarises the main outcomes from each of the individual study. It also provides suggestions of future work needed to improve the application of IP_{25} and $IPSO_{25}$ and other related biomarkers for paleo sea-ice reconstruction in the Arctic and Antarctic, respectively.

CHAPTER TWO

2 General laboratory and analytical methods

2.1 Introduction

The following chapter describes analytical procedures and methods employed to obtain the data required to achieve the objectives of the projects as described in Chapter 1. Most of the methods described here have been adopted from previous studies, where Highly Branched Isoprenoid (HBI) biomarkers, especially the Arctic sea-ice proxy IP_{25}, have been used for paleo reconstructions of oceanographic conditions in the polar regions (e.g. Belt et al., 2012; Brown, 2011; Cabedo-Sanz, 2013). These standardised methods particularly focus on the extraction and analysis of HBIs and other biomarkers in polar marine sediments and phytoplankton (Belt et al., 2014, 2015; Brown et al., 2015). The description of methods includes aspects of instrumentation and laboratory operating conditions, in addition to chemical identification and quantification.

As chemical analysis was carried out on different matrices (sediments, sea-ice, phytoplankton), the reader is referred to the relevant chapters (sediment material: **Chapters 3** and **5**, phytoplankton: **Chapter 4,** sea-ice: **Chapter 5**) for a description of the sample management and specific chemical extraction techniques.

2.2 Freeze-drying

Some of the sediment samples analysed here were freeze-dried in other laboratories. For those sediments freeze-dried in the Plymouth laboratory, a Christ Alpha 2-4 LD plus freeze-dryer was used. Frozen (-20ºC, ca 24h) sediments were freeze-dried at -80ºC and 0.001 mbar for ca 24-48 hours, depending on their water content and number of samples being dried. Water content (Wc; g) was determined by mass difference from wet (m_W) and dry (m_D) sediment masses, determined before and after freeze-drying (Equation 2.1).

Equation 2.1:

$$Wc = m_w - m_D$$

For the purposes of this research, only sediment material was freeze-dried prior to any further analysis.

2.3 Sample storage

Sediment samples held at Plymouth were stored in plastic bags and kept frozen (-20ºC) until analysis. The full history of the storage conditions under which sediments obtained from other laboratories (British Antarctic Survey (BAS), UK; British Ocean Sediment Core Research Facility (BOSCORF), UK; Geological Survey of Norway; Alfred Wegener Institute (AWI), Germany) were stored are not known. However it is believed that samples were stored under similar conditions, i.e. freeze-dried in plastic bags and kept in generally cool conditions (ca 5ºC).

Glass fibre filters (GF/F, Whatman, UK) containing phytoplankton samples were stored wrapped in aluminium foil and frozen (ca -20ºC) until analysis.

2.4 Internal standards for lipid quantification

The addition of internal standards to the sediment and phytoplankton samples prior to HBI and sterol extraction was used to enable quantification of the extracted compounds; 9-octylheptadec-8-ene (9-OHD, 10 μL; 1-10 μg mL^{-1}; Figure 2.1a) was added to allow for quantification of HBIs, while 5α-androstan-3β-ol (10 μL; 1-10 μg mL^{-1}; Figure 2.1b) was added for quantification of sterols. An additional internal standard, nonadecanoic acid (10 μL; 1 mg mL^{-1}, Figure 2.1c), was added only to phytoplankton samples to allow for quantification of fatty acids.

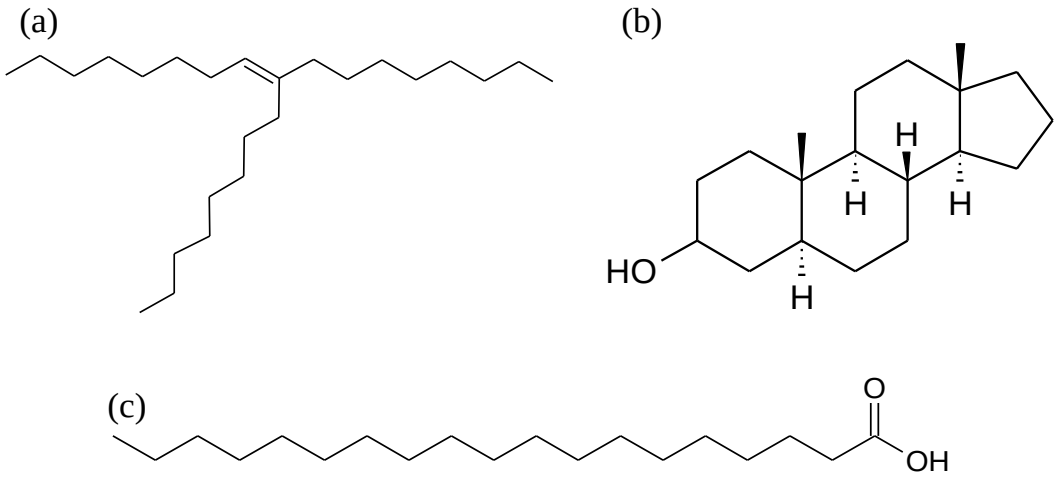

Figure 2.1: Chemical structures of internal standards used for biomarker quantification: (a) 9-octylheptadec-8-ene (9-OHD); (b) 5α-androstanol-3ß-ol; and (c) nonadecanoic acid.

2.5 Total organic extracts (TOEs)

For each sediment extraction, DCM/MeOH (2:1 *v/v*) was added in sufficient volume (ca.3 mL), to cover sediments (containing internal standards) with an excess of ca 1 mL above the sediment surface. The vials were then sealed using lined polypropylene screw caps (7 mL, Fisher, UK), ultra-sonicated (Transsonic T420, Camlab; ca 15min) to stimulate the disaggregation of sediments and thus permit more efficient organic extraction of the sample, and centrifuged (2500 rpm; 90s). The supernatant was then decanted into a clean pre-labelled 7 mL glass vial and the extraction procedure repeated

twice more (DCM/MeOH, 2:1 *v/v*, 1.5 mL) yielding the Total Organic Extract (TOE) (Figure 2.2, steps 1 to 5).

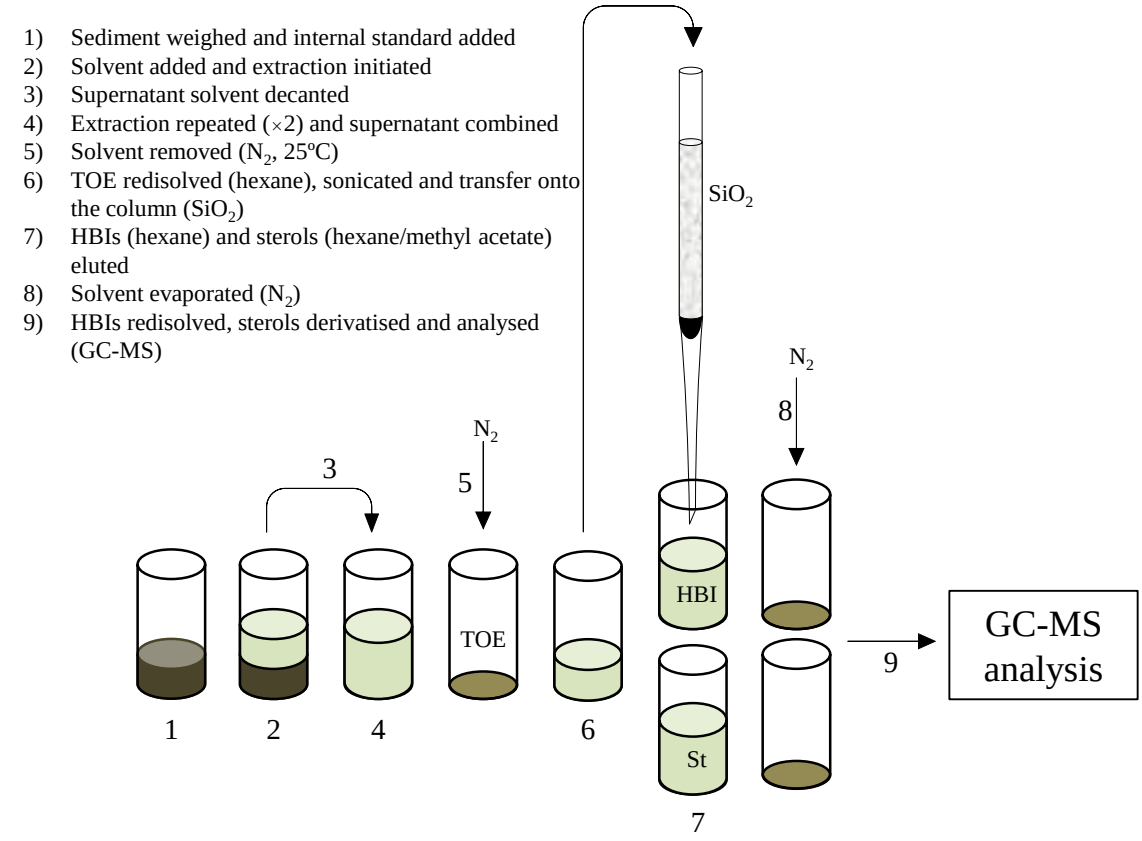

Figure 2.2: Schematic figure showing individual steps of the extraction and purification carried out for analysis of Arctic and Antarctic marine sediments (Belt et al., 2012). HBI and St refer to fractions containing highly branched isoprenoids and sterols, respectively. Individual steps of the extraction procedure are also briefly explained.

Typical sample quantities were 0.5-5 g of sediment, and ca 6-9 mL solvent was required for each extraction. Where higher quantities of sediments were extracted (4-5 g), two silica columns were used in the purification step (step 7, figure 2.2) in order to maximise interaction of the compounds of interest with the stationary phase, thus avoiding overload of the column with excess material, which could results in ineffective separation of the compounds of interest.

2.6 Saponification of fatty acid triglyceride esters

Following the addition of internal standards, filtered sea-ice and phytoplankton samples (GF/F) were saponified with sufficient methanolic potassium hydroxide (KOH, 5%; MeOH/H_2O, 90/10, *v/v*; ca 3 mL) to cover the sample in a 7 mL glass vial, which was capped using a lined polypropylene screw cap and heated (70ºC, 1h). The non-saponifiable lipids (NSL), including HBIs and sterols, were re-extracted into hexane (3×1 mL) and transferred to a clean vial using a glass pipette. Saponifiable lipids, including fatty acids, were obtained by adding concentrated HCl (1 mL) to the saponified samples with subsequent re-extraction with hexane (3×1 mL). A schematic showing the analytical steps undertaken during the analysis of phytoplankton samples is given in Figure 2.3.

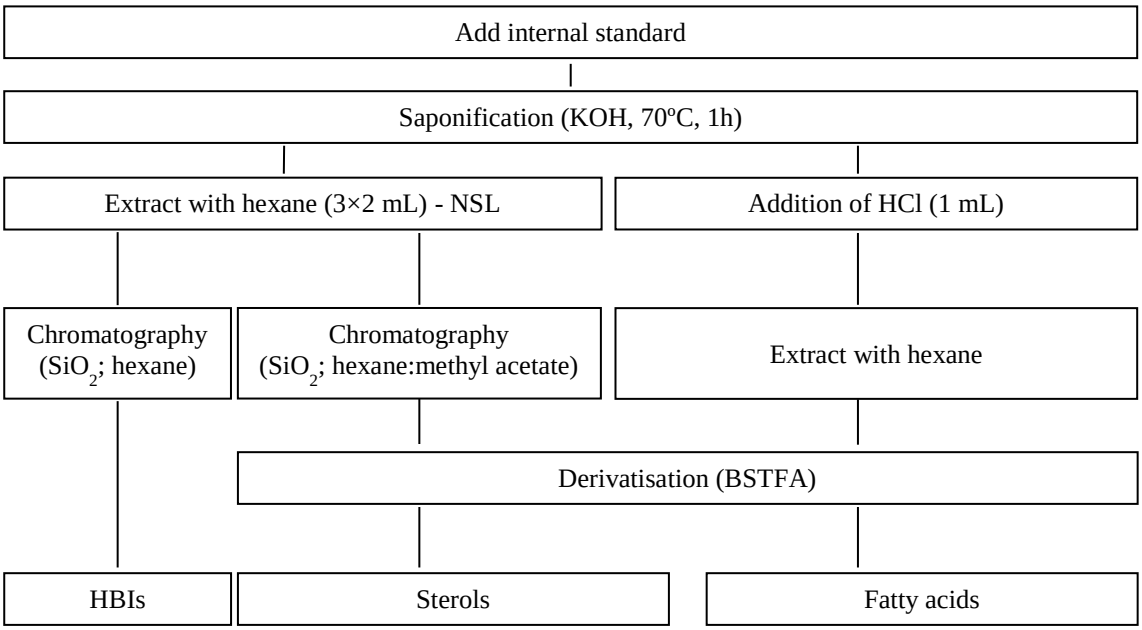

Figure 2.3: Schematic figure showing individual steps of the extraction and purification carried out for analysis of filtered sea-ice and phytoplankton samples.

2.7 Purification of biomarker lipids

2.7.1 Column chromatography

Total organic extracts (TOEs) from sediment analysis and non-saponifiable lipids (NSL) from phytoplankton analysis were partially purified prior to GC-MS analysis to remove complex mixtures of chemical compounds, which can interfere, chromatographically and spectrometrically, with the compounds of interest.

Following the removal of the solvent (N_2, ca 25°C) from the combined extracts, (e.g. step 5, Figure 2.2), the dried TOEs were re-suspended in hexane (0.5 mL) and sonicated (5 min). Extracts were then transferred into a small-scale chromatography column made of a glass pipette containing a small plug of cotton wool (Soxhlet extracted, DCM ca 8h) and deactivated chromatography grade silica (non-dried, ambient moisture, ca 0.7 g; 60-200 μm). Prior to addition of TOEs and NSLs, columns were pre-conditioned with hexane (ca 3 mL) to homogenise the stationary phase. Non-polar hydrocarbons, including IP_{25} and other HBIs of interest (HBI diene II, HBI trienes IIIa and IIIb), were eluted using hexane mobile phase (ca 6 mL), with more polar compounds, including sterols, eluted with hexane/methyl acetate (4:1, *v/v*; ca 6 mL). Both fractions were collected in pre-labelled 7 mL glass vials and solvents were removed by a N_2 stream (25°C) prior to GC-MS analysis. The purification steps typically undertaken for TOEs (sediment analysis) and NSL (phytoplankton samples) are illustrated in Figure 2.2, steps 5 to 9.

2.7.2 Silver-ion chromatography

Where identification of IP_{25} and other HBI compounds was difficult due to low abundance and/or the occurrence of other highly abundant co-eluting organic

compounds that prevented further concentration of the extracts, additional purification of hydrocarbon fractions by Ag-ion chromatography was required (Figure 2.4).

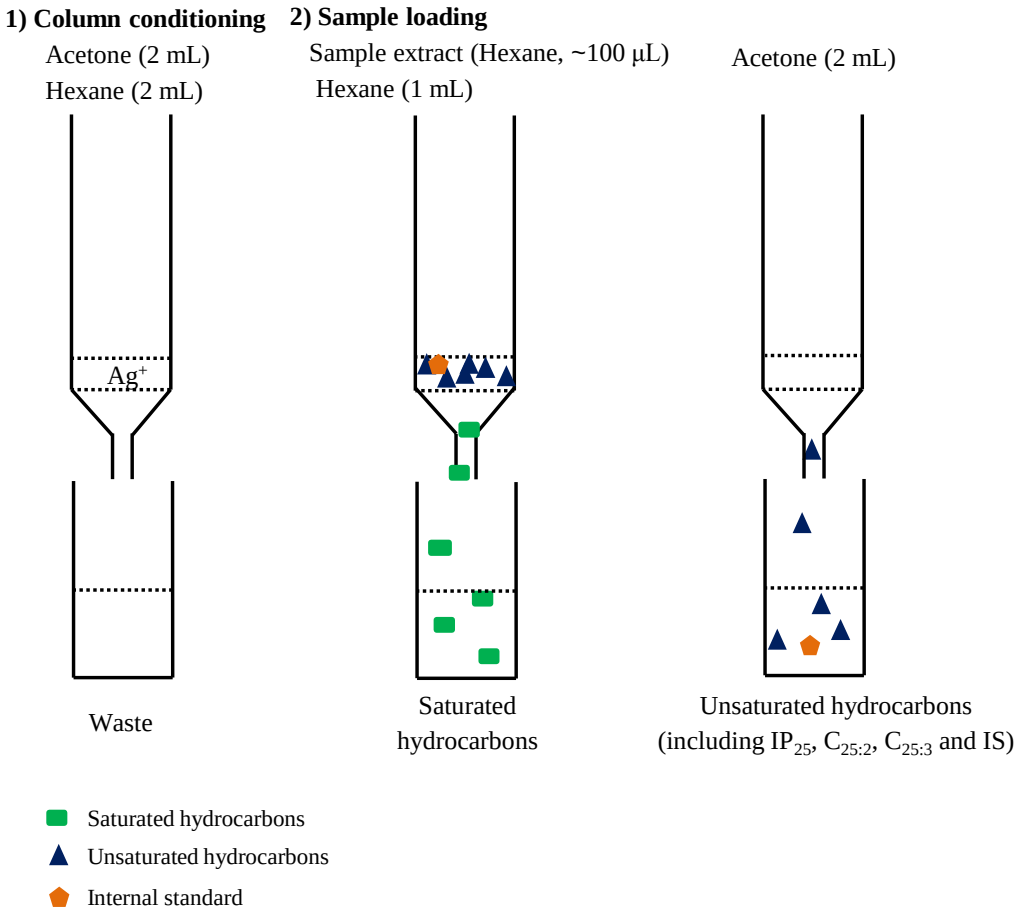

Figure 2.4: Schematic figure showing the Ag-ion chromatographic procedure for fractionation of saturated and unsaturated hydrocarbons (Cabedo-Sanz, 2013).

In these cases, extracts were further fractionated into saturated and unsaturated components using a glass pipette plugged with cotton wool (Soxhlet extracted, DCM, ca 8h) containing ca 100 mg of Ag-ion chromatography material (Supelco discovery® Ag-ion). Prior to the addition of partially purified hydrocarbon extracts re-dissolved in hexane (100 µL), Ag-Ion packed columns were conditioned with acetone followed by hexane (one column volumes each, ca 1 mL). Saturated hydrocarbons were eluted with hexane (1 mL), and unsaturated hydrocarbons, including IP_{25}, IS and other HBI compounds of interest in the study, were collected with acetone (2 mL), before being dried under a gentle stream of N_2 (25ºC).

2.7.3 Further purification and fractionation of partially purified hydrocarbon fractions

Where the abundance of certain HBIs was sufficiently high to allow for stable isotopic composition analysis to be undertaken (e.g. Antarctic surface sediments), further purification of partially purified extracts was carried out. In this case, compounds of interest were also fractionated into individual components depending on degree of unsaturation. The procedure (Figure 2.5) was similar to that described in Section 2.7.2, but used ca 300 mg rather than 100 mg of Ag-ion stationary phase.

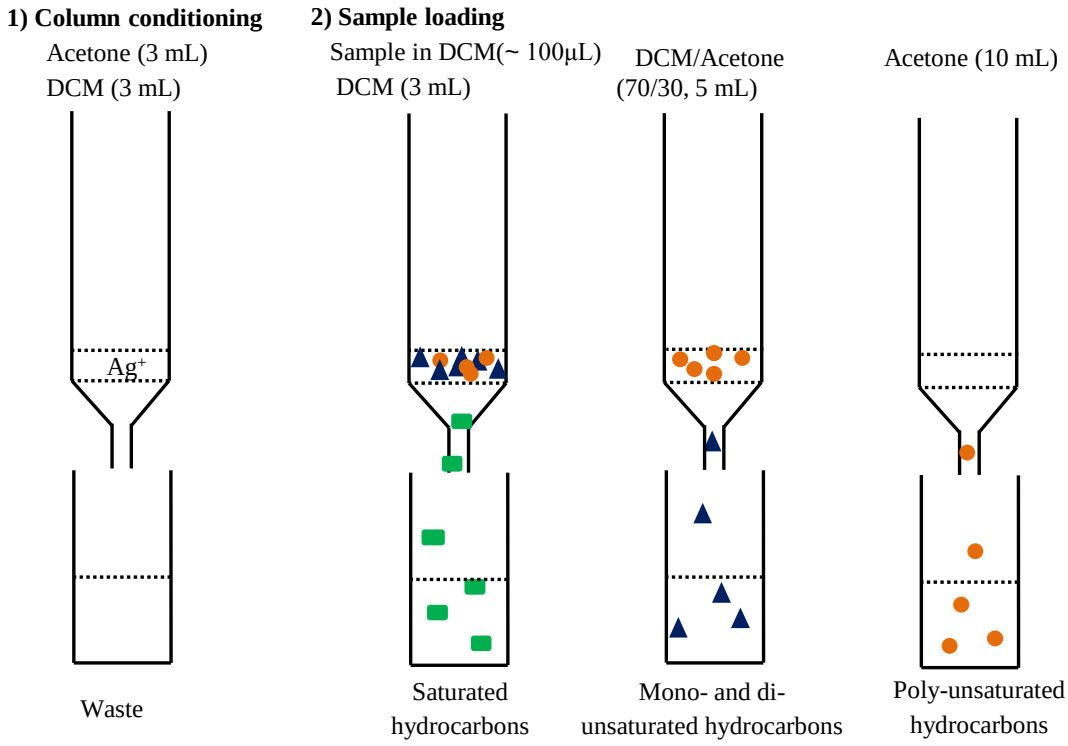

Figure 2.5: Schematic figure showing the Ag-ion chromatographic procedure for further fractionation of hydrocarbon compounds for stable isotope analysis.

Prior to separation, each column was conditioned with acetone followed by DCM (3 mL each). The partially purified extracts were then diluted in DCM and loaded onto the column. Gradual elution of extract containing columns with DCM (3 mL), DCM/Acetone 70/30 (5 mL) and Acetone (10 mL) resulted in three fractions containing

saturated, mono- and di-unsaturated (e.g. 9-OHD, HBI diene II) and polyunsaturated (e.g. HBI trienes IIIa and IIIb) hydrocarbons, respectively (Figure 2.5).

2.8 Removal of elemental sulfur

In some cases, TOEs were found to contain high concentrations of elemental sulphur (S_8, Figure 2.13) that interfered with the subsequent gas chromatographic analyses. Sulphur was removed from the TOEs before further purification based on a rapid, efficient and non-destructive method described by Jensen et al. (1977) based on the chemical reaction shown in Equation 2.2 (TBA^+ refers to tetrabutylammonium):

Equation 2.2:

$$(TBA^+)_2\ SO_3^{2-} + S_{(s)} \rightleftharpoons 2\ TBA^+ + S_2O_3^{2-}$$

A tetrabutylammonium sulphite reagent $(TBA^+)_2SO_3^{2-}$ (TBA reagent) was prepared by adding 3.39g of tetrabutylammonium hydrogen sulphate ($C_{16}H_{37}NO_4S$, Fisher Scientific) to 100 mL of ultra-high purified (UHP) water saturated with 25g of sodium sulphite anhydrous (Na_2SO_3, Fisher Scientific). Once the reagent was prepared, hexane (1 mL) was added to the dried TOEs, followed by some TBA reagent (1 mL) and 2-propanol (2 mL). This solution was then shaken by hand (1min). After adding UHP water (3 mL), the samples were shaken again (1min) and centrifuged (2500 rpm; 2min). The hexane layer containing the lipids of interest was transferred to a clean vial, and the procedure repeated twice more. After evaporation of the solvent (N_2, 25ºC), the TOEs were purified following the methods described in Section 2.7.1.

Previous investigation have found this method to be highly effective for removing sulphur from the Arctic marine sediments and TOEs tested, with comparable values of HBIs observed prior to and after the application of the method (Cabedo-Sanz, 2013).

The differences in concentrations observed (<18%) likely resulting from the inherent analytical variability (ca 7%) that is associated with analysis of HBIs in polar marine sediments (Belt et al., 2014).

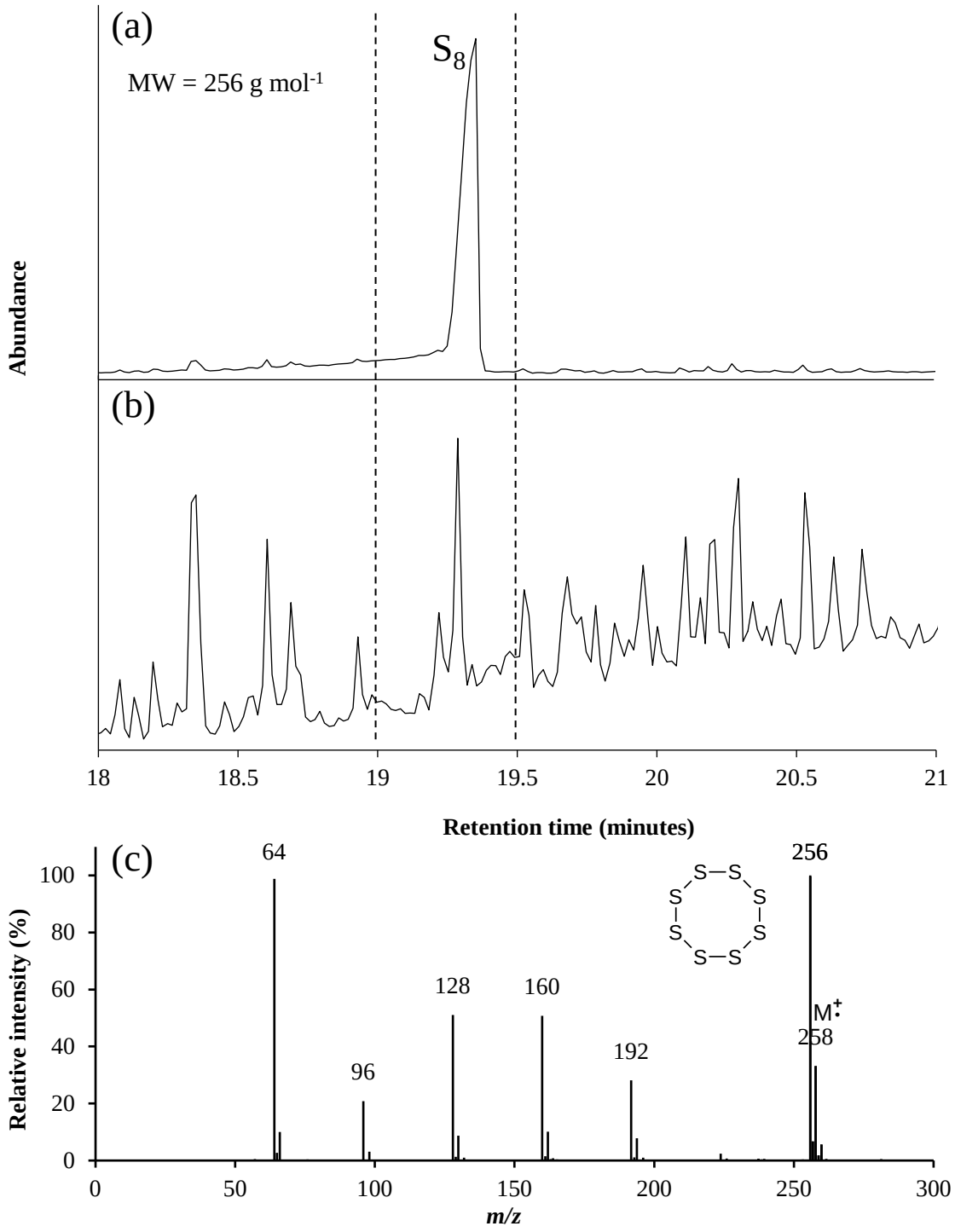

Figure 2.6: (a) TIC GC-MS chromatogram of sediment sample before sulphur removal; (b) TIC GC-MS chromatogram of sediment sample after desulphurisation; and (c) background-subtracted mass spectra and structure of elemental sulphur ($M^{+\bullet}$=*m/z* 256). Retention time window where all the HBIs of interest presented in this study elute (19.0-19.5 min) is indicated by dashed lines.

2.9 Derivatisation

Prior to analysis by GC-MS, fractions containing sterols and fatty acids were derivatised using N,O-bis(trimethylsilyl)trifluoroacetamide (BSTFA; 50 µL, 70ºC, 1h), to increase the volatility of the polar compounds and to improve their chromatographic behaviour.

2.10 Gas chromatography-mass spectrometry (GC-MS)

Prior to analysis by GC-MS, samples containing analytes of interest were transferred to GC vials (Chromacol, UK) and diluted to an appropriate concentration (100-500 µL). An Agilent 7890A GC coupled to a 5975 series mass selective detector (MSD) fitted with an Agilent HP-5ms (30 m×0.25 mm×0.25 µm) column was used, along with 1 µL split/splitless injection (300˚C) with helium carrier gas (1 mL min^{-1} constant flow). Total ion current (TIC; *m/z* 50-500 Da) and selective ion monitoring (SIM; -0.3 +0.7 *m/z* of interest) techniques were used to identify the compounds, with an electron voltage of 70 eV. The GC oven was heated from 40 to 300˚C at 10˚C min^{-1} and held at 300˚C for 10 minutes. The retention time and mass spectrum of individual compounds were obtained from TIC chromatograms, whereas compound quantification was normally performed from SIM chromatograms due to its generally high selectivity and sensitivity.

When concentrations of HBIs were particularly low, an additional GC-MS method was used. This co called `high-sensitivity method` utilised a modified mode of sample injection onto the column, involving injection of sample in splitless mode (all of the sample vaporised in the injector went onto the column) and a pulse pressure of 25 psi held for 0.35 minutes. This maximized sample introduction onto the column, while narrowing the sample bandwidth and increasing sensitivity of the instrument by ca 20% (Cabedo-Sanz, 2013). Further, a shorter detection window focused on the known

retention times of HBIs, allowed additional concentration of the sample (when possible) without affecting the MS detector. The high sensitivity method was only used for analysis of HBIs, due to their generally lower natural abundances in environmental samples compared to sterols or fatty acids (Belt et al., 2013; Brown, 2011). General features of GC-MS methods used in this research are summarised in Table 2.1.

Table 2.1: General features of GC-MS methods used for analysis of HBIs, sterols and FA.

Method	**HBI SIM-SCAN all HBI $M^{\ddagger\bullet}$ ions**	**HBI SIM-SCAN high sensitivity**	**STEROLS SIM SCAN**	**FA SIM SCAN**
Function	Routine detection of HBIs	Increased sensitivity for HBI analysis	Routine detection of sterols	Routine detection of FA
Mass range (*m/z*)	50-500	90-360	50-500	50-500
SIM ions (*m/z*)	350.3, 348.3, 346.3, 344.3,342.3, 99	350.3, 348.3, 346.3, 99	333, 343, 372, 382, 396, 470, 458, 500,	117
Total run time	36 min	36 min	36 min	36 min
GC Temp profile	40°C-300°C at 10°C min^{-1} (10 min isothermal)	40°C-300°C at 10°C min^{-1} (10 min isothermal)	40°C-300°C at 10°C min^{-1} (10 min isothermal)	40°C-300°C at 10°C min^{-1} (10 min isothermal)
Detection Time	10-36 min	18.5-20.5 min 21.8-22.5 min	20-36 min	14-36 min

2.11 Identification and quantification of biomarker lipids

2.11.1 Identification and quantification of HBI alkenes

Identification of HBIs isolated from marine sediments and phytoplankton samples was established by comparing their respective mass spectra with those of authentic compounds kept in the Plymouth laboratory. Specifically, each lipid was identified from their molecular ion ($M^{\ddagger\bullet}$; IP_{25} *m/z*=350.3; HBI diene II *m/z*=348.3 and HBI triene IIIa and IIIb *m/z*=346.3), their characteristic mass spectrum (Figure 2.7 and 2.8), and their retention indices (IP_{25}: 2080; HBI diene II: 2082; triene IIIa: 2047; triene IIIb: 2094), which was calculated using Equation 2.3.

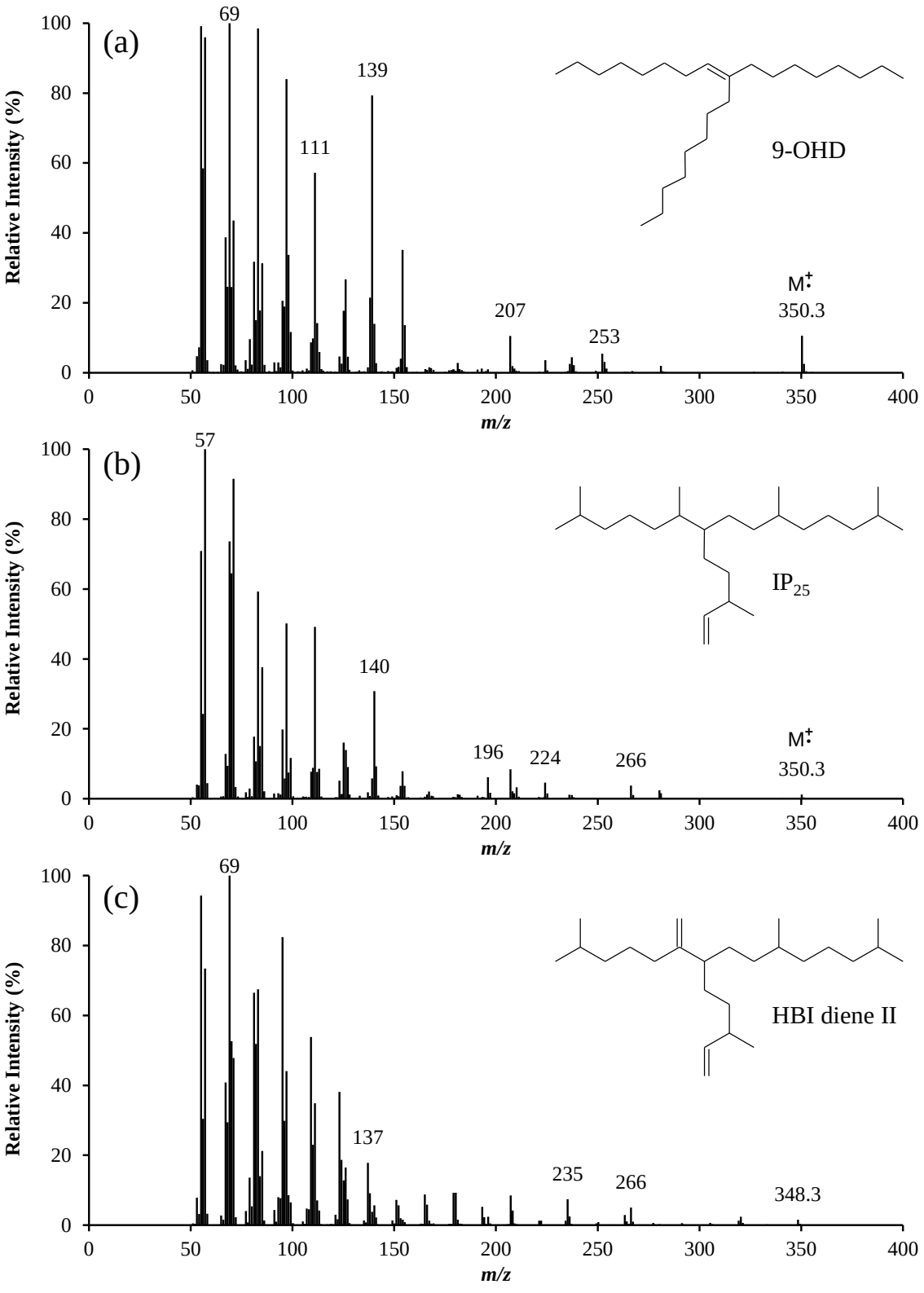

Figure 2.7: Background-subtracted mass spectra and structures of HBI alkenes described in the current study: (a) internal standard, 9-OHD ($M^{\bullet+}$=*m/z* 350.3); (b) IP_{25} ($M^{\bullet+}$=*m/z* 350.3) and (c) HBI diene II ($M^{\bullet+}$=*m/z* 348.3).

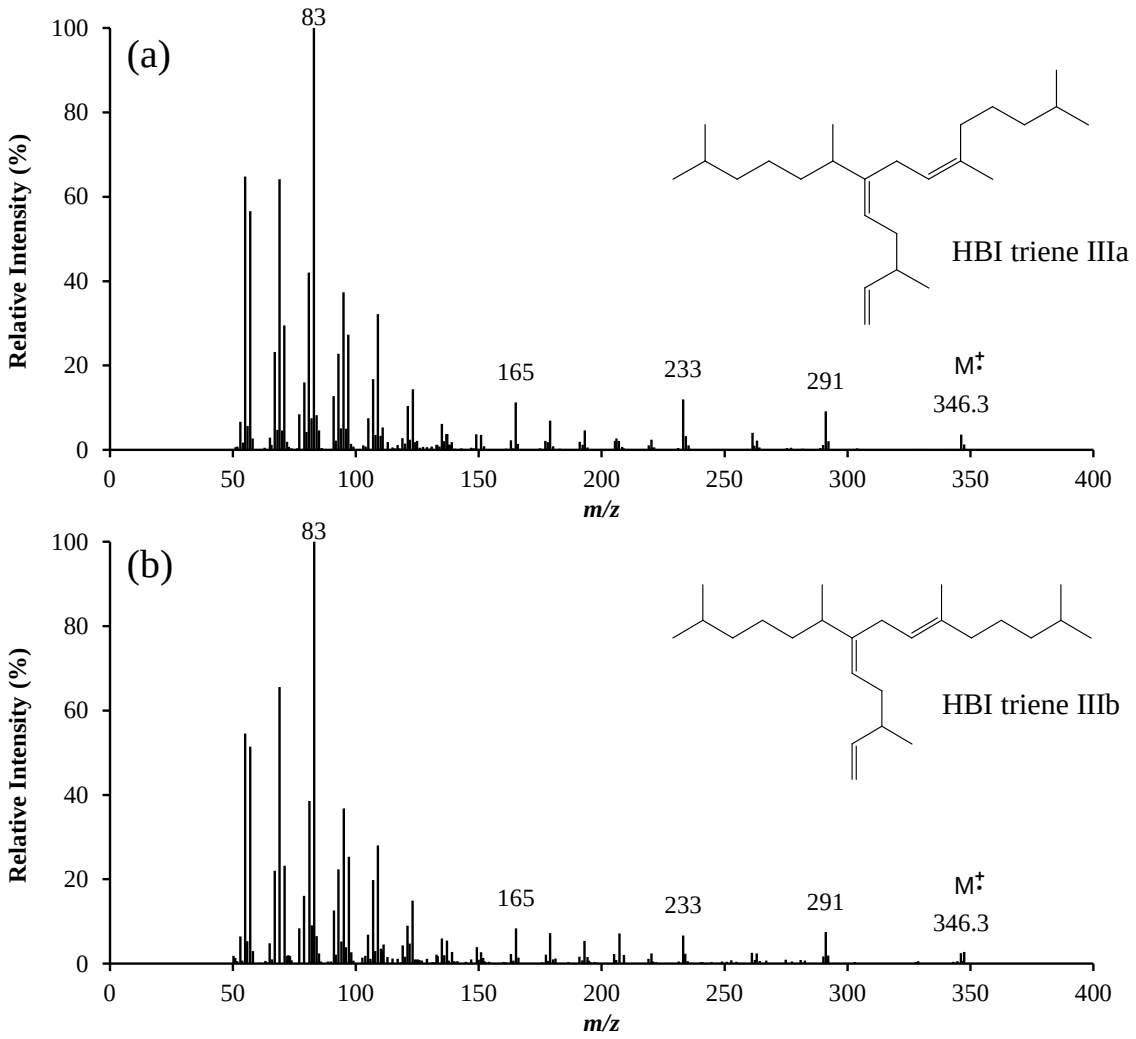

Figure 2.8: Background-subtracted mass spectra and structures of HBI alkenes described in the current study: (a) HBI triene IIIa ($M^{\bullet+}$=*m/z* 346.3) and (b) HBI triene IIIb ($M^{\bullet+}$=*m/z* 346.3).

Equation 2.3:

$$Ri = \frac{Rt^{HBI} - Rt^{nC_{20}}}{(Rt^{nC_{21}} - Rt^{nC_{20}})/100} + 2000$$

In Equation 2.3, *Ri* denotes the retention index and *Rt* is the retention time of individual lipids (e.g. HBI) and reference n-alkanes (e.g. nC_{20}).

Quantification of HBIs was achieved by manual integration (Chemstation, version C.03.00 software) of the molecular ion signal of each analyte as recorded by GC-MS SIM analysis (IP_{25}: *m/z* 350.3; HBI diene II: *m/z* 348.3; HBI triene IIIa and HBI triene IIIb: *m/z* 346.3; Figure 2.9). Factors such as extraction efficiency, mass of

sediment, or volume of water of samples extracted, and any differences in the relative response factors were accounted for using Equations 2.4 and 2.5, respectively.

Equation 2.4:

$$HBI\ (\mu g\ g^{-1} dry\ sediment) = \frac{\frac{P_A HBI}{P_A IS} * RF}{m\ dry\ sediment\ (g)} *\ m\ IS\ (\mu g)$$

Equation 2.5:

$$HBI\ (\mu g\ mL^{-1}) = \frac{\frac{P_A HBI}{P_A IS} * RF}{V\ filtered\ (mL)} *\ m\ IS\ (\mu g)$$

In Equation 2.4 and 2.5, P_A denotes the peak area of individual HBI lipid and internal standard (*IS*) obtained from GC-MS chromatograms. Mass of internal standard added and response factor applied is denoted by *mIS* and *RF*. Additionally, mass of sediment or volume of filtered water extracted is denoted as *m dry sediment* and *V filtered* respectively.

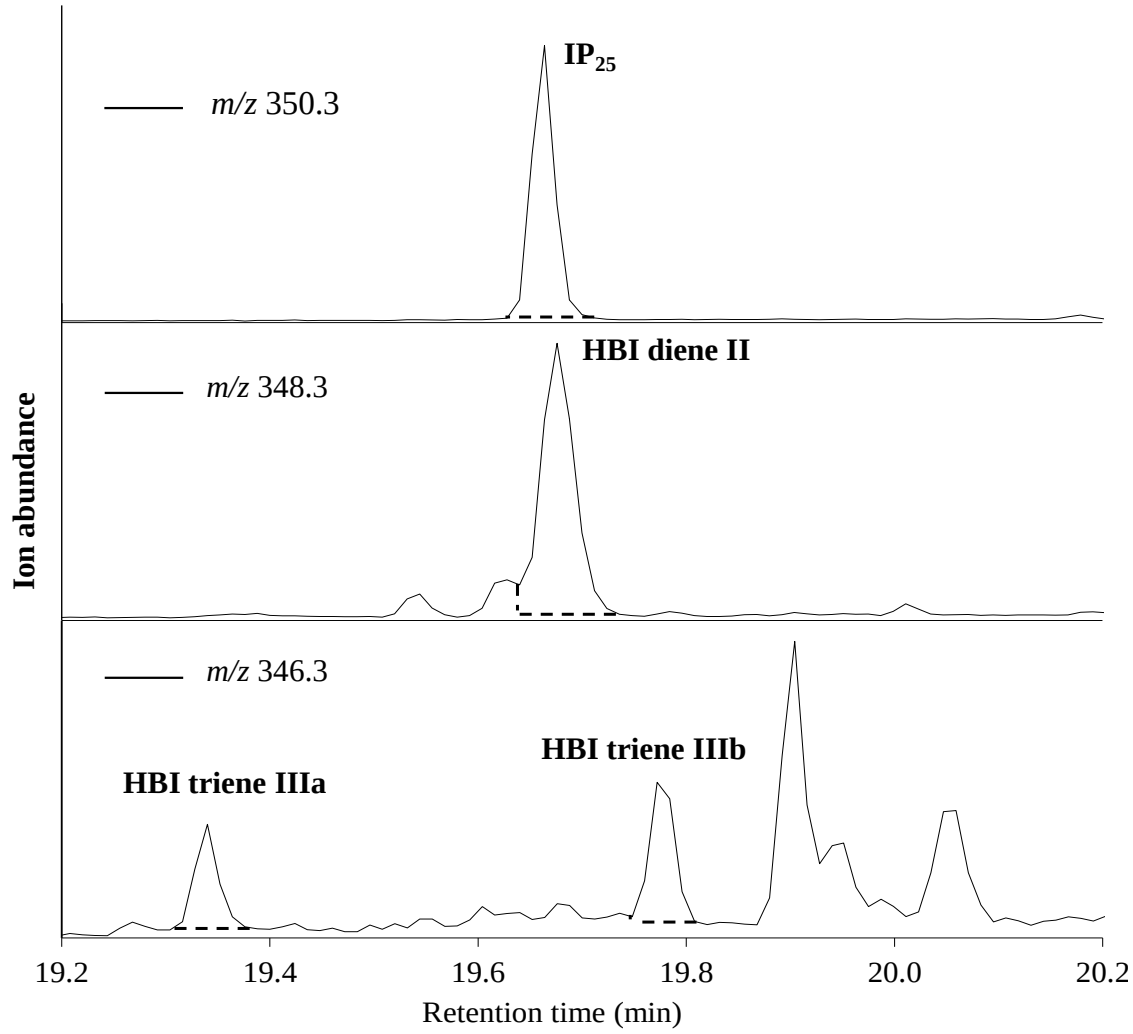

Figure 2.9: Partial GC-MS chromatograms (SIM, *m/z* 350.3, 348.3 and 346.3) of silica-purified sediment extract showing the relative elution order of HBIs of interest and the technique adopted for manual peak integration for quantification of HBIs (dashed lines).

The ratio between the peak area of a selected HBI (P_AHBI) and the peak area of the internal standard (P_AIS) was multiplied by a GC-MS response factor (RF) to account for different mass spectral responses between the particular HBI and the internal standard. The modified peak ratios were divided by either mass of dry sediment (g) or volume of water filtered (mL), and then multiplied by the mass of the internal standard (μg) added to the samples prior to extraction, yielding units for HBIs of μg g^{-1} (Equation 2.4; Table 2.2) and μg mL^{-1} (Equation 2.5) for sediment and phytoplankton analysis, respectively.

Table 2.2: Example of calculation steps needed to quantify HBI concentration in sediment samples using Equation 2.3. The example shown corresponds to the standard sediment sample from Barrow Strait. RF=response factor; sediment (g)=0.50; internal standard (IS, µg)=0.1. Calculation steps performed on GC-MS SIM-chromatogram given in Figure 2.8.

HBI	P_A HBI	P_A IS	RF	$\frac{P_A HBI}{P_A IS} * RF$	$\frac{\frac{P_A HBI}{P_A IS} * RF}{m\ dry\ sediment\ (g)}$	$\frac{\frac{P_A HBI}{P_A IS} * RF}{m\ dry\ sediment\ (g)} * m\ IS\ (\mu g)$
IP_{25}	141689	235321	5.22	3.14	6.29	0.629
HBI diene II	133997	235321	11.49	6.54	13.08	1.308
HBI triene IIIa	8843	235321	1.82	0.068	0.137	0.014
HBI triene IIIb	14844	235321	1.82	0.115	0.230	0.023

To account for the different mass spectral responses between the individual HBIs and the internal standard, response factors of individual HBIs were established experimentally from calibration curves of known HBI concentrations (0.2 µg mL^{-1}, 0.4 µg mL^{-1}, 0.6 µg mL^{-1}, 0.8 µg mL^{-1}, 1 µg mL^{-1}, $R^2 > 0.98$) against the internal standard (9-OHD) of equal concentration. Following the analysis by GC-MS, the RF for each of the standard solutions available at Plymouth University was calculated as a ratio of integrated peak areas (SIM mode) of selected ions for HBIs (e.g. *m/z* 350.3 for IP_{25}) and the internal standard (9-OHD). The final RF was calculated as an average of RFs obtained from the individual standards with periodic re-calibrations taking place every 3-6 months, depending on the frequency of analyses, to monitor for long-term sensitivity changes of the instrument.

Analytical reproducibility during each study was monitored using laboratory reference sediment with known abundances of biomarkers (Table 2.2). Reference sediment was used for approximately every 15 sediment samples extracted.

2.11.2 Identification and quantification of sterols

Identification of sterols isolated from marine sediments and phytoplankton samples (Table 2.3) was achieved by a combination of a comparison of the mass spectra of

derivatised compounds (trimethylsilyl, TMS) with those of authentic compounds or published spectra (e.g. NIST), to identify characteristic molecular and fragmentation ions (Figure 2.10 and Figure 2.11).

Table 2.3: Summary of the sterols studied as part of this research, and selected ions of their TMS ethers used for integration and quantification.

IUPAC name	Trivial name	Integration Ion
24-methylcholesta-5,22E-dien-3β-ol	brassicasterol	*m/z* 470
24-methylcholesta-5,24(28)-dien-3β-ol	24-methylenecholesterol	*m/z* 470
Cholest-5-en-3β -ol	cholesterol	*m/z* 458
Cholesta-5,22E-dien-3β-ol	22-dehydrocholesterol	*m/z* 327
5α-androstan-3β-ol	androstanol	*m/z* 333

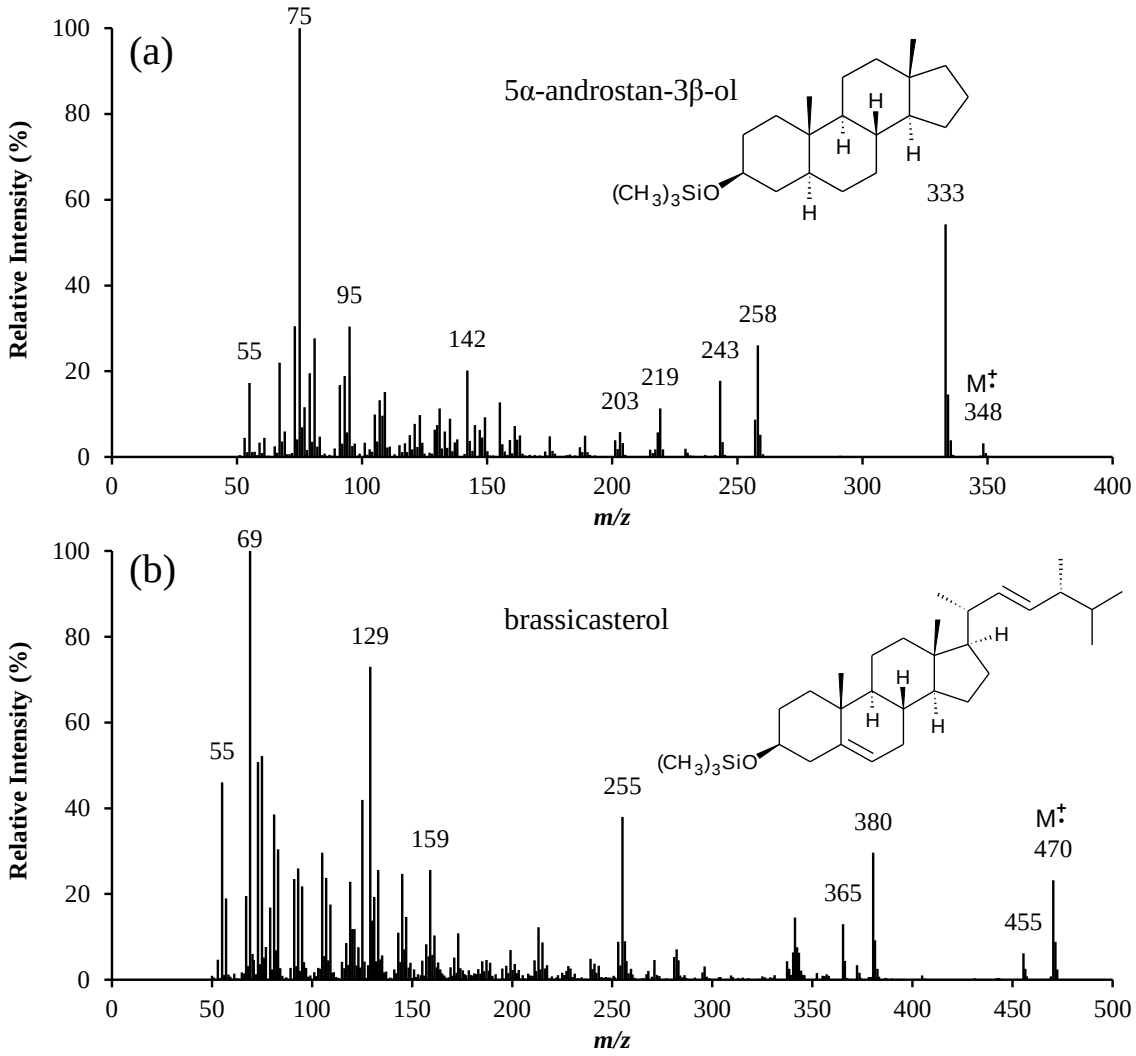

Figure 2.10: Background-subtracted mass spectra and structures of trimethylsilyl (TMS) sterols described in the current study: (a) 5α-androstan-3β-ol (internal standard, $M^{+\bullet}$=*m/z* 348); and (b) 24-methylcholesta-5,22E-dien-3β-ol (brassicasterol, $M^{+\bullet}$= *m/z* 470).

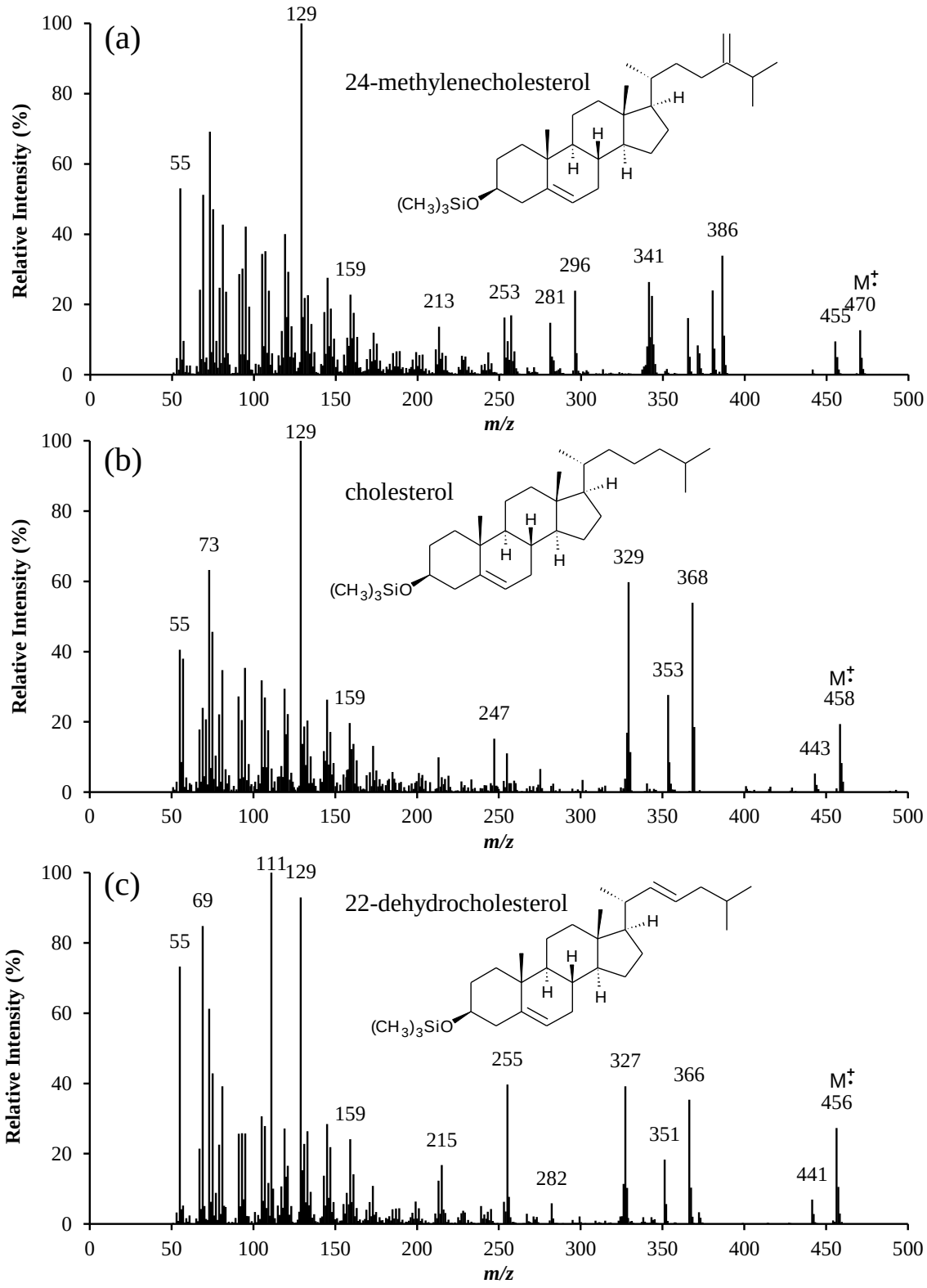

Figure 2.11: Background-subtracted mass spectra and structures of trimethylsilyl (TMS) sterols described in current study: (a) 24-methylcholesta-5,24(28)-dien-3β-ol (24-methylenecholesterol, $M^{+\bullet}$=*m/z* 470); (b) cholest-5-en-3β-ol (cholesterol, $M^{+\bullet}$=*m/z* 458); and (c) cholesta-5,22E-dien-3β-ol (22-dehydrocholesterol, $M^{+\bullet}$=*m/z* 456).

Quantification of sterols was achieved by the same method as for HBIs (Section 2.11.1) through manual integration (Chemstation, version C.03.00 software) of TMS molecular or fragmentation ion signal intensities obtained by GC-MS SIM mode (Table 2.3).

Factors such as extraction efficiency, mass of sediment or volume of water samplesextracted and any differences in the relative response factors were accounted for using Equations 2.6 and 2.7, respectively.

Equation 2.6:

$$sterol\ (\mu g\ g^{-1} dry\ sediment) = \frac{\frac{P_A sterol}{P_A IS} * RF}{m\ dry\ sediment\ (g)} *\ m\ IS\ (\mu g)$$

Equation 2.7:

$$sterol\ (\mu g\ mL^{-1}) = \frac{\frac{P_A sterol}{P_A IS} * RF}{V\ filtered\ (mL)} *\ m\ IS\ (\mu g)$$

In Equation 2.6 and 2.7, P_A denotes the peak area of individual sterol and internal standard (*IS*), obtained from GC-MS chromatograms. Mass of internal standard added and response factor applied is denoted by *mIS* and *RF*. Additionally, mass of sediment or volume of filtered water extracted is denoted as *m dry sediment* and *V filtered* respectively.

The response factor of the individual sterols was calculated from calibration curves of sterol concentrations (0.1 µg mL^{-1}, 0.2 µg mL^{-1}, 0.4 µg mL^{-1}, 0.6 µg mL^{-1}, 0.8 µg mL^{-1}, 1 µg mL^{-1}, R^2 >0.99) against the internal standard (5a-androstan-3β-ol) of equal concentration by the method described in Section 2.11.1.

2.11.3 Identification and quantification of fatty acids

Identification of fatty acids isolated from phytoplankton samples was undertaken as for sterols (Section 2.11.2) by a combination of a comparison of the mass spectra of derivatised compounds (trimethylsilyl, TMS) with those of authentic compounds or published spectra (e.g. NIST), to identify characteristic molecular and fragmentation ions (Figure 2.12 and Figure 2.13).

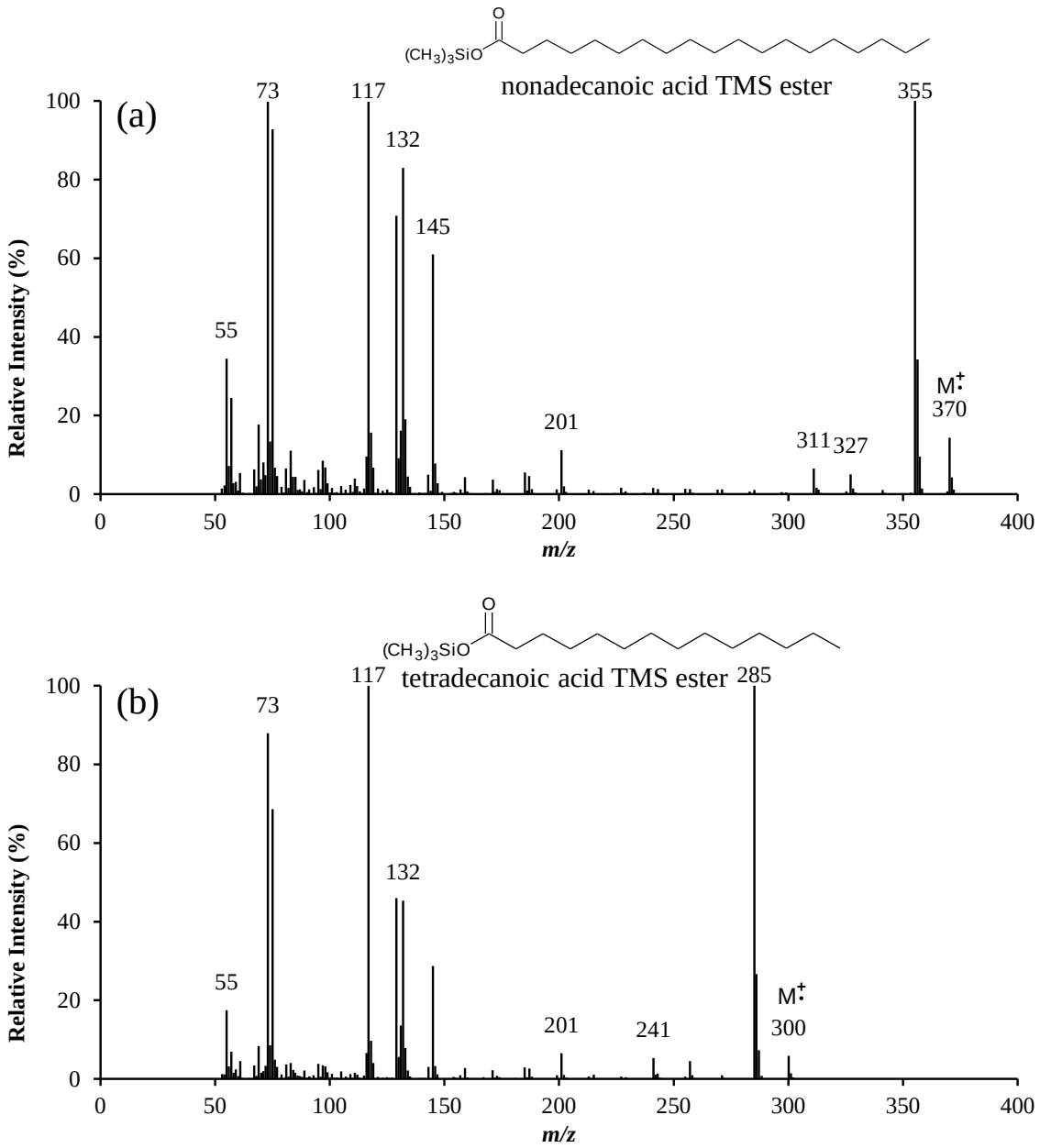

Figure 2.12: Background-subtracted mass spectra and structures of trimethylsilyl (TMS) ester of: (a) nonadecanoic acid (internal standard, $M^{+\bullet}$=*m/z* 370); and (b) tetradecanoic acid ($M^{+\bullet}$=*m/z* 300)

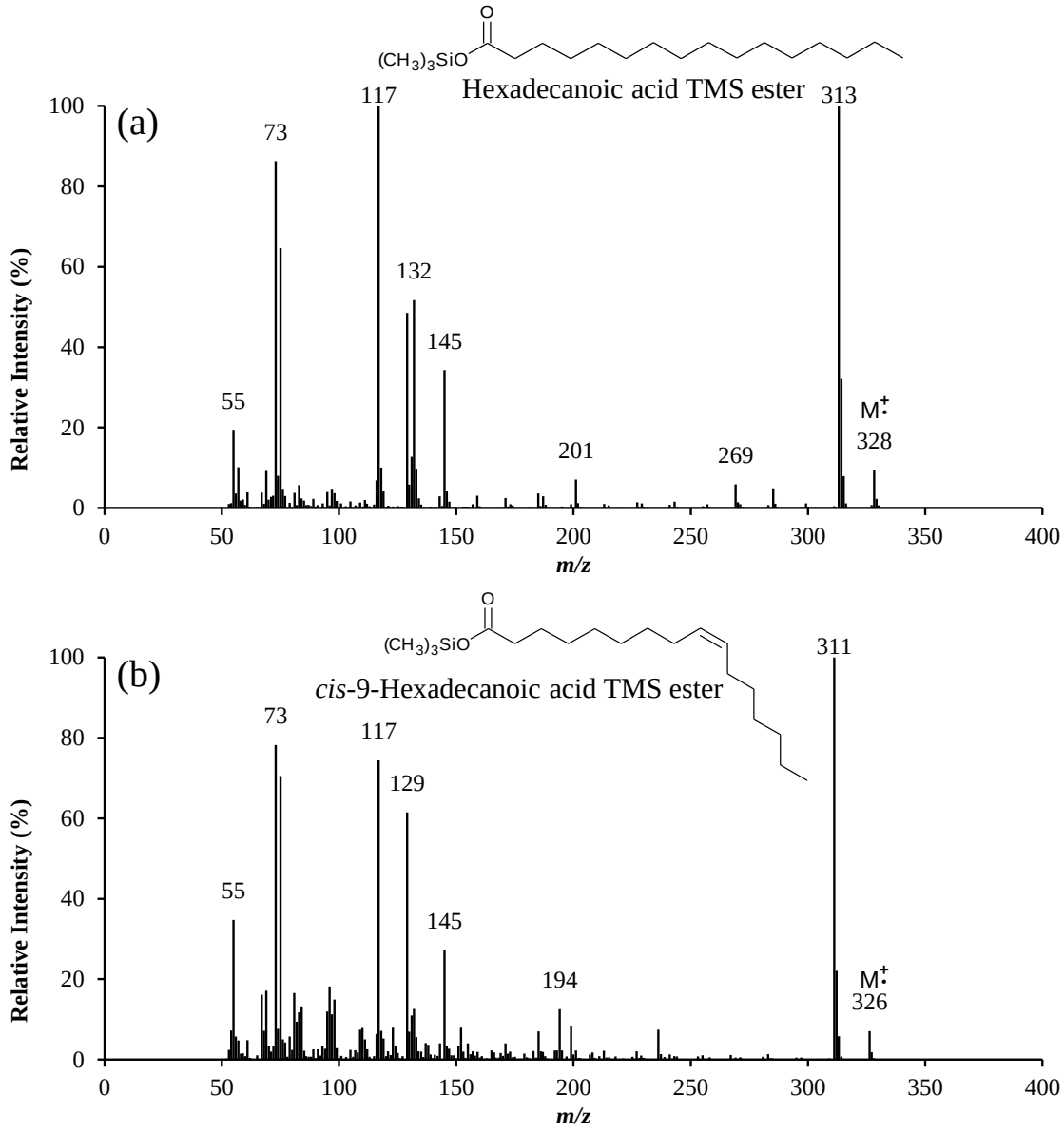

Figure 2.13: Background-subtracted mass spectra and structures of fatty acid trimethylsilyl (TMS) esters described in the current study: (a) hexadecanoic acid ($M^{+\bullet}$=*m/z* 328); and (b) *cis*-9-hexadecanoic acid ($M^{+\bullet}$=*m/z* 326).

Quantification of fatty acids isolated from phytoplankton was achieved by the method described for HBIs in Section 2.11.1, through manual integration (Chemstation, version C.03.00 software) of the common TMS fragmentation ion (*m/z* 117) signal intensities obtained by GC-MS SIM mode.

Factors such as extraction efficiency, volume of water sample filtered and any differences in the relative response factors were accounted for using Equation 2.8.

Equation 2.8:

$$FA\ (\mu g\ mL^{-1}) = \frac{\frac{P_A FA}{P_A IS} * RF}{V\ filtered\ (mL)} *\ m\ IS\ (\mu g)$$

In Equation 2.8, P_A is the peak area of individual fatty acid (*FA*) and internal standard (*IS*) obtained from GC-MS chromatograms. Mass of internal standard added and response factor applied is denoted by *mIS* and *RF*. Additionally volume of filtered water extracted is denoted as (*V filtered*).

The response factor of individual fatty acids was calculated from the calibration curves of fatty acid concentrations (1 µg mL^{-1}, 2 µg mL^{-1}, 4 µg mL^{-1}, 6 µg mL^{-1}, 8 µg mL^{-1} and 1 µg mL^{-1}, $R^2 > 0.98$) against the internal standard (nonadecanoic acid) of equal concentration using the approach described in section 2.11.1.

2.12 Calculation of the PIP_{25} indices

The PIP_{25} indices were calculated using the concentrations of IP_{25} and a biomarker derived from open-water phytoplankton (e.g. brassicasterol), as described by Müller et al. (2011). Where applied, a balance factor (*c*) for each set of samples was calculated by dividing the mean IP_{25} concentration by the mean phytoplankton biomarker concentration. The overall PIP_{25} calculation is shown in Equation 2.9, and the calculation of the balance factor shown in Equation 2.10.

Equation 2.9:

$$PIP_{25} = \frac{IP_{25}}{(IP_{25} + (phytoplankton\ biomarker * c\ ))}$$

Equation 2.10:

$$c = \frac{mean\ IP_{25}}{mean\ phytoplankton\ biomarker}$$

2.13 Stable isotope determinations

Following initial purification (Section 2.7.1), selected hydrocarbon fractions were further purified and isolated into fractions containing individual HBIs of interest (Section 2.7.3). The stable (carbon) isotopic composition ($\delta^{13}C$) of HBIs was then determined using gas chromatography-isotope ratio mass spectrometry (GC-IRMS). All GC-IRMS measurements were performed by Dr Kyle Taylor (Isoprime, UK) using an IsoPrime100 IRMS with GC5 interface and Agilent 7890B GC (Isoprime Ltd, Cheadle Hulme, UK) installed with an Agilent HP-5MS column (30 m×0.2m mm I.D., film thickness 0.25 μm). All samples were dissolved in hexane (10-150 μl) and injected in splitless mode with the following inlet conditions: 250°C, purge flow 25 ml min^{-1}, purge time 0.75 min. GC carrier gas (He) flow rate was 1 mL min^{-1}, oven program as follows: 1 minute hold at 50°C, ramp to 310°C at 10°C min^{-1}, then 13 minute hold. The combustion furnace consisted of a 0.7 mm I.D. quartz tube packed with CuO pellets, held at 850°C. GC-IRMS results were calibrated using the certified Indiana alkane standard mix A5 (Indiana University, Bloomington, IN, USA) and all results reported in delta notation ($\delta^{13}C$) relative to VPDB. IonOS software (Isoprime Ltd) was used to process GC-IRMS data; 'peak mapping' functionality was used to systematically designate specific compound identifications across multiple injections for robust data collation. The A5 alkane mix was analysed between every six sample injections in at least duplicate, with calibrations constructed from at least three interspersed measurements of the A5 mix. Reproducibility of individual alkanes was always ≤ 0.35‰. Root mean standard error (RMSE) of each of the calibrations was usually ≤ 0.25‰, with an overall RMSE for all calibrations combined of ≤ 0.21‰, reflecting both the reliability of each calibration, and the long-term stability of the system. Samples containing HBIs of interest were analysed at least duplicate measurements.

2.14 Microscopy

Identification of certain sea-ice diatom species (Chapter 5) was achieved using scanning electron microscopy (SEM). Preparation of cells for analysis by SEM was carried out by digestion of organic material (HCl; 30 mins; 70^{o}C) followed by washing of frustules (3×4 mL H_2O). Cleaned frustules were then dried onto glass and sputter-coated (Cr) prior to observation (JEOL 7001F SEM). Individual diatom cells for isolation were identified using a Nikon TS2000 inverted light microscope (×10 and 40 objectives) in phase contrast and isolated manually using a modified Pasteur pipette. All of the microscopic analysis of diatom species was carried out by Dr Thomas Brown at Plymouth University.

CHAPTER THREE

3 Results (1): Optimised biomarker-based reconstructions of Arctic sea-ice margins and concentrations in the Barents Sea

3.1 Introduction

Chapter three describes the investigation of diatom specific biomarker lipids, including the Arctic sea-ice proxy IP_{25}, in a suite of surface sediments from the Barents Sea. Specifically, the chapter demonstrates the usefulness of IP_{25}, which, when coupled with a structurally similar tri-unsaturated highly branched isoprenoid (HBI) alkene, that is believed to be produced by open water phytoplankton, can provide more detailed interpretation of sea-ice conditions within longer records. Moreover, a semi-quantitative aspect of this biomarker combined approach (via the so-called PIP_{25} index) is refined, with outcomes used to provide more specific, and quantitative, paleo sea-ice reconstructions within the Barents Sea.

The Barents Sea is one of the key areas for investigating the relationship between sea-ice and global climate, owing to its location at the crossroads of Arctic and Atlantic waters and the sensitivity of sea-ice cover to global warming (IPCC, 2007). The position of the modern winter ice limit in the western Barents Sea is fairly stable; whereas, further southeast it varies significantly on inter-annual and longer term timescales. From a local perspective, previous satellite and observational records have shown a retreat in the position of the overall maximum winter ice edge for the Barents Sea since ca 1870 AD (Divine and Dick, 2006). In the Barents Sea, these records have been further extended (ca 300 yr BP) through analysis of the Arctic sea-ice proxy $IP_{25,}$ in three sediment cores (Vare et al., 2010). Outcomes were in very good agreement with

observational records of sea-ice presence in the region, thus providing further evidence of the high selectivity of this biomarker with respect to the past occurrence of seasonal sea-ice cover.

A remaining question, however, concerns the extent to which the analysis of IP_{25} can provide more detailed or quantitative estimates of paleo sea-ice, especially for this region. In this respect, the parallel measurement of pelagic phytoplankton biomarkers, such as brassicasterol, that might be considered indicators of ice-free sea surface conditions, has been suggested and used to provide construction of sea-ice conditions for the Fram Strait over the last 30 kyr (Müller et al., 2009). This led to the subsequent development of the so-called PIP_{25} index, whereby concentrations of IP_{25} and a phytoplankton biomarker (typically brassicasterol) are combined to provide semi-quantitative estimates of sea-ice concentration (Müller et al., 2011). However, although relationships between PIP_{25} data and sea-ice concentrations are, in general, better than those using IP_{25} alone, this is not always the case (Navarro-Rodriguez et al., 2013) and the underlying reasons for such improved correlations are not fully resolved. Not least due to the uncertainties in the true inter-relationship between IP_{25} and phytoplankton lipids under different sea-ice settings, or the strict pelagic origin of brassicasterol in all cases (e.g. Belt et al., 2013; Fahl and Stein, 2012; Xiao et al., 2015). An alternative approach may be better focussed on improving our understanding of different sea-ice *conditions* (e.g. seasonal ice, drift ice) rather than sea-ice *concentrations*, especially if biological processes, and signatures of these, are particularly characteristic of the former. Indeed, establishing parameters such as the winter/summer ice margins or sea-ice seasonality are especially important since they are used as boundary parameters in climate forecasting and hindcasting models. In this respect, PIP_{25} data have also been interpreted in terms of categorisation of sea-ice conditions (Müller et al., 2011), although further caveats also exist. Amongst those identified (Belt and Müller, 2013),

the variable sources of brassicasterol and the potential lack of sensitivity of its production to individual environmental settings make reconstruction of different sea-ice conditions rather challenging, for certain regions at least.

The main aim of the current study, therefore, was to conduct analysis of IP_{25} and a different phytoplankton-derived HBI biomarker (HBI triene IIIa, Figure 3.1) that, like IP_{25}, has a well-defined or constrained source, whose production is more closely aligned with certain pelagic (or sea-ice) conditions, and has sedimentary concentrations closer to those of IP_{25} (compared to brassicasterol), thus potentially removing the need to employ a balance factor when calculating PIP_{25} indices. This tri-unsaturated HBI (HBI triene IIIa) has been hypothesised to represent a potential proxy for the pelagic environment adjacent to retreating sea-ice or the marginal ice zone (MIZ) in the Antarctic (Collins et al., 2013), a hypothesis based on the similarities in temporal profiles within Scotia Sea sediments, of HBI triene IIIa and a di-unsaturated HBI (HBI diene II), considered to be a sea-ice proxy in the Antarctic (Massé et al., 2011). However, the analyses of surface sediments or phytoplankton from such locations to support this hypothesis further have not, as yet, been presented.

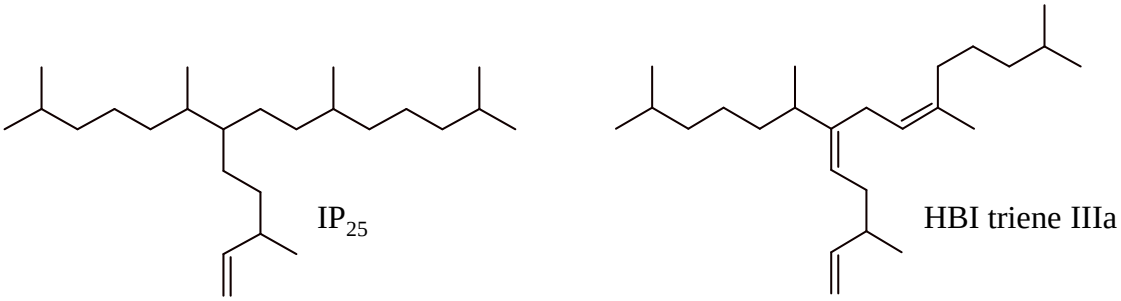

Figure 3.1: Chemical structures of HBI biomarker lipids IP_{25} and HBI triene IIIa.

The specific aims of the biomarker analysis were: 1) to investigate the sensitivity of sedimentary IP_{25} and HBI triene IIIa to the overlying sea-ice conditions; 2) to investigate the potential to make determinations of sea-ice extent more quantitative by

comparing biomarker-derived PIP_{25} data with satellite derived sea-ice concentrations and 3) to refine interpretations of previously published biomarker records to provide more detailed descriptions of sea-ice conditions.

In order to achieve these aims, the analysis of the biomarker lipids IP_{25}, HBI triene IIIa and brassicasterol in surface sediment material from locations across the Barents Sea was performed. The Barents Sea was selected as a study region because it has a reasonably well-defined annual sea-ice advance/retreat cycle, and also since complementary observational and proxy data were available. In addition, Vare et al. (2010) demonstrated that abundances of IP_{25} in dated short cores from the region aligned well with observational sea-ice records covering the last few hundred years. Further, biomarker data from three down-core records located within the study area were re-examined to provide more detailed information regarding paleo sea-ice conditions in the Barents Sea over the last ca 12 kyr BP.

3.2 Regional settings

The Barents Sea is a relatively shallow (mean depth 230 m) epicontinental shelf between the north Norwegian coast and the Svalbard archipelago that plays a crucial role in the Arctic climate system, largely, since it contributes to significant heat exchange between the ocean and the atmosphere (Serreze et al., 2007). Detailed descriptions of the main surface currents in the Barents Sea (and the adjacent northern Norwegian Sea) can be found elsewhere (Loeng, 1991) and a summary is shown in Figure 3.2a.

In brief, the North Atlantic Current (NAC) delivers relatively warm salty Atlantic water (> 2°C; > 35‰; (Hopkins, 1991)) into the northern North Atlantic (Swift, 1986) before

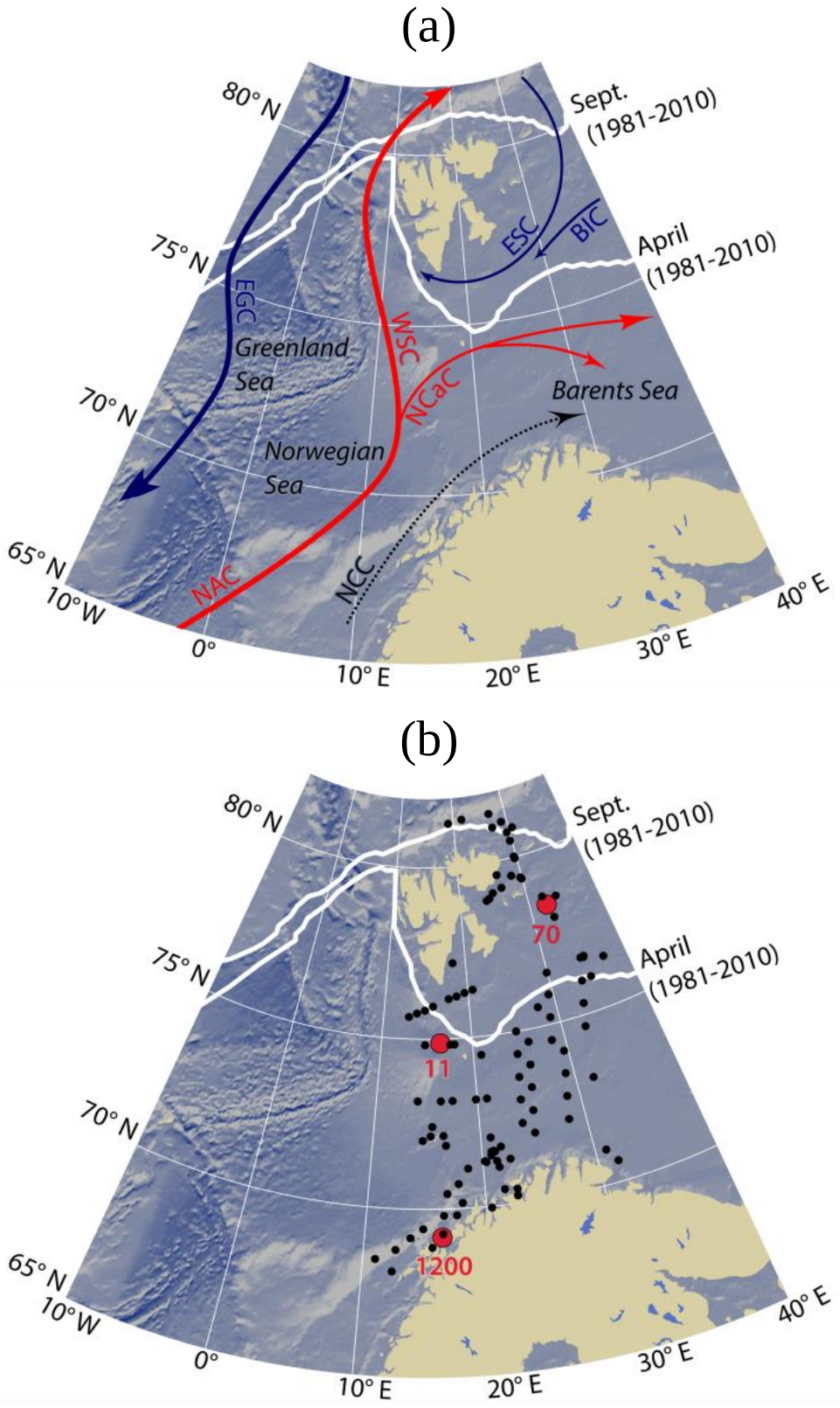

Figure 3.2: (a) Major surface currents of the study region. Red: North Atlantic Current (NAC), West Spitsbergen Current (WSC) and North Cape Current (NCaC). Blue: East Spitsbergen Current (ESC), East Greenland Current (EGC) and Bear Island Current (BIC). Black: Norwegian Coastal Current (NCC). (b) Sampling locations: surface sediments are indicated by black circles, and long cores by red circles. The positions of median April and September sea-ice extent (1981-2010; NSIDC, Fetterer et al., 2002) are also indicated.

dividing into the West Spitsbergen Current (WSC) and the North Cape Current (NCaC) which provide inflow to the Arctic Ocean and the Barents Sea, respectively, with a further branch of the NCaC flowing parallel with the coastal current system (Loeng, 1991). In contrast, colder and less saline Polar water (0-2°C; 33-34.4‰; (Hopkins, 1991)) is brought into the Atlantic Ocean from the Arctic Ocean by the East Greenland Current (EGC) and into the Barents Sea by the East Spitsbergen Current (ESC) and Bear Island Current (BIC). Polar and Atlantic water meet in the Barents Sea to form Arctic water (ca 0.5°C; ca 34.8‰; (Hopkins, 1991)), which is characterised by reduced temperature and salinity, as well as the occurrence of seasonal sea-ice (Hopkins, 1991). Warm and fresh coastal water (2-13°C, 32-35‰; (Hopkins, 1991)) is found on the shelves and off the coast of Norway and is transported northwards by the Norwegian Coastal Current (NCC) into the South-West Barents Sea and along the Norwegian and Russian coastline (Aure and Strand, 2001).

Of particular significance to this region, the boundaries between Polar/Arctic and Arctic/Atlantic waters correspond to the Polar Front and Arctic Front, respectively, both of which represent a sharp climatic gradient in terms of temperature, salinity and sea-ice coverage (Hopkins, 1991). The overall extent of sea-ice distribution in the northern North Atlantic and the Barents Sea, therefore, is closely related to the positions of the Polar and Arctic Fronts, which represent the average summer and winter sea-ice margins, respectively (Vinje, 1975). Consequently, sea-ice is formed during autumn and winter in the north-eastern Barents Sea (Loeng, 1991), while the southern Barents Sea is characterized by large seasonal and inter-annual sea-ice distribution changes, largely due to the strong (and variable) influence of inflowing Atlantic Water (AW) (Kvingedal, 2005). Such changes in sea-ice can be readily seen by the locations of the maximum, minimum and median April sea-ice extent for the period 1980-2015 derived from satellite data (NSIDC; Figure. 3.2b). A significant contribution to the annual

primary production in the Barents Sea results from a peak algal bloom during the spring as ice retreats along the ice edge or MIZ (Sakshaug et al., 2009).

3.3 Material and methods

3.3.1 Surface sediment material

Surface sediment samples (0-1 cm), were collected from a broad range of locations within the Barents Sea (Figure 3.2b) using box cores, multicores and gravity cores and were provided by Dr Jochen Knies (Geological Survey of Norway) and Professor Rüdiger Stein (Alfred Wegener Institute, Germany). Sediment material analysed in this study (n=49), was collected on-board the *James Clark Ross* (UK) and the *Polarstern* (Germany) research vessels during oceanographic cruises JR142 and ARK-VIII/2 in 2006 and 1991, respectively, with additional samples provided from the MAREANO program (2005-2010) (Knies and Martinez, 2009).

These data have been further supplemented with locations (n=53) where concentrations of IP_{25}, HBI triene IIIa and brassicasterol in surface sediments from the Barents Sea have previously been reported (Navarro-Rodriguez et al., 2013; Navarro-Rodríguez, 2014).

The dataset presented here (n=102) has been confined to the locations for which at least IP_{25} and HBI triene IIIa concentrations data were determined and all three biomarkers for the majority of locations. Exceptionally, brassicasterol was not measured previously in a small number of surface sediments from NW Norway, as the primary focus at the time was concentrated around HBIs only, and no extract fractions containing sterols was collected for these samples.

A detailed description of sediment material supplemented for this study is provided elsewhere (Navarro-Rodriguez et al., 2013) and a summary of all core locations and biomarker data can be found in Section 3.4, Table 3.1.

3.3.2 Biomarker analyses

Extraction and analysis of HBI and sterol lipids described in this chapter has followed the general scheme outlined in Figure 3.3. For a detailed description of individual steps (e.g. extraction, purification techniques) undertaken, the reader is referred to Chapter 2.

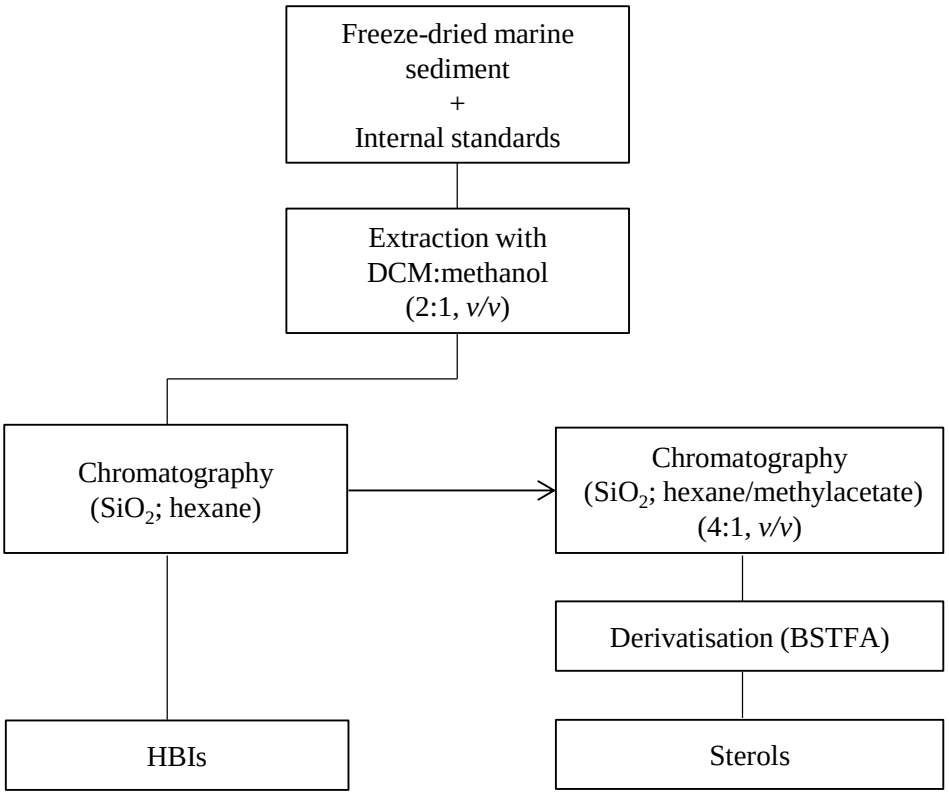

Figure 3.3: Flow diagram showing individual steps of biomarker analysis in marine sediments described in the study.

Briefly, ca 1-5 g of freeze dried and homogenised sediment material was extracted (DCM/MeOH; 3×3 mL; 2:1, *v/v*) by ultra-sonication following addition of internal standards (9-octylheptadec-8-ene (10 µL; 1 µg mL^{-1}) and 5α-androstan-3β-ol (10 µL;

1 µg mL^{-1}) for the quantification of HBI lipids and brassicasterol, respectively. Where necessary, elemental sulfur was removed from the resulting total organic extracts (TOEs) and these partially purified TOEs were then separated into fractions containing HBIs and sterols as described previously (Chapter 2, Section 2.7). Fractions containing brassicasterol were derivatized using *N*,*O*-bis(trimethylsilyl)trifluoroacetamide (BSTFA, 50 µL, 70°C; 1h). All fractions were analyzed by gas chromatography-mass spectrometry (GC-MS) with operating conditions as described in Chapter 2, Section 2.9.

Two-tailed *t*-tests were performed and interpreted (95% confidence limits) for statistical analyses, using Minitab17 Statistical Software (Version, Minitab®17.2.1)

3.3.3 Sea-ice data

In order to place the biomarker data into a spatial and recent temporal sea-ice context, estimates of sea-ice extent were obtained using polyline shapefiles derived from satellite data collected for the period 1981-2010 (National Snow and Ice Data Center; NSIDC). From these, the individual years of (overall) maximum and minimum extent for April (winter maximum), and the median positions of the maximum (April) and minimum (September) ice edge were identified (Figure 3.4b). This interval is suitable for contextualising surface (typically 0-1 cm) sediment data since accumulation rates in the region are generally of the order of 1 cm yr^{-1} (Maiti et al., 2010; Vare et al., 2010).

Estimates of mean spring (April-June) and summer (July-September) sea-ice concentrations (hereafter referred to as SpSIC and SuSIC, respectively) for the sampling region, used in the calibration of PIP_{25} indices, were obtained from Nimbus-7 SMMR and DMSP SSM/I-SSMIS passive microwave data for the period 1988-2007 (NSIDC). These data were selected, partly, because quantitative sea-ice data from this interval have been used in the most detailed PIP_{25}-based calibrations to date (Xiao et al., 2015)

and also since a 20-year interval reflects typical accumulation rates for the Barents Sea (Maiti et al., 2010; Vare et al., 2010). Further, Navarro-Rodriguez et al. (2013) stated that satellite-derived mean sea-ice concentration data are reasonably consistent between datasets covering recent decades, irrespective of their exact timeframe. Finally, although the position of the maximum winter ice edge in the Barents Sea has undergone a northerly retreat over the last ca 150 years (Divine and Dick, 2006), all of the sampling locations (n=45) selected for calibration of PIP_{25} indices, fall within a consistently spring ice-covered region during this time interval (Figure 3.4a), while the excluded sites have been ice-free (Figure 3.2b).

3.3.4 PIP_{25} indicex

The PIP_{25} indicex was calculated according to Equations 2.9 and 2.10 (Chapter 2), using HBI triene IIIa ($P_{IIIa}IP_{25}$) and brassicasterol (P_BIP_{25}) as the phytoplankton biomarkers. Additional P_BIP_{25} values were calculated using a global *c* factor (*c*=0.023), derived from analysis of data from a large number of surface sediment samples from different Arctic and sub-Arctic regions (Xiao et al., 2015). PIP_{25} values, using both phytoplankton biomarkers, were also calculated with exclusion of the *c* factor (i.e. *c*=1).

Only sedimentary biomarker data from locations that experience sea-ice cover at least part of the year (Figure 3.2b), were used. This corresponds to a region generally north of the position of maximum (spring) sea-ice extent (Figure 3.4a). Biomarker data available from ice-free locations were not included in the analysis here, in part, since the primary aim was to investigate the potential for different PIP_{25} indices to provide semi-quantitative estimates of sea-ice concentration (specifically, sea-ice concentration > 0%).

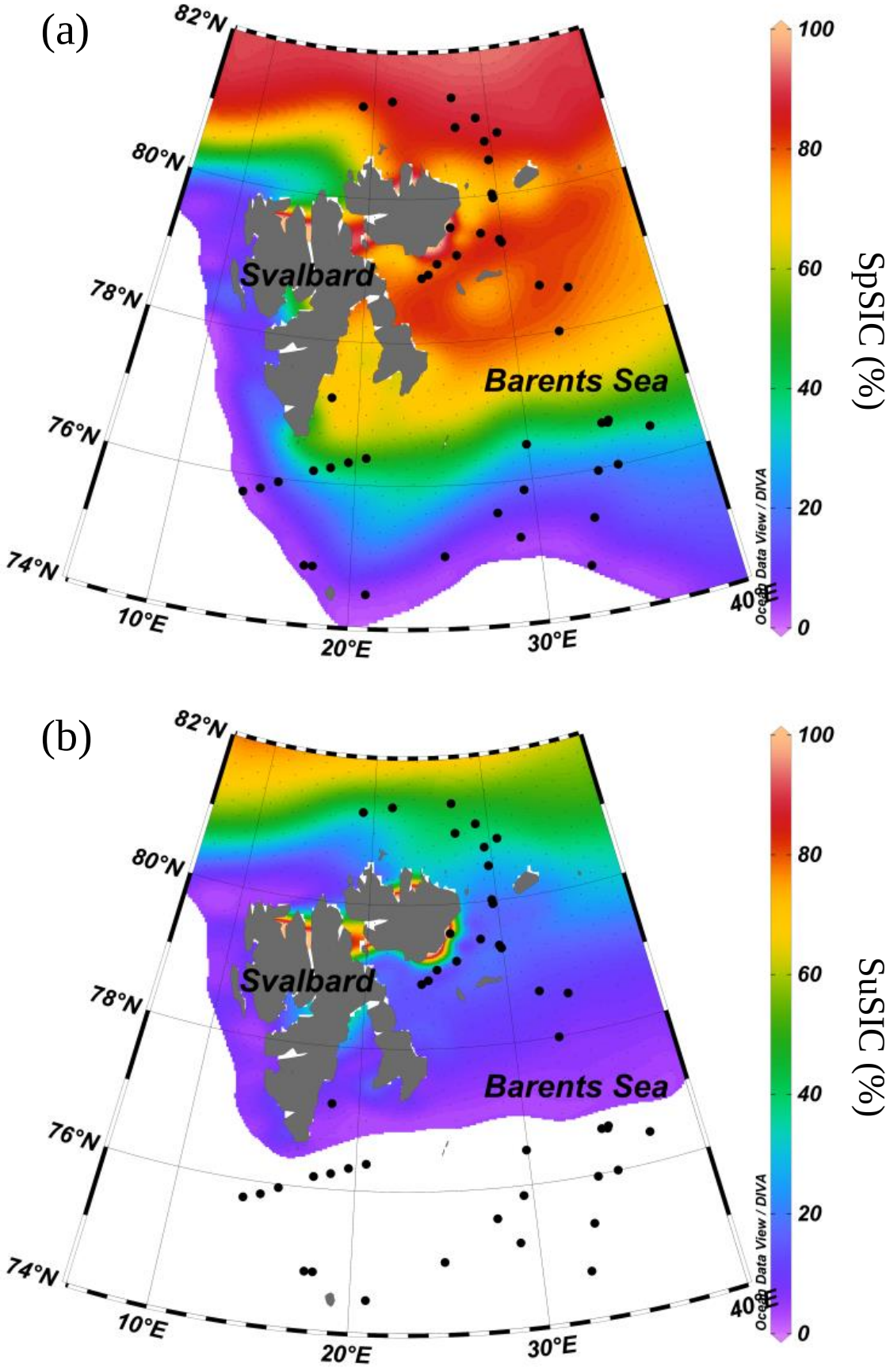

Figure 3.4: (a) Mean spring (April-June) sea-ice concentration (SpSIC) and (b) mean summer (July-September) sea-ice concentration (SuSIC) for the period 1988-2007 in study region used to evaluate PIP_{25} approach. Locations of surface sediments used for this study are indicated by black dots.

Furthermore, zero values for both PIP_{25} and sea-ice concentration for such regions would adversely skew the linear correlations between these two parameters for ice covered settings. Finally, since a zero value for PIP_{25} can only be obtained from the absence of IP_{25}, in any case, no additional information regarding sea-ice concentration is gained from this combined approach compared to measurement of IP_{25} alone. As such, the analysis presented here represents a regional calibration, as defined by locations experiencing sea-ice occurrence for at least part of the year (i.e. spring sea-ice concentration > 0%).

3.3.5 Down-core sediment material

To apply the findings from the surface sediment analysis to obtain more refined paleo reconstructions of sea-ice conditions in the Barents Sea, re-examination of previously published biomarker data from three sediment cores experiencing contrasting modern sea-ice conditions was also performed. More detailed descriptions of these sediment cores (70, 11 and 1200, Figure 3.2b), including core chronologies, can be found in more detail elsewhere. Briefly, core JM99-1200 (1200, Figure 3.2b) was collected from the Andfjorden, northern Norway (69.16˚ N, 16.25˚ E) and is described in Ebbesen and Hald (2004), Knies (2005) and Cabedo-Sanz et al. (2013). Core NP05-11-70GC (70, Figure 3.2b) was retrieved from the Olga Basin, northern Barents Sea (78.40° N, 32.42°E) and has been described previously by Berben (2014). Finally, core JM09-KA11-GC (11, Figure 3.2b) was collected from the Kveithola Trough, western Barents Sea (74.87° N; 16.48° E), and more details can be found in Rüther et al. (2012) and Berben et al. (2014). The age model for JM09-KA11-GC used in Berben et al. (2014) has been supplemented using a further ^{14}C date (ca 13.12 cal. kyr BP; Rüther et al. (2012) in order for the biomarker record to be extended to cover the Younger Dryas

(YD). Hereafter, cores JM99-1200, NP05-11-70GC and JM09-KA11-GC are referred to as 1200, 70 and 11, respectively.

3.4 Results and discussion

3.4.1 IP_{25} and HBI triene IIIa biomarkers in surface sediments- characterisation of the winter ice edge and the marginal ice zone (MIZ)

In total, 102 surface sediment samples were analysed for IP_{25} and HBI triene IIIa. Of these, 75 were also analysed for brassicasterol. Consistent with previous findings, the sea-ice biomarker IP_{25} was identified in 44 out of 45 (98%) extracts obtained from seasonally ice-covered locations (Figure. 3.5a). Exceptionally, IP_{25} was also identified in a few sediments (7 out of 57; 13%) from locations south of the maximum winter sea-ice extent and this has been attributed, previously, to some likely allochthonous input or sediment advection from locations further up the slope rather than local (autochthonous) production (Navarro-Rodriguez et al., 2013). Further, IP_{25} concentrations for locations further north of the median April sea-ice edge, with ice also persisting past June (1.1-12.4 ng g^{-1}, n=22), with mean concentration of 5.5±3.3 ng g^{-1}, were significantly higher (p=0.01) than for locations proximal to the winter sea-ice edge (0-9.8 ng g^{-1}, n=23) with a mean IP_{25} concentration of 3.1±2.5 ng g^{-1}. These findings are indicative of enhanced IP_{25} production (and subsequent deposition) for areas experiencing longer seasonal sea-ice cover, with melt only occurring during the late summer. In contrast, lower sedimentary IP_{25} abundances were found for locations that do not always experience sea-ice cover on an annual basis and where spring-summer ice retreat occurs earlier (e.g. May-June). Consistent with this difference, IP_{25} was normally absent (or

below the limit of detection) for the majority of locations to the south of maximum winter sea-ice margin.

Some quite different trends are apparent from the HBI triene IIIa data, however. For example, in contrast to IP_{25}, HBI triene IIIa was present in virtually all (101 out of 102; 99%) of the sediment extracts, consistent with a pelagic phytoplanktic origin for this biomarker rather than sea-ice diatoms. Indeed, HBI triene IIIa has, to date, not been identified in Arctic sea-ice. Concentrations of HBI triene IIIa were relatively low (0.1-1.6 ng g^{-1}; mean=0.40±0.38 ng g^{-1}, Figure 3.5b) for region that experience annual and extensive sea-ice cover, which contrasts the enhanced IP_{25} abundances for the same locations (Figure 3.5a), likely as a consequence of shorter (and cooler) summer seasons with lower phytoplankton productivity (Sakshaug et al., 2009). A somewhat higher mean HBI triene IIIa concentration of 1.7±1.6 ng g^{-1} (0-8.1 ng g^{-1}, n=57) was found for ice-free locations in the southern area (and warmer) of sampling, consistent with increased productivity in this region (Sakshaug et al., 2009). When compared against both of these two regions, however, a significantly higher ($p < 0.001$) mean HBI triene IIIa concentration of 13.0±8.3 ng g^{-1} (1.2-28.7 ng g^{-1}; n=23) was observed for locations bordered by the minimum (2006) and maximum (1981) April ice margins (Figure 3.5b). The enhancement of HBI triene IIIa in this MIZ, especially relative to locations further north, represents a clear reversal in trend compared to IP_{25}, and suggests increased production during late spring/early summer, which is reduced for regions with longer lasting sea-ice cover. However, it is also evident that the mean HBI triene IIIa concentration (13.0 ng g^{-1}) for this region of retreating ice edge is substantially (ca7-8 times) higher than for the annually ice-free locations (1.7 ng g^{-1}), and is thus indicative of the well-known enhanced phytoplankton production within the MIZ as sea-ice retreats during late spring (April-May) and into early summer (June) (Sakshaug et al., 2009).

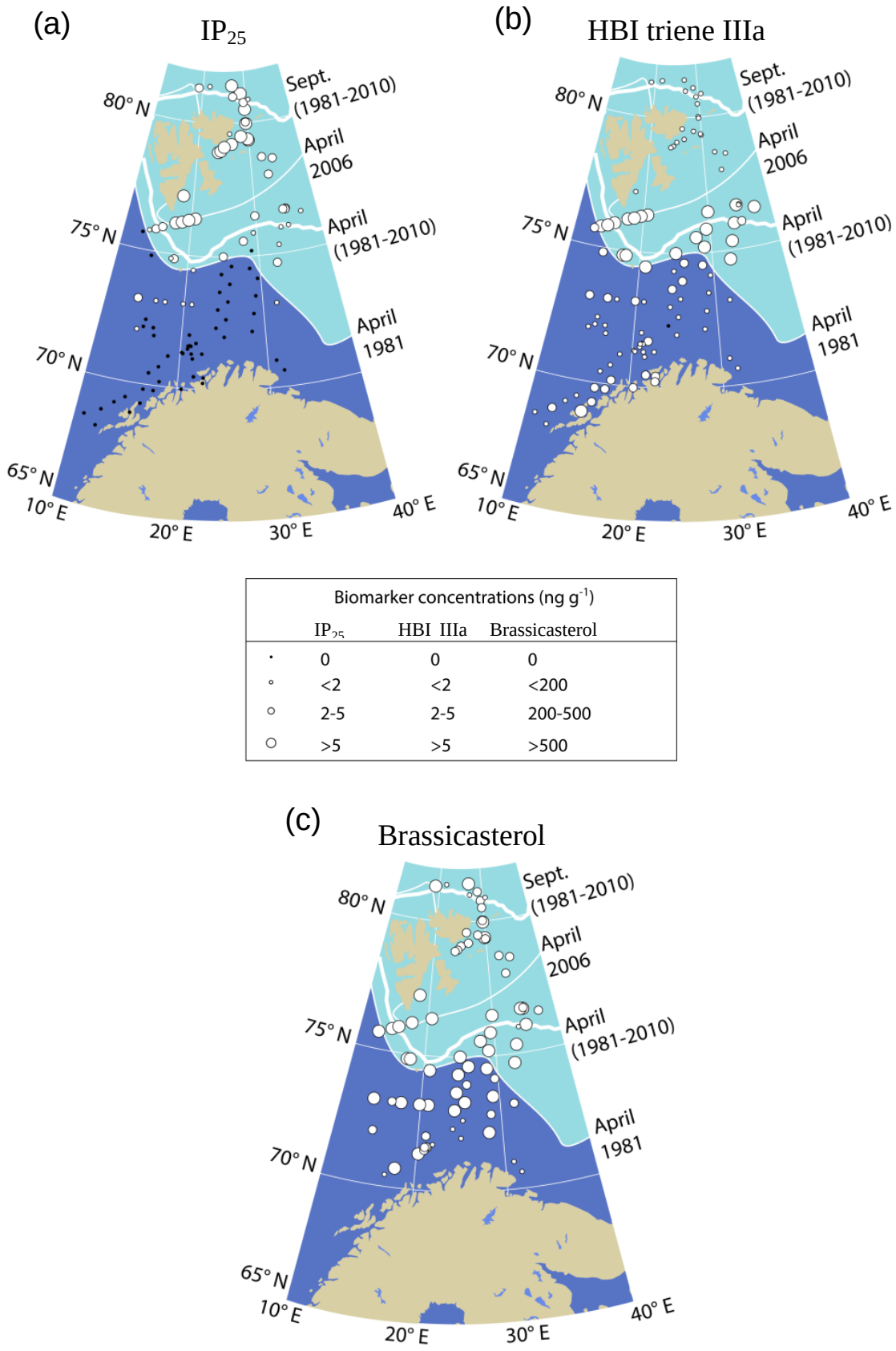

Figure 3.5: Surface sediment concentrations of: (a) IP_{25}; (b) HBI triene IIIa; and (c) brassicasterol. The positions of median April and September sea-ice extent (1981-2010; NSIDC, Fetterer et at., 2002), together with the maximum (1981) and minimum (2006) April sea-ice extent, are also indicated. Biomarker distribution maps were produced by means of QGis 2.14.2 (Essen) software.

Table 3.1: Details of sampling locations and associated biomarker data. (Note: Samples representing locations within the regions of extended sea-ice cover (i.e. north of the median April sea-ice edge) and proximal to the winter sea-ice edge (Figure 3.5) are indicated in bold and italic, respectively. All other samples are in normal text).

Station	Water Depth (m)	Lat.	Long.	IP_{25} (ng g^{-1})	HBI triene IIIa (ng g^{-1})	Brassicasterol (ng g^{-1})
JR142-GC12	**813**	**81.39**	**26.94**	**5.78**	**1.56**	**624**
JR142-GC13	**532**	**81.35**	**21.63**	**1.10**	**0.16**	**102**
JR142-GC19	**550**	**81.26**	**19.02**	**4.86**	**1.30**	**540**
JR142-GC11	**359**	**81.08**	**28.93**	**5.74**	**0.43**	**312**
PS2131-1	**106**	**80.98**	**27.10**	**2.43**	**0.13**	**117**
PS2142-3	**116**	**80.85**	**30.64**	**1.77**	**0.08**	**135**
PS2144-3	**505**	**80.75**	**29.47**	**2.20**	**0.16**	**228**
JR142-GC10	**443**	**80.49**	**29.65**	**8.15**	**0.66**	**300**
PS2148-1	**339**	**80.01**	**29.60**	**2.77**	**0.13**	**293**
JR142-GC9	**317**	**79.96**	**29.65**	**7.46**	**0.42**	**672**
JR142-GC20	**144**	**79.59**	**26.19**	**1.64**	**0.08**	**241**
JR142-GC8	**344**	**79.49**	**28.44**	**7.02**	**0.25**	**479**
JR142-GC23	**306**	**79.38**	**29.77**	**7.98**	**0.30**	**627**
JR142-GC22	**302**	**79.33**	**29.90**	**7.78**	**0.36**	**376**
JR142-GC7	**259**	**79.21**	**26.54**	**7.75**	**0.32**	**410**
JR142-GC6	**223**	**79.10**	**25.10**	**7.21**	**0.35**	**333**
JR142-GC5	**205**	**78.95**	**24.45**	**8.77**	**0.35**	**380**
JR142-GC4	**178**	**78.90**	**23.98**	**12.36**	**0.70**	**424**
PS2150-1	**283**	**78.67**	**32.13**	**2.79**	**0.10**	**271**
JR142-GC21	**212**	**78.57**	**34.06**	**2.28**	**0.59**	**231**
PS2151-1	**143**	**77.99**	**32.94**	**2.31**	**0.20**	**441**
PS2115-1	**101**	**77.20**	**18.33**	**11.34**	**0.15**	**710**
PS2111-2	*218*	*76.64*	*34.88*	*3.08*	*1.27*	*490*
679	*193*	*76.62*	*34.45*	*3.46*	*9.65*	*1818*
PS2153-1	*187*	*76.61*	*34.81*	*3.07*	*1.23*	*879*
643	*291*	*76.49*	*29.91*	*3.81*	*6.50*	*717*
681	*249*	*76.43*	*37.17*	*1.35*	*11.69*	*253*
St32	*228*	*76.38*	*20.58*	*9.84*	*10.99*	*4763*
St31	*258*	*76.31*	*19.57*	*6.92*	*9.32*	-
St30	*257*	*76.22*	*18.58*	*6.50*	*9.38*	-
St29	*309*	*76.16*	*17.62*	*7.39*	*13.85*	*3389*
PS2113-1	*260*	*76.00*	*34.90*	*0.32*	*2.13*	*519*
677	*276*	*75.97*	*33.73*	*1.34*	*8.79*	*131*
St27	*369*	*75.95*	*15.72*	*4.12*	*6.73*	*1320*
645	*296*	*75.86*	*29.46*	*1.54*	*17.60*	*689*
St26	*370*	*75.83*	*14.77*	*3.98*	*9.79*	*1295*
St25	*807*	*75.75*	*13.84*	*1.39*	*5.79*	-
St24	1500	75.64	12.92	0	4.00	1373
639	*263*	*75.57*	*27.90*	*2.47*	*27.13*	*1959*
675	*209*	*75.33*	*33.07*	*1.27*	*15.61*	*1484*
647	*343*	*75.20*	*29.01*	*0*	*22.66*	*1332*
635	*182*	*75.00*	*24.94*	*4.17*	*28.67*	*1878*
1241	*297*	*74.82*	*17.58*	*1.28*	*29.71*	*1919*
St20	*296*	*74.82*	*18.02*	*2.17*	*12.02*	*3452*
St23	1507	74.82	14.79	0	3.28	-
673	*165*	*74.67*	*32.49*	*2.82*	*19.07*	*520*
651	317	74.64	26.08	0	3.33	1005
649	394	74.54	28.58	0	3.54	803
1239	*178*	*74.46*	*20.83*	*0.51*	*17.70*	*575*
633	*373*	*74.34*	*24.69*	*0*	*1.89*	*709*
671	*366*	*74.15*	*29.55*	*0*	*0.82*	*403*
653	*441*	*73.97*	*25.81*	*0*	*2.42*	*366*
631	*451*	*73.67*	*24.47*	*0*	*2.02*	*658*

Table 3.1: continued

Station	Water Depth (m)	Lat.	Long.	IP_{25} (ng g^{-1})	HBI triene IIIa (ng g^{-1})	Brassicasterol (ng g^{-1})
669	414	73.50	29.15	0	1.92	512
655	412	73.31	25.54	0	0.42	635
PS2149-1	77	73.18	31.73	1.08	0.03	219
St14	675	73.17	16.38	1.74	4.98	461
St12	1030	73.17	14.09	2.35	2.23	520
St15	460	73.17	17.54	1.94	0.18	554
St18	463	73.17	20.95	0.56	1.55	842
St17	441	73.17	19.86	1.84	4.26	1286
629	04	73.01	24.25	0	0.56	540
667	305	72.84	28.76	0	0.31	339
657	268	72.64	25.27	0	0.30	184
R367 MC 026	610	72.42	15.50	0	0.85	-
627	264	72.32	24.06	0	0	121
665	289	72.17	28.41	0	0.47	7092
R421 MC 033	385	72.15	16.55	0	0.40	-
R405 MC 031	901	72.14	15.35	0	1.09	-
St02	371	72.02	20.92	0	1.20	475
St09	1317	72.01	14.62	1.14	1.27	244
659	256	71.98	25.06	0	0.31	108
R431 MC 035	357	71.86	16.75	0	0.61	-
625	360	71.72	21.76	0	3.97	13
St35	319	71.62	21.07	0	0.54	245
St37	335	71.60	21.19	0	0.70	211
St36	320	71.60	20.86	0	1.04	439
St38	310	71.49	20.82	0	0.90	407
St39	234	71.34	20.19	0	0.30	764
R4 MC 107	433	71.33	22.49	0	0.60	-
R18 MC98	319	71.31	21.28	0	0.11	-
R87 MC 006	240	71.31	20.32	0	0.33	-
R81 MC 002	262	71.16	18.65	0	0.32	-
R7 MC 89	355	71.13	21.44	0	0.69	-
690	283	71.02	30.96	0	0.23	38
St43	273	70.72	17.75	0	1.98	1253
692	252	70.62	31.72	0	0.12	29
R1 MC85	466	70.46	21.68	0	2.67	-
St45	1500	70.44	16.75	0	0.92	89
R35 MC 118	480	70.43	22.75	0	2.44	-
R35 MC 114	474	70.23	22.71	0	3.17	-
R100 MC 010	324	70.16	18.02	0	2.05	-
R77 MC 001	287	69.96	20.44	0	3.57	-
R209 MC 003	1592	69.80	16.42	0	2.78	-
R111 MC 004	365	69.80	17.50	0	2.82	-
R232 MC 009	1409	69.41	14.70	0	1.50	-
R223 MC 006	482	69.26	16.33	0	3.08	-
R229 MC 007	1107	69.14	13.68	0	1.54	-
R178 MC 010	125	68.86	15.44	0	8.09	-
R248 MC 010	1304	68.78	12.53	0	2.14	-
R276 BX 049	1315	68.48	10.97	0	0.48	-
R280 BMC 018	228	68.14	12.31	0	0.86	-

In order to assess whether the trends observed for HBI triene IIIa could be identified through other pelagic productivity indicators, the distribution pattern for the phytoplankton marker brassicasterol was also considered (Figure 3.5c). In accord with the trends identified for HBI triene IIIa, the mean brassicasterol concentration was lowest for the region with most persistent sea-ice cover (375±177 ng g^{-1}), slightly higher for ice-free settings (695±1200 ng g^{-1}), and highest for locations within the MIZ (1470±1200 ng g^{-1}). However, the relative changes between the three regions were clearly greater for HBI triene IIIa than for brassicasterol. Most noticeably, the enhancement of HBI triene IIIa between the MIZ and the region with more extended seasonal ice cover (×32.5) was more than eight times that of brassicasterol (×3.9), probably because the latter is a common component in marine phytoplankton and its distribution pattern reflects productivity spanning all growth seasons, while the former is likely biosynthesised by a much smaller number of sources, but whose growth is especially favoured by, or at least more tolerant to, the nutrient-rich and stratified upper water column found at the ice-edge. The differences in distribution of brassicasterol between regions may be further complicated or blurred by production of this sterol in certain sea-ice diatoms (e.g. Belt et al., 2013) and other sources (Volkman, 1986), especially for locations that may receive contributions from terrestrial sources (Fahl and Stein, 2012; Huang and Meinschein, 1979; Volkman, 1986; Xiao et al., 2015). In contrast, although the sources of HBI triene IIIa in the study region have not been firmly identified, its only known source are marine diatoms within the genera *Pleurosigma* (Belt et al., 2000b) and *Rhizosolenia* (Rowland et al., 2001). Further, when measured in Arctic marine sediments, HBI triene IIIa has a stable isotopic composition ($\delta^{13}C$ ca -35 to -40‰; Belt et al., 2008) consistent with a polar phytoplanktic origin (Massé et al., 2011) where cold and CO_2-enriched waters can result in highly depleted $\delta^{13}C$ organic matter (Tolosa et al., 2013).

A summary of mean biomarker concentrations, as well as ranges observed for each biomarker for individual regions described in the text (i.e. seasonal ice zone (SIZ); marginal ice zone (MIZ) and ice-free zone) are also summarised in Table 3.2.

Table 3.2: Summary of the mean (±1 standard deviation) and range of IP_{25}, HBI triene IIIa and brassicasterol concentrations in individual zones as described in text. All values are in ng g^{-1} of dry sediment.

	Seasonal Ice Zone (SIZ)	Marginal Ice Zone (MIZ)	Ice-free
IP_{25}	**5.5±**3.3 (n=22)	**3.1±**2.5 (n=23)	**0.2±**0.5 (n=57)
range	(1.1-12.4)	(0-9.8)	(0-2.35)
HBI triene IIIa	**0.40±**0.38 (n=22)	**13.0±**8.3 (n=23)	**1.7±**1.6 (n=57)
range	(0.1-1.4)	(1.2-29.7)	(0-8.1)
Brassicasterol	**375±**177 (n=22)	**1470±**1200 (n=20)	**695±**1200 (n=33)
range	(102-710)	(131-4760)	(13-7100)

3.4.2 Semi-quantitative estimates of paleo Arctic sea-ice concentrations in the Barents Sea; PIP_{25}

In Section 3.4.1 it was shown that concentrations of IP_{25} and HBI triene IIIa in surface sediments from seasonally ice-covered locations in the Barents Sea were strongly inversely correlated, with higher abundances of IP_{25} for regions of extended seasonal sea-ice cover, and enhanced HBI triene IIIa for locations proximal to the winter ice-edge or within the marginal ice zone (MIZ). As such, the respective responses of IP_{25} and HBI triene IIIa aligned particularly well with the original gradient model of biomarker production proposed by Müller et al. (2011) (Figure 3.6) that underpins the ratio-based format of the PIP_{25} index. Therefore, biomarker data from some of the Barents Sea surface sediments presented here were re-examined and their individual and combined (PIP_{25}) relationships to spring and summer sea-ice concentration investigated. All the analytical data used for this part of the study are also summarised in Table 3.3.

Table 3.3: Summary of PIP_{25} indices derived from surface sediments biomarker data (Table 3.1) located within the region of extended sea-ice cover and proximal to the winter sea-ice edge (Table 3.1, Figure 3.5). Corresponding mean spring (SpSIC) and summer (SuSIC) sea-ice concentrations for the period 1988-2007 (Xiao et al., 2015) for each station are also given.

Station ID	$P_{IIIa}IP_{25}$ c=0.63	$P_{IIIa}IP_{25}$ c=1	P_BIP_{25} c=0.0048	P_BIP_{25} c=0.023	P_BIP_{25} c=1	SpSIC (%)	SuSIC (%)
JR142-GC12	0.854	0.787	0.660	0.287	0.009	90.59	48.9
JR142-GC13	0.915	0.873	0.693	0.319	0.011	85.93	44.3
JR142-GC19	0.855	0.789	0.654	0.281	0.009	81.69	39.3
JR142-GC11	0.955	0.930	0.794	0.444	0.018	89.01	40.6
PS2131-1	0.967	0.949	0.813	0.475	0.020	86.58	30.6
PS2142-3	0.972	0.957	0.733	0.363	0.013	87.24	37.7
PS2144-3	0.956	0.932	0.669	0.296	0.010	86.63	35.9
JR142-GC10	0.951	0.925	0.851	0.542	0.026	79.55	30.0
PS2148-1	0.971	0.955	0.665	0.291	0.009	74.22	20.7
JR142-GC9	0.965	0.947	0.699	0.326	0.011	75.27	19.2
JR142-GC20	0.970	0.953	0.588	0.228	0.007	100.00	80.0
JR142-GC8	0.978	0.966	0.754	0.389	0.014	80.09	17.4
JR142-GC23	0.977	0.964	0.727	0.356	0.013	83.80	17.9
JR142-GC22	0.971	0.956	0.813	0.474	0.020	83.80	17.9
JR142-GC7	0.974	0.960	0.799	0.451	0.019	81.93	18.4
JR142-GC6	0.970	0.954	0.819	0.485	0.021	80.00	16.3
JR142-GC5	0.975	0.962	0.829	0.501	0.023	80.12	15.7
JR142-GC4	0.965	0.946	0.859	0.559	0.028	79.64	15.7
PS2150-1	0.978	0.965	0.683	0.309	0.010	80.89	11.7
JR142-GC21	0.859	0.794	0.674	0.300	0.010	80.53	10.8
PS2151-1	0.948	0.920	0.523	0.185	0.005	77.63	7.4
PS2115-1	0.992	0.987	0.770	0.410	0.016	66.80	6.0
PS2111-2	0.793	0.708	0.569	0.215	0.006	40.97	1.7
679	0.361	0.264	0.285	0.076	0.002	42.32	1.7
PS2153-1	0.797	0.714	0.423	0.132	0.003	40.97	1.7
643	0.480	0.370	0.527	0.188	0.005	36.36	2.0
681	0.154	0.104	0.528	0.188	0.005	37.44	0.0
St32	0.585	0.472	0.302	0.082	0.002	47.65	0.0
St31	0.539	0.426	-	-	-	44.52	0.0
St30	0.522	0.409	-	-	-	39.30	0.0
St29	0.457	0.348	0.314	0.087	0.002	33.77	0.0
PS2113-1	0.191	0.131	0.114	0.026	0.001	21.43	0.0
677	0.194	0.132	0.682	0.308	0.010	22.35	0.0
St27	0.491	0.380	0.396	0.119	0.003	18.11	0.0
645	0.121	0.080	0.319	0.089	0.002	18.49	0.0
St26	0.390	0.289	0.392	0.118	0.003	11.99	0.0
St25	0.274	0.194	-	-	-	9.64	0.0
639	0.125	0.083	0.209	0.052	0.001	14.44	0.0
675	0.114	0.075	0.152	0.036	0.001	11.18	0.0
647	0.000	0.000	0.000	0.000	0.000	8.10	0.0
635	0.186	0.127	0.318	0.088	0.002	10.50	0.0
1241	0.064	0.041	0.123	0.028	0.001	8.44	0.0
St20	0.221	0.153	0.116	0.027	0.001	9.32	0.0
673	0.189	0.129	0.532	0.191	0.005	6.53	0.0
1239	0.043	0.028	0.157	0.037	0.001	9.08	0.0

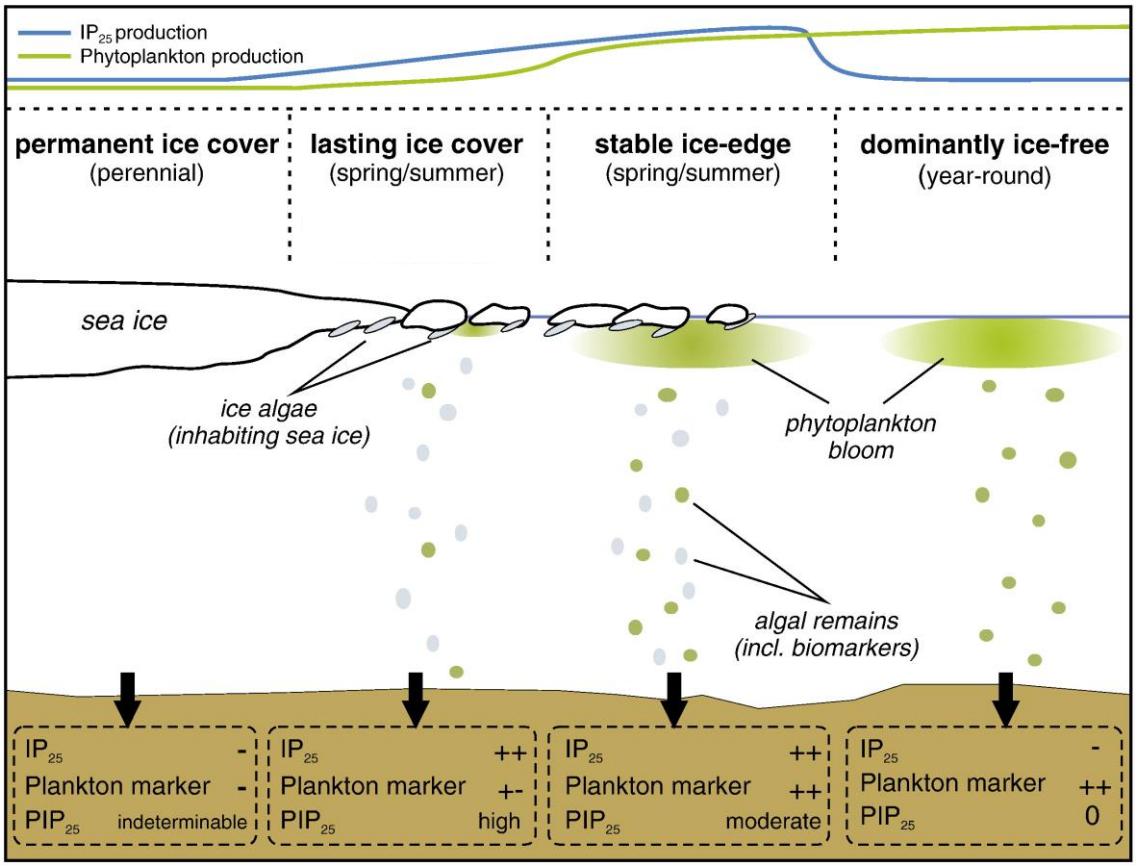

Figure 3.6: Generalised scheme illustrating distinct sea surface conditions and respective spring/summer productivities of ice algae and phytoplankton. An overview of sedimentary contents of IP_{25} and the phytoplankton-derived biomarkers is also presented together with resulting PIP_{25} indices indicated for each setting. Figure courtesy of Müller et al. (2011)

IP_{25} concentration in surface sediments (n=45) of the data set used for this study, shows a general increase with SpSIC, although a linear fit between the two is not strong (R^2=0.18; Figure 3.7a), and the relationship to SuSIC is even weaker (R^2 < 0.01; Figure 3.8a).

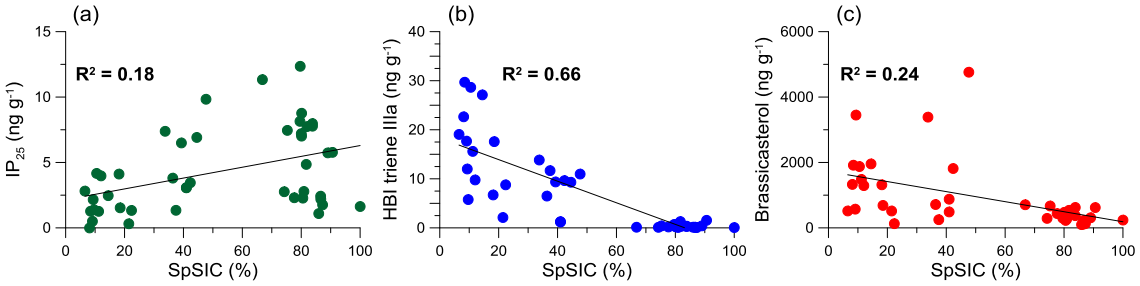

Figure 3.7: Relationships between individual biomarkers and SpSIC: (a) IP_{25}; (b) HBI triene IIIa; and (c) brassicasterol. R^2 values were obtained from linear regression fits.

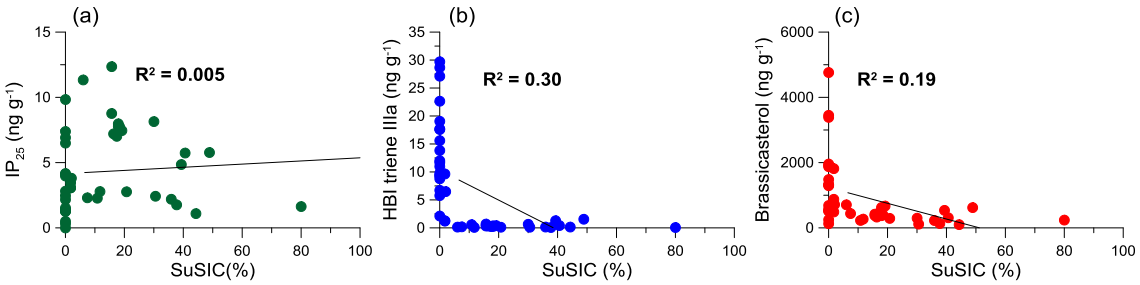

Figure 3.8: Relationships between individual biomarkers and SuSIC: (a) IP_{25}; (b) HBI triene IIIa; and (c) brassicasterol. R^2 values were obtained from linear regression fits

PIP_{25} indices for both phytoplankton lipids exhibit good linear relationships with SpSIC (Figure. 3.9a, c), however, with a particularly strong fit for $P_{IIIa}IP_{25}$ ($R^{2=}$0.88; Figure. 3.9a). Interestingly, the quality of the fit remains reasonably constant for $P_{IIIa}IP_{25}$ with exclusion of the *c* factor (i.e. *c*=1; R^2=0.9; Figure 3.9b), but outcomes for brassicasterol are strongly dependent on the magnitude of *c*. Thus, an R^2 value of 0.71, based on P_BIP_{25} values derived from Equations 2.9 and 2.10 in Chapter 2, reduces to 0.65 and 0.54 using a global *c* factor (Xiao et al., 2015), or for *c*=1 (Figure. 3.9d-e), respectively.

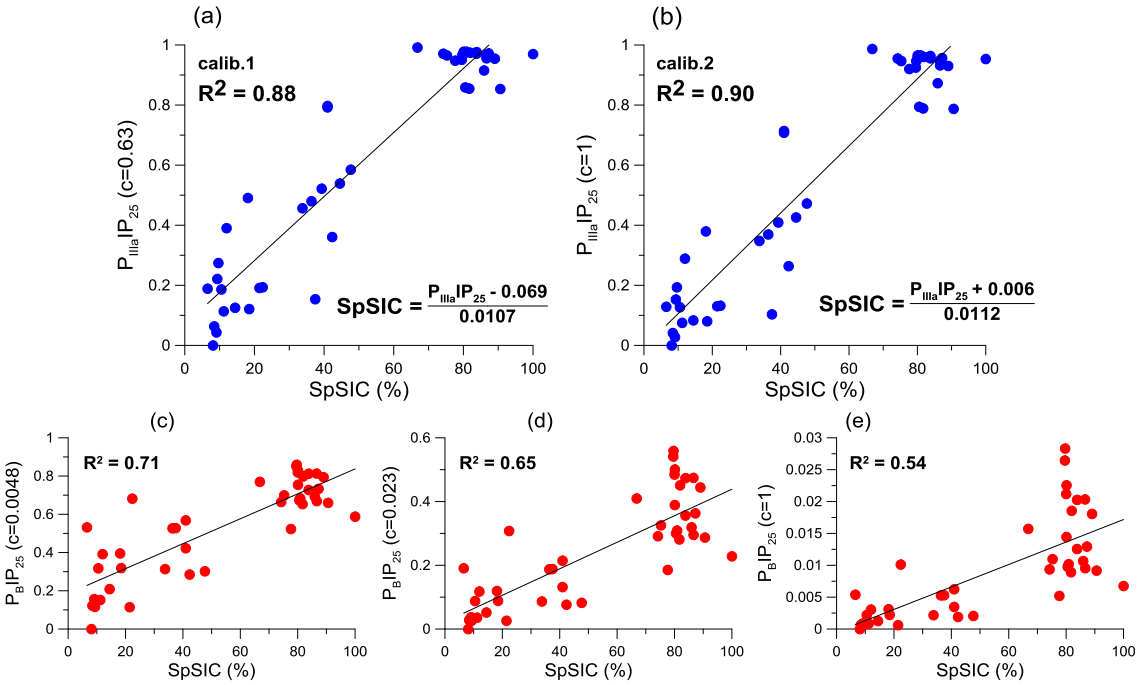

Figure 3.9: Relationship between PIP_{25} indices and SpSIC using different phytoplankton markers and *c* factors: (a) $P_{IIIa}IP_{25}$, *c* factor calculated from the current biomarker data; (b) $P_{IIIa}IP_{25}$, *c*=1; (c) P_BIP_{25}, *c* factor calculated from the current biomarker data; (d) P_BIP_{25}, global *c* factor as calculated by Xiao et al. (2015); and (e) P_BIP_{25}, *c*=1. R^2 values were obtained from linear regression fits.

Finally, all PIP_{25} indices show poor linear fits to SuSIC (Figure 3.10), although all (and only) $P_{IIIa}IP_{25}$ values greater than ca 0.8 correspond to locations with at least partial summer sea-ice cover (> 5%, Figure 3.10a, b).

SpSIC for the study region shows a generally northward increase, with approximate ranges of ca 5-20%, 20-60% and 60-100% for regions ca 74-76°N, 76-78°N and > 78°N, respectively (Figure. 3.4a). Following ice retreat during late spring, only locations north of ca 78°N experience some (> 5%) sea-ice cover during the summer months (July-September) with lower concentrations (typically < 50%; Figure. 3.4b) compared to spring.

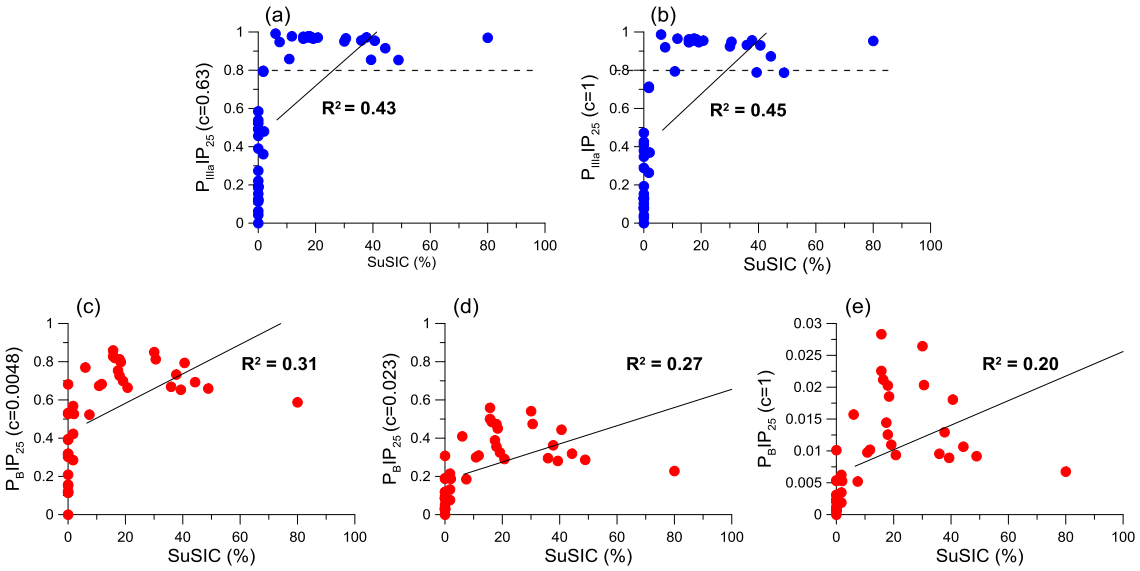

Figure 3.10: Relationship between PIP_{25} indices and SuSIC using different phytoplankton markers and *c* factors: (a) $P_{IIIa}IP_{25}$, *c* factor calculated from the current biomarker data; (b) $P_{IIIa}IP_{25}$ c=1; (c) P_BIP_{25}, *c* factor calculated from the current biomarker data; (d) P_BIP_{25}, global *c* factor as calculated by Xiao et al. (2015); (e) P_BIP_{25}, c=1. A possible threshold $P_{IIIa}IP_{25}$ value (ca 0.8) for summer sea-ice presence (>5%) is indicated with a horizontal dotted line. R^2 values were obtained from linear regression fits.

The improved linear relationship between P_BIP_{25} and SpSIC compared to that obtained using IP_{25} alone is consistent with observations made previously from other Arctic and sub-Arctic regions (e.g. Müller et al., 2011; Stoynova et al., 2013; Xiao et al., 2013, 2015). However, on the basis of the data presented here, even further improvements can

potentially be obtained by using HBI triene IIIa as the phytoplankton biomarker when deriving PIP_{25} indices. At this stage, the stronger linear fit between $P_{IIIa}IP_{25}$ and SpSIC (Figure 3.9a, b) may be attributed to a combination of the complementary sensitivities of IP_{25} and HBI triene IIIa to the surrounding sea-ice conditions, as demonstrated through the contrasting abundance distributions of these two biomarkers in the same sediments (Figure 3.5a, b), together with a greater selectivity of HBI triene IIIa (compared with brassicasterol) towards a marine phytoplankton origin; both factors aligning well with the underlying principles of the PIP_{25} approach (see Introduction; Müller et al., 2011). Indeed, Xiao et al. (2015) recently highlighted the importance of identifying a biomarker of exclusive marine origin for further development of the PIP_{25} index, especially as biomarkers such as brassicasterol can originate from a number of other environments (Belt et al., 2013; Huang and Meinschein, 1976; Volkman, 1986), with likely negative impacts on the sedimentary budget.

A further feature of the $P_{IIIa}IP_{25}$ data here is that the calculated range (ca 0-1), which is virtually identical with exclusion of the *c* factor, aligns well with the theoretical range (0-1) initially proposed by Müller et al. (2011) for describing different sea-ice settings (e.g. ice-free, marginal ice zone, extensive sea-ice), and also with the array of sea-ice concentrations pertinent to sampling sites (ca 5-95%) in this study, with linear fits providing reasonable estimates of low (12-18%), medium (40-45%) and high (68-72%) SpSIC based on $P_{IIIa}IP_{25}$ values of 0.2, 0.5 and 0.8, respectively. In contrast, in addition to the poorer linear fit that exists between P_BIP_{25} and SpSIC (Figure 3.9c-e), the range in P_BIP_{25} reflecting the extreme limits of sea-ice concentration (i.e. 0-100%) is extremely sensitive to the magnitude of c (i.e. 0-0.9, 0-0.6 and 0-0.03 for c=0.0048, 0.023 and 1, respectively) which causes clear difficulties when trying to make comparisons of values between different studies.

These outcomes are also illustrated well through visual comparison of various spatial distributions of PIP_{25} with seasonal sea-ice concentration (Figure. 3.11). For example, and in contrast to the spatial distributions of individual biomarkers (Figure. 3.11), $P_{IIIa}IP_{25}$ data (Figure. 3.11c) show an excellent relationship to SpSIC (Figure. 3.11a), as expected given the strong linear relationship between the two parameters, and the agreement is essentially unaffected following removal of the c factor (Figure. 3.11d). In contrast, the spatial distribution of P_BIP_{25} shows a generally poorer and less consistent association to SpSIC using each of the three c factors (Figures. 3.11e-g).

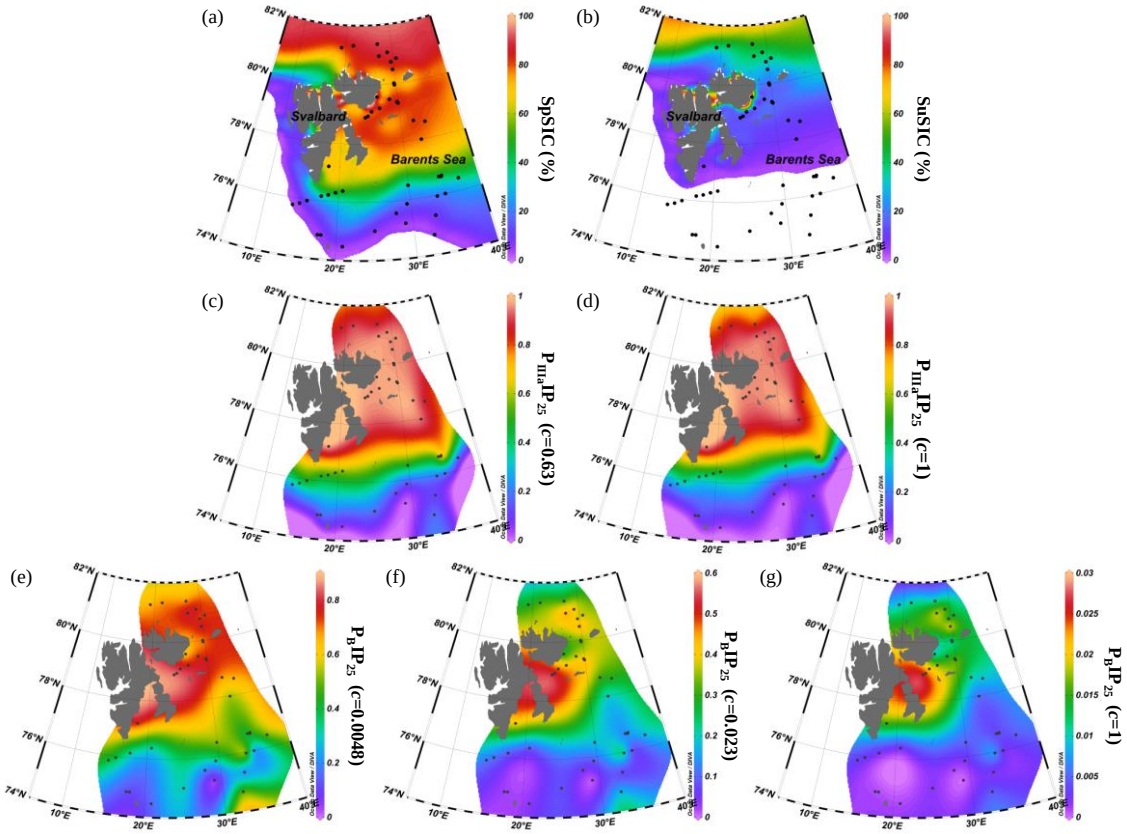

Figure 3.11: Spatial representations of sea-ice concentrations and PIP_{25} indices calculated using different phytoplankton markers and *c* factors: (a) mean SpSIC for the period 1988-2007 (Xiao et al., 2015); (b) mean SuSIC for the period 1988-2007 (Xiao et al., 20015); (c) $P_{IIIa}IP_{25}$, *c* factor calculated from the current biomarker data; (d) $P_{IIIa}IP_{25}$, c=1; (e) P_BIP_{25}, *c* factor calculated from the current biomarker data; (f) P_BIP_{25}, global *c* factor as calculated by Xiao et al. (2015); and (g) P_BIP_{25}, c=1. Note: figures showing SpSIC (a) and SuSIC (b) here are the same as those shown previously in Figure 3.4 and are presented to provide visual comparison with PIP_{25} derived indices.

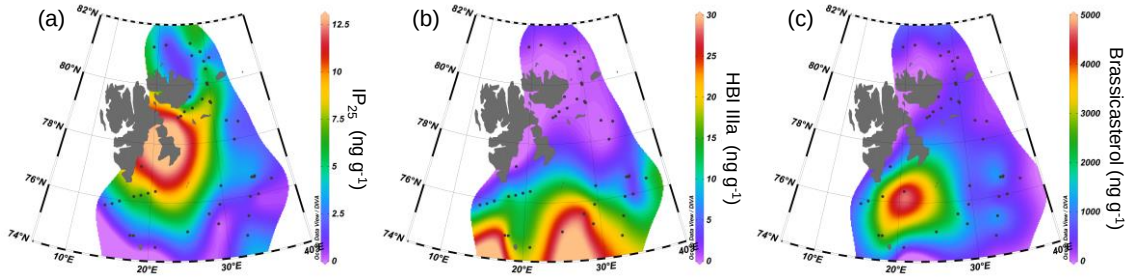

Figure 3.12: Spatial distribution of individual biomarker lipids in the study region used for PIP_{25} calibration: (a) IP_{25}; (b) HBI triene IIIa; and (c) brassicasterol.

This markedly better relationship between $P_{IIIa}IP_{25}$ and SpSIC (Figure 3.9a, b), compared to SuSIC (Figure 3.10a, b), likely reflects the specific or preferred environmental conditions under which each biomarker is biosynthesised, with IP_{25} being produced by certain sympagic diatoms during the spring algal bloom (Belt et al., 2013; Brown et al., 2011) and HBI triene IIIa by certain (as yet unknown) phytoplankton that thrive adjacent to the retreating ice edge or MIZ during the late spring melt. Although the latter conclusion is based on the surface sedimentary record rather than *in situ* water column measurements, it is noted that during analysis of HBIs and other biomarkers in surface waters off East Antarctica (Chapter 4), elevated abundances of HBI triene IIIa were apparent within the retreating MIZ compared to the adjacent regions of permanently open ocean conditions and extended sea-ice cover.

Despite the poor linear relationship between $P_{IIIa}IP_{25}$ and SuSIC (Figure 3.10a, b), only values greater than ca 0.8 are associated with at least partial (> 5%) summer sea-ice cover; a threshold value that might, therefore, provide a useful qualitative indicator of summer sea-ice occurrence. A corresponding value is less evident using P_BIP_{25} and, further, is highly dependent on the magnitude of *c* (Figure 3.10c-e).

Finally, the $P_{IIIa}IP_{25}$ threshold for summer ice occurrence (0.8) is also well demonstrated from a comparison of the spatial $P_{IIIa}IP_{25}$ distribution (Figure. 3.11c, d) compared to SuSIC (Figure 3.11b), with $P_{IIIa}IP_{25}$ generally < 0.8 for ice-free regions and values > 0.8

for those locations further north, and with SuSIC > 0%. Such a binary division is less evident from the P_BIP_{25} data, however (Figure. 3.11b, e-g).

The wider-scale applicability of these findings will clearly require analysis of surface sediments from other Arctic and sub-Arctic regions, including those that represent potentially different sea-ice settings to the consistent advance/retreat cycle that occurs within the Barents Sea. Nevertheless, the regional biomarker ($P_{IIIa}IP_{25}$)-based calibration described herein provides the necessary background for carrying out such studies, as well as longer-term and more detailed estimates of sea-ice concentration for the Barents Sea that are not currently available.

3.4.3 Temporal biomarker profiles and semi-quantitative estimates of SpSIC

In order to evaluate whether outcomes from surface sediment analysis could provide more detailed sea-ice descriptions (including estimates of SpSIC (%)) over longer timescales, previous biomarker data from three well dated marine sequences (Berben, 2014; Berben et al., 2014; Cabedo-Sanz et al., 2013) from locations with contrasting modern sea-ice cover (*viz*. long-lasting seasonal ice, inter-annual ice edge, ice-free) were re-examined and the outcomes compared with surface sediment data. Estimates of SpSIC (%) for each core were derived from calibration equations shown in Figure 3.9a (hereafter referred to as calib.1 (calibration1)) and 3.9b (hereafter referred to as calib.2 (calibration2)). The individual *c* factors used to calculate $P_{IIIa}IP_{25}$ indices in each core, correspond to values obtained from analysis of surface sediments from the Barents Sea (c=0.63), a value based on the ratio of the mean IP_{25} and HBI triene IIIa concentrations of each particular marine sequence (Section 3.4.2), and a value of c=1.

3.4.3.1 Olga Basin (northern Barents Sea)

Core 70 was retrieved from the Olga Basin in the northern Barents Sea (Figure 3.2b), a location that, in modern times, experiences long-lasting annual sea-ice cover. A biomarker record for core 70 (Figure 3.13) covers the last ca 9.5 cal. kyr BP and was previously discussed in detail by Berben (2014), who showed lowest IP_{25} concentrations during the early part of the record (Figure 3.13a), with a steady increase observed towards recent times. An opposite trend was, however, observed for HBI triene IIIa (Figure 3.13b) and a small decline in the brassicasterol concentration was also observed (Figure 3.13c), but this was not as pronounced as for HBI triene IIIa, possibly due to a lower sensitivity of the former to the overlying sea-ice conditions as demonstrated through the surface sediment data (Figure 3.5).

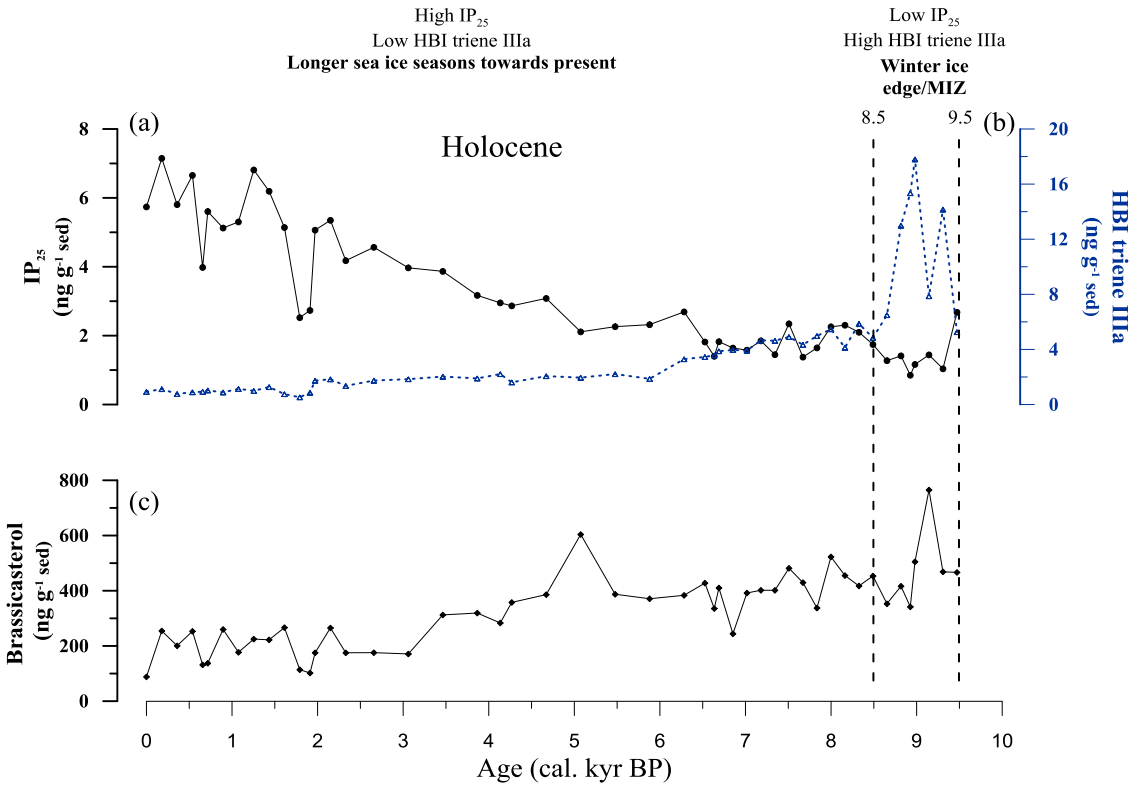

Figure 3.13: Down-core biomarker concentration profiles of: (a) IP_{25}; (b) HBI triene IIIa; and (c) brassicasterol in core 70 obtained from the northern Barents Sea. IP_{25} and brassicasterol data were obtained from Berben (2014) and HBI triene IIIa data were provided by Dr Patricia Cabedo-Sanz (personal communication, 2015). A summary of re-interpretations of environmental (sea-ice) conditions based on individual biomarker profiles is offered above each period described in text.

Berben (2014) suggested that the biomarker data indicated seasonal sea-ice cover throughout the record, but with shorter spring sea-ice cover and longer (and warmer) summers during the early Holocene (9.5-8.5 cal. kyr BP), with longer sea-ice seasons leading towards the present.

The SpSIC estimates in core 70 provided small differences for individual time slices, between the various approaches (Figure 3.14b). For the early Holocene part of the record (9.5-8.5 cal. kyr BP), mean estimates of SpSIC were never more than 20% (Table 3.4), with a range of values (9-20%) similar to those observed in the MIZ in modern times (ca 5-45%, Figure 3.4a). The rest of the Holocene (8.5-0 cal kyr BP) is characterised by a steady increase in SpSIC towards modern times (Figure 3.14).

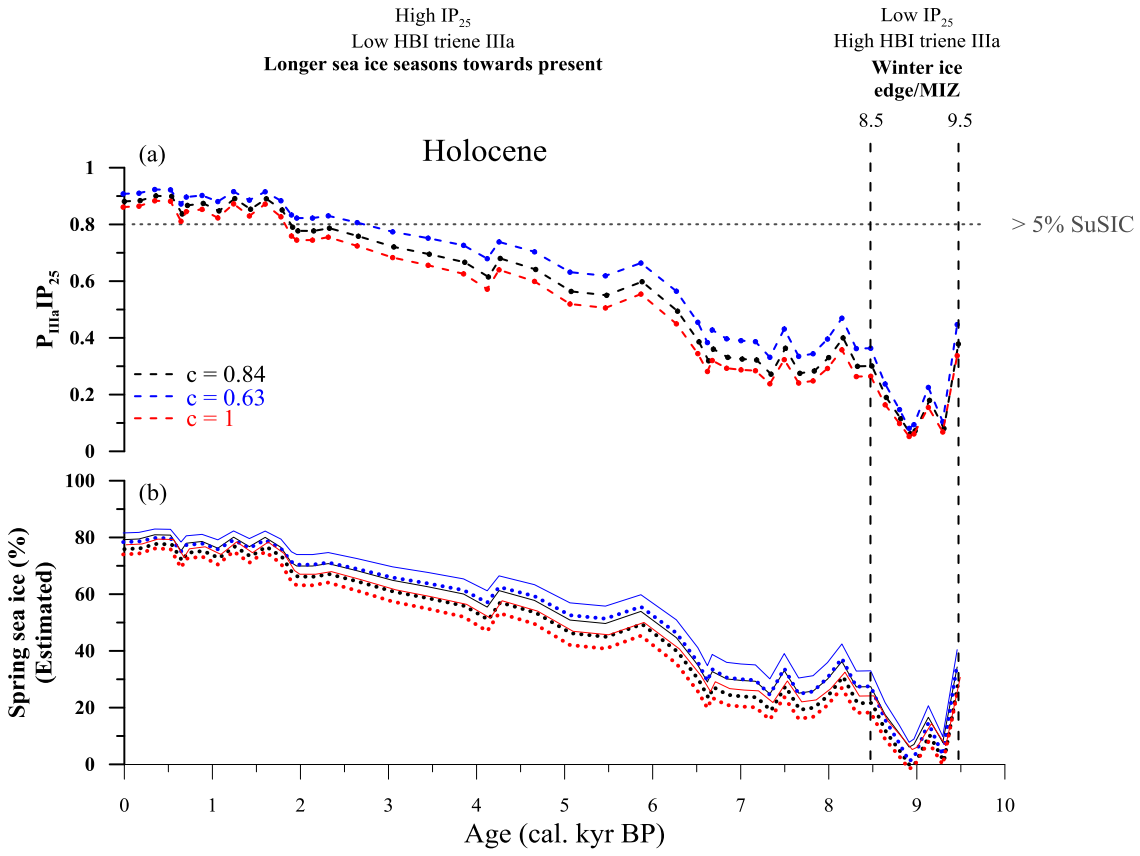

Figure 3.14: Down-core profiles of: (a) $P_{IIIa}IP_{25}$ indices in core 70 as calculated by application of *c* factors derived from core horizons (0.84, black), surface sediments (0.63, blue) or without application of *c* (1, red); (b) SpSIC (%) estimates calculated from calibration equations in Figure 3.9a (calib 1, dotted lines) and Figure 3.9b (calib 2, solid lines).

Table 3.4: The values in the table correspond to the mean estimates of SpSIC (%) for core 70 over specified time intervals described in text. Values derived from a combination of different calibration equations (Figure 3.9) and *c* factors used to calculate $P_{IIIa}IP_{25}$ indices. Individual *c* factors used in calculations of $P_{IIIa}IP_{25}$ correspond to the values obtained from the ratio of mean IP_{25} and HBI triene IIIa concentration in core 70 (*c*=0.84), an analysis of surface sediments from the Barents Sea (*c*=0.63), and a value of *c*=1.

	Mean estimates of SpSIC (%)					
Time interval (cal. kyr BP)	*c*=0.84		*c*=0.63		*c*=1	
	calib.1	calib.2	calib.1	calib.2	calib.1	calib.2
9.5-8.5	10	16	13	20	8	14
8.5-0	52	56	56	61	49	53
2.0-0	75	78	77	81	72	76

The range of mean estimate values (49%-61%) for the period was also significantly higher ($p < 0.05$) than in the early Holocene (9.5-8.5 cal. kyr BP). In addition, consistently high SpSIC estimates are observed for past ca 2 kyr (72%-81%), and occurrence of summer sea-ice ($P_{IIIa}IP_{25} > 0.8$) appears to be a persistent feature at the core site (Figure 3.14a).

3.4.3.2 Andfjorden (northern Norwegian Sea)

Core 1200, collected from the northern Norwegian Sea represents a location significantly further south of the modern winter sea-ice edge (Figure 3.2b). Detailed discussion of some of the biomarker data (IP_{25}, brassicasterol) was previously carried out by Cabedo-Sanz et al. (2013), who demonstrated that the site was covered by extensive seasonal sea-ice during the majority of the Younger Dryas (YD) (elevated IP_{25}), but was ice-free (IP_{25} absent) throughout the early-mid Holocene (ca 11.5-6.3 cal. kyr BP). During the termination of the YD (ca 11.9-11.5 cal. kyr BP), significantly lower IP_{25} abundance, compared to the previous millennium was hypothesised to reflect reduced/more variable sea-ice conditions or shorter seasonal sea-ice cover, but this was not investigated further. HBI triene IIIa concentrations (Figure. 3.15b) were extremely

low throughout the interval of elevated IP_{25} abundances during the YD (ca 12.9-11.9 cal. kyr BP), but increase markedly during the subsequent period (11.9-11.5 cal. kyr BP). In addition, the brassicasterol data for core 1200 do not reveal such clearly contrasting sea-ice conditions as IP_{25} and HBI triene IIIa, with alternating high and low abundances throughout the YD (Figure 3.15a-c), likely reflecting the variable sources of this biomarker.

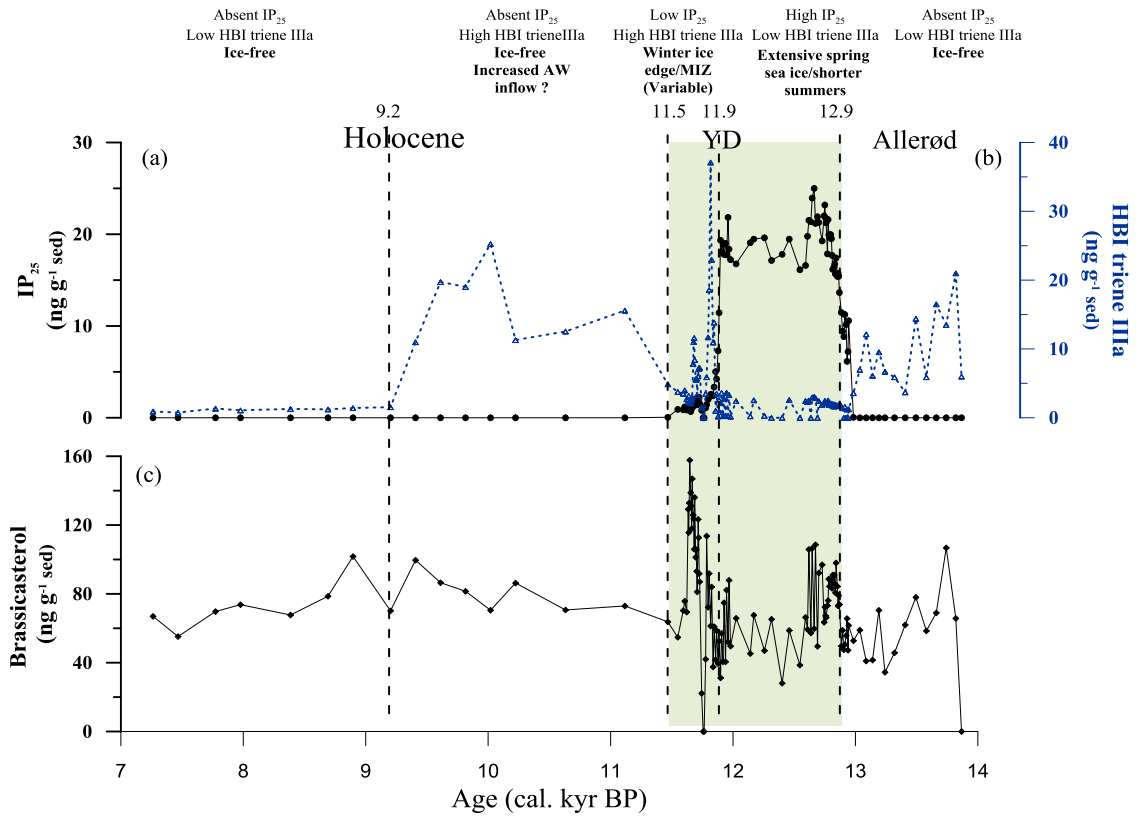

Figure 3.15: Down-core biomarker concentration profiles of: (a) IP_{25}; (b) HBI triene IIIa; and (c) brassicasterol in core 1200 obtained from northern Norwegian Sea. Biomarker data obtained from Dr Patricia Cabedo-Sanz (personal communication, 2015). The shaded areas correspond to the Younger Dryas (YD).

For the period of YD between 12.9 and 11.9 cal kyr BP, previously proposed as a period of extensive seasonal sea-ice at the core site (Cabedo-Sanz et al., 2013), new mean estimates of SpSIC are consistently high (71-85%), regardless of the method of determination used (Figure 3.16, Table 3.5). Slightly more variable estimates are observed for the period of YD termination (11.9-11.5 cal.kyr BP), when mean SpSIC

dropped to ca 25%, with a range of values (12-40%, Table 3.5) significantly lower than for the preceding period. Previously suggested ice free conditions for the early-mid Holocene period (ca 11.5-6.3 cal. kyr BP) as well as the interval preceding the YD (ca 13.6-12.9 cal. kyr BP) (Cabedo-Sanz et al., 2013) are further demonstrated by near zero estimates of SpSIC (Figure 3.16b, Table 3.5).

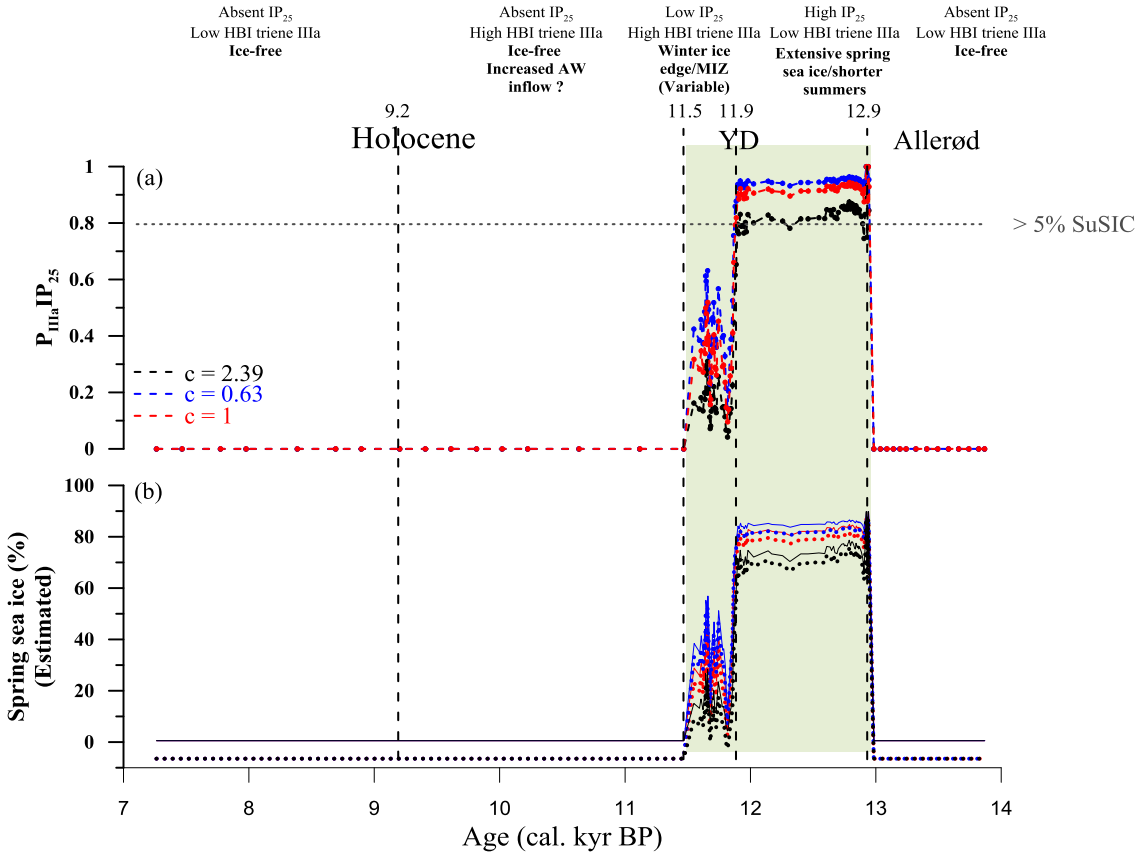

Figure 3.16: Down-core profiles of: (a) $P_{III}IP_{25}$ indices in core 1200 as calculated by application of *c* factors derived from core horizons (2.39, black), surface sediments (0.63, blue) or without application of *c* (1, red); (b) SpSIC (%) estimates calculated from calibration equations in Figure 3.9a (calib. 1, dotted lines) and Figure 3.9b (calib. 2, solid lines).

Table 3.5: The values in the table correspond to the mean estimates of SpSIC (%) for core 1200 over specified time intervals described in text. Values derived from a combination of different calibration equations (Figure 3.9) and *c* factors used to calculate $P_{IIIa}IP_{25}$ indices. Individual *c* factors used in calculations of $P_{IIIa}IP_{25}$ correspond to the values obtained from the ratio of mean IP_{25} and HBI triene IIIa concentration in core 1200 (*c*=2.39), an analysis of surface sediments from the Barents Sea (*c*=0.63), and a value of *c*=1.

	Mean estimates of SpSIC (%)					
Time interval (cal. kyr BP)	*c*=2.39		*c*=0.63		*c*=1	
	calib.1	calib.2	calib.1	calib.2	calib.1	calib.2
12.9-11.9	75	71	85	82	83	80
11.9-11.5	18	12	40	35	32	26
11.5-9.2	1	-6	1	-6	1	-6
9.2-6.3	1	-6	1	-6	1	-6

Therefore, the majority of the YD (12.9-11.9 cal kyr BP) in core 1200 was characterised by extensive spring sea-ice cover with SpSIC in the region of 85%. In addition the $P_{III}IP_{25}$ data also suggest the presence of summer sea-ice at the core site ($P_{IIIa}IP_{25} > 0.8$), regardless of the calibration method used. In the subsequent period (11.9-11.5 cal. kyr BP), the transition from extensive sea-ice cover to the one of a winter ice edge scenario, is further characterised by the estimates of SpSIC that are significantly lower (ca 25%) than for most of the YD.

3.4.3.3 Kveithola Trough (western Barents Sea)

Core 11 was obtained from a location in the western Barents Sea close to the modern maximum winter sea-ice extent and thus experiences variable sea-ice cover (presence/absence) on an annual basis and, in any case, for shorter periods (e.g. November-April). Some of the biomarker data were discussed previously in detail by Berben et al. (2014), who showed relatively low abundances of IP_{25} in core 11 throughout the Holocene (Figure 3.17a), although some elevation in values was noted

for the early Holocene and the last ca 1.0 cal. kyr BP. A similar concentration profile was noted for brassicasterol, although some temporal variation between the two biomarkers was observed for the early part of the record, at the end of the YD (ca 11.9-11.5 cal kyr BP, Figure 3.17c). These observations were interpreted as reflecting stable MIZ conditions (favourable for both biomarkers) during the early Holocene, preceded by a period of more extensive sea-ice cover during the latter stages of the YD. Additional biomarker data for this core (Cabedo-Sanz, personal communication) that extend those of Berben at al. (2014), with new IP_{25} data for the YD (to ca 13.0 cal. kyr BP, Figure 3.17a), and HBI triene IIIa concentrations for the entire record (Figure 3.14b), reveal highest IP_{25} concentrations during the majority of the YD (ca 13-11.9 cal. kyr BP) accompanied by extremely low HBI triene IIIa abundance.

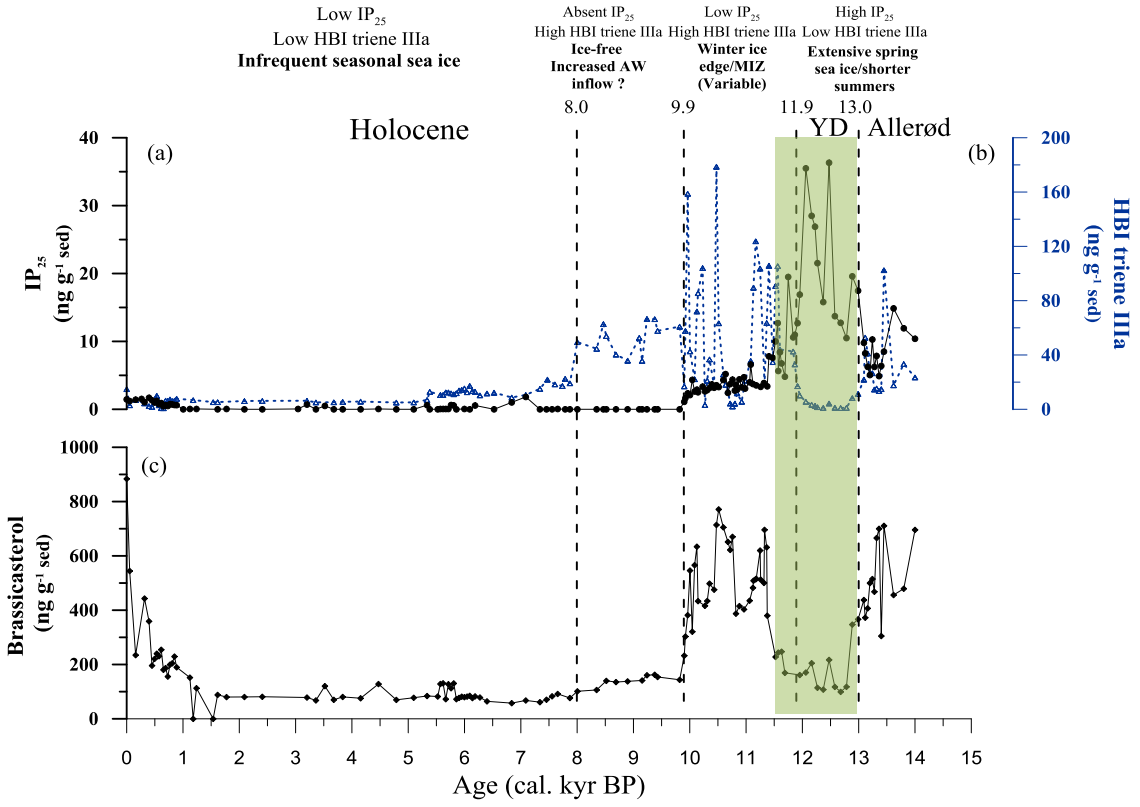

Figure 3.17: Down-core biomarker concentration profiles of: (a) IP_{25}; (b) HBI triene IIIa; and (c) brassicasterol in core 11 obtained from western Barents Sea. Some IP_{25} and brassicasterol data are obtained from Berben et al. (2014). Remaining biomarker data were provided by Dr Patricia Cabedo-Sanz (personal communication, 2015). The shaded area corresponds to the Younger Dryas (YD).

Exceptionally, during the early Holocene (ca 9.9-8.0 cal. kyr BP), IP_{25} is absent (or below our limit of detection) and is accompanied by relatively high HBI triene IIIa concentrations, although this is not the case for brassicasterol (see Section 3.4.4 for a discussion of this observation).

Unlike for core 70 and 1200, estimates of SpSIC in core 11 were somewhat more variable between the different approaches (Figure 3.18, Table 3.6). Variation in SpSIC values can be readily observed throughout the record, with the exception of the YD between ca 13.0 and 11.9 cal kyr BP, when the variation in values is considerably reduced, likely due to relatively large temporal changes between IP_{25} and HBI triene IIIa. For that period, mean SpSIC estimates are relatively high, with a range of 69-86% (Table 3.6) suggesting a period of extensive seasonal sea-ice cover at the site, an observation similar to that for core 1200. In addition, occurrence of the summer sea-ice appears to be a permanent feature at the core site ($P_{IIIa}IP_{25} > 0.8$, Figure 3.18a). For the period between 11.9 and 9.9 cal. kyr BP the range of mean SpSIC estimates varied between 9 and 42% (Figure 3.18, Table3.6), with similar variation in mean SpSIC values (2-24%) also observed in later part of the record (8.0-0 cal. kyr BP) (Figure 3.18, Table 3.6). Additionally, values of mean SpSIC estimates between 17 and 54% were observed for the period 14.0-13.0 cal. kyr BP (Figure 3.18, Table3.6). This variability in outcomes, is not seen to the same extent in cores 70 and 1200, and is likely caused by generally more variable (and higher) sedimentary abundances of HBI triene IIIa in core 11 (Figure 3.17b) when compared to cores 70 (Figure 3.13b) and 1200 (Figure 3.15b).

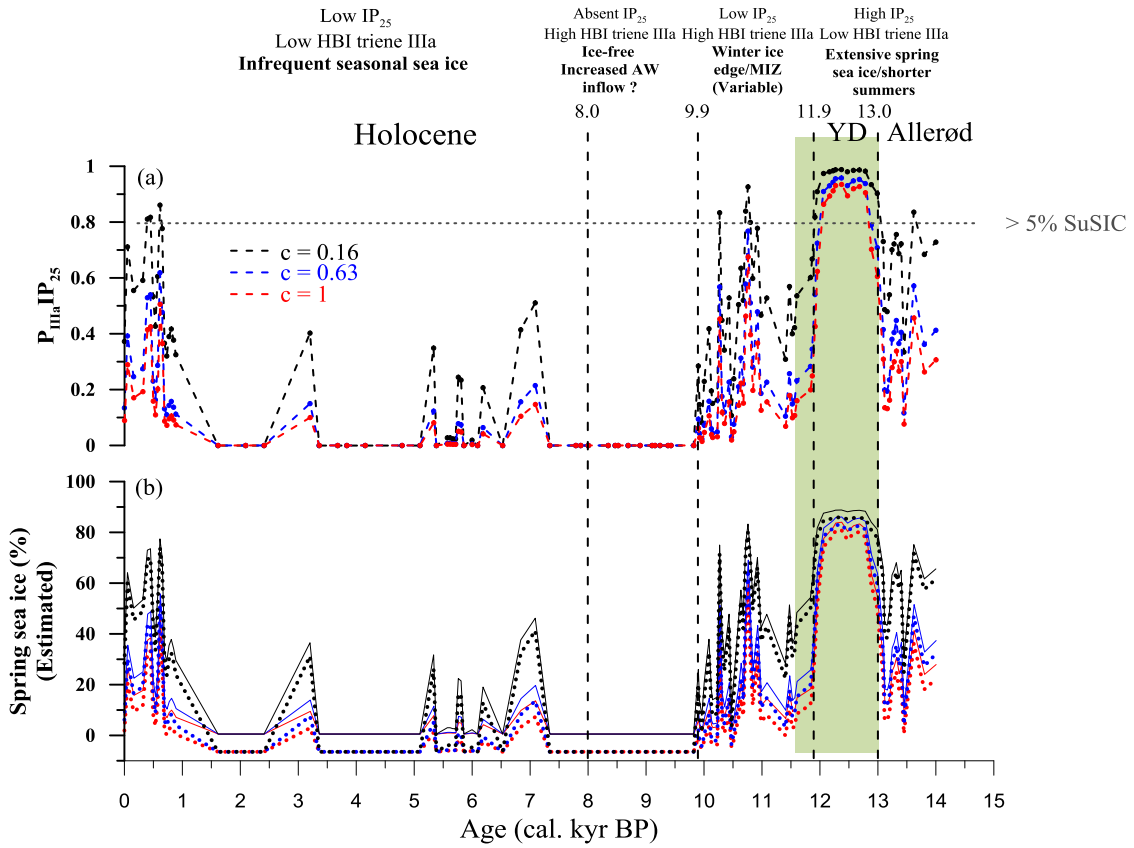

Figure 3.18: Down-core profiles of: (a) $P_{IIIa}IP_{25}$ indices in core 11, calculated by application of *c* factors derived from core biomarker data (0.16, black), surface sediments (0.63, blue) and without application of *c* (1, red); (b) SpSIC (%) estimates calculated from calibration equations in Figure 3.9a (calib.1, dotted lines) and Figure 3.9b (calib.2, solid lines).

Table 3.6: The values in the table correspond to the mean estimates of SpSIC (%) for core 11 over specified time intervals described in text. Values derived from a combination of different calibration equations (Figure 3.9) and *c* factors used to calculate $P_{IIIa}IP_{25}$ indices. Individual *c* factors used in calculations of $P_{IIIa}IP_{25}$ correspond to the values obtained from the ratio of mean IP_{25} and HBI triene IIIa concentration in core 11 (*c*=0.16), an analysis of surface sediments from the Barents Sea (*c*=0.63), and a value of *c*=1.

	Mean estimates of SpSIC (%)					
Time interval (cal. kyr BP)	*c*=0.16		*c*=0.63		*c*=1	
	calib.1	calib.2	calib.1	calib.2	calib.1	calib.2
14.0-13.0	58	54	32	26	23	17
13.0-11.9	86	83	78	74	73	69
11.9-9.9	42	37	21	15	15	9
9.9-8	1	-6	1	-6	1	-6
8.0-0	24	18	12	5	9	2

Data presented here, therefore, suggest that the most severe sea-ice conditions for this site only existed during the YD, with SpSIC in the region of 75%. Reasonably similar-to-modern conditions were reached by the early Holocene, with more variable SpSIC (9-42%), but which are considerably and consistently lower than for the preceding period. The conditions remained reasonably consistent for the rest of the Holocene, with biomarker abundances similar to those seen for surface sediments from ice-free locations further south (Figure. 3.5b), indicating only infrequent sea-ice cover at the core locations and SpSIC that are consistently less than 25%.

3.4.4 Early Holocene anomalies-enhanced Atlantic water inflow?

For cores 1200 and 11, there are intervals during the early Holocene for which IP_{25} is absent, but where levels of HBI triene IIIa are relatively high, before declining and remaining low for the remainder of the records. Specifically, elevated HBI triene IIIa (but absent IP_{25}) occurred ca 11.2-9.3 cal. kyr BP and ca 9.9-8.0 cal. kyr BP in cores 1200 and 11, respectively (Figures 3.15 and 3.17). This combination of IP_{25} and HBI triene IIIa does not occur for the northern Barents Sea site (core 70), since IP_{25} is present throughout the record (Figure 3.13a). Of course, the occurrence of HBI triene IIIa (but not IP_{25}) is not unexpected given the ubiquity of this biomarker in surface sediments from across the study region, but the elevated abundances compared to modern values represents something of an anomaly. At this stage, since the exact sources (and depth habitats) of HBI triene IIIa are not known, it is not possible to conclude with certainty whether its occurrence reflects near-surface or sub-surface conditions, especially as the likely diatom sources inhabit a dynamic range across the photic zone. Potentially, therefore, enhanced HBI triene IIIa during the early Holocene could be explained by increased surface layer productivity during the Holocene Thermal Maximum (HTM). However, since the HTM for the Nordic/Barents Seas is believed to

have occurred ca 9.0-6.0 kyr BP (summarised by Risebrobakken et al., 2011), this explanation seems unlikely. Alternatively, increased HBI triene IIIa levels may better reflect the consequences of increased Atlantic Water inflow (with associated enhanced productivity) to the northern Norwegian Sea and Barents Sea, established as occurring ca 10.0±1.0 kyr BP, through examination, mainly, of foraminiferal data obtained from cores across the region (Risebrobakken et al., 2011). Additionally, elevated HBI triene IIIa concentrations (but absent IP_{25}) also occur in core 1200 during the Allerød (ca 13.8-12.9 cal. kyr BP; Figure 3.15). Previously, Cabedo-Sanz et al. (2013) interpreted the absence of IP_{25} during this interval as indicative of ice-free conditions at this time, although an alternative explanation involving glacial re-advance could not be discounted. HBI triene IIIa data are not at all consistent with this latter hypothesis; however, it is likely that ice-free conditions prevailed during this warm interval, with environmental conditions similar to those from ca 11.5-9.2 cal. kyr BP.

Determination of the sources (and major environmental habitats) of HBI triene IIIa is clearly important, therefore, before elevated abundances of this biomarker can be interpreted fully, but the quantification of this biomarker has the potential to add to the existing proxies used to probe climatic and oceanographic shifts in the Norwegian and Barents Seas, especially when measured alongside the sea-ice biomarker proxy IP_{25}.

3.5 Conclusions

In summary, the primary aim here was to investigate the potential for selected biomarkers to provide complementary (at least) information to the qualitative (IP_{25}) and semi-quantitative (PIP_{25}) methods established previously. With regards to the aims outlined in Section 3.1, the following summary of findings is presented:

Analysis of >100 surface sediments from diverse regions across the Barents Sea has shown that the relative abundances of the diatom-derived biomarkers IP_{25} and HBI triene IIIa are strongly dependent on the overlying oceanographic conditions, with the position of the seasonal sea-ice edge playing a major role. These observations are consistent with production of these biomarkers from source-specific diatoms, whose habitats are strongly dependent on the occurrence of seasonal sea-ice. Thus, IP_{25} appears to be produced, selectively, by a small number of Arctic sea-ice diatom species, while HBI triene IIIa is made by other diatom species, whose habitat preference appears to be adjacent to the retreating sea-ice edge. Therefore, enhanced sedimentary abundances of IP_{25} were observed for regions experiencing more frequent and longer-lasting spring sea-ice cover, with HBI triene IIIa common to all seasonally ice-free regions, but especially enhanced in sediments for locations that reflect the retreating ice edge or MIZ during late spring-summer. Therefore, more accurate descriptions of spring sea-ice conditions are achievable by measuring IP_{25} alongside other source-specific biomarkers (e.g. HBI triene IIIa) whose production is particularly reflective of the neighbouring sea-ice conditions (e.g. winter sea-ice margin, marginal ice zone) as shown in the current study.

Semi-quantitative estimates of spring sea-ice concentration for the Barents Sea, using the PIP_{25} index may be improved by means of a tri-unsaturated HBI (HBI triene IIIa) as a phytoplankton biomarker, possibly as a result of the greater sensitivity of this biomarker to the seasonal sea-ice conditions compared to brassicasterol, with enhanced production in the MIZ compared to regions of longer lasting sea-ice cover. In particular, reasonably strong linear relationships between PIP_{25} indices and SpSIC have been found for biomarker data obtained from locations representing contrasting overlying sea-ice settings in the Barents Sea. Consistent with the strong linear fit between $P_{IIIa}IP_{25}$ and SpSIC, the spatial distribution of $P_{IIIa}IP_{25}$ exhibited a strong association with the

corresponding SpSIC. Since the abundances of IP_{25} and HBI triene IIIa were much closer in magnitude than between IP_{25} and brassicasterol, the linear relationships, the range in PIP_{25} and the spatial agreement between PIP_{25} and SpSIC were also less dependent on the balance factor *c* for $P_{IIIa}IP_{25}$ than for $P_BIP_{25.}$ Considerably weaker linear relationships were observed between individual biomarkers and SpSIC or SuSIC, or between PIP_{25} values and SuSIC. However, data presented here suggest that a lower limit threshold for $P_{IIIa}IP_{25}$ (ca 0.8) might represent a useful qualitative proxy for the past occurrence of summer sea-ice for the Barents Sea, at least.

The potential for the combined analysis of IP_{25} and HBI triene IIIa to provide more detailed assessments of past sea-ice conditions has been tested by their (and related PIP_{25} indices) quantification in three down-core records representing contrasting modern settings. The outcomes are not only consistent with previous general findings, but have allowed more detailed descriptions of sea conditions to be deciphered. For cores 11 and 1200, high IP_{25}, low HBI triene IIIa and concentrations estimates of SpSIC (>70%) during the YD are consistent with extensive sea cover, with relatively short periods of ice-free conditions resulting from late summer retreat. Towards the end of the YD (ca 11.9 cal. kyr BP), a general amelioration of conditions resulted in a near winter maximum ice edge scenario and SpSIC in the region of 20-40%, although this was somewhat variable and the eventual transition to predominantly ice-free conditions was later for the western Barents Sea site (core 11; ca 9.9 cal. kyr BP) compared to NW Norway (core 1200; ca 11.5 cal. kyr BP), likely as a result of its more northerly location. In contrast, the northern Barents Sea site (core 70) was characterised by seasonal sea-ice cover throughout the Holocene with a gradual shift from winter ice edge conditions and SpSIC in the region of 10-20% during the early Holocene to more sustained ice cover, with SpSIC of ca 55% in the Neoglacial; a transition that has undergone something of a reverse in the last ca 150 yr according to observational records (Divine and Dick, 2006).

CHAPTER FOUR

4 Results (2): Distribution of highly branched isoprenoid alkenes and other algal lipids in surface and water column waters from East Antarctica: further insights for biomarker-based paleo sea-ice reconstruction

4.1 Introduction

Chapter four provides further insights into the use of certain HBIs (HBI diene II and HBI triene IIIa) as proxies for Antarctic sea-ice. Specifically, the content of the current chapter will demonstrate the sensitivity of these lipids in the surface waters in East Antarctica to the overlaying, sea-ice influenced, oceanographic conditions especially when compared to more generic indicators of marine primary productivity. The possible influence of a coastal polynya as well as alterations within the water column with regards to the sedimentary interpretations of these lipids will be discussed.

The Southern Ocean sea-ice is critical to Earth's climate regulation. It is one of the most seasonal and variable features of the Earth's surface, and has a significant influence on key oceanic and atmospheric processes, which in turn drive the global climate (Brandon et al., 2010; Comiso, 2010). Determining the paleo sea-ice record is widely recognised as critical to elucidating past (and future) climate conditions (Thomas and Dieckmann, 2010; Vaughan et al., 2013).

Although the analysis of fossil diatoms has been used with great success for reconstruction of Antarctic winter sea-ice extent over the last 220,000 years (Armand and Leventer, 2010; de Vernal et al., 2013a; Gersonde et al., 2005), this approach is not

applicable for longer timeframes and does not provide complementary information on the occurrence of summer sea-ice; a parameter critical in determining the net area of sea-ice coverage and loss (Esper and Gersonde, 2014; Ferry et al., 2015). As such, there is a need to develop new and complementary proxies for reconstructing geophysical parameters associated with Antarctic sea-ice.

In recent years, the organic geochemical lipid, HBI diene II (Chapter 1, Figure 1.1) has been identified in both sea-ice diatoms and sediments from a number of Antarctic locations (Johns et al., 1999; Massé et al., 2011; Nichols et al., 1988), with an isotopic ($\delta^{13}C$) signature that is also characteristic of a sea-ice origin (Johns et al., 1999; Massé et al., 2011; Sinninghe Damsté et al., 2007). Since this HBI diene II is co-produced with IP_{25} by Arctic sea-ice diatoms (Brown et al., 2014b) and is positively correlated with IP_{25} when quantified in sediments (Cabedo-Sanz et al., 2013; Massé et al., 2008; Vare et al., 2009), it too can be used as a proxy for Arctic sea-ice, and also has the potential to provide the basis for paleo sea-ice reconstruction for the Southern Ocean. In fact, a number of Antarctic sea-ice reconstruction studies based on the variable abundance of HBI diene II in Antarctic sediments have begun to appear (Barbara et al., 2010, 2013, 2016; Campagne et al., 2015, 2016; Collins et al., 2013; Denis et al., 2010; Etourneau et al., 2013; Massé et al., 2011). A further HBI (HBI triene IIIa) has been reported in Antarctic phytoplankton and sediments, although this isomer has not been identified in Antarctic sea-ice. Further, its significantly lighter stable isotopic composition ($\delta^{13}C$) in phytoplankton ($\delta^{13}C$=-40.2± 0.5‰) and sediments (e.g. $\delta^{13}C$=-41.6±1.1‰) (Massé et al., 2011), compared to HBI diene II, indicates an exclusive origin in the pelagic phytoplankton (Trull and Armand, 2001), possibly from species that thrive within the marginal ice zone or retreating ice margin (Collins et al., 2013). As such, measurement of HBI diene II in Antarctic sediments has generally been used to provide proxy evidence for variability in past sea-ice extent for the Southern Ocean (Barbara et al.,

2010, 2016; Barbara et al., 2013; Campagne et al., 2015, 2016; Denis et al., 2010; Etourneau et al., 2013; Massé et al., 2011), while parallel quantification of HBI triene IIIa has been used to demonstrate open-water conditions and possibly changes in seasonality of Antarctic sea-ice (Collins et al., 2013). Presence of HBI triene IIIa in study by Massé et al (2011) was also always accompanied by occurrence of another triunsaturated isomer, HBI triene IIIb (Chapter 1, Figure 1.1), with stable isotopic composition ($\delta^{13}C$) values in the same phytoplankton ($\delta^{13}C$=-38.3± 0.6‰) and sediment ($\delta^{13}C$=-36.1± 4.2‰) samples similar to those of HBI triene IIIa. Despite this, only quantifications based on HBI triene IIIa have thus far been used in number of Antarctic paleo studies (Barbara et al., 2010, 2016; Barbara et al., 2013; Campagne et al., 2015, 2016; Denis et al., 2010; Etourneau et al., 2013). Other common lipid biomarkers such as sterols and fatty acids have received less attention as possible sea-ice proxies, likely due to their ubiquity and low environmental specificity, at least compared to HBIs such as IP_{25}. However, development of HBIs as proxies for Antarctic sea-ice is much less advanced than that of IP_{25} for the Arctic (see Belt and Müller, 2013) and has relied almost entirely on their analysis in a small number of sediments, rather than within their source environments.

Hence, to provide further insights into the use of certain HBIs, and particularly HBI diene II and HBI triene IIIa, as proxies for Antarctic sea-ice, the aim of this study was: 1) to investigate the occurrence and abundance distribution of HBI diene II, and HBI trienes IIIa and IIIb, within water samples taken from a transect in the East Antarctica, and from locations directly influenced by contrasting sea-ice settings; 2) to compare the outcomes from 1) with distributions of algal sterols and fatty acids as more generic indicators of marine primary productivity; 3) to explore any environmental influence on the ratio between HBI diene II and HBI triene IIIa (II/IIIa)-a parameter that

has been used in several previous paleo studies as an indicator of past sea-ice changes in the Southern Ocean.

4.2 Regional setting

A detailed description of the oceanographic and topographic features of the area under study can be found elsewhere (e.g. Gwyther et al., 2014; Miles et al., 2016; Williams et al., 2011). Briefly, the Sabrina Coast (ca 115ºE-130ºE) is a relatively small coastal area of much larger landmass, generally known as Wilkes Land (ca 110ºE-142ºE). The coast is characterised by marine terminating glaciers, ice shelves (such as the Totten, Moscow University and Dalton Ice Shelves, Figure 4.1), large tracts of year-round ice adjoining the land (fast ice), extensive seasonal sea-ice growth and a region of strong sea-ice formation (the Dalton ice tongue polynya) (Gwyther et al., 2014). The continental shelf seas of the Sabrina Coast are approximately 1000 m deep, with the shelf break occurring between 65.0°S to 65.5°S (Gwyther et al., 2014). The area is dominated by two major ocean currents (Figure 4.1); the eastward flowing Antarctic Circumpolar Current (ACC), located in the deep abyssal waters to the north of the continental shelf break (Orsi et al., 1995) and the westwards flowing Antarctic Coastal Current (ACoC), which flows within 50 km of the coast and is associated with the east wind drift. Offshore of the shelf break, the two major water masses are cold, fresh Antarctic Surface Waters (AASW) above warm, saline Circumpolar Deep Water (CDW). The CDW properties weaken poleward through mixing with cold Antarctic water masses and, when cooler than 1.5ºC (also known as the Southern Boundary), it is referred to as 'modified' CDW (mCDW) (Williams et al., 2011). Over the upper continental slope and continental shelf break, this boundary between AASW and mCDW is termed the Antarctic Slope Front (ASF, Jacobs, 1991; Whitworth et al., 1998).

In general, sea-ice formation in the area begins in March-April, with relatively rapid retreat beginning to occur in November/December (Massom et al., 2013). The marginal ice zone in the area is relatively narrow (Figure 4.1), especially when compared to some other areas of the Antarctic (e.g. the Weddell Sea), but is subject to a strong inter-annual variability (Massom et al., 2013). Coastal polynyas play a crucial role on sea-ice formation in the region, with high levels of production as a consequence of their activity (Tamura et al., 2008). The occurrence of easterly driven katabatic winds also plays a controlling factor with respect to sea-ice formation (Massom et al., 1998). During sea-ice production (April-October), brine rejection leads to the deepening of the cold surface mixed layer and de-stratification of the water column (Petty et al., 2014), thus contributing to the formation of Antarctic bottom waters (AABW), an important contributor to the global overturning circulation (e.g. Johnson 2008).

4.3 Experimental

4.3.1 Surface water samples

Water samples were obtained as part of the NBP1402 cruise aboard the RVIB *Nathaniel B Palmer* in February-March 2014 and were provided by Dr Leanne Armand (Macquarie University Australia). At each sampling site (Figure 4.1), surface water (ca 0-10 m water depth) was obtained either from the ship's intake line or from CTD rosettes. In total, sampling was carried out at 47 sites, with 38 locations within the polynya region (in the Seasonal Ice Zone (SIZ)), west of the Dalton Iceberg Tongue (East Antarctica), and a further 9 locations representing a transect to ca 56°S in the Marginal Ice Zone (MIZ) and the Permanently Open Ocean (POOZ) (Figure 4.1). In each case, 1.5-3.0 L of water was filtered onto 25 mm Whatman GF/F filters (as supplied), wrapped in aluminium foil and stored frozen (-80°C) until further analysis.

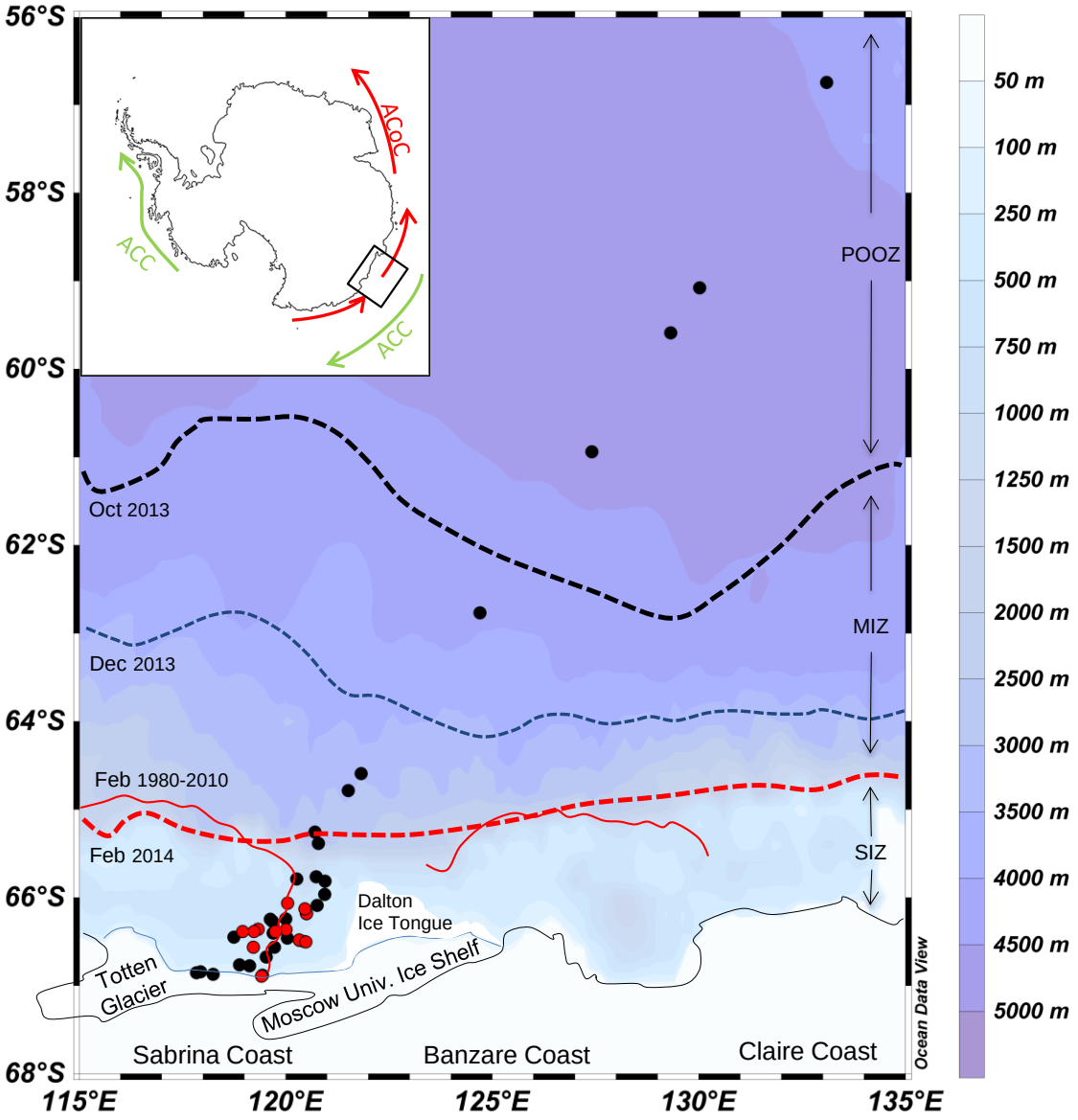

Figure 4.1: Map of the main study region and location of individual sampling sites. Samples collected by CTD are indicated by red circles and those collected through intake line by black circles respectively. Antarctic Circumpolar Current (ACC), Antarctic Coastal Current (ACoC) and other landmarks are also indicated. Dated lines refer to mean satellite-derived sea-ice extent (NSIDC, Fetterer et al., 2002) and the regions designated as the permanently open ocean zone (POOZ), the marginal ice zone (MIZ) and the seasonal ice zone (SIZ) are also shown. The main polynya region described in the text includes samples located further south than ca 66°S.

4.3.2 Water column samples

Distribution of biomarkers within the water column was investigated through analysis of water samples collected by CTD rosette (Figure 4.1). In total, 12 stations, all located within SIZ, were sampled at three depths; surface (0-10 m), subsurface (20-60 m) and near the bottom of the water column (480-1300 m). Due to CTD instrumentation not

being calibrated prior to deployment, environmental variables, such as temperature, salinity or chlorophyll *a* data, were not considered to complement biomarker analysis. Details of volumes filtered and samples preservation prior to analysis are described in Section 4.3.1

4.3.3 Lipid extraction and analysis

Filtered water samples were extracted and analysed by the methods described in Chapter 2. Extraction of filter samples was carried out according to methods outlined in Section 2.6, with purification of non-saponifiable lipids (NSL) carried out according to Section 2.5. Prior to analysis by GC-MS (Section 2.9), fractions containing fatty acids and sterols were derivatised (BSTFA; 50 µl; 70°C; 60 min), with individual biomarker data obtained via methods outlined in Section 2.10. Individual concentrations were normalised to the volume of water filtered.

4.3.4 Sea-ice and chlorophyll *a* data

Mean monthly satellite-derived sea-ice extent and chlorophyll *a* data were obtained from the National Snow and Ice Data Center (Fetterer et al., 2002) and NASA (http://oceandata.sci.gsfc.nasa.gov/), respectively. Sea-ice imagery was derived from MODIS (on-board Terra and Aqua spacecraft) and provided by NASA Worldview (https://earthdata.nasa.gov/earth-observation-data/near-real-time).

4.4 Results

4.4.1 HBIs in surface waters

HBI diene II was identified and quantified in all of the surface water samples from the SIZ with a range in concentration of 0.10-0.48 pg mL^{-1} (mean 0.25 pg mL^{-1}, Figure 4.2a, Table 4.1). The mean concentration of HBI diene II in samples from the MIZ (0.10 pg mL^{-1}) was lower than that for the SIZ and this biomarker was absent (or below the limit of quantification; 0.025 pg mL^{-1}) in the sample from the most northerly location within the MIZ and in each of the four samples from the POOZ (Figure 4.2a). In contrast, HBI triene IIIa could be quantified in all samples from the three zones (Figure 4.2b, Table 4.1). The concentration of HBI triene IIIa was 0.21-3.97 pg mL^{-1} in the SIZ with generally higher values in the MIZ (2.24-8.99 pg mL^{-1}). Indeed, the mean HBI triene IIIa concentration in the MIZ (6.00 pg mL^{-1}) was ca six times higher than that in the SIZ (1.06 pg mL^{-1}). However, HBI triene IIIa was present in much lower amounts (0.06-0.09 pg mL^{-1}) in samples from the POOZ, with a mean concentration (0.07 pg mL^{-1}) ca 14 and 85 times lower compared to the SIZ and MIZ, respectively.

An additional tri-unsaturated HBI, HBI triene IIIb, was also detected in all samples, although at lower concentration than for HBI triene IIIa (Figure 4.2c, Table 4.1). Consistent with observations for HBI triene IIIa, concentrations of HBI triene IIIb in the SIZ (0.07-1.17 pg mL^{-1}) were generally lower than in the MIZ (0.80-2.8 pg mL^{-1}), with lowest values observed for samples in the POOZ (0.01-0.02 pg mL^{-1}). The relative enhancement of concentration in the MIZ was also evident from the mean concentration recorded in each of the zones. Thus, the mean HBI triene IIIb concentration in the MIZ (1.92 pg mL^{-1}) was ca 6 and 94 times larger than that in the SIZ (0.31 pg mL^{-1}) and POOZ (0.02 pg mL^{-1}), respectively. Additionally, an enhancement of HBI triene IIIb in SIZ was ca 15 times higher compared to the POOZ (Table 4.1). These observations are

in very good agreement to those seen for HBI triene IIIa, a relationship confirmed by a good correlation between the two biomarkers ($R^{2=}$0.99, Figure 4.3, Table 4.2).

Although the abundances of all HBIs were not sufficiently high in individual samples to enable stable isotopic composition ($\delta^{13}C$) to be determined, a value of -35± 1.5‰ for HBI triene IIIa was acquired by combining several extracts together; however, the

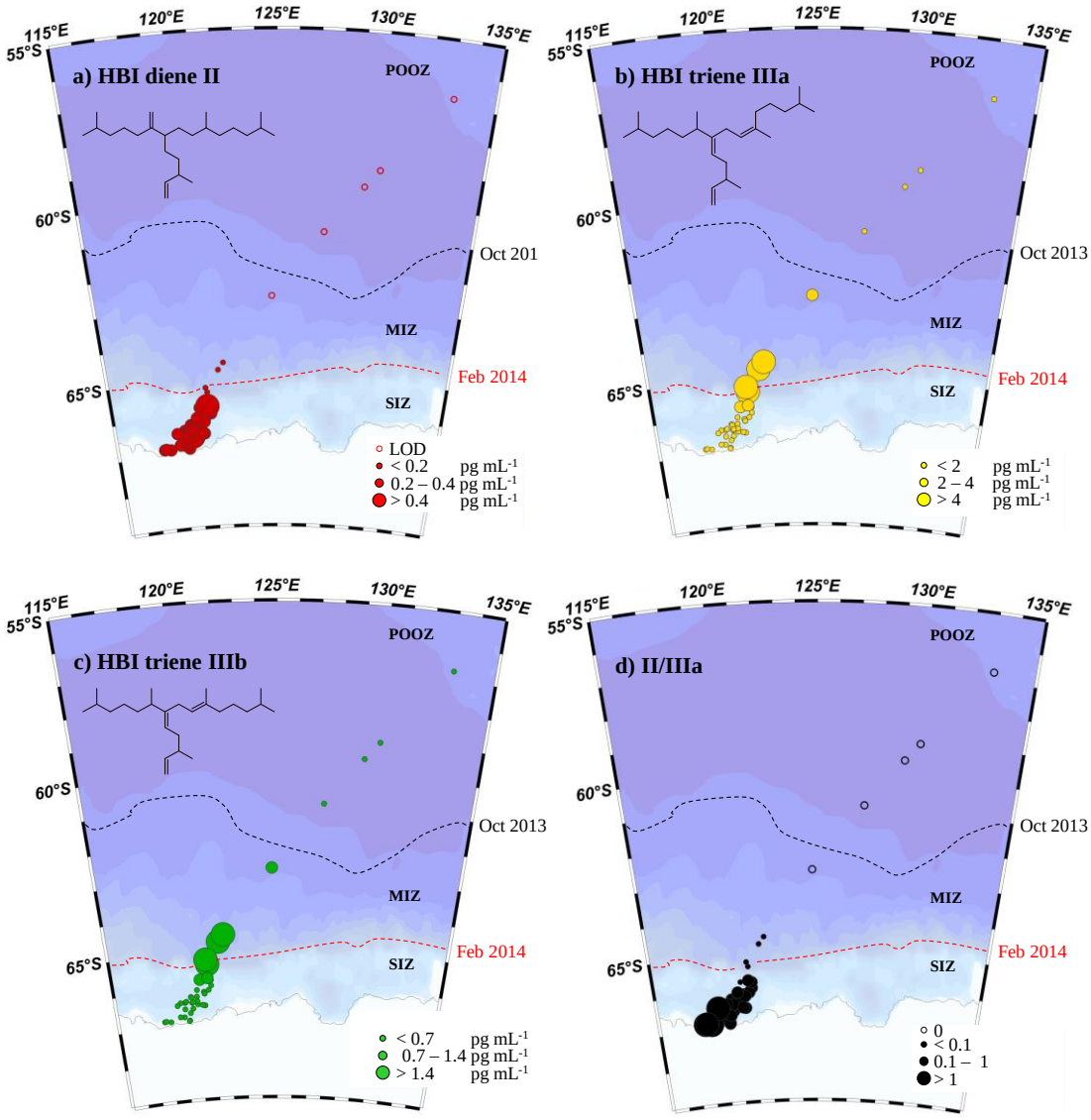

Figure 4.2: Distributions of HBIs in East Antarctic surface waters: a) HBI diene II; b) HBI triene IIIa; c) HBI triene IIIb; and d) the ratio between HBI diene II and HBI triene IIIa (II/IIIa). The position of maximum (October 2013) sea-ice extent prior to sample collection is indicated by black stippled line (NSIDC, Fetterer et al., 2002). The position of the following minimum (February 2014) sea-ice extent in the study area is indicated by the red stippled line (NSIDC, Fetterer et al., 2002). Regions designated as the permanently open ocean zone (POOZ), the marginal ice zone (MIZ) and the seasonal ice zone (SIZ) are also shown.

Table 4.1: The mean (±1 standard deviation) and range in concentrations (pg mL^{-1}) of HBIs in surface water samples from the seasonal ice zone (SIZ), the marginal ice zone (MIZ) and the permanently open ocean zone (POOZ). A summary of the ratio between HBI diene II and HBI triene IIIa (II/IIIa) is also given.

		SIZ (n=38)	MIZ (n=5)	POOZ (n=4)
HBI diene II	mean	**0.25**±0.1	**0.10**±0.07	**0**
	range	(0.10-0.48)	(0-0.17)	-
HBI triene IIIa	mean	**1.06**±0.8	**6.00**±2.85	**0.07**±0.01
	range	(0.21-3.97)	(2.24-8.99)	(0.06-0.09)
HBI triene IIIb	mean	**0.31**±0.2	**1.92**±0.86	**0.02**±0.01
	range	(0.07-1.17)	(0.80-2.80)	(0.01-0.03)
II/IIIa	mean	**0.34**±0.3	**0.02**±0.02	**0**
	range	(0.09-1.33)	(0-0.04)	-

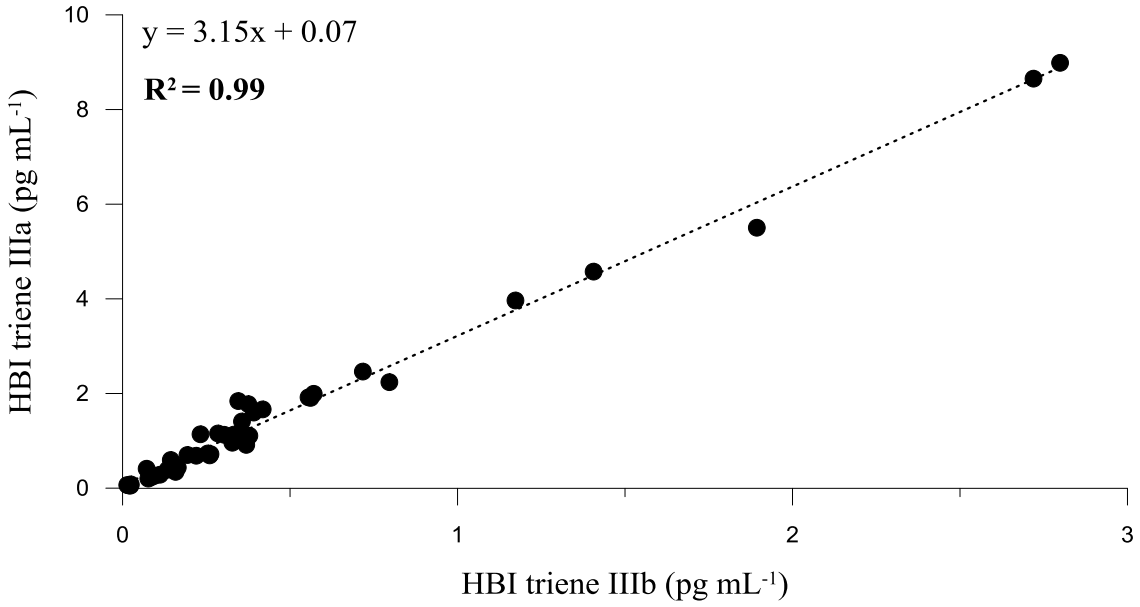

Figure 4.3: The relationship between HBI triene IIIa and HBI triene IIIb in surface water samples.

combined abundances of HBI diene II and HBI triene IIIb was too low to obtain the corresponding values for these HBIs.

Consistent with differences in HBI distributions between zones, concentrations of HBI diene II and both HBI trienes were not at all correlated (Table 4.2). Further, the mean II/IIIa ratio was ca 22 times larger in the SIZ (0.344) compared to the MIZ (0.016) with all individual values also higher in the SIZ (Figure 4.2, Table 4.1).

Table 4.2: Pearson's correlation (r) between biomarkers in surface water samples. Values in bold indicate a significant correlation (p<0.05). The name of each sterol is expressed in short notation, i.e. bras=brassicasterol, 24-metchol=24 methylenecholesterol, 22-dehchol= 22-dehydrocholesterol, chol=cholesterol. For fatty acids (FA), $C_{14:0}$ refers to tetradecanoic FA, $C_{16:0}$ refers to hexadecanoic FA and $C_{16:1}$ refers to *cis*-9-hexadecanoic FA.

	HBI diene II	HBI triene IIIa	HBI triene IIIb	bras	24-metchol	22-dehchol	chol	$C_{14:0}$ FA	$C_{16:0}$ FA
HBI diene II									
HBI triene IIIa	-0.028								
HBI triene IIIb	-0.084	**0.994**							
bras	-0.005	0.223	0.245						
24-methchol	0.042	**0.651**	**0.668**	**0.808**					
22-dehchol	0.111	-0.024	-0.009	**0.820**	**0.543**				
chol	0.238	**0.291**	**0.298**	**0.575**	**0.557**	**0.490**			
$C_{14:0}$ FA	0.094	**0.706**	**0.700**	**0.587**	**0.785**	**0.309**	**0.676**		
$C_{16:0}$ FA	0.100	**0.526**	**0.526**	**0.452**	**0.588**	0.218	**0.848**	**0.885**	
$C_{16:1}$ FA	0.170	**0.687**	**0.680**	**0.521**	**0.746**	0.268	**0.775**	**0.949**	**0.920**

p=0.05;
n=47

4.4.2 Sterols and fatty acids in surface waters

The major sterols in all samples were 24-methylcholest-5,22-dien-3β-ol (brassicasterol), 24-methylenecholesterol, 22-dehydrocholesterol and cholesterol. For brassicasterol (Figure 4.4a, Table 4.3), the mean concentration of 479 pg mL^{-1} in the MIZ was slightly higher than for the SIZ (358 pg mL^{-1}) and this value further decreased in the POOZ (236 pg mL^{-1}), an enhancement of ca 1.3 and 2.0 in the concentration of this lipid in the MIZ compared to the SIZ and the POOZ respectively. The mean concentration of 24-methylenecholesterol in the MIZ (125 pg mL^{-1}) was ca 1.9 and 3.8 times higher than in the SIZ (66 pg $mL^{-1)}$ and in the POOZ (33 pg mL^{-1}), respectively (Figure 4.4b, Table 4.3). A similar trend was observed for cholesterol, the mean concentration of which, was ca 1.8 and 2.3 times higher in the MIZ (452 pg mL^{-1}) compared to the SIZ (251 pg mL^{-1}) and to the POOZ (198 pg mL^{-1}) (Figure 4.4c, Table 4.3). The trend for 22-dehydrocholsetrol (Figure 4.4d, Table 4.3) is somewhat different in that the highest concentration, unlike the other three sterols, was found in the SIZ, with a value of 511 pg mL^{-1} only marginally higher than for the MIZ (452 pg mL^{-1}), an outcome affected by an unusually high concentration of this lipid in station T20 (2612 pg mL^{-1}).

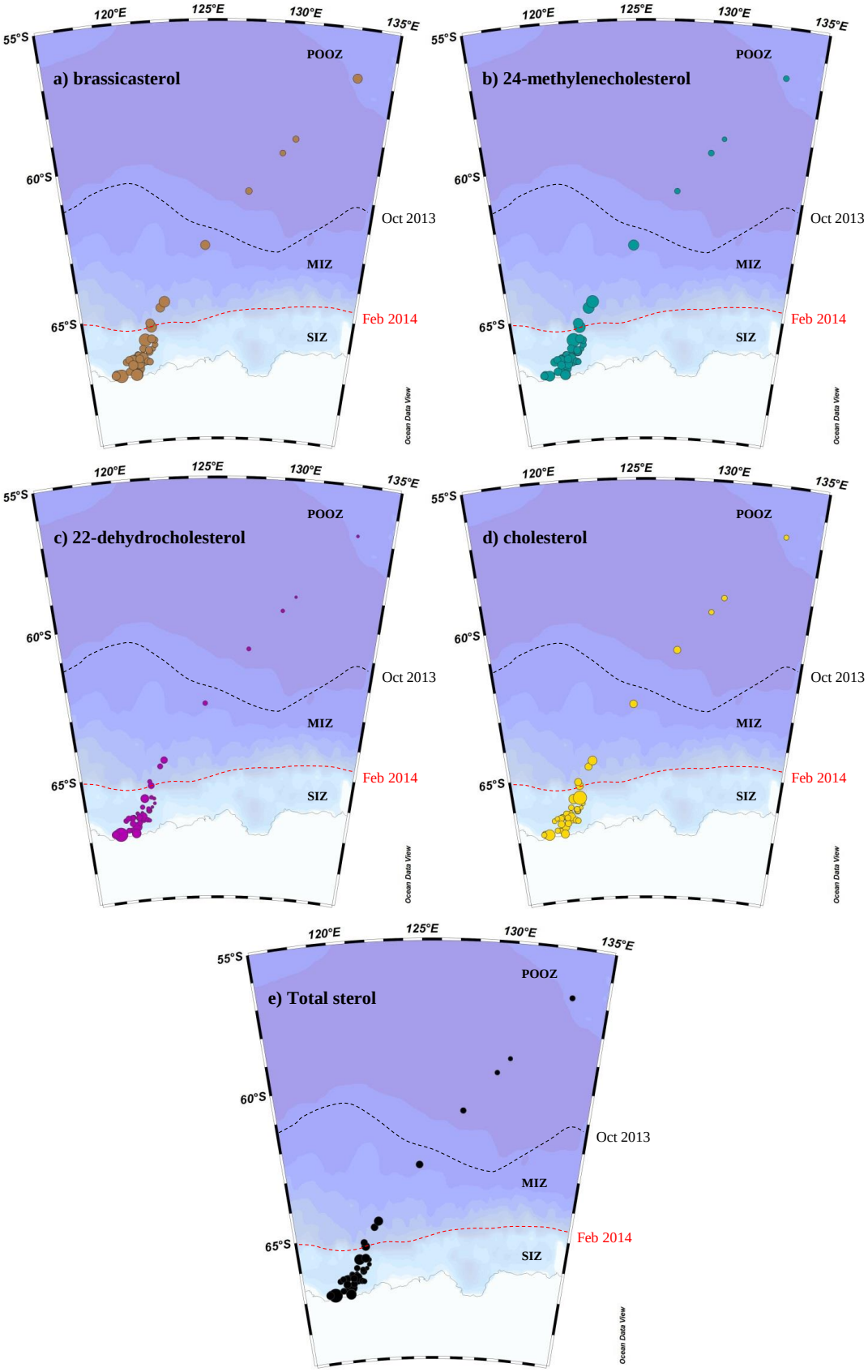

Figure 4.4: Concentrations (pg mL^{-1}) of major and total sterols in East Antarctic surface waters. Circe size in each map normalised to the highest concentration of respective (individual and total) sterol. Position of maximum (October 2013) sea-ice extent prior to sample collection is indicated by black stippled line (NSIDC, Fetterer et al., 2002). Position of following minimum (February 2014) sea-ice extent in the study area is indicated by the red stippled line (NSIDC, Fetterer et al., 2002).

Table 4.3: Mean (±1 standard deviation) and the range of concentrations (pg mL^{-1}) of major and total sterol in surface water from the seasonal ice zone (SIZ), the marginal ice zone (MIZ) and the permanently open ocean zone (POOZ).

		SIZ (n=38)	MIZ (n=5)	POOZ (n=4)
brassicasterol	mean	**358**±196	**479**±92	**272**±123
	range	(132-906)	(381-597)	(188-454)
24-methylenecholesterol	mean	**66**±29	**125**±22	**33**±6
	range	(28-182)	(99-157)	(25-38)
22-dehydrocholestrol	mean	**511**±457	**452**±157	**187**±71
	range	(130-2612)	(291-670)	(118-270)
cholesterol	mean	**251**±167	**340**±61	**198**±68
	range	(97-1007)	(295-445)	(152-299)
Total sterol	mean	**1186**±757	**1397**±318	**691**±146
	range	(419-4186)	(1075-1868)	(528-839)

This value was the highest for any single sterol across the all of the samples analysed, and more than two times higher than the next highest concentration (1171 pg mL^{-1}) of any individual sterol within the sample set. The mean concentration of 22-dehydrocholesterol was at its lowest (187 pg mL^{-1}) in the POOZ and was ca 2.7 times lower than the value in the SIZ. When considering all sterols together, the mean total sterol (brassicasterol + 24-methylenecholesterol + 22-dehydrocholesterol + cholesterol) concentration in the SIZ, MIZ and POOZ was 1190, 1400 and 690 pg mL^{-1} (Figure 4.3e, Table 4.3), respectively. In addition, concentrations of sterols were generally well correlated (Table 4.2), indicating reasonable consistency in the relative composition between sampling sites.

The FA GC-MS chromatograms were dominated by C_{14}, C_{16} and $C_{16:1}$, again consistent with diatoms as the major components in the filtered biota (e.g. Opute, 1974; Volkman et al., 1989; Reuss and Poulsen, 2002). Concentrations of C_{14}, C_{16} and $C_{16:1}$ were also well correlated across all samples (Table 4.2) with some variation in mean concentrations of individual and total FAs (C_{14} + C_{16} + $C_{16:1}$) between the different sampling zones (Figure 4.5; Table 4.4). The mean concentration for C_{14} FA was highest

in the MIZ, with a value of 2636 pg mL^{-1} being ca 2 and 4 times higher than the mean concentration in the SIZ (1264 pg mL^{-1}) and the POOZ (673 pg mL^{-1}), respectively. The same degree of enhancement in the MIZ over the SIZ and the POOZ was also seen for $C_{16:1}$ FA, with a mean concentration of 1910 pg mL^{-1} in the MIZ being ca 2 and 4 times higher than the mean concentration in the SIZ (932 pg mL^{-1}) and the POOZ (475 pg mL^{-1}), respectively. The concentration of C_{16} FAs (Figure 4.5, Table 4.4) was

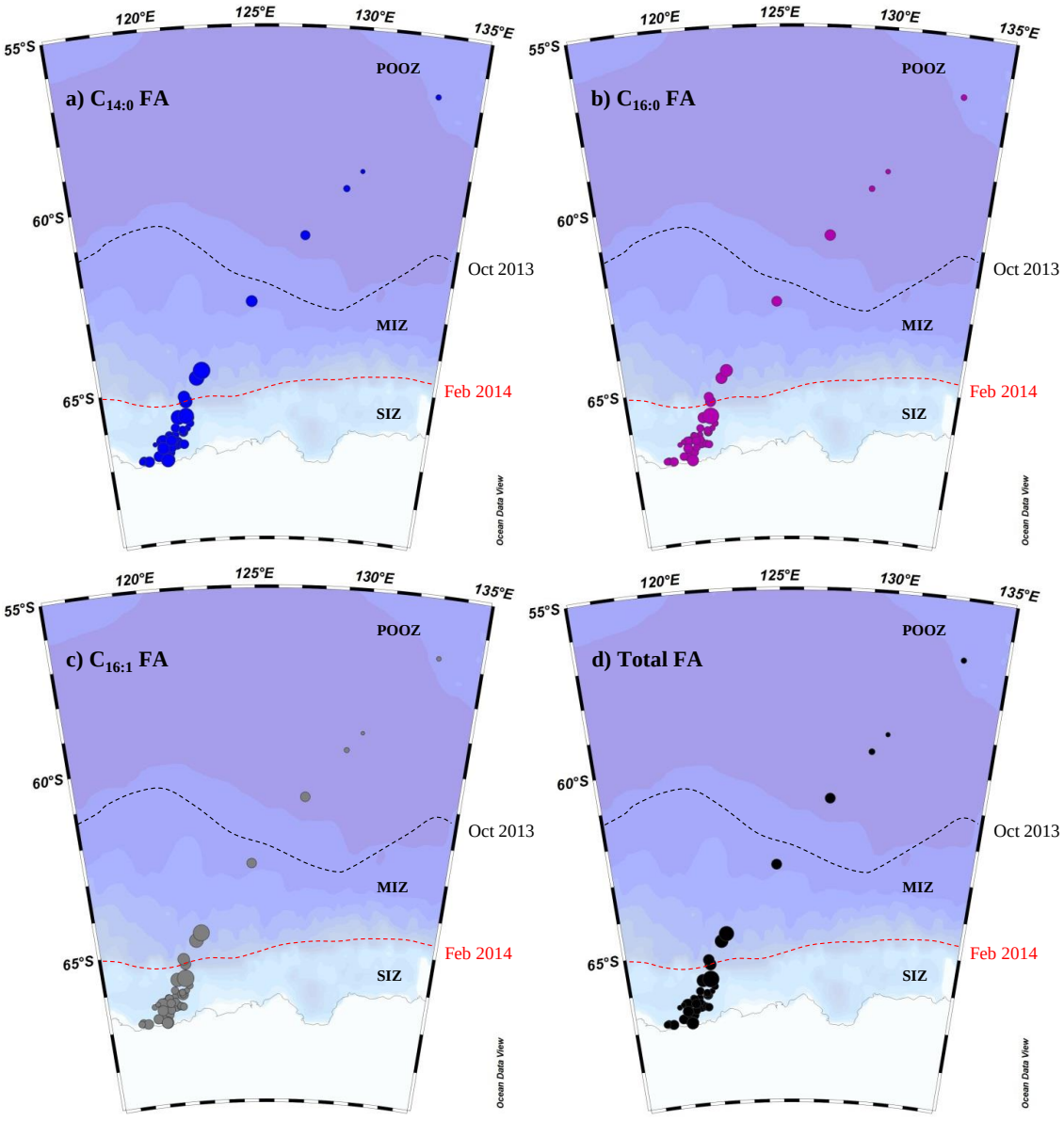

Figure 4.5: Concentrations (pg mL^{-1}) of major and total fatty acids in East Antarctic surface waters. Circe size in each map normalised to the highest concentration of respective (individual and total) sterol. Position of maximum (October 2013) sea-ice extent prior to sample collection is indicated by black stippled line (NSIDC, Fetterer et al., 2002). Position of following minimum (February 2014) sea-ice extent in the study area is indicated by the red stippled line (NSIDC, Fetterer et al., 2002).

Table 4.4: Mean (±1 standard deviation) and the range of concentrations (pg mL^{-1}) of major and total fatty acids in surface water from the seasonal ice zone (SIZ), the marginal ice zone (MIZ) and the permanently open ocean zone (POOZ).

		SIZ (n=38)	MIZ (n=5)	POOZ (n=4)
$C_{14:0}$ FA	mean	**1264±**730	**2636±**920	**673±**425
	range	(279-3352)	(1762-4000)	(322-1282)
$C_{16:0}$ FA	mean	**1817±**1074	**3214±**767	**1504±**1203
	range	(674-7006)	(2354-4304)	(685-3293)
$C_{16:1}$ FA	mean	**932±**582	**1910±**804	**475±**47
	range	(259-3301)	(1100-3094)	(159-1120)
Total FA	mean	**4014±**2317	**7759±**2435	**2652±**2059
	range	(1265-13658)	(5630-11398)	(1166-5696)

generally higher across all the zones, when compared to the other FA (Table 4.4),with the values of 3214 pg mL^{-1}, 1817 pg mL^{-1} and 1504 pg mL^{-1} for the MIZ, the SIZ and the POOZ, respectively; an enhancement of ca 1.8 and 2.1 in the MIZ compared to the SIZ and the POOZ. Consistent with these observations, the mean total FA concentration was higher in the MIZ (7759 pg ml^{-1}) compared to the SIZ (4014 pg ml^{-1}) and POOZ (2652 pg ml^{-1}), an enhancement of ca 1.9 and 2.9 for the MIZ compared to the SIZ and the POOZ, respectively.

4.4.3 HBIs in the water column

In the water column (Figure 4.1), HBI diene II could be identified and quantified in all the water samples from the surface (0-10 m), subsurface (20-60 m) and benthic layer (480-1300 m) of the water column (Figure 4.6, Table 4.5). In the surface layer, concentrations of HBI diene II ranged from 0.10 to 0.35 pg mL^{-1} (mean 0.19 pg mL^{-1}). The concentrations were generally higher in the subsurface layer (Table 4.5) and the mean concentration of 0.30 pg mL^{-1} was ca 1.6 times higher than in surface layer. The lowest concentrations of HBI diene II were observed in the benthic layer, with a mean

concentration of 0.11 pg mL^{-1} being ca 2-3 times lower compared to the surface and subsurface layers.

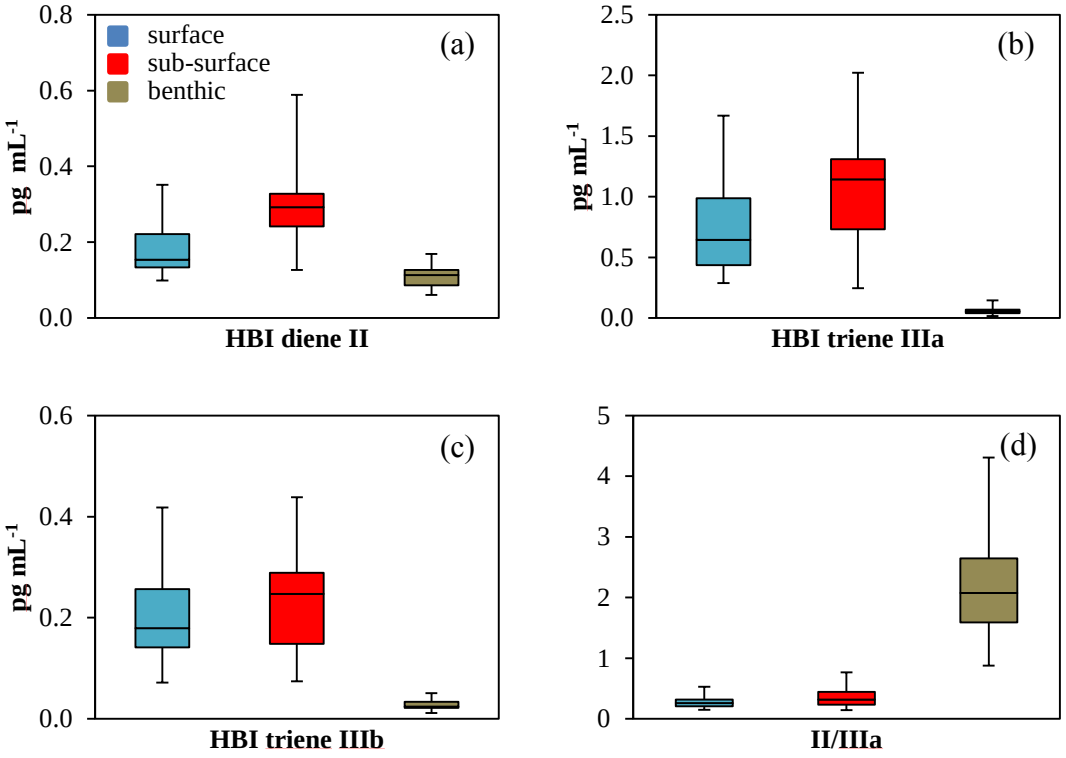

Figure 4.6: Box and whisker plots of HBI concentrations in surface (blue), subsurface (red) and benthic (brown) layers of the water column from the seasonal ice zone (SIZ) in East Antarctica.

Table 4.5: Mean (±1 standard deviation) and range of concentrations (pg mL^{-1}) of HBIs in surface, subsurface and benthic layers of the water column from the sasonal ice zone (SIZ) in East Antarctica (n=12).

		surface	sub-surface	benthic
HBI diene II	mean	**0.19**±0.09	**0.30**±0.12	**0.11**±0.03
	range	(0.10-0.35)	(0.13-0.59)	(0.06-0.17)
HBI triene IIIa	mean	**0.74**±0.40	**1.04**±0.52	**0.06**±0.04
	range	(0.29-1.67)	(0.24-2.02)	(0.02-0.15)
HBI triene IIIb	mean	**0.21**±0.11	**0.24**±0.11	**0.03**±0.01
	range	(0.07-0.42)	(0.07-0.44)	(0.01-0.05)
II/IIIa	mean	**0.28**±0.11	**0.35**±0.17	**2.2**±0.99
	range	(0.15-0.53)	(0.14-0.77)	(0.88-4.31)
IIIb/IIIa	mean	**0.29**±0.06	**0.24**±0.05	**0.52**±0.21
	range	(0.17-0.37)	(0.20-0.38)	(0.16-0.89)

HBI trienes could also be identified and quantified in all the samples (Figure 4.6, Table 4.5), with a trend in concentrations similar to those of HBI diene II. Thus, the mean concentration of HBI trienes IIIa in the surface layer (0.74 pg mL^{-1}) was lower than in the subsurface layer (1.04 pg mL^{-1}). The concentration of HBI triene IIIa was substantially reduced in the benthic layer (Table 4.5), with a mean concentration (0.06 pg mL^{-1}) ca 12 and 17 times lower than in the surface and subsurface layers, respectively. The mean concentration of HBI triene IIIb in the sub-surface layer (0.24 pg mL^{-1}) was marginally higher than the mean concentration in the surface layer (0.21 pg mL^{-1}). The concentration of HBI triene IIIb was similarly as for HBI IIIa, significantly reduced in the benthic layer (0.03 pg mL^{-1}).

4.4.4 Sterols and fatty acids in water column

Unlike for HBIs, concentrations of each major sterol within the water column were highest in the surface water layer and showed a general decrease in values towards the benthic layer (Figure 4.7, Table 4.6). Thus, for brassicasterol, the mean concentration in the surface layer (355 pg mL^{-1}), dropped to 201 and 44 pg mL^{-1} in the subsurface and benthic water layers, respectively. For 24-methylenecholesterol, the mean concentration of 60 pg mL^{-1} in the surface layer fell to 35 pg mL^{-1} in the sub-surface layer and 8 pgmL^{-1} in the benthic layer. The concentration of 22-dehydrocholesterol was generally highest amongst all of the sterols, with a mean concentration of 500 pg mL^{-1}. In the subsurface and benthic layers, this value reduced to 284 and 49 pg ml^{-1}, respectively. Finally, the mean concentration of cholesterol in the surface layer was 237 pg mL^{-1}, which reduced to 124 and 76 pg mL^{-1} in the subsurface and benthic layers. When considering all sterols together, the mean total sterol (brassicasterol + 24-methylenecholesterol + 22-dehydrocholesterol + cholesterol) concentration in the

surface layer (1150 pg mL^{-1}) was ca 1.8 and 6.5 higher than in the subsurface (644 pg mL^{-1}) and benthic (177 pg ml^{-1}) layers, respectively.

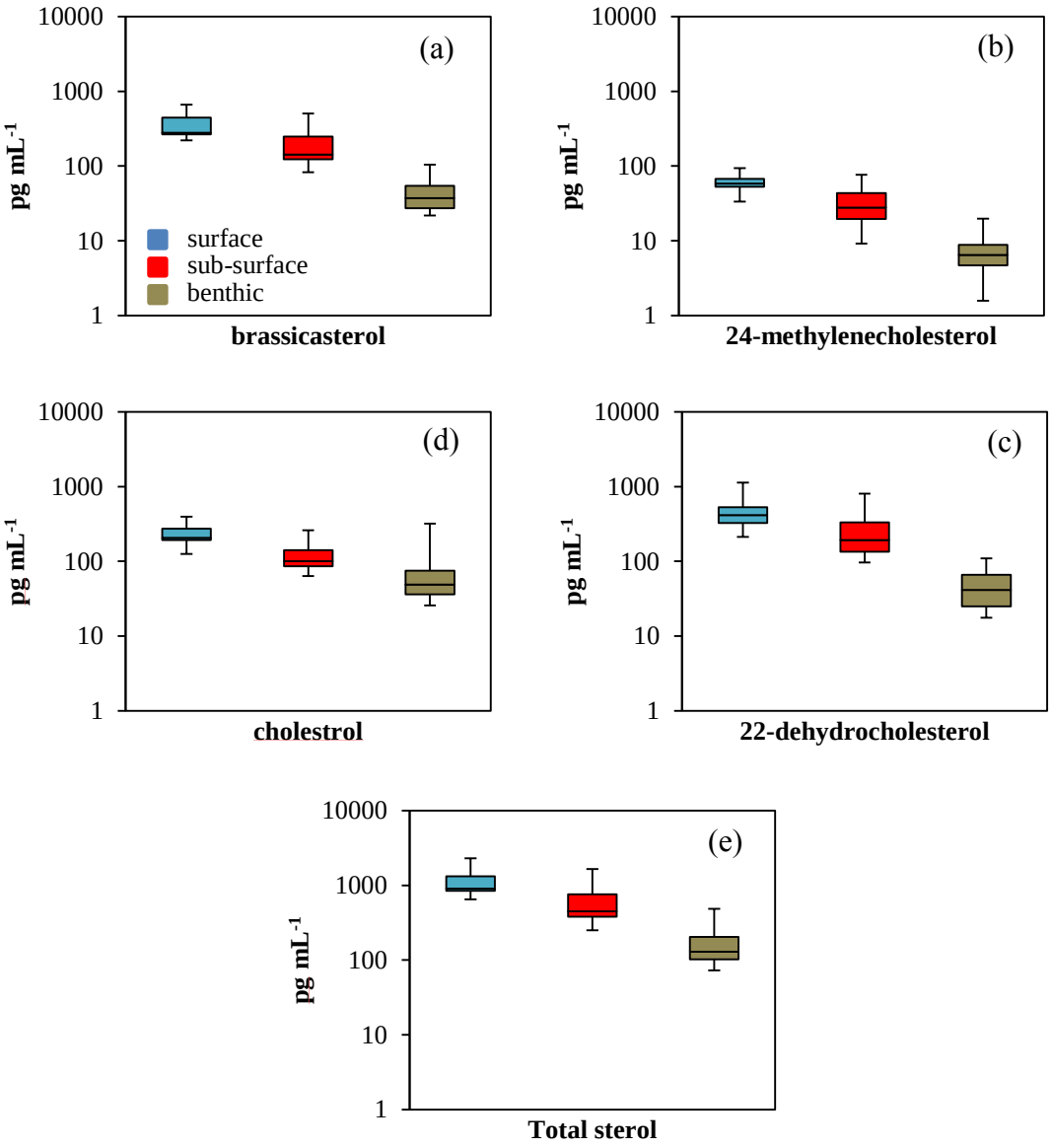

Figure 4.7: Box and whisker plots of major and total sterols concentration in surface (blue), sub-surface (red) and benthic (brown) layer of the water column from the seasonal ice zone (SIZ) in East Antarctica. Concentrations of individual and total sterols are displayed in log_{10} scale.

Table 4.6: Mean (±1 standard deviation) and range of concentrations (pg mL^{-1}) of individual and total sterols in surface, subsurface and benthic layers of the water column from the surface ice zone (SIZ) in East Antarctica (n=12).

		surface	sub-surface	benthic
brassicasterol	mean	**355**±138	**201**±122	**44**±24
	range	(221-664)	(82-506)	(22-104)
24-methylene cholesterol	mean	**60**±16	**35**±22	**8**±5
	range	(33-94)	(9-76)	(2-20)
22-dehydrocholesterol	mean	**500**±283	**284**±221	**49**±31
	range	(212-1135)	(97-801)	(18-110)
cholesterol	mean	**237**±80	**124**±62	**76**±81
	range	(125-397)	(63-259)	(26-319)
Total sterol	mean	**1151**±503	**644**±415	**177**±120
	range	(650-2290)	(252-1634)	(73-487)

Concentrations of fatty acids in general, showed the same trend within the water column as the sterols (Figure 4.8, Table 4.7). Thus, highest concentrations were observed in the surface layer, with a gradual drop in concentration towards the benthic layer. The mean concentration of C_{14} FA in the surface layer was 1226 pg mL^{-1}. This value then dropped to 895 and 296 pg mL^{-1} in the subsurface and benthic layers, respectively. For $C_{16:1}$ FA, the mean concentrations of 784 pg mL^{-1} observed in the surface layer fell to 552 pg mL^{-1} in the subsurface layer and 342 pg mL^{-1} in the benthic layer. The concentrations of C_{16} FAs were generally higher than the other FAs across all the water column layers. In line with the observations for the other two FAs, the mean concentration of 1824 pg mL^{-1} in the surface layer, reduced to 1542 pg mL^{-1} and 952 pg mL^{-1} in the subsurface and benthic layers. Consistent with these observations, the mean total FA concentration was higher in the surface layer (3834 pg ml^{-1}) compared to the subsurface (2898 pg ml^{-1}) and benthic (1589 pg ml^{-1}) layer, an enhancement of ca 1.3 and 2.4, respectively.

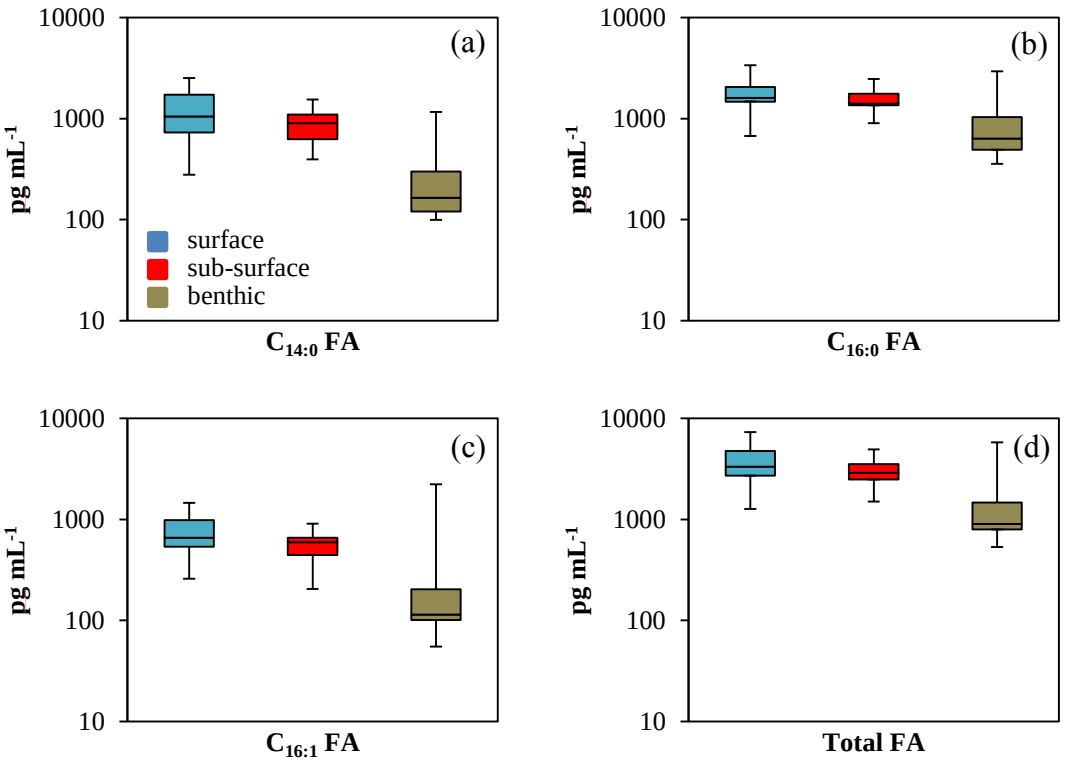

Figure 4.8: Box and whisker plots of major and total fatty acid concentrations in surface (blue), subsurface (red) and benthic (brown) layers of the water column from the seasonal ice zone (SIZ) in East Antarctica. Concentrations of individual and total sterols are displayed in $\log_{10}$ scale.

Table 4.7 Mean (±1 standard deviation) and range of concentrations (pg mL^{-1}) of individual and total fatty acids (FA) in surface, subsurface and benthic layers of the water column from the seasonal ice zone (SIZ) in East Antarctica (n=12).

		surface	sub-surface	benthic
$C_{14:0}$ FA	mean	**1226**±739	**895**±358	**296**±311
	range	(279-2509)	(394-1542)	(100-1162)
$C_{16:0}$ FA	$C_{14:0}$ FA	**1824**±735 (674-3367)	**1542**±423 (899-2463)	**952**±784 (357-2937)
$C_{16:1}$ FA	mean	**784**±402	**552**±197	**342**±613
`	range	(251-1452)	(205-908)	(55-2230)
Total FA	mean	**3834**±836	**2898**±945	**1589**±1588
	range	(1265-7288)	(1498-4913)	(533-5759)

4.5 Discussion

4.5.1 Lipid distributions within different sea-ice settings

The occurrence of the di-unsaturated HBI diene II in seasonally sea-ice covered surface waters within the polynya, west of the Dalton Iceberg Tongue, and further offshore in the MIZ is consistent with production of this biomarker by sea-ice diatoms during the spring bloom (Johns et al., 1999; Nichols et al., 1988), followed by their release into the upper water column during sea-ice melt. In addition, the absence of HBI diene II within the POOZ further supports the notion of selective production of this biomarker by certain (as yet unknown) diatoms affiliated with sea-ice. Consistent with both of these observations, sympagic diatoms have previously been identified in near-coastal surface waters off Adélie Land (also East Antarctica) soon after ice melt, while the species composition further offshore was dominated by pelagic counterparts (Riaux-Gobin et al., 2011). Unfortunately, the abundance of HBI diene II in the SIZ and MIZ samples was too low for its stable isotopic composition (and thus confirmation of its sea-ice origin) to be determined, although this HBI has been reported previously in sea-ice from a nearby location (ca 66°S; 110°E) (Massé et al., 2011) with an isotopic signature ($\delta^{13}C$=-5.7‰) characteristic of a sea-ice diatom source. In fact, HBI diene II, identified previously in sea-ice and sediments from other Antarctic locations, is always isotopically heavy, and has not been reported in Antarctic phytoplankton, suggesting that its production is highly specific to certain sea-ice diatoms. The source of HBI diene II in water samples analysed here is therefore believed to be sea-ice diatoms that were released into the surface waters during ice melt. Further, the overall increased concentration of HBI diene II in the SIZ samples compared to those from the MIZ is likely reflecting more favourable conditions for sea-ice diatom growth due, mainly, to longer seasonal sea-ice cover. Indeed, at the time of sampling

(9 February-10 March 2014), remnant sea-ice was still evident in the SIZ (L. Armand, personal communication), but the MIZ was characterised by clear, open water conditions. The maximum winter sea-ice extent in the region is normally reached during September and October (Figure 4.1) with spring retreat occurring during November and December, coincident with (at least some) sea-ice diatom growth (e.g. Arrigo et al., 2010). Although there have been no systematic time-series investigations of the production of HBI diene II in Antarctic sea-ice, the accumulation of IP_{25} in Arctic sea-ice has been shown to closely parallel the spring bloom (Belt et al., 2013; Brown et al., 2011). As such, the corresponding accumulation of HBI diene II in Antarctic sea-ice might be expected to be highest in regions of longer spring sea-ice duration (i.e. within the SIZ), with lower amounts within the MIZ due to competing sea-ice melt. Consistent with this suggestion, HBI diene II was not detected in the most northerly sampling location within the MIZ, where the sea-ice margin had already retreated further south by December 2013 (Figure 4.1). Finally, the selective production of HBI diene II by sea-ice diatoms likely explains the poor overall correlations between its concentration and those of the other lipids (Table 4.3), which could all be identified in each of the SIZ, MIZ and POOZ.

The distribution pattern of HBI triene IIIa is substantially different to that of HBI diene II, indicating contrasting environmental control over its production. For example, HBI triene IIIa could be identified and quantified in samples from all locations, consistent with biosynthesis by phytoplankton rather than sea-ice diatoms, a conclusion supported further by an extremely light isotopic signature of this lipid in the current study ($\delta^{13}C$=-35±1.5‰) and in previous reports when measured in Antarctic phytoplankton ($\delta^{13}C$=-40.2±0.5‰, Massé et al., 2011) and sediments from both the Antarctic ($\delta^{13}C$=-41.6±1.1‰, Massé et al., 2011) and the Arctic ($\delta^{13}C$=-35 to -40‰, Belt et al., 2008). Although the sources of HBI IIIa in Antarctic (or Arctic)

phytoplankton is not known, diatoms belonging to the *Pleurosigma* genus are likely candidates, since some of these, including planktonic species, are known producers of HBI trienes (including HBI triene IIIa) in culture (Belt et al., 2000a, 2001b; Grossi et al., 2004). Curiously, despite the ubiquity of HBI triene IIIa in samples from each zone, the mean concentrations were markedly higher in the SIZ compared to the POOZ and even higher in the MIZ (Figure 4.2). In previous paleo Antarctic sea-ice studies based on HBI lipids in marine sediments, the down-core variability of HBI triene IIIa in particular has been interpreted in terms of changes in the extent or duration of open-water conditions, with the corresponding abundances of HBI diene II providing the complementary responses in terms of sea-ice duration (Barbara et al., 2010, 2013; Denis et al., 2010; Massé et al., 2011; Collins et al., 2013; Etourneau et al., 2013). In general, opposing trends in HBI diene II and HBI triene IIIa provide some support to such interpretations. However, in a study focussing on glacial age sediments (35-65 ka) from the Scotia Sea in the South Atlantic, Collins et al. (2013) observed in-phase changes in HBI diene II and HBI triene IIIa concentrations and suggested that these might be better interpreted in terms of the latter being produced by phytoplankton that thrive at the ice edge, with low seasonality shifts favouring production of both biomarkers. Further, Etourneau et al. (2013) interpreted late Holocene increases in HBI diene II and HBI triene IIIa within a western Antarctic Peninsula record as indicating increasing sea-ice extent during colder winters (increased HBI diene II) coeval with warmer summers (increased HBI IIIa). However, no *in situ* data have thus far been presented to test either hypothesis further. In the current study, surface water data certainly indicate enhancement of HBI triene IIIa within the MIZ (relative to the POOZ) as the sea-ice edge retreats during spring, but with concentrations of HBI diene II that are lower than for the SIZ. Conversely, a reduction in HBI triene IIIa in the SIZ (relative to the MIZ) is accompanied by the highest HBI diene II concentrations as described earlier. Such shifts

in the relative concentrations of HBI diene II and HBI triene IIIa in particular are even more evident in the II/IIIa ratio between the three zones with all values in the SIZ being larger than those for the MIZ (Figure. 4.2, Table 4.1). Therefore, surface water sample data indicate that relatively low HBI diene II and high HBI triene IIIa (and thus low II/IIIa) are characteristic of the MIZ, while high HBI diene II and low HBI triene IIIa (high II/IIIa) reflect conditions of longer seasonal sea-ice cover found in the SIZ.

The abundance distribution of another tri-unsaturated HBI, HBI triene IIIb, shows a very strong relationship to HBI triene IIIa, indicating the same environmental control over its production. The strength of the relationship between HBI triene IIIa and HBI triene IIIb also suggests that they are likely originated from the same source. Indeed, it is noted that these two biomarkers have been identified in a diatom culture of *Pleurosigma intermedium* (Belt et al., 2000b). They have also been observed previously in phytoplankton and sediment material from Antarctica (Massé et al., 2011), with a light isotopic signature ($\delta^{13}C$=-35 to 38‰) supporting their likely phytoplankton origin. The apparent environmental sensitivity of HBI triene IIIb to the overlying oceanographic conditions potentially makes it an additional biomarker of phytoplankton within the Southern Ocean.

In order to investigate the sensitivity of HBI triene IIIa and HBI triene IIIb to the local sea-ice conditions in more detail and, in particular, to assess the significance of the enhancement in the MIZ compared to the POOZ, their distributions were compared to the concentrations of selected marine diatom sterols and FAs as more generic indicators of primary productivity. In contrast to the data for HBIs IIIa and IIIb, the concentrations of both lipid classes (individual and totals) were much more evenly distributed between the SIZ, the MIZ and the POOZ. The mean concentrations of total sterols and FAs were, however, highest in the MIZ, although the relative enhancements were not as large as those of the HBI trienes (Figures 4.2-4.4). As such, all three markers of marine diatom

productivity (HBI trienes, sterols, FAs) show increased values within the MIZ, and elevated mean (February/March) Chl *a* concentration was also evident within the MIZ (0.75 mg m^{-3}) compared to the POOZ (0.11 mg m^{-3}) and the SIZ (0.3 mg m^{-3}) (Figure 4.9). The largest (clearest) change in mean lipid concentration between the different sampling zones is especially evident through inspection of triene III (IIIa+IIIb)/total sterol and triene III/total FA ratios (Figure 4.10 a and b, Table 4.8), with the highest values within the MIZ due to enhanced concentrations of HBIs IIIa and IIIb (Figure 4.2).

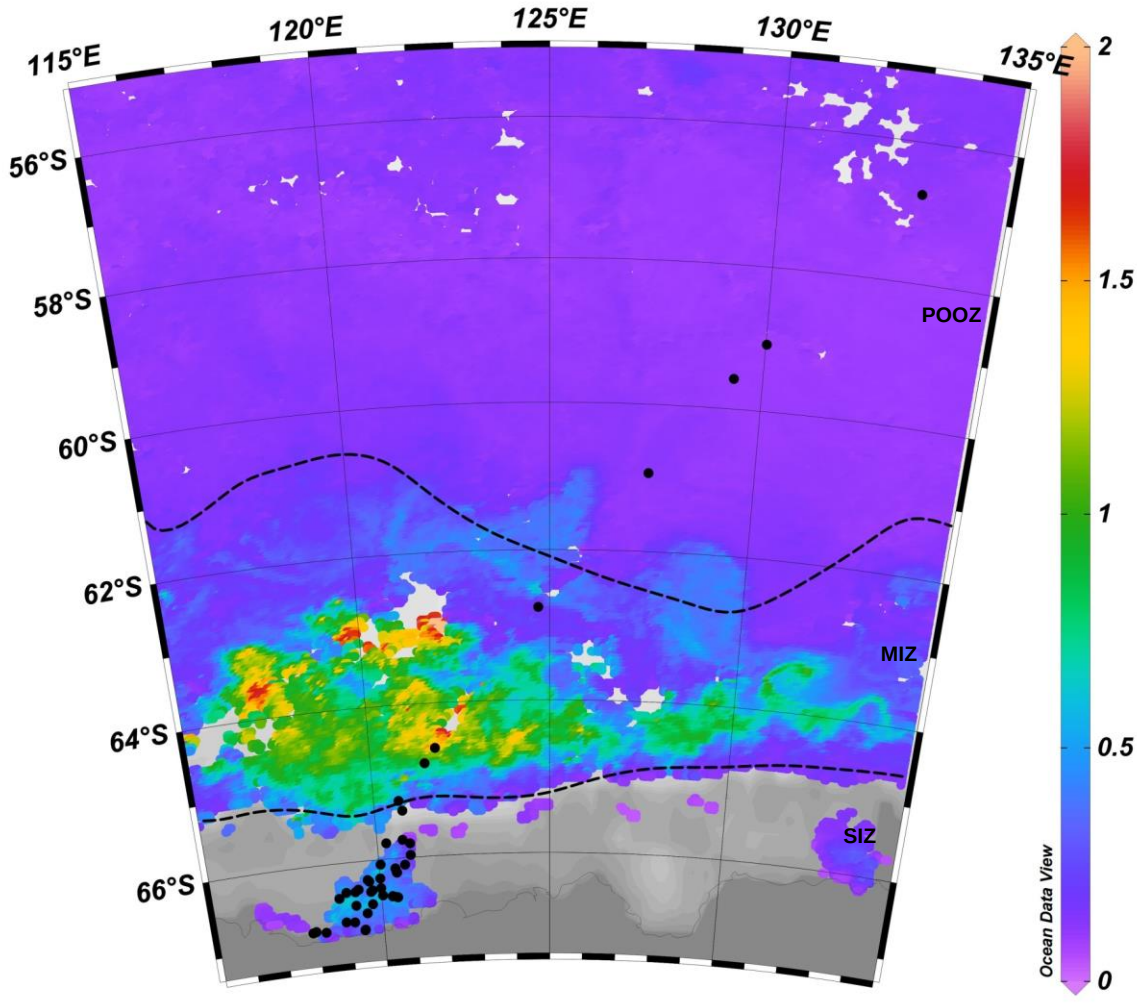

Figure 4.9: Mean February chlorophyll *a* (Chl *a*, mg m^{-3}) distribution across the sampling region. Data courtesy of NASA (2014). Position of maximum (October 2013) and following minimum (February 2014) sea ice extent, prior to and after sample collection, are indicated by black stippled lines (NSIDC, Fetterer et al., 2002).

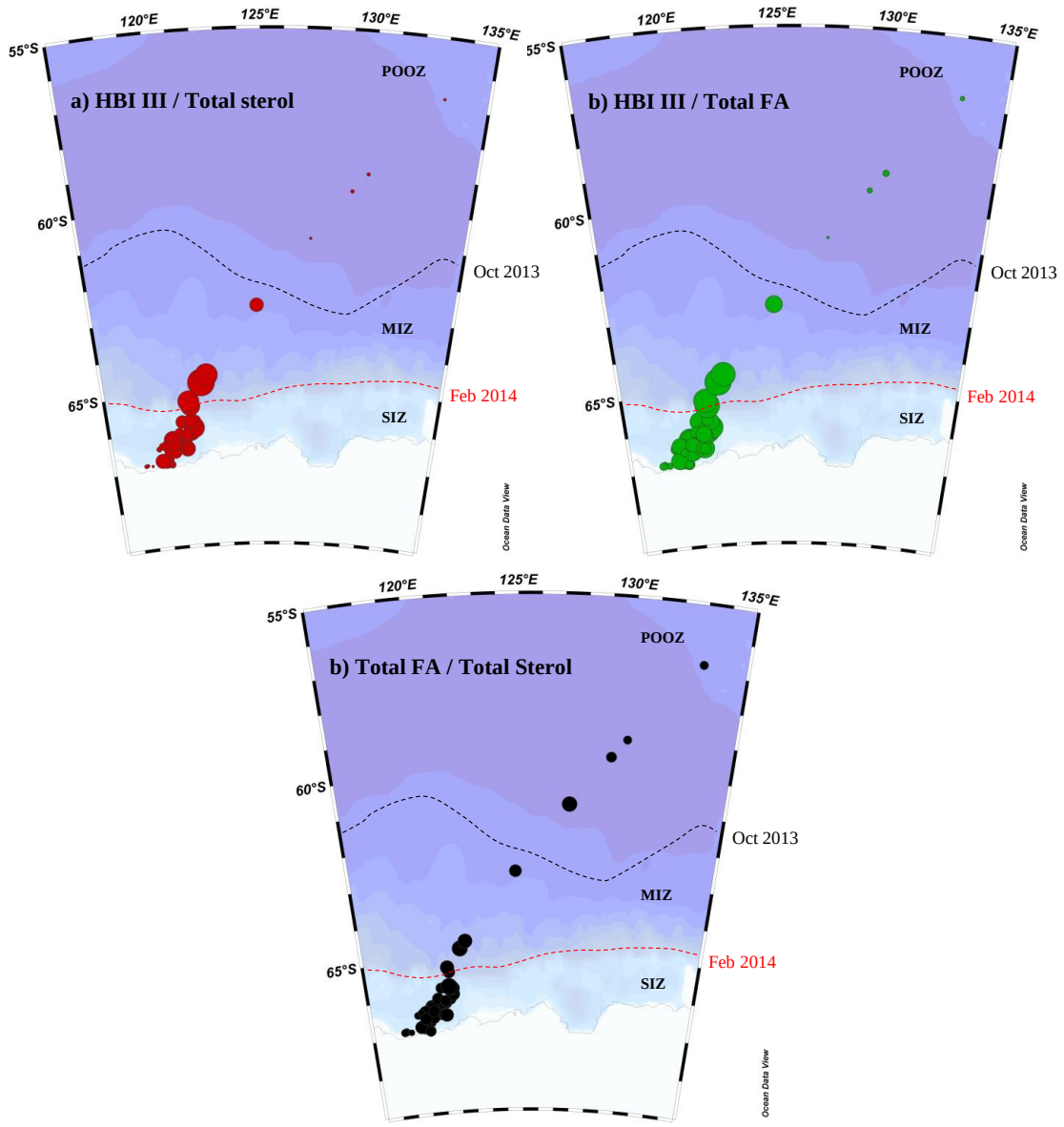

Figure 4.10: Distribution of: (a) HBI III/total sterol; (b) HBI III/total fatty acids (FA); and (c) total FA/total sterol in East Antarctic surface waters. Circe size in each map normalised to the highest ratio. The position of maximum (October 2013) sea-ice extent prior to sample collection is indicated by the black stippled line (NSIDC, Fetterer et al., 2002). The position of the following minimum (February 2014) sea-ice extent in the study area is indicated by the red stippled line (NSIDC, Fetterer et al., 2002).

Table 4.: Mean and range of biomarker ratios in the surface ice zone (SIZ), marginal ice zone (MIZ) and the permanently open ocean zone (POOZ) in East Antarctic surface waters.

		SIZ (n=38)	MIZ (n=5)	POOZ (n=4)
HBI III/ Total sterol	mean	**1.5×10^{-3}**	**5.7×10^{-3}**	**1.3×10^{-4}**
	range	(9.6×10^{-5}-5.1×10^{-3})	(2.5×10^{-3}-9.2×10^{-3})	(9.8×10^{-5}-1.8×10^{-4})
HBI III/ Total FA	mean	**3.8×10^{-4}**	**9.9×10^{-4}**	**4.7×10^{-5}**
	range	(8.3×10^{-5}-9.5×10^{-4})	(5.4×10^{-4}-1.3×10^{-3})	(1.5×10^{-5}-7.2×10^{-5})
Total FA/ Total sterol	mean	**3.8**	**5.6**	**3.6**
	range	(1.2-8.1)	(4.3-7.3)	(2.2-6.8)

At this stage, it is not clear what the reason behind the particular enhancement of HBI trienes in MIZ is, although it may, potentially, be attributed to a preference (or tolerance) of the species that biosynthesise these HBIs to the stratified and nutrient-rich surface waters found at the sea-ice edge, which are well-known to promote phytoplankton productivity in the Antarctic (e.g. Niebauer and Alexander, 1985; Smith and Nelson, 1985; Korb et al., 2005) and the Arctic (Perrette et al., 2011; Sakshaug and Skjoldal, 1989).

In contrast, the smaller changes in relative concentration of total sterols and total FAs between the different sampling regions likely reflect more general variations in diatom productivity, especially as these are lipids common to all diatoms. In addition, there may also be additional contributions to the FA budget from some other microalgae or bacteria (e.g. Volkman et al., 1989; Nichols et al., 1993) that further influence the distributions between zones, and this may explain, in part, the slightly different distributions of sterols and FAs between sampling regions (Figures 4.4 and 4.5, Tables 4.4 and 4.6), most clearly observed through somewhat variable (mean and range) total FAs/total sterol ratios (Figure 4.7c, Table 4.5). However, certain signature bacterial FAs such as iso- and anteiso-branched C_{15} acids were either extremely low in abundance (total concentration always less than ca 1.5% of total FAs) or absent (e.g. C_{17} FAs), suggesting that bacteria probably had a relatively small impact on total FA content.

4.5.2 The role of the polynya

Sea-ice cover within the SIZ typically reaches a maximum during late September/early October, with some partial break-up by the end of October (Figure 4.11a). A distinctive feature of the SIZ within the current study, however, is the polynya, located west of the Dalton Iceberg Tongue (Figure 4.11b). Polynya formation occurs as a consequence of a

natural embayment between the Dalton Iceberg Tongue to the east and landfast ice off Law Dome to the west, which limits sea-ice export via the westward-flowing Antarctic Coastal Current. Together with katabatic winds that funnel along the Moscow University Ice Shelf, this embayment results in recurrent ice formation and break-up leading to a 'sea-ice factory' scenario that is responsible for sea-ice retention even into summer, which contrasts the advance/retreat cycle that occurs further north. Importantly, from a marine sediment-based proxy perspective, with horizons representing multi-year accumulation, a polynya scenario is a common feature for the SIZ on an annual basis. In any case, extended sea-ice duration within the polynya is likely favourable for enhanced sea-ice diatom growth and thus, production of HBI diene II, as seen in the SIZ samples (Figure 4.2a). On the other hand, the occurrence of transient phases of open-water within the polynya (Figure 4.11b) potentially explains the somewhat higher abundances of HBI trienes (and of sterols and FAs; Figures 4.4, 4.5), at least when compared with values in the POOZ. Therefore, relatively high abundances of HBI diene II and HBI triene IIIa in the sedimentary record, as observed here within the SIZ water samples, may reflect polynya-type conditions rather than long seasonal sea-ice cover followed by warmer summers, as has been suggested previously (Etourneau et al., 2013). In addition, the II/IIIa ratio, within the SIZ samples presented here, span at least one order of magnitude (Table 4.1), which is typical of the range seen in sedimentary records, and interpreted previously as indicating quite major shifts in either sea-ice extent and/or open water conditions during summers (Barbara et al., 2010, 2013; Etourneau et al., 2013). Of course, whether sedimentary II/IIIa ratios closely reflect those of the overlying water samples, or if the variation seen in the latter becomes homogenised within sediments, is in need of further investigation; however, on the basis of the data presented here, it is possible that some control over substantial variations in

sedimentary II/IIIa may not be limited to large-scale changes in sea-ice extent, but may also be influenced by polynya-driven processes.

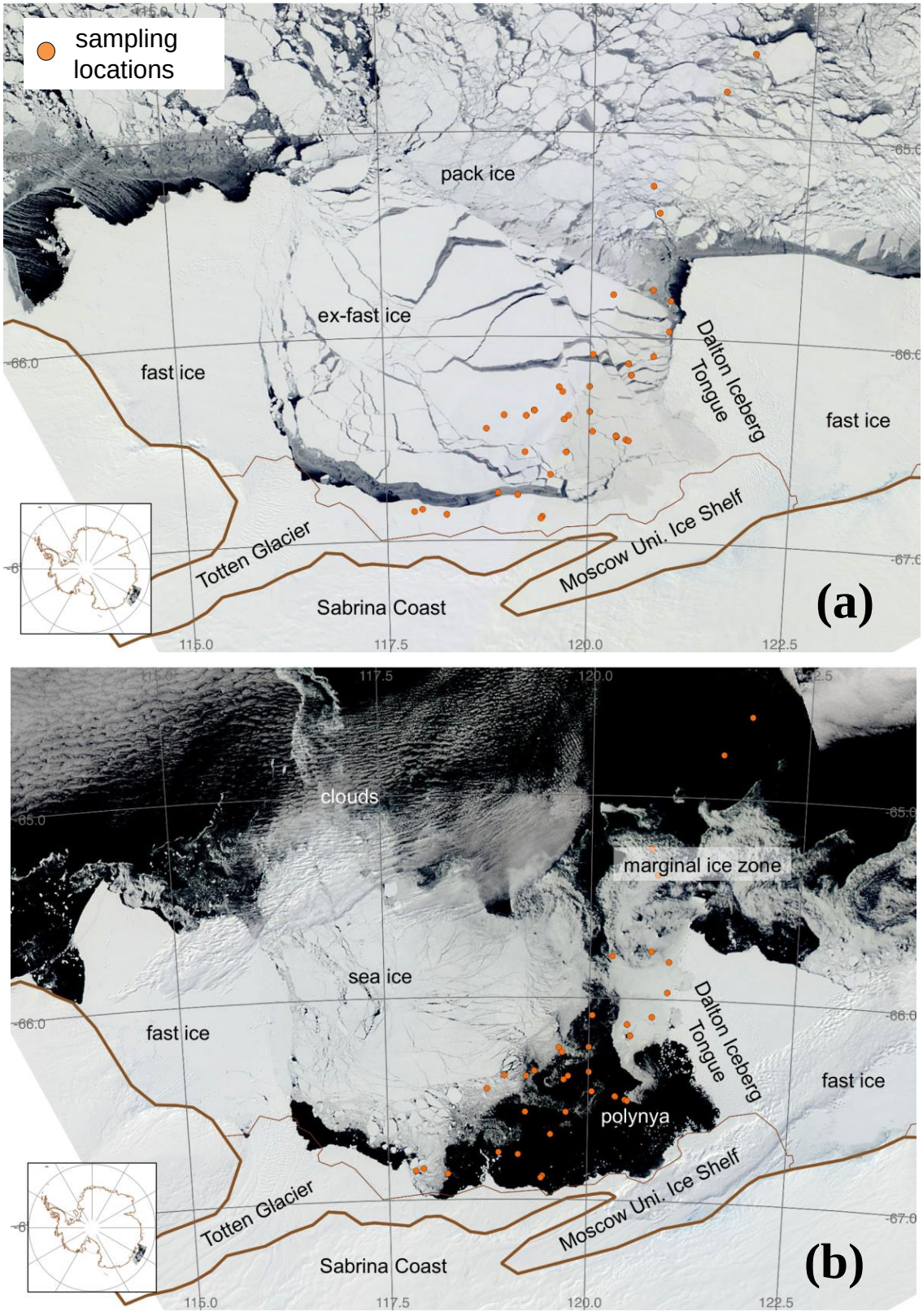

Figure 4.11: Satellite-derived visible images of the study region (composite of data from the MODerate Resolution Imaging Spectroradiometer (MODIS), flown on two NASA spacecraft (Terra and Aqua)). Imagery was recorded on (a) 26 October 2013 and (b) 18 February 2014.

4.5.3 Lipid distributions in the water column

In order to investigate how the abundances of various biomarker lipids change during the sedimentation process, analysis of water column samples was conducted from 12 CTD stations (Figure 4.1). Each station was located within the SIZ and water samples from three different depths of the water column were analysed. Accordingly, the water samples collected within the top 10 m of the water column were considered as the surface layer (e.g. Section 4.3.1). The subsurface layer, also thought to represent the chlorophyll maximum depth within each station, was collected between 20 and 60 m water depth. Samples analysed at the bottom of the water column (benthic layer) represent a considerable increase in the water depth in comparison to surface and subsurface layers. Thus, samples analysed from the benthic layer were collected at water depths between 480 and 1300 m.

When considering all three lipids classes (HBIs, sterols and FA), different observations can be seen for the HBIs compared to those of sterols and FA (sections 4.4.3 and 4.4.4). Thus, within the water column, the mean concentrations of HBIs showed a relative increase form the surface to the subsurface layers (Figure 4.6). This was then followed by a considerable reduction in concentration in the benthic layer. The reason behind this slight increase within the photic part of the water column (surface to sub-surface) is as yet not clear, although one explanation might be an increased number of the specific diatom species responsible for biosynthesis of these biomarkers in the subsurface layer compared to the surface layer. This could result from accumulation of diatom species towards the strong pycnocline layer that prevents vertical migration of the species towards the benthic layer. Alternatively, the increase in subsurface layer might represent a combination of species accumulation (in the case of HBI diene II) and biosynthesis of some biomarkers (in the case of HBI trienes) by species thriving in the nutrient rich parts of the water column. Additionally, relatively high variation in abundances of all

three HBIs in the photic part of the water column might be characteristic of a number of other processes, such as wind mixing, that occur in the uppermost part of the water column. Therefore, further analysis of water column samples, along with measurements of some other variables, such as temperature, salinity or species composition might provide more information behind these observations. Species composition, of selected samples is currently being conducted by a collaborating institution in Australia.

Concentrations of HBI diene II and both HBI trienes were considerably reduced in the benthic layer of the water column. The largest reduction was observed with HBI triene IIIa, with concentrations between the subsurface and benthic layers being reduced by ca 17 times. Somewhat smaller reductions were observed for HBI triene IIIb (×8) and the smallest degree of reduction was observed for HBI diene II, where concentrations fell by only ca 3 times between the subsurface and benthic layers. In general, the variation in the level of reduction of each of the HBIs towards the benthic layer, agrees well with variable degradation rates of these biomarkers under laboratory conditions (Rontani et al., 2011, 2014) and represents a plausible explanation behind the observations. Alternatively, variation in the HBI composition in benthic layer could be explained by different sinking rates of sea-ice vs phytoplankton diatoms once released into the water column, a suggestion that will require further confirmation through, for example, taxonomic investigation of the samples. A generally greater reduction in HBI trienes compared to HBI diene II can also be observed through the change in the ratio of HBI diene II to HBI triene IIIa. Thus, while the mean ratio was relatively constant between the surface (0.28) and subsurface layers (0.35) of the water column (Table 4.5), a considerable increase in the ratio was evident in the benthic layer (2.2). Further, individual II/IIIa ratios (i.e. from each CTD station) were always higher in the benthic layer compared to the surface/subsurface layers.

Under laboratory conditions, the reactivities of HBI trienes IIIa and IIIb have been shown to be approximately the same, although with slightly higher reactivity rates observed for HBI triene IIIb over HBI triene IIIa (Rontani et al., 2014). In line with this, the ratio between HBI trienes IIIb and IIIa (IIIb/IIIa) might be expected to decrease throughout the water column, although this is not the case in water samples from this study (Table 4.6). While the ratio IIIb/IIIa is relatively constant in the photic part of the water column (0.29 and 0.24), in the benthic layer, this ratio increases (0.52). This suggests preferential alteration of HBI triene IIIa over HBI triene IIIb during the vertical transport in the water column, an observation that will also require further investigation.

Unlike the HBIs, the abundances of sterols and fatty acids showed a consistent decreasing trend throughout the water column. The same major sterols and fatty acids, observed in the surface waters (Section 4.5.1), were also detected in the subsurface and benthic layers, and some degree of variation in the proportion of individual lipids within each layer was observed (Tables 4.6 and 4.7). The general drop in values of each individual and total lipid, most evident in the benthic layer (Figures 4.7 and 4.8, Tables4.6and 4.7), is in good agreement with higher degradation rates of sterols and fatty acids observed under laboratory condition. Under such conditions, reactivity rates between HBIs and sterols or fatty acids are between one and three orders of magnitude lower. Alternatively, a general decrease in the values in sterol and FA composition might simply reflect an overall lower biomass. However, this would not explain the general increase in the values of HBIs observed in the subsurface layer.

Therefore, it is clear that further investigations of water column samples from a number of Antarctic locations are needed in order to provide some explanations of the observations for sterols and FA. However, given the apparent higher sensitivity of the HBIs towards sea-ice conditions (Section 4.5.1), which might have an implications for future paleo sea-ice reconstructions, efforts might be better concentrated towards

making our understanding of environmental signatures of HBIs within Antarctic environment more complete.

4.6 Conclusions

Distributions of an HBI diene II and HBI trienes IIIa and IIIb in surface waters from an offshore transect within the region north of the polynya west of the Dalton Iceberg Tongue (East Antarctica) were found to be extremely sensitive to the local sea-ice conditions. Thus, HBI diene II was only detected for sampling sites that experienced seasonal sea-ice, with highest concentrations found in coastal locations with longer-lasting ice cover and a recurrent polynya. In contrast, HBI triene IIIa and triene IIIb were observed in surface waters from the POOZ, the MIZ and the SIZ, but with highest concentrations within the region of the retreating sea-ice edge (the MIZ). Production of intermediate level concentrations of HBIs IIIa and IIIb within the SIZ likely reflects favourable conditions associated with the polynya. These observations are consistent with significant environmental control over the biosynthesis of HBI diene II and HBI trienes (IIIa and IIIb) by sea-ice diatoms and open water phytoplankton, respectively, with the production of HBI trienes being especially favoured within the vicinity of the retreating ice-edge or the polynya. Although some environment-specific trends were also identified in the sterol and FA distributions, these were not as striking as those for HBI diene II and two HBI trienes, IIIa and IIIb. Data presented here generally support various previous deductions based on sedimentary records of HBIs (only HBI diene II and HBI triene IIIa) in dated marine archives, especially the abundance of HBI diene II as an indicator of seasonal sea-ice extent. The occurrence of HBI triene IIIa at all sites is consistent with the previous use of this biomarker as an open water indicator, while enhanced concentrations within the MIZ supports the notion of a more specific indicator of increased productivity adjacent to the sea-ice edge, as

suggested by Collins et al. (2013). However, additional local factors, such as those associated with polynya formation, may also exert significant control over the distribution of HBI triene IIIa and the relative concentrations of II and IIIa, in particular. The tri-unsaturated biomarker HBI triene IIIb has also been quantified and shown to be highly correlated with abundances and distributions of HBI triene IIIa, suggesting that both biomarkers have the same source origin within the Southern Ocean. Further, HBI triene IIIb exhibits the same general response to the variable oceanographic conditions within the study area as HBI triene IIIa, potentially making it an alternative biomarker of phytoplankton in the Southern Ocean. However abundances of HBI triene IIIb were consistently lower than those of HBI triene IIIa (ca 3 times), which may have implications for detection when these biomarkers are only present in low amounts, as is often the case (Massé et al., 2011).

Within the water column, abundances of all three HBIs showed variation between the three water depths analysed. Namely, an increase in abundances from surface to subsurface layer of the photic zone, followed by decrease in concentrations observed towards the bottom of the water column. These variations could result from variable composition of the diatom species in the respective depths or their alteration in the water column during vertical transport. Additional alteration, due to biological activity, cannot be ruled out, as yet. To confirm any of these suggestions, however, further analysis of, for example, species composition will be required, especially as some variation in lipid concentration between individual stations was observed. In contrast to the HBI profiles, abundances of sterols and fatty acids showed a decreasing trend throughout the water column. This is in general agreement with their higher reactivities under laboratory conditions, although further investigations are needed in order for such changes to be interpreted with greater confidence.

CHAPTER FIVE

5 Results (3): Source, distribution and environmental significance of an organic geochemical proxy for Antarctic sea-ice: $IPSO_{25}$

5.1 Introduction

Chapter Five describes the identification of an environmental source of the diatom specific di-unsaturated HBI lipid HBI diene II (hereafter termed $IPSO_{25}$; Ice Proxy for the Southern Ocean with 25 carbon atoms; Figure 5.1) as the tube-dwelling diatom *Berkeleya adeliensis* Medlin, which is a common constituent of Antarctic sea-ice diatom communities. In addition, this chapter describes the surface sedimentary distribution of $IPSO_{25}$ together with tri-unsaturated HBIs, IIIa and IIIb. More specifically, this chapter will demonstrate that sedimentary abundances of $IPSO_{25}$ are consistent with the ecologically preferred habitat of its source. Further, and in relation to the ecological habitat of *Berkeleya adeliensis*, a re-interpretation of sedimentary occurrence and abundances of $IPSO_{25}$ in previous paleo records is offered. The sedimentary occurrences and distributions of HBI trienes IIIa and IIIb are also presented.

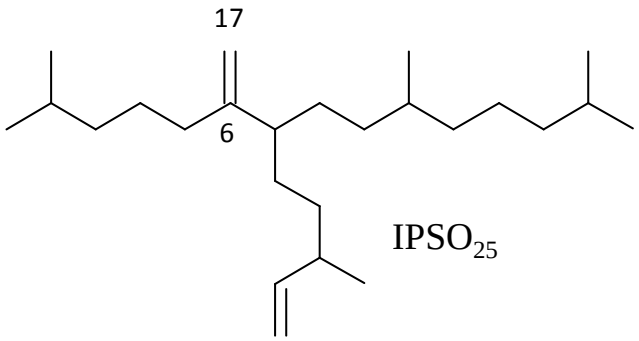

Figure 5.1: Structure of HBI biomarker $IPSO_{25}$.

In Chapter 4, it is shown that the presence and abundance of HBI diene II (referred to in this chapter as $IPSO_{25}$) in surface waters from East Antarctic was closely associated with locations that experience seasonal sea-ice, with highest concentrations found in coastal locations with longer-lasting ice cover and a recurrent polynya, an observation that aligned well with the previous identification of $IPSO_{25}$ in coastally bound sea-ice and near-surface sediments (Johns et al., 1999; Massé et al., 2011; Nichols et al., 1993; Sinninghe Damsté et al., 2007). However, these aforementioned investigations only represent a relatively small number of studies reporting the occurrence of this biomarker either in sea-ice, the water column or sediment samples within Antarctica (Figure 5.2a). Despite this, and unlike for the Arctic, where the distribution pattern of IP_{25} has been determined following analysis of sea-ice and several hundred surface sediments from different Arctic regions (Belt and Müller, 2013; Xiao et al., 2015) (Figure 5.2b), a number of Antarctic sea-ice reconstructions, based on $IPSO_{25}$, have been reported.

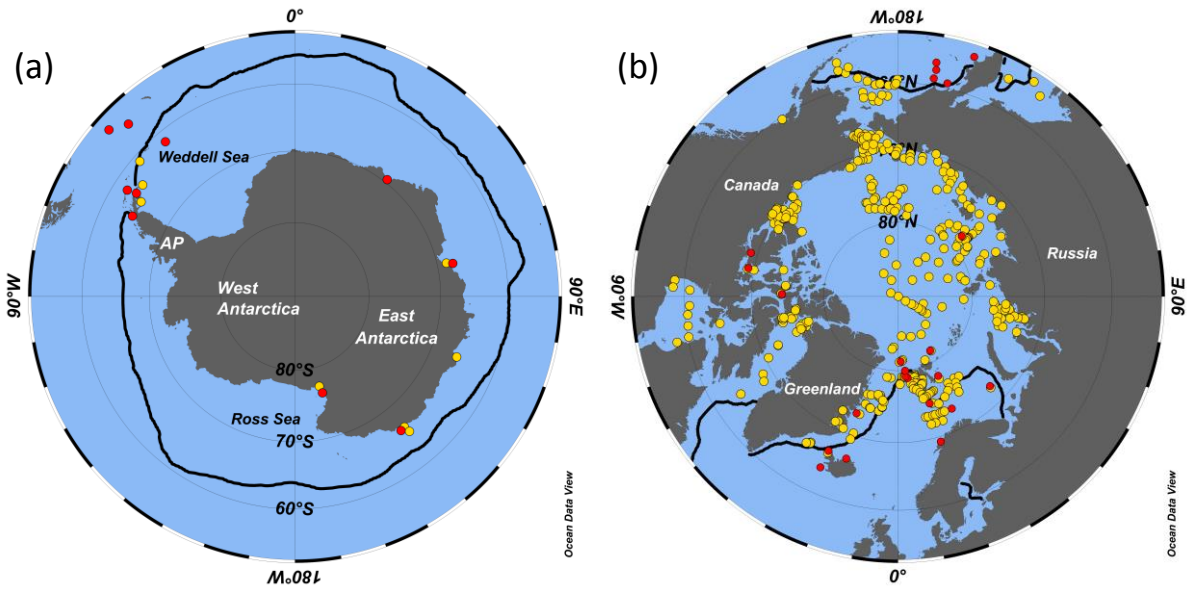

Figure 5.2: Summary maps of: (a) Antarctica and; (b) the Arctic, showing locations where HBI diene II ($IPSO_{25}$) in Antarctic and IP_{25} in Arctic have been identified in either sea-ice or surface sediments (yellow dots). Paleo records where these biomarkers have been used are indicated on each map by red dots. The black lines correspond to the median winter sea-ice extent for the interval 1979-2010 (NSIDC; Fetterer et al., 2002), in October (Antarctica) and March (Arctic).

These studies span recent decades, the Holocene (Barbara et al., 2010, 2013, 2016; Campagne et al., 2015, 2016; Denis et al., 2010; Etourneau et al., 2013; Massé et al., 2011) and the last glacial (ca 60 kyr BP (Collins et al., 2013)).

Further, a lack of knowledge of the environmental source of $IPSO_{25}$, has almost certainly had a significant impact on the interpretation of its sedimentary occurrence and abundance characteristics.

The interpretation of $IPSO_{25}$ abundances in paleo reconstruction studies in the Southern Ocean has generally been accompanied by analysis of HBI triene IIIa (Figure 5.3) as a phytoplankton indicator (e.g. Barbara et al., 2010; Campagne et al., 2015; Denis et al., 2010; Etourneau et al., 2013). This is believed to be favourably biosynthesised in the waters adjacent to the ice edge (Collins et al., 2013), a suggestion that, to some extent, has been supported by the data shown in Chapter 4. Finally, it is noted that, despite the usual co-occurrence of HBI triene IIIa and a further tri-unsaturated HBI (HBI triene IIIb, Figure 5.3) in some cultures of HBI producing diatoms (Belt et al., 2000a) only HBI triene IIIa has, to date, been used as a proxy indicator of open water phytoplankton in paleo records.

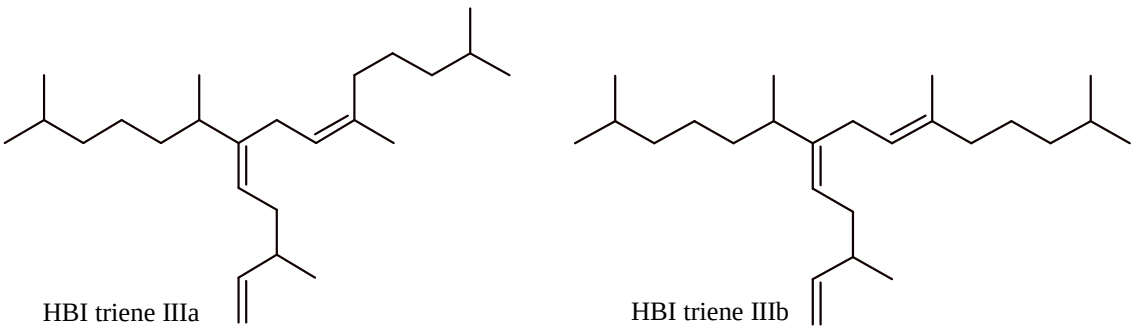

Figure 5.3: Structures of C_{25} highly branched isoprenoids (HBI) trienes IIIa and IIIb.

Therefore, the aim of this study was to investigate the sedimentary abundances of $IPSO_{25}$ and HBI trienes IIIa and IIIb in almost 150 surface sediments covering different

regions of (mainly) West Antarctica, including the Weddell Sea, the Antarctic Peninsula (AP), the Bellingshausen Sea (BS), Amundsen Sea (AS) and the Ross Sea. In addition, the stable isotopic composition of individual HBIs in some of the samples from different regions was also determined. A final aim was to conduct hydrocarbon analysis of bulk sea-ice samples from the Western Antarctic Peninsula (WAP), mixed sea-ice diatom assemblages obtained from these sea-ice samples, and picked cells of the sea-ice diatom *Berkeleya adeliensis*.

5.2 Methods

5.2.1 Sample description

Two landfast sea-ice cores were collected by Ms. Mairi Fenton (British Antarctic Survey) from Ryder Bay (Figure 5.4), situated close to the British Antarctic Survey Rothera Research Station (Adelaide Island; 67°35'8"S, 68°7'59"W) on December 3 2014. Bottom sections (ca 10 cm) of each core were sliced from the main cores and left to melt in the dark at 4°C. Aliquots of the thawed samples were then filtered (GF/F; 0.7 µm), with the remaining material re-frozen and stored at -20°C until further use. Surface sediment material (Figure 5.4) from the Antarctic Peninsula, the Bellingshausen Sea, the Amundsen Sea and the Weddell Sea was taken from the upper 0-1 cm of archived box cores, multi-cores and gravity cores held at the British Antarctic Survey, the British Ocean Sediment Core Research Facility (BOSCORF, UK) and the Alfred Wegener Institute for Polar Marine Research (AWI, (Germany) and provided by Dr Claire Allen (BAS), Dr. Suzanne MacLachlan (BOSCORF) and Dr Rainer Gersonde (AWI). Additional sediment samples from the Antarctic Peninsula and the Ross Sea were collected during several R/V ARAON cruises between 2001 and 2015 and

provided by Dr Jung-Hyun Kim (Hanyang University, South Korea). All surface sediment material was assumed to represent accumulation during the modern era.

Figure 5.4: Summary map showing locations of surface sediments (yellow dots) analysed as part of this study. The location of sea-ice sampling is indicated by the red triangle. The black and white stippled lines refer to the median winter (October) and summer (February) sea-ice margins for the interval 1979-2010 (NSIDC, Fetterer et al., 2002), respectively. AP: Antarctic Peninsula, BS: Bellingshausen Sea, AS: Amundsen Sea

5.2.2 Species identification

Species identification and isolation from sea-ice samples was performed by Dr Thomas Brown (Plymouth University) by the methods described in Chapter 2, Section 2.14.

5.2.3 Extraction and analysis of lipids

HBI lipids were extracted from thawed and filtered sea-ice samples, picked cells of *B. adeliensis* and freeze-dried sediments, using methods described in Chapter 2 (section 2.5-2.10). Briefly, for sea-ice samples, lipids were extracted from freeze-dried filters by saponification (20% KOH; 80°C; 60 min) and then re-extracted with hexane. For isolated cells of *B. adeliensis*, a total hexane extract (THE) only was obtained (hexane; 3×1 mL, ultrasonication; 3×5 min). In each case, the resulting THE suspensions were filtered through pre-extracted (dichloromethane/methanol) cotton wool to remove cells before being partially dried (N_2 stream) and fractionated into non-polar lipids by column chromatography (hexane (3 mL)/SiO_2). For sediments, ca 1 g of freeze-dried sediment material was extracted by sonication (dichloromethane/methanol; 2:1 *v/v*, 3×3 mL) to obtain a total organic extract (TOE). Each TOE was partially purified to remove polar components, elemental sulphur, and saturated non-polar components using silver-ion chromatography. For all sample types, an internal standard (9-octylheptadec-8-ene; 0.01-0.1 µg) was added prior to extraction, to enable subsequent quantification of HBIs by GC-MS methods. Analysis of partially purified non-polar lipids was carried out using GC-MS with identification of $IPSO_{25}$ achieved by comparison of its retention index and mass spectrum with those obtained from a purified reference compound. Quantification of $IPSO_{25}$ was achieved by integrating individual ion responses (*m/z* 348.3) in single ion monitoring mode, and normalising these to the corresponding peak area of the internal standard and an instrumental response factor derived from a purified standard. GC-MS-derived masses of $IPSO_{25}$ were converted to sedimentary concentrations using the mass of sediment extracted, while a cellular concentration of $IPSO_{25}$ in *B. adeliensis* was obtained by dividing the normalised GC-MS response obtained from picked cells by the number of cells extracted.

5.2.4 Stable isotope determinations

The stable (carbon) isotopic composition ($\delta^{13}C$) of sedimentary $IPSO_{25}$ was determined by Dr Kyle Taylor (Isoprime, UK) by the method outlined in Chapter 2, Section 2.13.

5.3 Results

The diatom assemblage in a bulk sea-ice sample collected from the WAP in December 2014 consisted of *B. adeliensis* as the major diatom species (> 86%). Morphometric assessment of this tube-dwelling diatom, included elongated central area, apical and transapical length (36 and 8 µm, respectively), number of parallel striae in 10 µm (50) and asymmetric axial area adopting a distinct urn-shape around the simple helictoglossa. Further, the lipid biomarker $IPSO_{25}$ was identified in non-polar extracts obtained from both the bulk sea-ice sample and picked cells of *B. adeliensis*, with an estimated cellular concentration (ca 6 pg $cell^{-1}$;Brown T.A., personal communications) consistent with that of other HBI-producing diatoms (Brown et al., 2014b). No other HBI lipids were identified in the bulk sea-ice sample or the picked cells of *B. adeliensis*.

Within the surface sediments, $IPSO_{25}$ could be identified and quantified in 125 out of the 149 samples analysed, with a concentration ranging from 0.22 to 1830 ng g^{-1} (Figure 5.6; Table 5.1). The highest concentrations (>500 ng g^{-1}) were always associated with samples taken from coastal locations, with a general drop-off in abundance for offshore sites. In some cases, there were also substantial abundance variations in $IPSO_{25}$, even for relatively nearby study sites. The stable isotopic composition ($\delta^{13}C$) of $IPSO_{25}$ in surface sediments from Marguerite Bay, the SE Weddell Sea and the northern Antarctic Peninsula was found to be -15.00± 0.03‰, -13.46± 0.02‰, and -14.39± 0.07‰, respectively. In contrast to $IPSO_{25}$, HBI triene IIIa could be identified in 86 out of 149 sediment samples, (Figure 5.7) with

concentrations (0.05-11.6 ng g^{-1}) (Table 5.1) that were generally lower than those of $IPSO_{25}$. In fact, in all of the samples where both biomarkers have been detected (81), concentrations of HBI triene IIIa were always smaller (Table 5.1). Interestingly, in five samples where HBI triene IIIa was detected, $IPSO_{25}$ was either absent or below the LOD. It is noted, however, that where this was the case, the concentration of HBI triene IIIa was very low (<0.2 ng g^{-1}) and all five stations were located further off-shore.

HBI triene IIIb was identified in 52 out of 149 surface sediments (Figure 5.8) with concentrations in the range 0.05-5.0 ng g^{-1} (Figure 5.8, Table 5.1). When detected, concentrations of HBI triene IIIb were similar to those of HBI triene IIIa, and always lower than those of $IPSO_{25.}$ In only one sample where HBI triene IIIb was detected, $IPSO_{25}$ was either absent or below the LOD. However, in all of the samples where HBI triene IIIb was detected, HBI triene IIIa was also observed, with concentrations that were generally ca 2 times higher than those of HBI triene IIIb. For two stations, however (Marian Cove, King George Island), HBI triene IIIb was either equal to, or marginally higher, than that of HBI triene IIIa (Table 5.1). Additionally, in 19 stations, none of the HBIs were detected. A relatively good correlation between both HBI trienes (R^2=0.88) was also observed (Figure 5.9), although this was not as strong as in the surface water samples (Chapter 4, R^2=0.99). Unlike for surface waters, sedimentary abundances of both HBI trienes were further correlated with those of $IPSO_{25}$. Finally, sedimentary abundances of HBI trienes were too low for their stable isotopic composition ($\delta^{13}C$) to be determined.

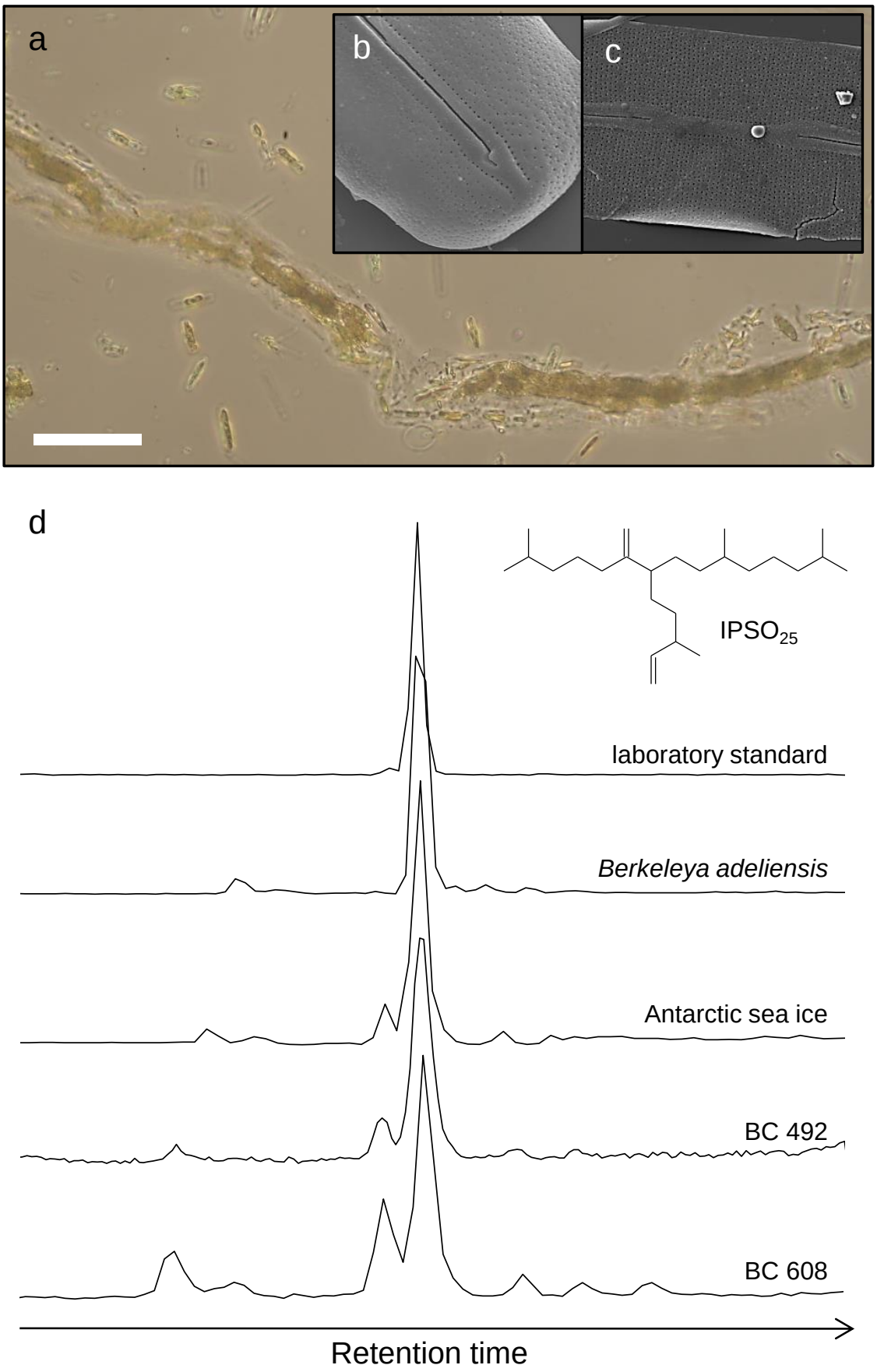

Figure 5.5: $IPSO_{25}$-producing species and lipid extracts containing $IPSO_{25}$: (a) light microscopy image of *B. adeliensis* in Antarctic sea-ice; (b) and (c) scanning electron micrographs of outer and inner cell of *B. adeliensis* isolated from Antarctic sea-ice; and (d) structure of $IPSO_{25}$ and partial GC-MS chromatograms of $IPSO_{25}$ in various samples (SIM mode; *m/z* 348.3).

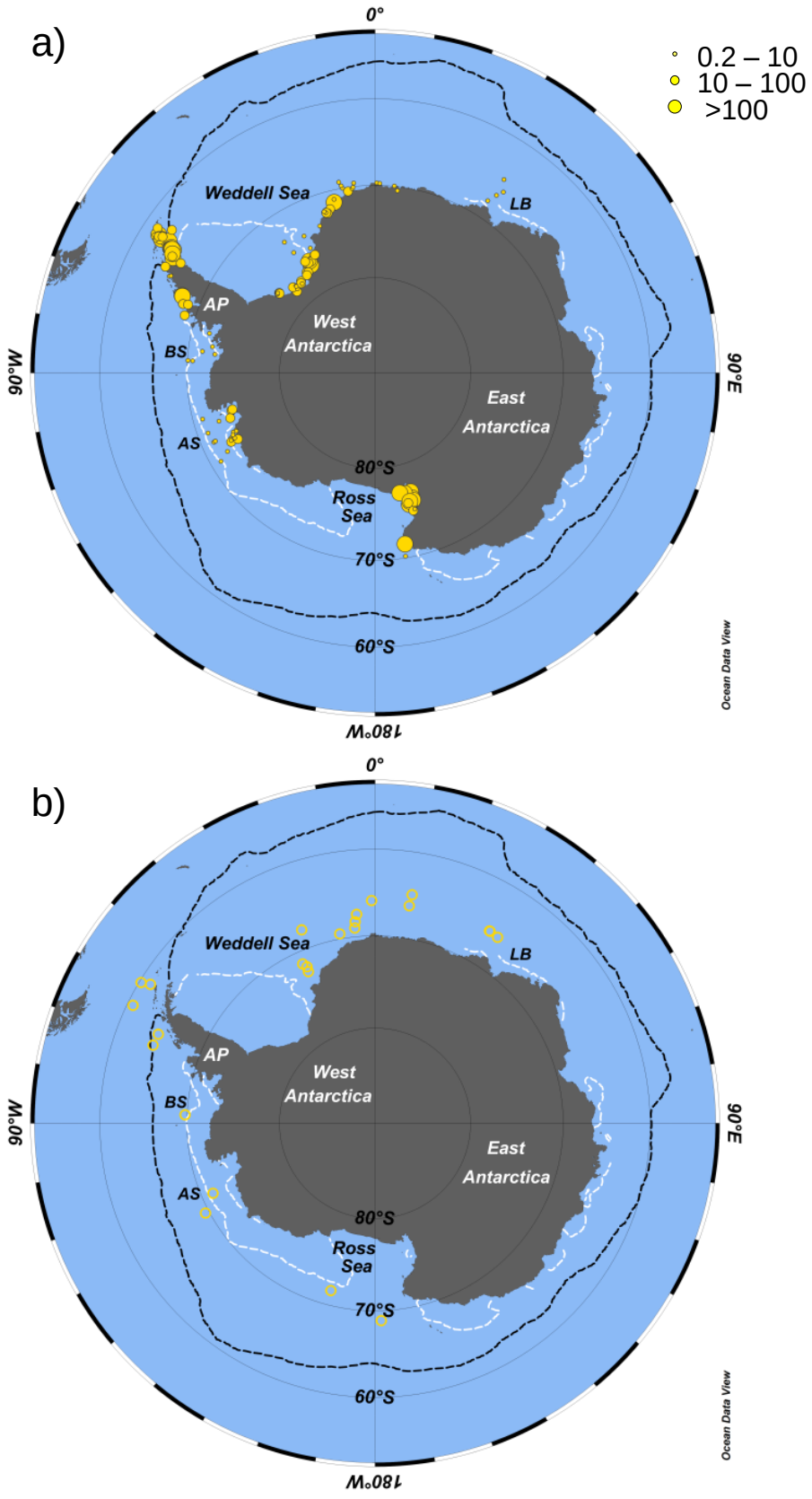

Figure 5.6: Distribution map showing: (a) the variable concentrations of $IPSO_{25}$ in Antarctic surface sediments (ng g^{-1} dry sediment); and (b) locations where $IPSO_{25}$ was below the limit of detection (i.e. <0.2 ng g^{-1} dry sediment). The black and white stippled lines refer to the median winter (October) and summer (February) sea-ice margins for the period 1979-2010 (NSIDC; Fetterer et al., 2002), respectively. AP: Antarctic Peninsula; BS: Bellingshausen Sea; AS: Amundsen Sea; LB: Lützow-Holm Bay.

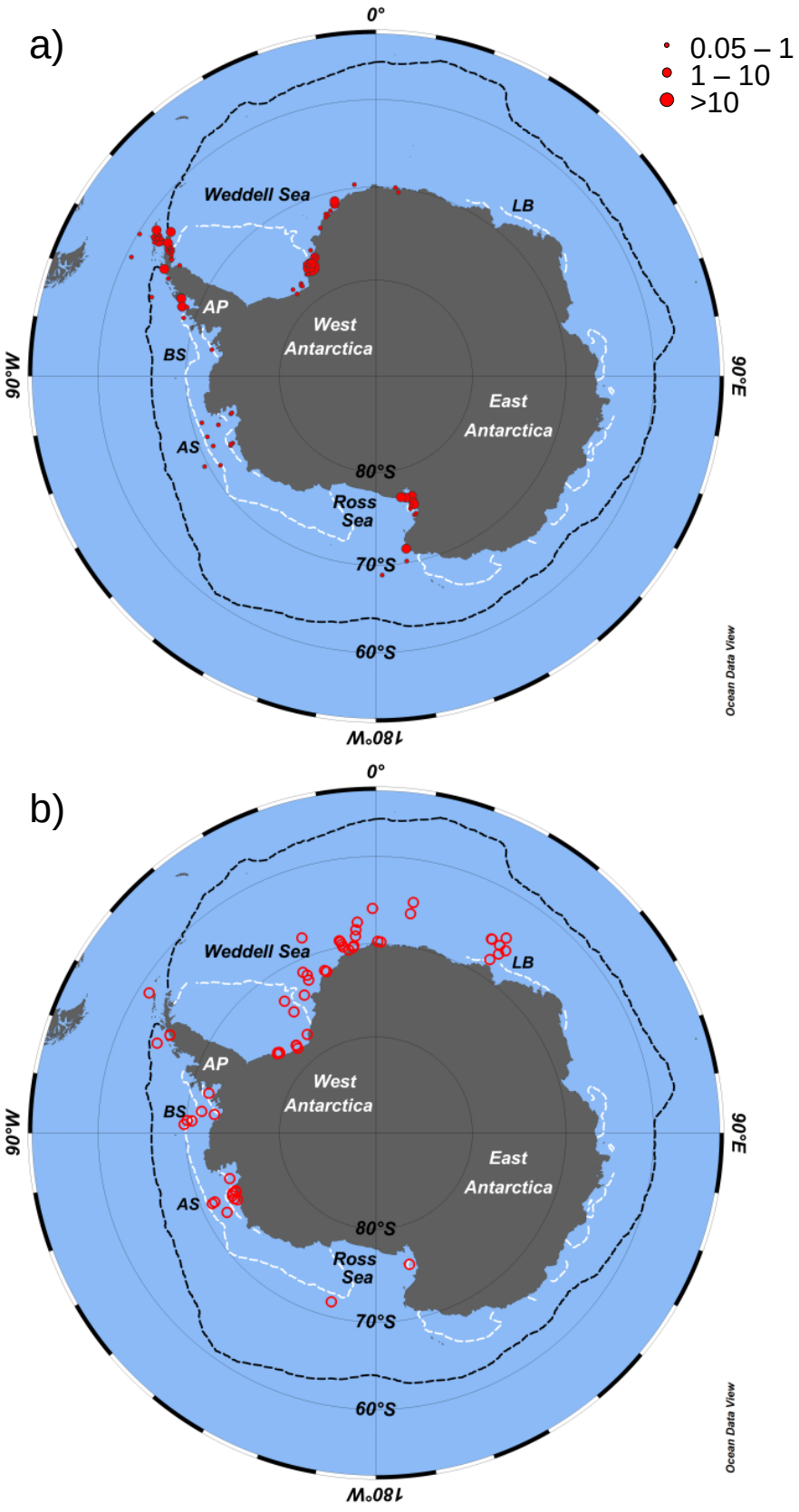

Figure 5.7: Distribution map showing: (a) the variable concentration of HBI triene IIIa in Antarctic surface sediments (ng g^{-1} dry sediment), and (b) locations where HBI triene IIIa was below the limit of detection (i.e. <0.05 ng g^{-1} dry sediment). The black and white stippled lines refer to the median winter (October) and summer (February) sea-ice margins for the period 1979-2010 (NSIDC, Fetterer et al., 2002), respectively. AP: Antarctic Peninsula; BS: Bellingshausen Sea; AS: Amundsen Sea; LB: Lützow-Holm Bay.

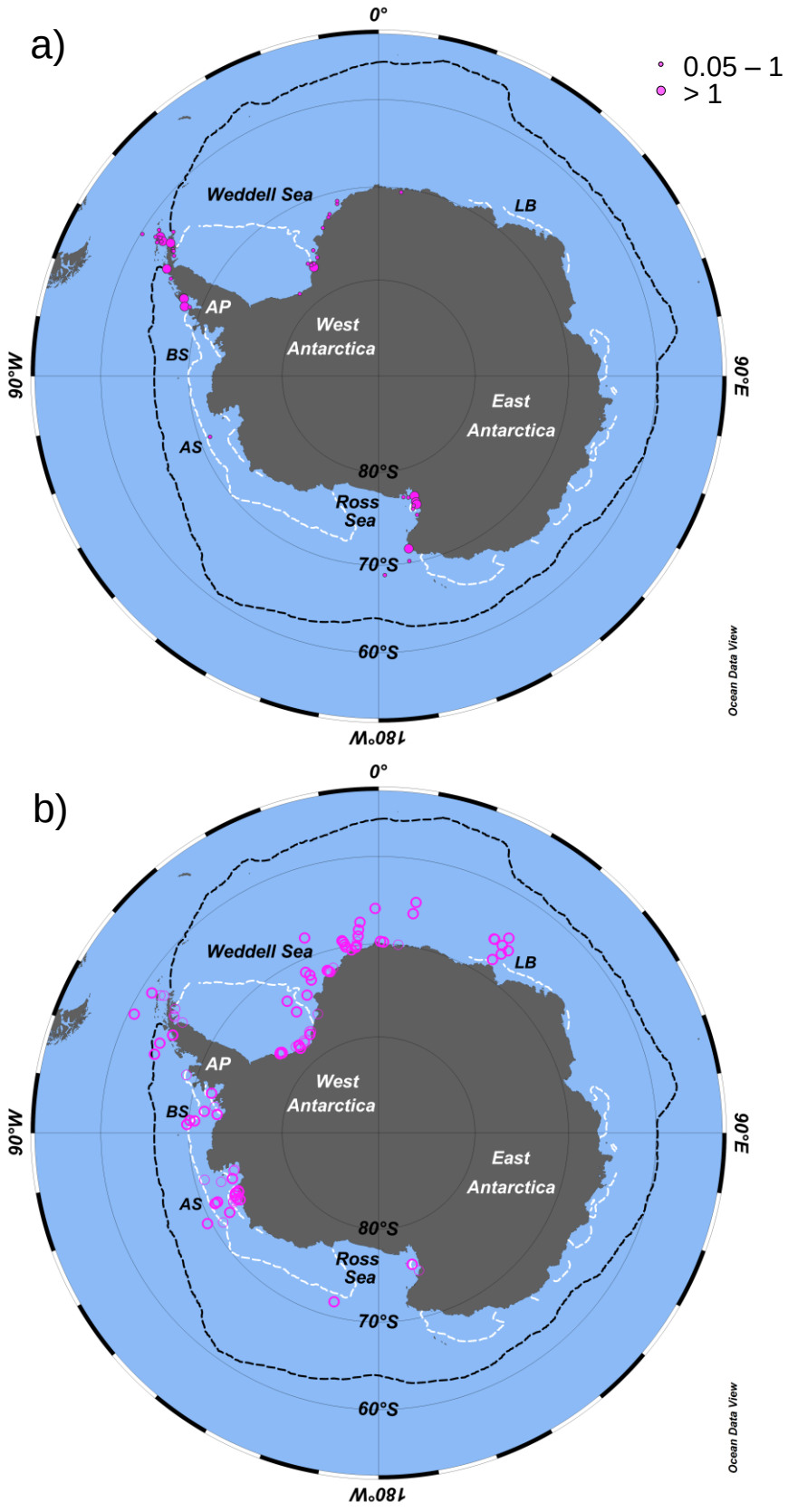

Figure 5.8: Distribution map showing (a) the variable concentration of HBI triene IIIb in Antarctic surface sediments (ng g^{-1} dry sediment); and (b) locations where HBI triene IIIb was below the limit of detection (i.e. <0.05 ng g^{-1} dry sediment). The black and white stippled lines refer to the median winter (October) and summer (February) sea-ice margins for the period 1979-2010 (NSIDC; Fetterer et al., 2002), respectively. AP: Antarctic Peninsula; BS: Bellingshausen Sea; AS: Amundsen Sea; LB: Lützow-Holm Bay.

Table 5.1: Concentrations of HBI biomarkers in surface sediments and the ratio between $IPSO_{25}$ and HBI triene IIIa (II/IIIa). All biomarker concentrations expressed as ng g^{-1} of dry sediment.

Station ID	Lat	Long	$IPSO_{25}$	HBI triene IIIa	HBI triene IIIb	II/IIIa
BC 312	-64.15	-58.53	739.4	0.74	0.44	999
BC 313	-64.22	-58.30	1201.4	0.77	0.34	1560
BC 314	-64.22	-58.48	836.9	1.00	0.60	837
BC 315	-64.29	-58.60	348.5	0.51	0.29	683
BC 316	-64.38	-58.51	396.2	0.36	0.12	1101
BC 317	-64.57	-58.49	153.8	0.27	0	570
BC 319	-64.69	-59.44	99.6	0.39	0.10	255
BC 320	-64.83	-60.01	78.4	0.22	0	356
BC 321	-64.96	-60.24	295.5	0.20	0	1478
BC 351	-70.09	-86.19	0.8	0	0	
BC 361	-71.99	-76.55	3.3	0	0	
BC 363	-72.60	-80.83	2.3	0.13	0	18
BC 364	-72.98	-83.44	3.9	0	0	
BC 369	-71.58	-82.86	2.0	0	0	
BC 373	-70.61	-86.25	0.8	0	0	
BC 379	-69.77	-87.42	0	0	0	
BC 398	-71.40	-113.39	2.0	0.16	0	13
BC 403	-71.60	-113.29	1.4	0	0	
BC 407	-73.21	-115.24	6.9	0.10	0	69
BC 409	-73.80	-112.82	4.5	0	0	
BC 412	-73.92	-115.86	16.2	0	0	
BC 416	-74.14	-112.45	5.2	0	0	
BC 420	-74.14	-112.86	4.2	0	0	
BC 421	-73.62	-113.71	2.0	0	0	
BC 423	-73.45	-115.20	10.4	0.20	0	52
BC 426	-73.67	-114.98	5.9	0	0	
BC 429	-73.14	-115.70	11.6	0.19	0	61
BC 431	-72.30	-118.16	4.2	0	0	
BC 439	-71.60	-113.30	1.9	0	0	
BC 443	-71.28	-113.46	0	0	0	
BC 455	-71.07	-105.08	1.2	0.08	0	15
BC 476	-74.48	-104.42	53.4	0.34	0	157
BC 477	-74.36	-104.67	54.5	0.58	0	94
BC 483	-73.99	-107.38	37.4	0	0	
BC 485	-72.73	-107.29	6.1	0.07	0	87
BC 487	-71.18	-109.90	3.6	0.55	0.10	7
BC 490	-69.59	-117.98	0	0.19	0	0
BC 492	-71.15	-119.96	0.4	0.18	0	2
BC 516	-68.79	-69.88	49.1	0.60	0.13	82
BC 518	-68.24	-70.20	34.3	8.88	2.97	4
BC 519	-68.24	-70.20	34.1	5.81	1.84	6
BC 521	-67.79	-68.08	612.3	9.09	4.18	67
BC 523	-67.86	-68.20	750.6	9.44	3.81	80
BC 566	-77.27	-33.45	42.2	0.18	0	234
BC 571	-78.15	-43.65	13.6	0.30	0.10	45
BC 574	-78.00	-42.50	2.1	0	0	
BC 577	-77.65	-42.10	6.9	0	0	
BC 580	-77.73	-42.17	2.0	0	0	
BC 584	-77.91	-39.15	3.7	0.29	0	13
BC 590	-77.61	-38.72	29.6	0.48	0	62
BC 591	-77.77	-39.39	13.8	0.34	0	41
BC 605	-77.18	-34.16	28.1	0.27	0	104
BC 607	-76.79	-30.57	448.8	4.37	1.26	103
BC 608	-76.79	-30.57	1108.4	11.59	3.31	96

Table 5.1: continued

Station ID	Lat	Long	$IPSO_{25}$	HBI triene IIIa	HBI triene IIIb	II/IIIa
BC 608	-76.79	-30.57	1108.4	11.59	3.31	96
BC 612	-76.42	-29.81	54.4	1.15	0.27	47
BC 615	-76.47	-29.69	92.6	1.04	0.25	89
BC 621	-76.15	-32.04	50.7	0.26	0.05	195
BC 623	-76.47	-31.13	37.8	0.58	0.10	65
BC 624	-76.34	-30.28	129.6	2.14	0.44	61
BC 627	-76.05	-27.15	25.6	1.19	0.30	22
BC 628	-76.02	-26.91	29.4	0.26	0	113
BC 639	-63.57	-57.29	685.5	2.24	1.03	306
BC04-BS05	-61.63	-56.22	12.7	1.02	0.40	12
BC06-DP05	-60.69	-63.96	0	0.07	0	0
BC08-DP03	-60.23	-58.86	0	0.12	0.07	0
BF10-BC01	-62.72	-57.88	119.4	4.21	1.49	28
BF10-BC02	-62.60	-58.12	55.8	3.16	0.93	18
BF10-BC03	-62.19	-57.32	116.0	3.53	1.97	33
EAP13-BC16	-66.07	-60.46	24.3	0.69	0	35
GC 112	-64.68	-70.54	0	0.11	0	0
GC 513	-68.79	-73.11	14.2	0.71	0	20
JV10-BC01	-63.13	-54.78	84.6	1.22	0.41	69
MC10-BC01	-62.22	-58.79	3.0	0.24	0.25	13
MC10-BC02	-62.21	-58.77	1.5	0.20	0.20	8
PS 1138-8	-62.27	-57.65	50.9	0.17	0	299
PS 1273-1	-75.17	-27.34	5.3	0.39	0.16	14
PS 1277-1	-77.53	-43.66	11.0	0.13	0	85
PS 1282-1	-73.40	-20.51	4.0	0.50	0.15	8
PS 1284-1	-72.51	-17.46	6.0	0.20	0.11	30
PS 1345-8	-62.26	-57.55	11.7	0.42	0.21	28
PS 1364-1	-67.85	-20.72	0	0	0	
PS 1366-2	-70.44	-8.42	10.4	0	0	
PS 1367-1	-72.34	-16.52	27.4	0.17	0	161
PS 1370-1	-72.05	-17.44	0.5	0	0	
PS 1371-1	-72.43	-23.63	0	0	0	
PS 1372-2	-72.21	-16.72	23.4	0.31	0.13	75
PS 1373-2	-72.24	-16.88	12.4	0	0	
PS 1374-2	-72.22	-16.93	5.8	0	0	
PS 1375-2	-72.17	-17.13	1.8	0.13	0	14
PS 1376-2	-71.97	-15.30	58.9	0.18	0	327
PS 1377-1	-69.27	-10.73	0.5	0	0	
PS 1378-1	-69.43	-10.50	0	0	0	
PS 1379-1	-69.73	-10.25	0.2	0	0	
PS 1380-1	-70.01	-9.99	0.4	0	0	
PS 1386-1	-68.33	-5.62	0	0	0	
PS 1388-1	-69.03	-5.89	0	0	0	
PS 1390-1	-69.62	-6.40	0.3	0.09	0	3
PS 1394-1	-70.09	-6.68	0.5	0	0	
PS 1395-1	-70.22	-6.98	2.2	0	0	
PS 1396-1	-76.95	-50.10	10.0	0	0	
PS 1397-1	-76.88	-50.03	12.0	0	0	
PS 1398-2	-76.77	-50.57	5.5	0	0	
PS 1399-1	-76.82	-51.02	8.4	0	0	
PS 1402-2	-77.48	-34.73	41.4	0	0	
PS 1406-1	-71.34	-13.42	109.9	1.33	0.50	83
PS 1412-1	-71.04	-13.24	4.9	1.47	0.35	3
PS 1421-1	-74.67	-33/96	7.5	0	0	
PS 1453-1	-66.03	-0.86	0	0	0	

Table 5.1: continued

Station ID	Lat	Long	$IPSO_{25}$	HBI triene IIIa	HBI triene IIIb	II/IIIa
PS 1539-1	-62.67	-57.26	43.1	0.12	0	359
PS 1540-1	-61.74	-57.90	6.8	0.38	0.18	18
PS 1542-1	-61.29	-58.16	0	0	0	
PS 1544-1	-62.08	-57.65	7.9	2.21	0.69	4
PS 1559-1	-64.78	-67.61	0	0	0	
PS 1635-2	-71.87	-23.45	0	0	0	
PS 1798-2	-73.70	-27.36	2.0	0	0	
PS 1802-2	-73.17	-34.67	1.3	0	0	
PS 1803-2	-67.51	-5.01	0	0	0	
PS 1805-5	-66.19	35.31	0.3	0	0	
PS 1812-5	-66.06	33.28	0	0	0	
PS 1813-5	-64.96	33.63	2.1	0	0	
PS 1817-5	-67.99	33.19	4.4	0	0	
PS 1822-1	-66.92	34.30	0.3	0	0	
PS 1823-1	-65.93	30.83	0	0	0	
PS 1824-2	-65.93	30.64	0	0	0	
PS 1825-5	-66.33	8.89	0	0	0	
PS 1826-2	-65.03	9.18	0	0	0	
PS 2006-1	-71.40	-24.31	0	0	0	
PS 2024-3	-69.97	5.91	6.8	0.13	0	52
PS 2062-2	-69.78	1.45	1.1	0	0	
PS 2065-1	-69.72	0.56	2.6	0	0	
PS 2067-1	-70.44	7.00	7.3	0.18	0.09	41
RS15-BC16	-75.66	165.48	358.6	0.81	0.72	443
RS15-BC18	-74.91	164.52	20.4	0.10	0.06	204
RS15-BC19	-75.00	163.72	8.5	0.11	0	77
RS15-BC25	-75.82	165.69	60.7	0	0	
RS15-BC40	-71.62	-165.29	0	0	0	
RS15-GC54	-70.17	170.54	3.3	0.12	0.06	28
RS15-GC57	-71.54	170.06	1174.9	4.36	2.57	269
RS15-GC70	-75.96	164.91	320.8	0.92	0.65	349
RS15-GC71	-77.09	168.44	309.7	1.51	0.85	205
RS15-GC76	-76.92	163.36	1829.1	7.05	5.01	259
RS15-GC78	-76.26	163.48	729.4	3.15	2.27	232
RS15-GC82	-76.94	166.29	629.5	1.21	0.98	520
RS15-GC84	-76.01	163.46	378.8	1.93	1.17	196
RS15-LC48	-68.90	178.16	0	0.05	0	0
WAP13-BC22	-64.70	-63.02	10.8	3.25	1.44	3
WAP13-BC45	-65.75	-64.53	1.0	0	0	
WAP13-BC46	-65.75	-64.47	1.1	0	0	
WAP13-BC47	-65.61	-64.76	4.1	0.67	0.28	6

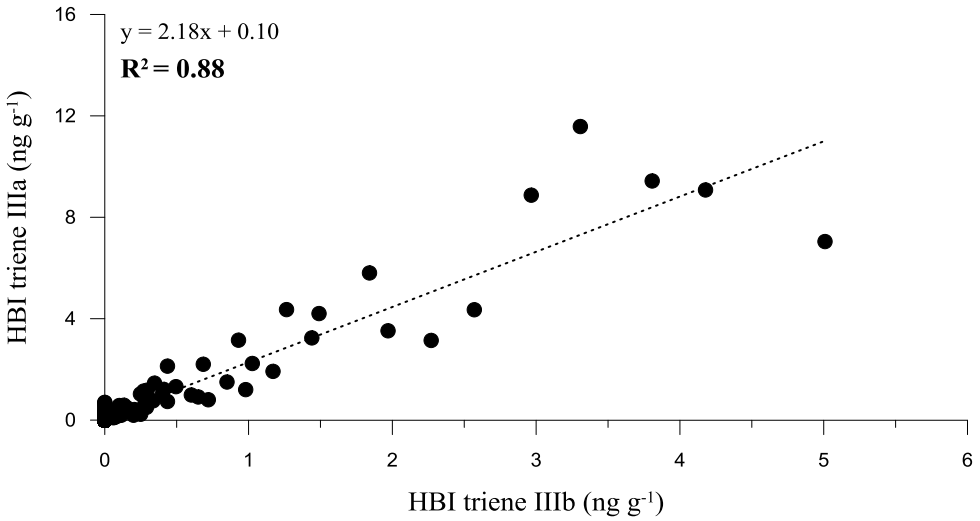

Figure 5.9: Relationship between HBI triene IIIa and HBI triene IIIb abundances in surface sediments.

Table 5.2: Pearson correlation coefficients between HBI biomarkers in surface sediments

	$IPSO_{25}$	HBI triene IIIa
HBI triene IIIa	**0.611**	
HBI triene IIIb	**0.736**	**0.938**
n=149, $p < 0.05$		

5.4 Discussion

One of the outcomes of this study was the identification of a sea-ice diatom source responsible for the biosynthesis of $IPSO_{25}$ (namely *Berkeleya. adeliensis*). Therefore, the sedimentary distribution of this biomarker will be mainly discussed with regards to preferred ecological habitat of *B. adeliensis*. The strong coastal association of sedimentary $IPSO_{25}$ is consistent with the presence of *B. adeliensis* as a common and relatively abundant species within Antarctic landfast ice diatom communities (McMinn, 1998; McMinn et al., 2000; Medlin, 1990; Riaux-Gobin et al., 2003). On a more specific regional basis, $IPSO_{25}$ has previously been reported in sea-ice and/or sediments from locations where *B. adeliensis* has also been identified in sea-ice, including Ellis Fjord (McMinn, 1996; Sinninghe Damsté et al., 2007), Adélie Land (Campagne et al., 2016; Denis et al., 2010; Massé et al., 2011; Riaux-Gobin et al., 2003, 2013),

Lützow-Holm Bay (Matsumoto et al., 1992; Tanimura et al., 1990), the WAP (Barbara et al., 2013; Etourneau et al., 2013, this study) and the Ross Sea/McMurdo Sound (Johns et al., 1999; McMinn et al., 2000; Ryan et al., 2012; Venkatesan, 1988) (Figure 5.10). For the Windmill Islands, East Antarctica, *B. adeliensis* has also been identified in sediments from Stephenson Cove (Cremer et al., 2003), while $IPSO_{25}$ has been reported in sea-ice from the same location and nearby O'Brien Bay (Massé et al., 2011) (Figure 5.10).

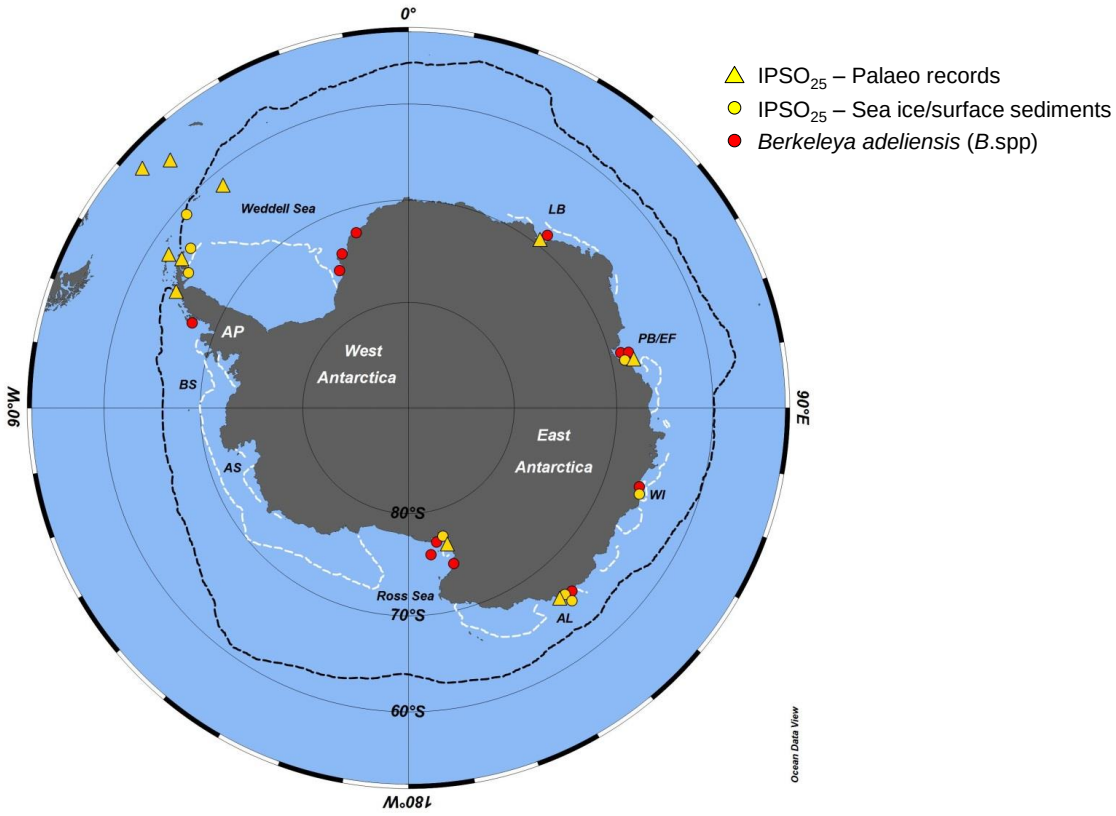

Figure 5.10: Summary map of Antarctica showing locations where *Berkeleya adeliensis* and HBI diene II ($IPSO_{25}$) have been identified in sea-ice, surface sediments and paleo records The black and white stippled lines refer to the median winter and summer sea-ice margins for the period 1979-2010 (NSIDC, Fetterer et al., 2002), respectively. AP: Antarctic Peninsula; BS: Bellingshausen Sea; AS: Amundsen Sea; AL: Adélie Land; WI: Windmill Islands; PB/EF: Prydz Bay/Ellis Fjord; LB: Lützow-Holm Bay.

B. adeliensis is a constituent species of the tube-dwelling genus *Berkeleya Grunow*, found frequently in Antarctic coastal waters and sea-ice (McMinn et al., 2000; Riaux-Gobin et al., 2003, 2011, 2013; Riaux-Gobin and Poulin, 2004), and is commonly

associated with landfast ice, where it can colonise both consolidated bottom ice and platelet ice; in some cases forming elongated strands that extend below the ice surface (Riaux-Gobin et al., 2003, 2011, 2013; Riaux-Gobin and Poulin, 2004). On the other hand, *B. adeliensis* has not been reported outside of the Antarctic, so cannot be a source of $IPSO_{25}$ in sediments from the Arctic, for example, despite the common occurrence of this biomarker in sediments from high latitude northern hemisphere settings (Belt and Müller, 2013). A more specific habitat preference for *B. adeliensis* in Antarctic sea-ice is not entirely clear, since elevated cell numbers have been reported in bottom ice and platelet ice (Riaux-Gobin et al., 2003, 2013), although some migration to the latter has been noted during ice melt (Riaux-Gobin et al., 2013). Indeed, Riaux-Gobin et al. (2013) suggested that *B. adeliensis* may be more tolerant towards the contrasting environments of bottom ice and platelet ice than many other sympagic species, with the more open-channel network of platelet ice possibly more compatible with such tube-dwelling species (Riaux-Gobin et al., 2003). Further, Riaux-Gobin et al. (2003) identified substantially higher abundances of *B. adeliensis* in sea-ice from coastal locations compared to offshore settings around Adélie Land, East Antarctica, while in the water column, generally low abundances of *B. adeliensis*, attributed to ice melt release, were restricted to under-ice waters or polynyas proximal to coastal locations (Riaux-Gobin et al., 2003, 2011).

The close association of *B. adeliensis* with landfast ice prompted Riaux-Gobin et al. (2011) to suggest that the occurrence of the cells of such sympagic species may represent suitable proxies in sedimentary records, adding the caveat that the poor preservation potential of the cells may prevent such an application, in practice. Indeed, *B. adeliensis* was not identified in sediment assemblage counts from Lützow -Holm Bay, despite being abundant in overlying sea-ice and the water column (Tanimura et al., 1990), and the organism is rarely (if ever) a constituent of diatom

inventories used in paleoceanographic reconstructions (Crosta et al., 2004; Ferry et al., 2015; Gersonde and Zielinski, 2000; Leventer et al., 1996).

Further, abundances of *B. adeliensis* have been shown to exhibit a high-to-low abundance trend for coastal to offshore sites for Adélie Land in both sea-ice (Riaux-Gobin et al., 2003) and surface waters soon after ice-melt (Riaux-Gobin et al., 2011), and a similar trend in $IPSO_{25}$ distribution has been observed previously in surface sediments from the same region, with highest concentrations for near-shore settings, lower values offshore, and absence for sites beyond the marginal ice zone (Massé et al., 2011). A similar offshore depletion in abundances of $IPSO_{25}$ was also identified previously in sediments from Lützow-Holm Bay (Matsumoto et al., 1992), from where *B. adeliensis* has been reported in coastal landfast ice (Tanimura et al., 1990) and the generality of this gradient can be readily seen through inspection of the surface sediment data for $IPSO_{25}$ presented here, with highest concentrations (up to ca 1800 ng g^{-1}) for coastal locations and substantially lower abundances offshore (ca 0.22-8.51 ng g^{-1}) (Figure 5.11).

Additionally, it is also noted that concentrations of $IPSO_{25}$ in surface waters from East Antarctica during late spring (i.e. during and shortly after ice melt) were shown to be strongly dependent on the nature and length of seasonal ice cover, with highest values for coastal locations experiencing at least partial ice cover extending into the summer (Chapter 4).

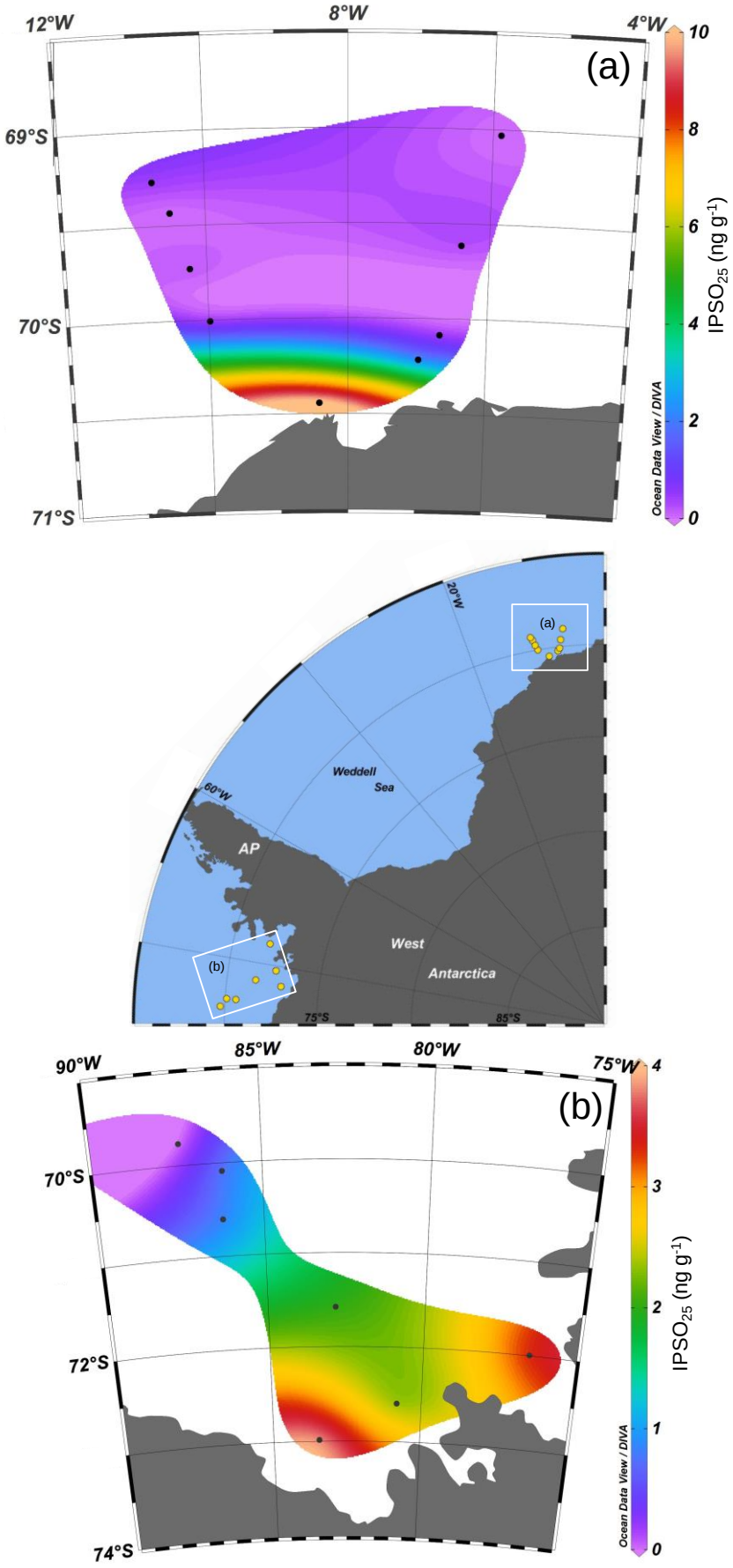

Figure 5.11: Regional maps illustrating the gradient drop-off in $IPSO_{25}$ concentration in surface sediments from coastal to offshore settings in: (a) the SE Weddell Sea and (b) the Bellingshausen Sea

Collectively, these observations suggest that distributions of $IPSO_{25}$ in Antarctic sediments are closely related to the ecology of the source diatom, *B. adeliensis*.

The apparently strict association of *B. adeliensis* to landfast ice might limit the value of $IPSO_{25}$ as a general Antarctic sea-ice proxy. However, instead, the environmental specificity of its source should enable more detailed insights into defining past sea-ice conditions to be made with confidence. Thus, since it has been shown previously that *B. adeliensis* increases in abundance towards the end of the spring bloom and during the onset of ice melt (Riaux-Gobin et al., 2003; Ryan et al., 2012), it follows that the occurrence of sedimentary $IPSO_{25}$ likely signifies the past presence of landfast ice during late spring/early summer. Such an interpretation parallels, to some extent, that for IP_{25} in the Arctic, whose presence in sediments is interpreted as reflecting spring sea-ice cover (Belt et al., 2007; Belt and Müller, 2013), although this is not restricted to landfast ice.

Previous paleo sea-ice reconstructions based on $IPSO_{25}$ have largely been conducted on sediment cores retrieved from near coastal locations around the Antarctic Peninsula (Barbara et al., 2013, 2016; Etourneau et al., 2013), Adélie Land (Campagne et al., 2016; Denis et al., 2010) and Prydz Bay (Barbara et al., 2010), so its occurrence in these is consistent with the source and surface sediment data presented herein. Interestingly, however, *B. adeliensis* was not reported in the taxonomic inventories of any of these previous studies, which presumably reflects the susceptibility of this species towards dissolution in the water column and in sediments. Indeed, it has been suggested previously that many sea-ice diatoms such as *B. adeliensis* may be under-represented in Antarctic sediments (Leventer, 1998), likely as a result of their only lightly silicified frustules. However, on the basis of readily detectable quantities of $IPSO_{25}$ in surface sediments described here, and in previous down-core investigations (Barbara et al., 2010, 2013, 2016; Campagne et al., 2015, 2016; Campagne et al., 2016; Collins et al.,

2013; Denis et al., 2010; Etourneau et al., 2013; Massé et al., 2011), at least partial deposition of *B. adeliensis* from the melting sea-ice to underlying sediments, even if subsequent dissolution of its silica frustules is significant, must have occured.

By combining the intracellular concentration of $IPSO_{25}$ in *B. adeliensis* with its abundance distribution in surface sediments, it can be estimated that the corresponding contribution of *B. adeliensis* falls within the range ca 10^{2}-10^{5} cells per gram of sediment, which is lower than typical total diatom cell concentrations in Antarctic sediments (ca 10^{5}-10^{7} cells g^{-1}) (Buffen et al., 2007; Stockwell et al., 1991) and certainly below the 2-3% threshold generally used in taxonomy-based paleoceanographic reconstructions (Armand et al., 2005; Gersonde and Zielinski, 2000). On the other hand, the occurrence of $IPSO_{25}$ likely offers complementary information to taxonomic-based sea-ice reconstructions, not least, since a clear distinction can be made between the respective signatures of $IPSO_{25}$ and commonly employed sea-ice diatom taxa in sediments. Thus, $IPSO_{25}$ is biosynthesised by at least one individual diatom species (*B. adeliensis*) that resides and blooms within the sea-ice matrix itself, and therefore represents a proxy measure of late spring/summer (permanent) sea-ice. In contrast, the frequently used diatom taxa for paleo sea-ice reconstruction (e.g. *Fragilariopsis curta* and *Fragilariopsi cylindrus* (Armand et al., 2005; Crosta et al., 2004; Gersonde and Zielinski, 2000)) bloom within the open waters of the marginal ice zone (Leventer and Dunbar, 1996; Mangoni et al., 2008), and their sedimentary distribution corresponds to seasonal (winter) sea-ice cover.

In previous studies, semi-quantitative interpretations of temporal changes to sea-ice conditions have been inferred from the variability of $IPSO_{25}$ in down-core records in much the same way that distributions of IP_{25} has been interpreted in Arctic sea-ice reconstructions (Belt and Müller, 2013). However, in contrast to IP_{25}, there have not been, as yet, any published reports that calibrate sedimentary $IPSO_{25}$ concentrations

with known sea-ice conditions, including seasonal sea-ice concentration, so such interpretations are based largely on conjecture and comparisons with IP_{25}. Further studies are therefore required to place the interpretations of abundance changes of $IPSO_{25}$ on a firmer footing. In practice, however, the greater heterogeneity of Antarctic sea-ice may limit the feasibility of performing such calibrations, especially for coastal locations, owing to the myriad of ice types that exist, the prevalence of polynyas, and the fluctuations that occur within these, both seasonally and annually. In the meantime, substantial (orders of magnitude) abundance changes in $IPSO_{25}$, even for sediments from proximate locations within each of the Antarctic Peninsula, the Weddell Sea and Ross Sea are evident. For example, the concentration ranges of $IPSO_{25}$ are 34-750, 150-1200, 37-1100 and 8-1800 ng g^{-1} in Marguerite Bay (AP), the NW and SE Weddell Sea, and the Ross Sea, respectively (Figure 5.12).

It is likely that number of features other than sea-ice concentration and/or duration likely have influence over (considerably variable) $IPSO_{25}$ abundances and consideration of the ecology of *B. adeliensis* may offer particularly useful insights. For example, unlike the source diatoms of IP_{25} in Arctic sea-ice, which have a generally consistent contribution of ca 1-5% of the total diatom taxa (Brown et al., 2014b), the proportion of *B. adeliensis* in Antarctic sea-ice diatom communities is highly variable, both spatially and temporally, with seasonal shifts in composition also having been observed in previous studies (Riaux-Gobin et al., 2003, 2013). *B. adeliensis* represented the major taxon in our sea-ice samples from the WAP, but much lower percentages (and absences) have been reported from the same (Henley et al., 2012) and other regions (Mangoni et al., 2008; McMinn, 1996; Riaux-Gobin et al., 2013), and inter-annual variability is also high. As such, sedimentary $IPSO_{25}$ may be much more strongly influenced by variations in Antarctic sea-ice diatom assemblages than is the case for IP_{25} in the Arctic. *B adeliensis* is also known to flourish in platelet ice, where diatom communities, in

general, can proliferate to yield significantly elevated biomass compared to consolidated ice or other sea-ice forms (Arrigo et al., 1995; Günther and Dieckmann, 1999; Thomas et al., 2001). In addition, larger and chain-forming sea-ice diatoms such as *Porosira pseudodenticulata* are known to have higher sinking rates compared to solitary pennate species in the Antarctic (Ichinomiya et al., 2008), a phenomenon commonly associated with aggregated sea-ice diatoms (Riebesell et al., 1991). The seemingly effective transfer of *B. adeliensis* from sea-ice to the underlying sediments, despite its general fragility towards dissolution may, therefore, reflect its propensity to form elongated strands and mats within platelet ice that have elevated sinking rates. Abundances of *B. adeliensis* (and thus $IPSO_{25}$) may thus potentially provide a sensitive proxy indicator of platelet ice, whose occurrence and concentration is commonly associated with the provision of super-cooled low density sub-surface water derived from nearby ice shelves (Arrigo et al., 1995; Dieckmann et al., 1986; Foldvik and Kvinge, 1974; Jeffries et al., 1993). Certainly, the widespread occurrence of *B. adeliensis* and $IPSO_{25}$, with elevated abundances of both for coastal locations, is consistent with ice shelves occupying almost half of the Antarctic coastline and enhanced platelet ice formation within the trajectory of super-cooled surface waters (Jeffries et al., 1993).

The production of $IPSO_{25}$ by *B. adeliensis* is not restricted to platelet ice, and both have been observed in samples of bottom ice. In fact, production of $IPSO_{25}$ in both platelet ice and consolidated bottom ice communities may potentially explain some of the differences in one of the frequently cited characteristics of $IPSO_{25}$ in Antarctic settings; namely, its relatively enriched ^{13}C content (compared to pelagic organic carbon), a feature found previously for other individual lipids and bulk organic matter derived within sea-ice (Dunbar and Leventer, 1992; Gibson et al., 1999; McMinn et al., 1999; Munro et al., 2010; Thomas et al., 2001; Tortell et al., 2013).

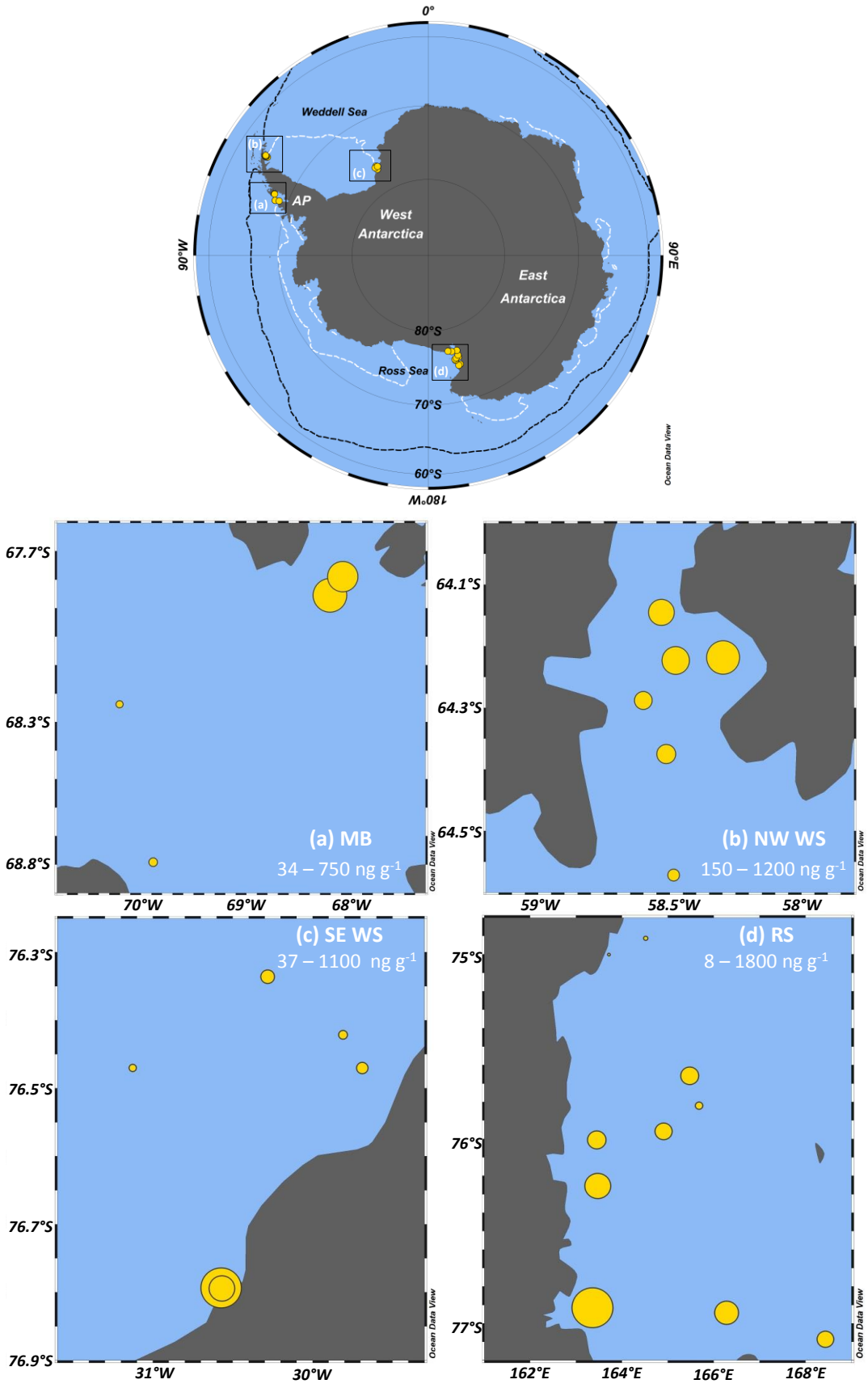

Figure 5.12: Regional variation of $IPSO_{25}$ concentration in surface sediments from: (a) Marguerite Bay (MB); (b) Northwest Weddell Sea (NW WS); (c) Southeast Weddell Sea (SE WS); and (d) and Ross Sea (RS). Range of concentrations of $IPSO_{25}$ for each region is also given. Smallest and largest circle in each respective map correspond to lower and upper limit of concentration respectively.

Although the causes of the $\delta^{13}C$ enrichment of sea-ice-derived particulate organic matter (POM) are still debated, CO_2 limitation represents the general consensus view, which effectively partially reverses the photosynthetic preference for ^{12}C assimilation pertinent to CO_2-replete, open water environments, resulting in increased (less negative) $\delta^{13}C$ values (Dunbar and Leventer, 1992; Gibson et al., 1999; McMinn et al., 1999; Munro et al., 2010; Thomas et al., 2001; Tortell et al., 2013). Indeed, consistent with lower CO_2 concentrations in the brine channels of sea-ice (Gleitz et al., 1995), it has been shown that Antarctic sea-ice POM can become increasingly enriched in ^{13}C with greater distance from the ice/water interface (McMinn et al., 1999), and with the seasonal transition from late winter (October) to spring (December), concomitant with increasing biomass (Dunbar and Leventer, 1992), as CO_2 potentially becomes depleted. It has also been demonstrated that interstitial CO_2 drawdown has a significant impact on $\delta^{13}C$ for POC (Munro et al., 2010), although the precise relationship between $\delta^{13}C$ and CO_2 supply/demand is probably complicated by variable (and inconsistent) nutrient exchange (Tortell et al., 2013), leading to large ranges in $\delta^{13}C$ for sea-ice-derived particulate organic carbon (POC) (Dunbar and Leventer, 1992; Gibson et al., 1999; McMinn et al., 1999; Munro et al., 2010; Thomas et al., 2001; Tortell et al., 2013), with only relatively minor ^{13}C enrichment in some cases (Dunbar and Leventer, 1992; Thomas et al., 2001; Tortell et al., 2013). In accordance with these previous studies, although some $\delta^{13}C$ data for $IPSO_{25}$ are consistent with significant enrichment of ^{13}C within a relatively enclosed (and potentially CO_2-limited) sea-ice matrix, with $\delta^{13}C$=-5.7 to -8.5‰ in sea-ice (Massé et al., 2011) and ca -9‰ in Ellis Fjord sediments (Sinninghe Damsté et al., 2007), a relatively depleted value ($\delta^{13}C$=-17.8‰) was found for $IPSO_{25}$ in surface sediment material from Adélie land, East Antarctica (Massé et al., 2011). Massé et al. (2011) suggested that this might be attributed to the formation of $IPSO_{25}$ at a time of sea-ice melt, when the ice matrix would probably have been more

permeable to CO_2 and nutrient replenishment. However, given new findings presented here, a more likely explanation for the lighter isotopic composition of $IPSO_{25}$ in Adélie Land sediment is biosynthesis of this biomarker by *B. adeliensis* in the relatively open channels of platelet ice, with comparably free supplementation of CO_2 from surrounding waters. An alternative suggestion, involving production of $IPSO_{25}$ in CO_2-replete open waters following ice melt seems unlikely given the sensitivity of *B. adeliensis* towards dissolution in the water column. Consistent with this suggestion, Thomas et al. (2001) found only a small ^{13}C enrichment in POC in the interstitial waters of platelet ice from the eastern Weddell Sea (highest $\delta^{13}C$ =-20.9‰) with a mean $\delta^{13}C$ value (-24.0‰) only slightly higher than that for the underlying open water ($\delta^{13}C$=-25.6‰). On the other hand, a relative enrichment in ^{13}C for $IPSO_{25}$ in sediments from Ellis Fjord (Sinninghe Damsté et al., 2007), likely reflects its biosynthesis in the semi-enclosed environment of consolidated bottom ice, which *B. adeliensis* is known to colonise for this region (McMinn, 1996). Within sediment samples analysed as part of this study, $\delta^{13}C$ values for $IPSO_{25}$ in selected surface sediments from the WAP, the northern AP and the SE Weddell Sea were in the range ca -13.5 to -15‰, (i.e. intermediate between typical sea-ice and open water values) and thus indicative of a semi-enclosed sea-ice host. Interestingly, $IPSO_{25}$ abundances in these samples were also amongst the highest across all samples, consistent with the higher biomass generally associated with platelet ice (Arrigo et al., 1995; Günther and Dieckmann, 1999; Thomas et al., 2001).

By further consideration of the environmental sensitivity of *B. adeliensis* (and thus of $IPSO_{25}$) towards nearby glacial and ice shelf water inflow, potentially new insights into the impacts of past changes to such processes is provided by re-inspection of some previous paleo sea-ice reconstructions based on $IPSO_{25}$. For example, enhanced $IPSO_{25}$ in sediment core JPC24 from Prydz Bay (East Antarctica) between ca 10.9 and

10.4 cal. kyr BP (Figure 5.13c), previously interpreted as reflecting heavier sea-ice conditions during the deglaciation at this site, also coincided with an interval where the retreating Amery Ice Shelf was probably in the vicinity of, but not over, the core site (Barbara et al., 2010). Interestingly, lower $IPSO_{25}$ concentrations were observed both before this interval, likely reflecting an ice shelf covering the site, and afterwards, indicative of a more retreated ice shelf edge, as deduced previously, based largely on taxonomic distributions (Barbara et al., 2010). Similarly, elevated $IPSO_{25}$ in a high resolution (sub-decadal) record from the WAP since ca 1950 AD (core MTC 18A; Figure 5.10a), likely reflects enhanced meltwater-induced platelet ice formation during the recent (and abrupt) retreat of ice shelves and glaciers around the WAP (Cook et al., 2005; Pike et al., 2013), rather than an increase in sea-ice. Finally, as part of a Holocene paleoclimate record for the WAP, Etourneau et al. (2013) interpreted elevated concentrations of $IPSO_{25}$ in a core from Palmer Deep (JPC10; Figure 5.14d) during the late Holocene (last ca 3 kyr) as an indication of increased sea-ice presence and duration compared to the early and mid-Holocene, stating that glacial ice probably only had a relatively minor influence on $IPSO_{25}$ abundance. An apparent paradox between increased sea-ice and coeval increases to surface temperatures within the same record, and enhanced glacial ice melt derived from a nearby core site (ODP1098) (Pike et al., 2013), was reconciled by proposition of a late Holocene transition towards colder winter/spring seasons and warmer summers. On the other hand, Pike (2013) questioned the possible influence of other ice sources on the production and distribution of biomarkers such as $IPSO_{25}$, and the new data help resolve this. Thus, enhanced $IPSO_{25}$, observed especially after ca 3 kyr in Palmer Deep (JPC10; Figure 5.13d) (Etourneau et al., 2013), likely reflects the positive influence of increasing meltwater discharge from neighbouring ice shelves and glaciers (ODP1098) (Pike et al., 2013), on platelet sea-ice formation, with further (slightly) elevated concentrations of $IPSO_{25}$ in the earliest part

of the JPC10 record (ca 8-9 kyr BP; Figure 5.13d), and also in core JPC38 from the northeastern AP (Figure 5.13b) (Barbara et al., 2016), coincident with enhanced glacier discharge or accelerated glacier/iceberg melt during the final stages of the deglaciation (Peck et al., 2015; Pike et al., 2013). Finally, although most of the previous Antarctic studies incorporating $IPSO_{25}$ data have been conducted on near-coastal environments (Barbara et al., 2010, 2013, 2016; Campagne et al., 2015, 2016; Denis et al., 2010; Etourneau et al., 2013), exceptionally, Collins et al. (2013) investigated the broader potential of this biomarker for paleo sea-ice reconstruction by determining its distribution in glacial age sediments from three sites in the northern, central and southern sectors of the Scotia Sea, all of which are located further north of the boundary between $IPSO_{25}$ presence/absence in modern surface sediments (Figure 5.6). The occurrence of $IPSO_{25}$ in sediments from all three core locations, especially during MIS 2 (ca 12-24 cal. kyr BP), during which time, sea-ice diatom indicator species (i.e. *F. curta* and *F. cylindrus*) were also relatively abundant, either suggests that a different source may be responsible for $IPSO_{25}$ biosynthesis in such settings, or that *B. adeliensis* is also able to colonise sea-ice for non-coastal marine settings, especially for those under the influence of nearby glacial meltwater. To resolve this, the analysis of sea-ice samples from other Antarctic regions and settings, and individual diatom species within these will be required. In the meantime, it is noted that, amongst the more common and abundant Antarctic sea-ice diatom genera, *Fragilariopsis*, *Chaetoceros and Nitzschia*, are not producers of HBI lipids (Sinninghe Damsté et al., 2004). In fact, of the known HBI-producing diatom genera, only *Haslea, Pleurosigma, Navicula* and *Berkeleya* are found in Antarctic sea-ice, and only the latter two contain species that are generally considered to be common and abundant (*viz. N. glaciei* and *B. adeliensis*); however, no HBI lipids (including $IPSO_{25}$) were identified previously in *N. glaciei* (Massé et al., 2011). In addition, species within the *Pleurosigma* genus do not biosynthesise HBIs

with a 6-17 double bond (Belt et al., 2000a), which is one of the structural characteristics of $IPSO_{25}$ (Figure 5.1).

In previous studies of HBI lipids in Antarctic sea-ice and sea-ice diatoms (Johns et al., 1999; Massé et al., 2011; Nichols et al., 1993), only $IPSO_{25}$ has been identified as a common and abundant component, despite analyses having been conducted on mixed diatom assemblages of varying composition. This either means that *B. adeliensis* is a unique source of $IPSO_{25}$ in Antarctic sea-ice or that other species also only produce this particular HBI, and no others. However, the latter seems unlikely given the large number of HBIs of different structural type made by various diatoms and, unlike all other HBI-producing diatom genera, which have thus far, always been shown to produce a suite of HBIs (typically >3) (for a recent review, see Brown et al. 2014 and references therein), the genus *Berkeleya* appears to biosynthesise predominantly only one (di-unsaturated) isomer. Further, the occurrence of up to seven HBI isomers in Arctic sea-ice (Brown, 2011) can be attributed to the presence of several HBI-producing diatoms, and not just those that biosynthesise IP_{25} (Belt et al., 2007; Brown et al., 2011; Brown et al., 2014b). Therefore, although it is feasible that species other than *B. adeliensis* may be producers of $IPSO_{25}$ in Antarctic sea-ice, these are likely to be only relatively minor contributors of this biomarker. As such, *B. adeliensis* probably represents a major source of $IPSO_{25}$ in coastal Antarctic sea-ice and underlying sediments, as further supported by outcomes of surface sediments analysis.

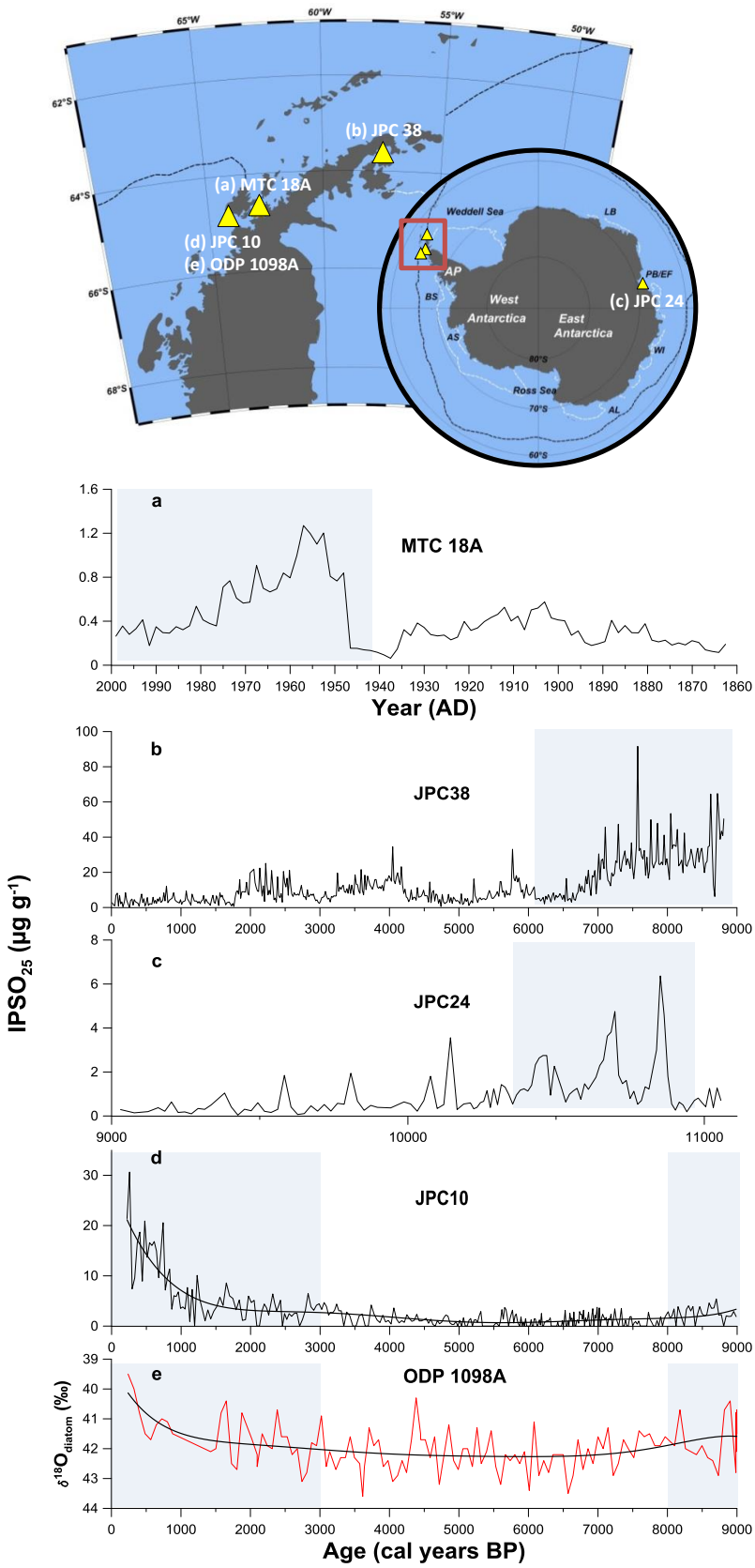

Figure 5.13: $IPSO_{25}$ in down-core records; (a)-(d), distribution of $IPSO_{25}$ in previously published down-core records covering different timescales. The relationship between enhanced $IPSO_{25}$ and increased meltwater inflow from nearby ice shelves and glaciers is highlighted by shaded area in each case. (a) WAP (Barbara et al., 2013); (b) Prydz Bay, East Antarctica (Barbara et al., 2010); (c) northeastern AP (Barbara et al., 2016); (d) Palmer Deep (WAP) (Etourneau et al., 2013); (e) Meltwater record from core ODP1098 (Pike et al., 2013) which is at the same site as JPC10.

Thus far, the presence and sedimentary abundance distribution of HBI trienes within the samples presented here have not been discussed, mainly as the search for a source responsible for their biosynthesis in the Southern Ocean is still ongoing. Identification of a source identification of the HBI trienes would potentially provide vital information that would enable their sedimentary occurrence and distribution to be better deciphered (cf. $IPSO_{25}$). In the meantime, some preliminary discussion regarding the sedimentary distribution of both HBI trienes is offered.

As already mentioned (Section 5.1), the sedimentary occurrence of HBI triene IIIa has been used in some previous paleo records as an open water indicator (e.g. Etourneau et al., 2013, Barbara et al., 2013, Campagne et al., 2016). This generalisation has, however, been suggested as potentially misleading (Collins et al., 2013), since the term 'open water' could, refer to permanently ice free locations, but also open waters associated with the MIZ or even pockets of open water within the SIZ. Therefore, and based on the good sedimentary correlation of $IPSO_{25}$ and HBI triene IIIa in glacial age sediments, Collins et al. (2013) suggested a close association of both biomarkers with sea-ice, but with the MIZ playing a crucial role in the distribution of HBI triene IIIa, in particular. This observation was also seen through analysis of surface waters from East Antarctica as part of the current study (Chapter 4). A similar amplification of HBI triene IIIa abundances in the MIZ is, however, not especially evident from the surface sediments presented here. In fact, the highest concentrations of HBI triene IIIa (up to 12 ng g^{-1}) were observed in coastal locations (cf $IPSO_{25}$) with generally lower abundances observed further offshore (Figure 5.7). In line with this, a positive correlation of sedimentary $IPSO_{25}$ and HBI triene IIIa abundance is observed ($r=0.611$, $p<0.05$), suggesting an association of both biomarkers to the same, coastally bound sea-ice environment. Indeed, the sedimentary occurrence of HBI triene IIIa is also closely coupled with $IPSO_{25}$. For example, out of 86 samples where HBI triene IIIa was

detected, 81 also contained $IPSO_{25}$. On the other hand, HBI triene IIIa was only present in 5 samples where $IPSO_{25}$ was absent (or below the LOD), and the concentrations of HBI triene IIIa in these were very low and the stations were located further offshore. Therefore, based on the data presented here, it appears that sedimentary distribution of HBI triene IIIa is extremely similar to that of $IPSO_{25}$ (i.e. coastal settings). Sedimentary abundances of HBI triene IIIa were, however, far less variable than those of $IPSO_{25,}$ as shown through the ratio between the two biomarkers (II/IIIa, Figure 5.14), which varied by ca four orders of magnitude (3-1560), with the highest values (>1000) observed in location from North-West Weddell Sea (Figure 5.14). On a more regional scale, however, the variation in the II/IIIa ratio was smaller and values varied by about one to two orders of magnitude. Thus, for example, ranges in II/IIIa ratio from Ross Sea, Amundsen Sea, South-East and North-West Weddell Sea were 77-520, 2-156, 250-1560 and 3-330 respectively. The reason behind this relatively high regional and inter-regional variation is not clear, although the influences of regionally-driven environmental processes in each region will likely play an important role. In the meantime, it is noted that sedimentary changes in II/IIIa ratio spanning approximately an order of magnitude within temporal records, have previously been interpreted as indicative of major changes in sea-ice extent (e.g. Barbara et al., 2013, Etourneau et al., 2013). On the basis of the surface sediment data presented, however, such interpretations might need to be re-considered.

As suggested previously (Chapter 4), the sedimentary occurrence of HBI triene IIIb might provide a suitable alternative indicator of phytoplankton production in the Southern Ocean. However, the generally lower abundances of HBI triene IIIb might hinder its detection, in practice. In line with this, HBI triene IIIb was only detected in 52 out of 149 samples. In each of the 52 samples, however, sedimentary occurrence of HBI triene IIIb was always accompanied by the presence of HBI triene IIIa and abundances

of both HBI trienes were also highly correlated (r=0.938, p<0.05). Concentrations of HBI triene IIIb were almost exclusively lower than those of HBI triene IIIa (Table 5.1), an exception being two stations within the Antarctic Peninsula (King George Island), where, although very low, concentrations of HBI triene IIIb were equal or marginally higher than those of HBI triene IIIa (Table 5.1)

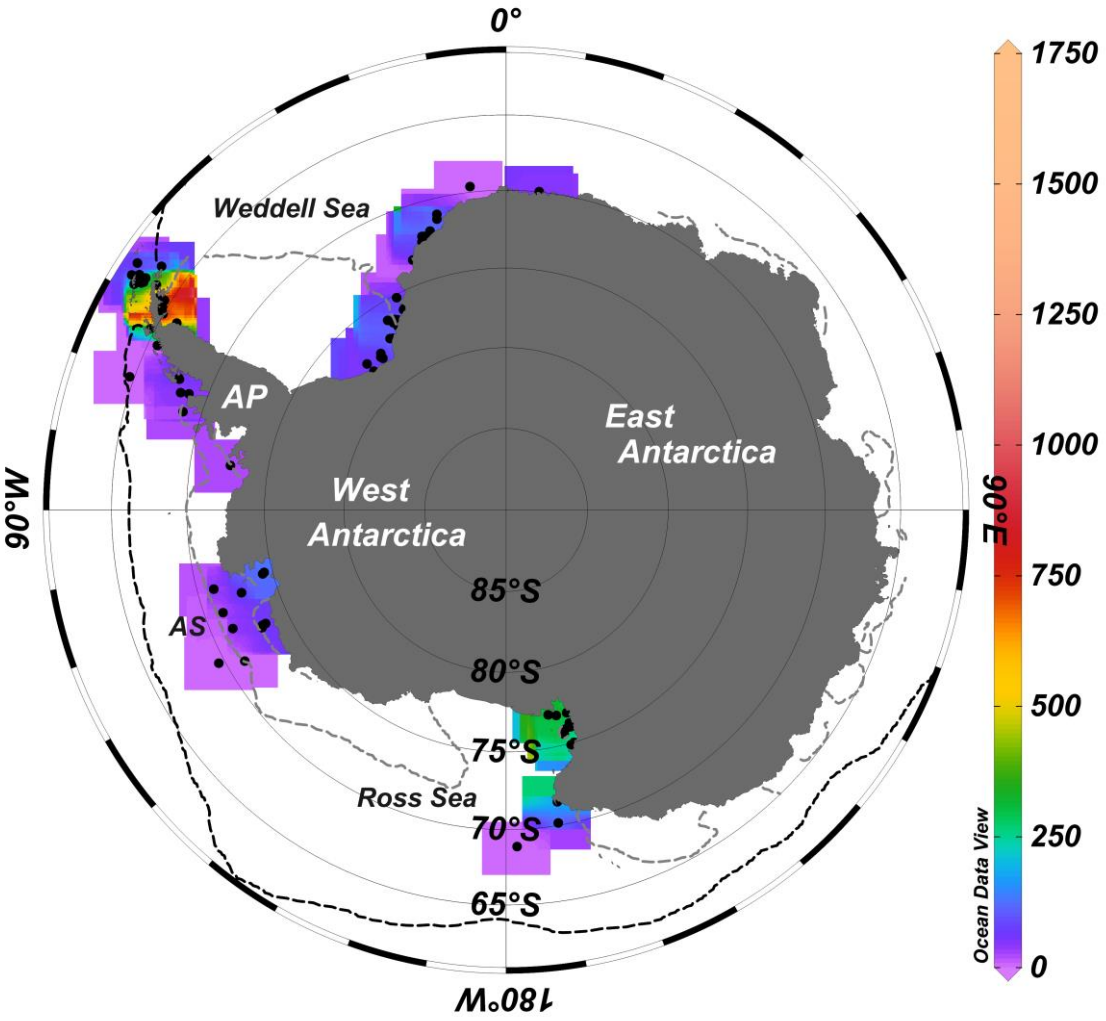

Figure 5.14: Map showing regional variation of ratio between sedimentary $IPSO_{25}$ and HBI triene IIIa (II/IIIa). Black and grey stippled lines correspond to median maximum (October) and minimum (February) sea-ice extent, respectively (NSIDC; Fetterer et al., 2002). AS: Amundsen Sea.

Although well correlated, a linear relationship between both trienes (in sediments) was not as strong (R^2=0.88) as for surface waters (R^2=0.99), possibly as a result of variable degradation of each biomarker within the water column or sediments themselves. This

seems possible given the slight differences in their respective oxidation rates under controlled conditions (Rontani et al., 2014), although further analysis of environmental samples, including water column and sediment traps, is required to confirm this. Alternatively, variable abundances of sedimentary HBI triene IIIa and IIIb may reflect an additional environmental source of one or both of these biomarkers. Confirmation of this will require analysis of marine diatoms in the Southern Ocean, including those from the genera *Pleurosigma* and *Rhisoselinia*, that are known to biosynthesise HBI trienes (Belt et al., 2001b). This, in part, could explain the higher concentration of HBI triene IIIb in two sediment samples collected from King George Island in the Antarctic Peninsula. With relation to $IPSO_{25,}$ HBI triene IIIb was detected in 51 out of 52 stations when $IPSO_{25}$ was identified and their sedimentary abundances were relatively well correlated (Table 5.2) (cf. $IPSO_{25}$ and HBI triene IIIa; Table 5.2).

5.5 Conclusions

In summary, the sedimentary distribution of $IPSO_{25}$ showed significant variation (up to four orders of magnitude) in abundance between different regions of Antarctica, but also on a more local scale. The highest concentrations of $IPSO_{25}$ (up to ca 1800 ng g^{-1}) were generally observed in near coastal settings, with a general decrease in concentration seen in locations further off shore. In addition, $\delta^{13}C$ values for $IPSO_{25}$ in selected surface sediments suggest the biosynthesis of the biomarker in a semi-enclosed sea-ice environment. The sedimentary occurrence of HBI trienes shows a similarity with that of $IPSO_{25}$ and hence, a strong coastal relationship to their biosynthesis, likely reflecting the preferred habitat of their (as yet unknown) source(s). Individually, abundances of HBI triene IIIa show generally higher sedimentary abundances compared to HBI triene IIIb; however, it is clear that the identification of the environmental

sources of HBI trienes in the Southern Ocean is still needed in order to better evaluate the distribution of these biomarkers in the samples presented here.

The outcomes of the sedimentary analysis of $IPSO_{25}$ are consistent with the ecology of the tube-dwelling diatom *Berkeleya adeliensis* Medlin, now identified as a previously unknown source of $IPSO_{25}$. In particular, the strong coastal association of sedimentary $IPSO_{25}$ is consistent with the presence of *B. adeliensis* as a common and relatively abundant species within Antarctic landfast ice diatom communities and distributions of $IPSO_{25}$ in Antarctic sediments are closely related to its ecology. Thus, in addition to representing a qualitative measure of the past occurrence of Antarctic landfast ice during late spring/summer, variability in sedimentary $IPSO_{25}$ could potentially provide further insights into changes to ice shelf and glacial melt processes in long-term records. Additionally, determination of the stable isotopic composition ($\delta^{13}C$) may also be particularly enlightening for understanding the structural characteristics of the sea-ice from which $IPSO_{25}$ was derived (i.e. platelet versus consolidated bottom ice). However, measuring the $IPSO_{25}$ content in a larger number of sea-ice diatoms, in sea-ice of different types and from other regions is required before the interpretation of its precise sedimentary signature can be fully deciphered.

CHAPTER SIX

6 Conclusions and Future work

6.1 Conclusions

The main aim of this study was to improve biomarker-based methods for sea-ice reconstruction in the Arctic and Antarctic. In particular, a more quantitative aspect of paleo sea-ice reconstruction was investigated for the Arctic, through the combined application of the sea-ice proxy IP_{25} and other structurally similar biomarkers of phytoplankton origin. In the Southern Ocean, efforts were concentrated to provide further knowledge about occurrence and distribution of various biomarker lipids in a number of matrices (sea-ice, water column, sediments), in order to better evaluate their environmental significance for paleo sea-ice reconstructions. Particular attention was placed on HBIs and a di-unsaturated analogue (termed here as HBI diene II or $IPSO_{25}$) of IP_{25}.

In order to achieve these overall aims, the following investigations were carried out:

1. In the Arctic (Barents Sea), analysis of surface sediments for IP_{25} and a tri-unsaturated HBI (HBI triene IIIa) from locations influenced by contrasting sea-ice settings was conducted. Along with previously published data from the Barents Sea, the sedimentary occurrence and abundance of these biomarkers were evaluated in order to provide more detailed sea-ice descriptions in historical records.

2. A combined biomarker-based approach (i.e. PIP_{25}) was carried out to evaluate HBI triene IIIa as a phytoplankton counterpart to $IP_{25,}$ and to provide semi-quantitative sea-ice estimates for the Barents Sea.

3. In the Southern Ocean, analysis of HBI biomarkers in various matrices was carried out to provide further knowledge and understanding about their potential use in paleo reconstructions

4. In both polar regions, the possibility of common environmental relationships between a number of biomarker lipids was investigated.

The **first aim** of this study was to improve the application of the IP_{25} proxy for sea-ice reconstructions in the Arctic by examining means of making them more quantitative, or, at least, for improving definitions of sea-ice conditions.

Analysis and evaluation of certain HBI lipids in a large number of surface sediments from locations within Barents Sea revealed that the relative sedimentary abundances of IP_{25} and a structurally similar HBI biomarker (HBI triene IIIa), were characteristic of the overlying surface oceanographic conditions. In particular, the location of the seasonal sea-ice edge appears to have a significant influence on their distributions. Thus, while IP_{25} was generally limited to locations experiencing seasonal sea-ice, with higher abundance found for locations with longer periods of ice cover, HBI triene IIIa was significantly enhanced in sediments within the vicinity of the retreating sea-ice edge or marginal ice zone (MIZ). This was suggested to reflect production of these biomarkers from source-specific diatoms, whose habitats are strongly dependent on the occurrence of seasonal sea-ice. Thus, by measuring IP_{25} alongside other source-specific biomarkers (e.g. HBI IIIa) whose production is particularly reflective of the neighbouring sea-ice conditions (e.g. winter sea-ice margin, marginal ice zone), it should be possible to provide more accurate descriptions of spring sea-ice conditions. Additionally, the response of HBI triene IIIa to this well-defined sea-ice scenario also appeared to be more selective than that of the more generic phytoplankton biomarker, brassicasterol.

A combined biomarker approach resulted in reasonably good positive linear relationship between PIP_{25} indices and spring sea-ice concentration, with the strongest correlation found when using a tri-unsaturated HBI (HBI triene IIIa, $P_{IIIa}IP_{25}$) as the open-water counterpart to IP_{25}. This was suggested to reflect a possibly greater sensitivity of HBI triene IIIa to the seasonal sea-ice conditions compared to brassicasterol, with enhanced production in the MIZ compared to regions of longer lasting sea-ice cover. The quality of the linear fits between $P_{IIIa}IP_{25}$ and spring sea-ice concentration (SpSIC) together with their respective spatial distributions were also far less dependent on the balance factor c, than for P_BIP_{25} (PIP_{25} index derived from brassicasterol). This was suggested to have positive consequences for semi-quantitative reconstructions of sea-ice conditions in downcore records, and when making comparisons between outcomes from different Arctic regions or climatic epochs.

In contrast, linear relationships between individual biomarkers and spring (SpSIC) and summer (SuSIC) sea-ice concentrations or between PIP_{25} values and SuSIC were much weaker. However, a lower limit threshold for $P_{IIIa}IP_{25}$ (ca. 0.8) was suggested to represent a useful qualitative proxy for the past occurrence of summer sea-ice for the Barents Sea, at least.

The re-evaluation of biomarker data from three dated marine sequences in the Barents Sea showed that combined analysis of IP_{25} and HBI triene IIIa has the potential to provide more detailed and semi-quantitative description of sea-ice conditions in the Barents Sea.

The **second aim** of this study was to improve our understanding of biomarker-based reconstructions in Southern Ocean, through analysis of HBIs in sea-ice, sediments and water column samples.

Analysis of surface water samples from an East Antarctic transect off the Sabrina Coast (Chapter 4) revealed that distributions of a di-unsaturated HBI (HBI diene II), and tri-unsaturated HBIs (HBI trienes IIIa and IIIb) were extremely sensitive to the local sea-ice conditions. Thus, HBI diene II was only detected for sampling sites that experienced seasonal sea-ice, with highest concentrations found in coastal locations with longer-lasting ice cover and a recurrent polynya. In contrast, HBIs triene IIIa and triene IIIb were observed in surface waters from the POOZ, the MIZ and the SIZ, but with highest concentrations within the region of the retreating sea-ice edge (the MIZ). Production of HBI trienes in the SIZ was suggested to reflect favourable conditions associated with a polynya-type environment. Observations were consistent with significant environmental control over the biosynthesis of HBI diene II and HBI trienes by sea-ice diatoms and open water phytoplankton, respectively, with the production of HBI trienes being especially favoured within the vicinity of the retreating ice-edge.

Within the water column, abundances of all three HBIs showed variation between the three water depths analysed. In particular, the abundances increased from the surface (0-10m) to the subsurface (20-60 m) layer of the photic zone, with a decrease in concentrations observed towards the bottom of the water column (480-1300 m), with concentrations of HBI trienes particularly reduced. These variations were suggested to result from a possible variation in composition of the diatom species in the respective depths or alteration of each biomarker in the water column due to degradation. Each of those will require further investigation.

Although some environment-specific trends were also identified in the sterol and FA distributions, these were not as striking as those for HBI diene II and two HBI trienes, IIIa and IIIb.

Outcomes of this study generally supported various previous deductions based on sedimentary records of HBIs (only HBI diene II and HBI triene IIIa) in dated marine archives, especially the abundance of HBI diene II as an indicator of seasonal sea-ice extent and HBI triene IIIa as an open water indicator. Additionally, enhanced concentrations within the MIZ also supported the notion of a more specific indicator of increased productivity adjacent to the sea-ice edge, as suggested by Collins et al. (2013). However, a number of factors, such as those associated with polynya formation and processes within the water column were suggested to potentially have important implications for use of these biomarkers for paleo sea-ice reconstructions.

The sedimentary distribution of HBI diene II (termed here as $IPSO_{25}$, Chapter 5) showed significant variation (up to four orders of magnitude) in abundances between different regions of Antarctica, but also on a more local scale. Highest concentrations of $IPSO_{25}$ were generally observed in near coastal settings, with a general downward gradient in concentration seen for locations further offshore. Further, $\delta^{13}C$ values for $IPSO_{25}$ in selected surface sediments indicated the biosynthesis of this biomarker in a semi-enclosed sea-ice environment. These outcomes of sedimentary analysis of $IPSO_{25}$ are consistent with the ecology of tube-dwelling diatom *Berkeleya adeliensis* Medlin, identified as previously unknown source of $IPSO_{25.}$ Through biomarker and species composition analysis of sea-ice it was suggested that *Berkeleya adeliensis* might represent a major source of this biomarker in Antarctic settings. Further it was hypothesised that the tendency of *Berkeleya adeliensis* to flourish in platelet ice might provide a useful sedimentary signal of landfast sea-ice, influenced by meltwater discharge from nearby glaciers and ice shelves, especially, since platelet ice formation is strongly associated with super-cooled freshwater inflow. Additionally, determination of the stable isotopic composition ($\delta^{13}C$) may also be particularly enlightening for

determining the structural characteristics of the sea-ice from which $IPSO_{25}$ was derived (i.e. platelet versus consolidated bottom ice).

The sedimentary occurrence of HBI trienes shows a similarity with that of $IPSO_{25}$ and hence, a strong coastal relationship to their biosynthesis, likely reflecting their (as yet unknown) source(s). Individually, abundances of HBI triene IIIa show a generally higher sedimentary concentrations compared to HBI triene IIIb, which as although sedimentary occurrence of HBI trienes generally supports however, it is clear that identification of the environmental sources of HBI trienes in the Southern Ocean is needed in order to better evaluate their distribution in samples presented here.

The **third aim** of this study was to investigate, and identify, any common environmental relationships between several HBI biomarkers in both polar regions.

Along these lines, it was noted (Chapter 3) that the sedimentary abundances between HBI triene IIIa and brassicasterol showed similar response to the overlaying oceanographic conditions. Thus, brassicasterol concentration was lowest for the region with most persistent sea-ice cover, slightly higher for ice-free settings, and highest for locations within the MIZ. However, the relative changes between the three regions were clearly greater for HBI triene IIIa than for brassicasterol. This was suggested to reflect brassicasterol being common constituent in marine phytoplankton, with a distribution pattern reflecting productivity spanning all growth seasons. On the other hand, enhancement of HBI triene IIIa was suggested to indicate likely biosynthesis by a much smaller number of sources, but whose growth is especially favoured by, or at least more tolerant to, the nutrient-rich and stratified upper water column found at the ice-edge.

In the surface waters of Southern Ocean (Chapter 4), the most striking environmental relationship was observed between HBI trienes IIIa and IIIb. The abundance distribution of both HBI trienes shown the similar enhancement in concentrations in MIZ with lower

abundances observed in SIZ and ice-free locations. Additionally, a high linear relationship (R^2=0.99) between the two HBI trienes was suggested to indicate the same environmental control over their production. The strength of the relationship between HBI triene IIIa and HBI triene IIIb also suggests that these lipids are likely made by the same source. This relationship also led to the suggestion that HBI IIIb could potentially be used as an additional biomarker of phytoplankton within the Southern Ocean, which might also have positive implications for studies in the Arctic.

Relatively strong relationship between HBI trienes was also observed within surface sediments (Chapter 5), although it was not as strong (R^2=0.88) as for surface waters (R^2=0.98). This was suggested to result either from variable degradation of each biomarker within the water column or sediments themselves or reflect an additional environmental source of one or both of these biomarkers. The sedimentary occurrence and distribution of both HBI trienes were also found to be similar to that of $IPSO_{25}$. This strong coastal relationship to their biosynthesis was suggested to likely reflect the preferred habitat of their (as yet unknown) source(s).

6.2 Future Work

To evaluate the applicability of combined biomarker approach presented here (Chapter 3), and to provide more detailed description of sea-ice conditions in other Arctic areas, future PIP_{25}-style investigations will be required. It will be of particular importance to establish relationships between sedimentary abundances of IP_{25} and HBI triene IIIa in other parts of the Arctic Ocean and for locations where the annual sea-ice cycle is not as well defined as for the Barents Sea. An additional interest would be to investigate other phytoplankton derived biomarkers that, as with HBI triene IIIa, might enable more detailed descriptions of sea-ice conditions to be proposed.

The identification of the organic geochemical biomarker $IPSO_{25}$ in the Antarctic sea-ice diatom *Berkeleya adeliensis* likely ensures that future interpretations of the sedimentary occurrence of this sea-ice proxy can be made with greater confidence and in more detail. However, measuring the $IPSO_{25}$ content in a larger number of sea-ice diatoms, in sea-ice of different types, in sea-ice from other regions and over the seasonal cycle are all required before the interpretation of its precise sedimentary signature can be fully deciphered.

Investigations into the reasons behind the variation in HBI distribution within the water column will need to be confirmed through further studies of water column samples and from other regions. Additional interest should be aimed at identification of environmental source(s) of HBI trienes, which would enable the sedimentary occurrence and distribution of these to be better evaluated.

Finally, the proposed application of $IPSO_{25}$ as a useful indicator of changes to ice shelf and glacial melt processes in long-term records will require further testing through down-core investigations. With this in mind, it is noted that ODP site 1098 from Palmer Deep is one of the best studied core sites from Antarctica, with a suite of proxy data available, including a melt water record (Pike et al.; 2013) that would provide for a direct proxy comparison.

REFERENCES

Ackley, S., 1981. A review of sea-ice weather relationships in the Southern Hemisphere., in Sea Level, Ice, and Climatic Change. Proceedings of the Camberra Symposium, IAHS Publ., 131, 127-159.

Allen, C. S., Pike, J., Pudsey, C. J., Leventer, A., 2005. Submillennial variations in ocean conditions during deglaciation based on diatom assemblages from the southwest Atlantic. Paleoceanography 20, PA2012.

Allen, C. S., Pike, J., Pudsey, C. J., 2011. Last glacial-interglacial sea-ice cover in the SW Atlantic and its potential role in global deglaciation. Quaternary Science Reviews 30, 2446-2458.

Andrews, J. T., Eberl, D. D., 2007. Quantitative mineralogy of surface sediments on the Iceland shelf, and application to down-core studies of Holocene ice-rafted sediments. Journal of Sedimentary Research 77, 469-479.

Armand, L. K., Leventer, A., 2003. Palaeo sea ice distribution-reconstruction and palaeoclimatic significance., in Sea Ice: An Introduction to its Physics, Chemistry, Biology and Geology, ed. Thomas, D. N.and Dieckmann, G. S., Blackwell Science Ltd., Oxford, pp. 333-362.

Armand, L. K., Crosta, X., Romero, O., Pichon, J.-J., 2005. The biogeography of major diatom taxa in Southern Ocean sediments: 1. Sea ice related species. Palaeogeography, Palaeoclimatology, Palaeoecology 223, 93-126.

Armand, L. K.,Leventer, A., 2010. Palaeo sea ice distribution and reconstruction derived from the geological records., in Sea ice, ed. Thomas, D. N.and Dieckmann, G. S., Blackwell Science Ltd., Oxford,UK, pp. 469-530.

Arrigo, K., Dieckmann, G., Gosselin, M., Robinson, D., Fritsen, C., Sullivan, C., 1995. High resolution study of the platelet ice ecosystem in McMurdo Sound, Antarctica biomass, nutrient, and production profiles within a dense microalgal bloom. Marine Ecology-Progress Series 127, 255-268.

Arrigo, K. R., Worthen, D. L., Lizotte, M. P., Dixon, P., Dieckmann, G., 1997. Primary production in Antarctic sea ice. Science 276, 394-397.

Arrigo, K. R., Van Dijken, G., Pabi, S., 2008. Impact of a shrinking Arctic ice cover on marine primary production. Geophysical Research Letters 35, L19603

Arrigo, K. R., Mock, T., Lizotte, M. P., 2010. Primary producers and sea ice, in Sea ice, ed. Thomas, D. N.and Dieckmann, G. S., Blackwell Publishing Ltd, Oxford, pp. 283-325.

Arrigo, K. R., Van Dijken, G. L., 2015. Continued increases in Arctic Ocean primary production. Progress in Oceanography 136, 60-70.

Arzel, O., Fichefet, T., Goosse, H., 2006. Sea ice evolution over the 20th and 21st centuries as simulated by current AOGCMs. Ocean Modelling 12, 401-415.

Aure, J., Strand, Ø., 2001. Hydrographic normals and long-term variations at fixed surface layer stations along the Norwegian coast from 1936 to 2000. Fisken og havet 13, 1-24.

Barbara, L., Crosta, X., Massé, G., Ther, O., 2010. Deglacial environments in eastern Prydz Bay, East Antarctica. Quaternary Science Reviews 29, 2731-2740.

Barbara, L., Crosta, X., Schmidt, S., Massé, G., 2013. Diatoms and biomarkers evidence for major changes in sea ice conditions prior the instrumental period in Antarctic Peninsula. Quaternary Science Reviews 79, 99-110.

Barbara, L., Crosta, X., Leventer, A., Schmidt, S., Etourneau, J., Domack, E., Massé, G., 2016. Environmental responses of the Northeast Antarctic Peninsula to the Holocene climate variability. Paleoceanography 31, 131-147.

Belt, S. T., Cooke, D. A., Robert, J.-M., Rowland, S., 1996. Structural characterisation of widespread polyunsaturated isoprenoid biomarkers: A C_{25} triene, tetraene and pentaene from the diatom Haslea ostrearia simonsen. Tetrahedron Letters 37, 4755-4758.

Belt, S. T., Allard, W. G., Massé, G., Robert, J.-M., Rowland, S. J., 2000a. Highly branched isoprenoids (HBIs): identification of the most common and abundant sedimentary isomers. Geochimica et Cosmochimica Acta 64, 3839-3851.

Belt, S. T., Allard, W. G., Massé, G., Robert, J. M., Rowland, S. J., 2000b. Important sedimentary sesterterpenoids from the diatom *Pleurosigma intermedium*. Chemical Communication, 501-502.

Belt, S. T., Allard, W. G., Massé, G., Robert, J.-M., Rowland, S. J., 2001a. Structural characterisation of C_{30} highly branched isoprenoid alkenes (rhizenes) in the marine diatom *Rhizosolenia setigera*. Tetrahedron Letters 42, 5583-5585.

Belt, S. T., Massé, G., Allard, W. G., Robert, J.-M., Rowland, S. J., 2001b. C_{25} highly branched isoprenoid alkenes in planktonic diatoms of the *Pleurosigma genus*. Organic Geochemistry 32, 1271-1275.

Belt, S. T., Massé, G., Rowland, S. J., Poulin, M., Michel, C., Leblanc, B., 2007. A novel chemical fossil of palaeo sea ice: IP_{25}. Organic Geochemistry 38, 16-27.

Belt, S. T., Massé, G., Vare, L. L., Rowland, S. J., Poulin, M., Sicre, M.-A., Sampei, M., Fortier, L., 2008. Distinctive ^{13}C isotopic signature distinguishes a novel sea ice biomarker in Arctic sediments and sediment traps. Marine Chemistry 112, 158-167.

Belt, S. T., Vare, L. L., Massé, G., Manners, H. R., Price, J. C., Maclachlan, S. E., Andrews, J. T., Schmidt, S., 2010. Striking similarities in temporal changes to spring sea ice occurrence across the central Canadian Arctic Archipelago over the last 7000 years. Quaternary Science Reviews 29, 3489-3504.

Belt, S. T., Brown, T. A., Navarro-Rodriguez, A., Cabedo-Sanz, P., Tonkin, A., Ingle, R., 2012. A reproducible method for the extraction, identification and quantification of the Arctic sea ice proxy IP_{25} from marine sediments. Analytical Methods 4, 705-713.

Belt, S. T., Brown, T. A., Ringrose, A. E., Cabedo-Sanz, P., Mundy, C. J., Gosselin, M., Poulin, M., 2013. Quantitative measurement of the sea ice diatom biomarker IP_{25} and sterols in Arctic sea ice and underlying sediments: Further considerations for palaeo sea ice reconstrucion. Organic Geochemistry 62, 33-45.

Belt, S. T., Müller, J., 2013. The Arctic sea ice biomarker IP_{25}: a review of current understanding, recommendations for future research and applications in palaeo sea ice reconstructions. Quaternary Science Reviews 79, 9-25.

Belt, S. T., Brown, T. A., Ampel, L., Cabedo-Sanz, P., Fahl, K., Kocis, J. J., Masse, G., Navarro-Rodriguez, A., Ruan, J.,Xu, Y., 2014. An inter-laboratory investigation of the Arctic sea ice biomarker proxy IP_{25} in marine sediments: key outcomes and recommendations. Climate of the Past 10, 155-166.

Belt, S. T., Cabedo-Sanz, P., Smik, L., Navarro-Rodriguez, A., Berben, S. M. P., Knies, J., Husum, K., 2015. Identification of paleo Arctic winter sea ice limits and the marginal ice zone: Optimised biomarker-based reconstructions of late Quaternary Arctic sea ice. Earth and Planetary Science Letters 431, 127-139.

Berben, S. 2014. A Holocene palaeoceanographic multi-proxy study on the variability of Atlantic water inflow and sea ice distribution along the pathway of Atlantic water. University of Tromsø (PhD thesis).

Berben, S., Husum, K., Cabedo-Sanz, P., Belt, S., 2014. Holocene sub-centennial evolution of Atlantic water inflow and sea ice distribution in the western Barents Sea. Climate of the Past 10, 181-198.

Bi, D., Budd, W. F., Hirst, A. C., Wu, X., 2001. Collapse and reorganisation of the Southern Ocean overturning under global warming in a coupled model. Geophysical Research Letters 28, 3927-3930.

Bischof, J. F., Darby, D. A., 2000. Quaternary ice transport in the Canadian Arctic and extent of Late Wisconsinan glaciation in the Queen Elizabeth Islands. Canadian Journal of Earth Sciences 36, 2007-2022.

Bond, G., Showers, W., Cheseby, M., Lotti, R., Almasi, P., Priore, P., Cullen, H., Hajdas, I., Bonani, G., 1997. A pervasive millennial-scale cycle in North Atlantic Holocene and Glacial Climates. Science 278, 1257-1266.

Bond, G., Kromer, B., Beer, J., Muscheler, R., Evans, M. N., Showers, W., Hoffmann, S., Lotti-Bond, R., Hajdas, I., Bonani, G., 2001. Persistent solar influence on North Atlantic climate during the Holocene. Science 294, 2130-2136.

Brandon, M. A., Cottier, F. R., Nilsen, F., 2010. Sea ice and oceanography., in Sea Ice, ed. Thomas, D. N.and Dieckmann, G. S., Blackwell Science Ltd., Oxford,UK, pp. 79-111.

Brassell, S. C., Eglinton, G., Marlowe, I. T., Pflaumann, U., Sarnthein, M., 1986. Molecular stratigraphy-A new tool for climatic assessment. Nature 320, 129-133.

Brown, T. A. 2011. Production and preservation of the Arctic sea ice diatom biomarker IP_{25}. University of Plymouth (PhD thesis).

Brown, T. A., Belt, S. T., Philippe, B., Mundy, C. J., Massé, G., Poulin, M., Gosselin, M., 2011. Temporal and vertical variations of lipid biomarkers during a bottom ice diatom bloom in the Canadian Beaufort Sea: further evidence for the use of the IP_{25} biomarker as a proxy for spring Arctic sea ice. Polar Biology 34, 1857-1868.

Brown, T. A., Belt, S. T., Cabedo-Sanz, P., 2014a. Identification of a novel di-unsaturated C_{25} highly branched isoprenoid in the marine tube-dwelling diatom Berkeleya rutilans. Environmental Chemistry Letters 12, 455-460.

Brown, T. A., Belt, S. T., Tatarek, A.,Mundy, C. J., 2014b. Source identification of the Arctic sea ice proxy IP_{25}. Nature Communications 5, 4197

Brown, T. A., Hegseth, E. N., Belt, S. T., 2015. A biomarker-based investigation of the mid-winter ecosystem in Rijpfjorden, Svalbard. Polar Biology 38, 1-14.

Buffen, A., Leventer, A., Rubin, A., Hutchins, T., 2007. Diatom assemblages in surface sediments of the northwestern Weddell Sea, Antarctic Peninsula. Marine Micropaleontology 62, 7-30.

Cabedo-Sanz, P. 2013. Identification of variability in sub-arctic sea ice conditions during the Younger Dryas and Holocene. University of Plymouth (PhD Thesis).

Cabedo-Sanz, P., Belt, S. T., Knies, J., Husum, K., 2013. Identification of contrasting seasonal sea ice conditions during the Younger Dryas. Quaternary Science Reviews 79, 74-86.

Campagne, P., Crosta, X., Houssais, M., Swingedouw, D., Schmidt, S., Martin, A., Devred, E., Capo, S., Marieu, V., Closset, I., 2015. Glacial ice and atmospheric forcing on the Mertz Glacier Polynya over the past 250 years. Nature Communications 6, 6642

Campagne, P., Crosta, X., Schmidt, S., Houssais, M. N., Ther, O., Massé, G., 2016. Sedimentary response to sea ice and atmospheric variability over the instrumental period off Adélie Land, East Antarctica. Biogeosciences 13, 4205-4218.

Collins, L. G., Allen, C. S., Pike, J., Hodgson, D. A., Weckström, K., Massé, G., 2013. Evaluating highly branched isoprenoid (HBI) biomarkers as a novel Antarctic sea-ice proxy in deep ocean glacial age sediments. Quaternary Science Reviews 79, 87-98.

Comiso, J. C., Nishio, F., 2008. Trends in the sea ice cover using enhanced and compatible AMSR‐E, SSM/I, and SMMR data. Journal of Geophysical Research: Oceans 113, C02S07

Comiso, J. C., Parkinson, C. L., Gersten, R., Stock, L., 2008. Accelerated decline in the Arctic Sea ice cover. Geophysical Research Letters 35, L01703.

Comiso, J. C., 2010. Variability and Trends of the Global Sea Ice Cover, in Sea Ice, ed. Thomas, D. N.and Dieckmann, G. S., Wiley-Blackwell, Chichester, pp. 205-246.

Cook, A., Fox, A., Vaughan, D., Ferrigno, J., 2005. Retreating glacier fronts on the Antarctic Peninsula over the past half-century. Science 308, 541-544.

Cremer, H., Roberts, D., Mcminn, A., Gore, D., Melles, M., 2003. The Holocene diatom flora of marine bays in the Windmill Islands, East Antarctica. Botanica Marina 46, 82-106.

Cronin, T. M., Holtz, T. R., Whatley, R. C., 1994. Quaternary paleoceanography of the deep Arctic Ocean based on quantitative analysis of Ostracoda. Marine Geology 119, 305-332.

Cronin, T. M., Holtz, T. R., Stein, R., Spielhagen, R., Futterer, D., Wollenburg, J., 1995. Late Quaternary Palaoceanography of the Eurasian Basin Arctic Ocean. Paleoceanography 10, 259-281.

Cronin, T. M., Gemery, L., Briggs Jr, W. M., Jakobsson, M., Polyak, L., Brouwers, E. M., 2010. Quaternary Sea-ice history in the Arctic Ocean based on a new Ostracode sea-ice proxy. Quaternary Science Reviews 29, 3415-3429.

Cronin, T. M., Polyak, L., Reed, D., Kandiano, E. S., Marzen, R. E., Council, E. A., 2013. A 600-ka Arctic sea-ice record from Mendeleev Ridge based on ostracodes. Quaternary Science Reviews 79, 157-167.

Crosta, X., Pichon, J. J., Burckle, L. H., 1998. Application of modern analog technique to marine Antarctic diatoms: Reconstruction of maximum sea-ice extent at the Last Glacial Maximum. Paleoceanography 13, 284-297.

Crosta, X., Sturm, A., Armand, L., Pichon, J. J., 2004. Late Quaternary sea ice history in the Indian sector of the Southern Ocean as recorded by diatom assemblages. Marine Micropaleontology 50, 209-223.

Crosta, X., Romero, O., Armand, L. K., Pichon, J.-J., 2005. The biogeography of major diatom taxa in Southern Ocean sediments: 2. Open ocean related species. Palaeogeography, Palaeoclimatology, Palaeoecology 223, 66-92.

Crosta, X., Koç, N., 2007. Diatoms: from micropaleontology to isotope geochemistry., in Proxies in Late Cenozoic Paleoceanography, ed. Hillaire-Marcel, C., de Vernal, A., Elsevier, Amsterdam, pp. 327-369.

de Vernal, A., Hillaire-Marcel, C., Turon, J. L., Matthiessen, J., 2000. Reconstruction of sea-surface temperature, salinity, and sea-ice cover in the northern North Atlantic during the last glacial maximum based on dinocyst assemblages. Canadian Journal of Earth Sciences 37, 725-750.

de Vernal, A., Henry, M., Matthiessen, J., Mudie, P. J., Rochon, A., Boessenkool, K. P., Eynaud, F., Grøsfjeld, K., Guiot, J., Hamel, D., Harland, R., Head, M. J., Kunz-Pirrung, M., Levac, E., Loucheur, V., Peyron, O., Pospelova, V., Radi, T., Turon, J.-L., Voronina, E., 2001. Dinoflagellate cyst assemblages as tracers of sea-surface conditions in the northern North Atlantic, Arctic and sub-Arctic seas: the new n=677 data base and its application for quantitative palaeoceanographic reconstruction. Journal of Quaternary Science 16, 681-698.

de Vernal, A., Eynaud, F., Henry, M., Hillaire-Marcel, C., Londeix, L., Mangin, S., Matthiessen, J., Marret, F., Radi, T., Rochon, A., Solignac, S., Turon, J. L., 2005. Reconstruction of sea-surface conditions at middle to high latitudes of the Northern Hemisphere during the Last Glacial Maximum (LGM) based on dinoflagellate cyst assemblages. Quaternary Science Reviews 24, 897-924.

de Vernal, A., Gersonde, R., Goosse, H., Seidenkrantz, M.-S., Wolff, E. W., 2013a. Sea ice in the paleoclimate system: the challenge of reconstructing sea ice from proxies-an introduction. Quaternary Science Reviews 79, 1-8.

de Vernal, A., Hillaire-Marcel, C., Rochon, A., Fréchette, B., Henry, M., Solignac, S., Bonnet, S., 2013b. Dinocyst-based reconstructions of sea ice cover concentration during the Holocene in the Arctic Ocean, the northern North Atlantic Ocean and its adjacent seas. Quaternary Science Reviews 79, 111-121.

de Vernal, A., Rochon, A., Fréchette, B., Henry, M., Radi, T., Solignac, S., 2013c. Reconstructing past sea ice cover of the Northern Hemisphere from dinocyst assemblages: status of the approach. Quaternary Science Reviews 79, 122-134.

Denis, D., Crosta, X., Barbara, L., Massé, G., Renssen, H., Ther, O., Giraudeau, J., 2010. Sea ice and wind variability during the Holocene in East Antarctica: insight on middle-high latitude coupling. Quaternary Science Reviews 29, 3709-3719.

Dickson, R., Rudels, B., Dye, S., Karcher, M., Meincke, J., Yashayaev, I., 2007. Current estimates of freshwater flux through Arctic and subarctic seas. Progress in Oceanography 73, 210-230.

Dieckmann, G. S., Rohardt, G., Hellmer, H., Kipfstuhl, J., 1986. The occurrence of ice platelets at 250 m depth near the Filchner ice shelf and it's significance for sea ice biology. Deep-sea research. Part A, Oceanographic research papers 33, 141-148.

Dieckmann, G. S.,Hellmer, H. H., 2010. The importance of sea ice: an overview., in Sea ice, ed. Thomas, D. N.and Dieckmann, G. S., Wiley-Blackwell, Chichester, pp. 1-22.

Divine, D. V., Dick, C., 2006. Historical variability of sea ice edge position in the Nordic Seas. Journal of Geophysical Research 111, C01001.

Dunbar, R., Leventer, A., 1992. Seasonal variation in carbon isotopic composition of Antarctic sea ice and open-water plankton communities. Antarctic Journal of the United States 27, 79-81.

Ebbesen, H., Hald, M., 2004. Unstable Younger Dryas climate in the northeast North Atlantic. Geology 32, 673-676.

Eglinton, T. I., Eglinton, G., 2008. Molecular proxies for paleoclimatology. Earth and Planetary Science Letters 275, 1-16.

Eiríksson, J., Knudsen, K. L., Haflidason, H., Heinemeier, J., 2000. Chronology of late Holocene climatic events in the northern North Atlantic based on AMS ^{14}C dates and tephra markers from the volcano Hekla, Iceland. Journal of Quaternary Science 15, 573-580.

Esper, O., Gersonde, R., 2014. New tools for the reconstruction of Pleistocene Antarctic sea ice. Palaeogeography, Palaeoclimatology, Palaeoecology 399, 260-283.

Etourneau, J., Collins, L. G., Willmott, V., Kim, J. H., Barbara, L., Leventer, A., Schouten, S., Sinninghe Damsté, J. S., Bianchini, A., Klein, V., Crosta, X., Massé, G., 2013. Holocene climate variations in the western Antarctic Peninsula: evidence for sea ice extent predominantly controlled by changes in insolation and ENSO variability. Climate of the Past 9, 1431-1446.

Fahl, K., Stein, R., 2012. Modern seasonal variability and deglacial/Holocene change of central Arctic Ocean sea-ice cover: New insights from biomarker proxy records. Earth and Planetary Science Letters 351, 123-133.

Ferry, A. J., Prvan, T., Jersky, B., Crosta, X., Armand, L. K., 2015. Statistical modeling of Southern Ocean marine diatom proxy and winter sea ice data: Model comparison and developments. Progress in Oceanography 131, 100-112.

Fetterer, F., K. Knowles, W. Meier, and M. Savoie. 2002, updated daily. Sea Ice Index, Version 1. G02135. Boulder, Colorado USA. NSIDC: National Snow and Ice Data Center. doi: http://dx.doi.org/10.7265/N5QJ7F7W.

Foldvik, A., Kvinge, T. Conditional instability of sea water at the freezing point. Deep Sea Research and Oceanographic Abstracts, 1974. Elsevier, 169-174.

Gersonde, R., Zielinski, U., 2000. The reconstruction of late Quaternary Antarctic sea-ice distribution—the use of diatoms as a proxy for sea-ice. Palaeogeography, Palaeoclimatology, Palaeoecology 162, 263-286.

Gersonde, R., Crosta, X., Abelmann, A., Armand, L., 2005. Sea-surface temperature and sea ice distribution of the Southern Ocean at the EPILOG Last Glacial Maximum—a circum-Antarctic view based on siliceous microfossil records. Quaternary Science Reviews 24, 869-896.

Gibson, J. A. E., Trull, T., Nichols, P. D., Summons, R. E., McMinn, A., 1999. Sedimentation of ^{13}C-rich organic matter from Antarctic sea-ice algae: A potential indicator of past sea-ice extent. Geology 27, 331-334.

Gleitz, M., v.d. Loeff, M. R., Thomas, D. N., Dieckmann, G. S.,Millero, F. J., 1995. Comparison of summer and winter inorganic carbon, oxygen and nutrient concentrations in Antarctic sea ice brine. Marine Chemistry 51, 81-91.

Gooday, A. J., 2003. Benthic foraminifera (Protista) as tools in deep-water palaeoceanography: environmental influences on faunal characteristics. Advances in Marine Biology 46, 1-90.

Grossi, V., Beker, B., Geenevasen, J. A. J., Schouten, S., Raphel, D., Fontaine, M.-F., Sinninghe Damsté, J. S., 2004. C_{25} highly branched isoprenoid alkene from the marine benthic diatom *Pleurosigma strigosum*. Phytochemistry 65, 3049-3055.

Günther, S., Dieckmann, G. S., 1999. Seasonal development of algal biomass in snow-covered fast ice and the underlying platelet layer in the Weddell Sea, Antarctica. Antarctic Science 11, 305-315.

Gwyther, D., Galton-Fenzi, B., Hunter, J., Roberts, J., 2014. Simulated melt rates for the Totten and Dalton ice shelves. Ocean Science 10, 267-279.

Henley, S., Annett, A., Ganeshram, R., Carson, D., Weston, K., Crosta, X., Tait, A., Dougans, J., Fallick, A., Clarke, A., 2012. Factors influencing the stable carbon isotopic composition of suspended and sinking organic matter in the coastal Antarctic sea ice environment. Biogeosciences 9, 1137-1157.

Holland, M. M., Bitz, C. M., Tremblay, B., 2006. Future abrupt reductions in the summer Arctic sea ice. Geophysical Research Letters 33, L23503

Hopkins, T. S., 1991. The GIN Sea-a synthesis of its physical oceanography and literature review 1972-1985. Earth Science Reviews 30, 175-318.

Horner, R., Ackley, S. F., Dieckmann, G. S., Gulliksen, B., Hoshiai, T., Legendre, L., Melnikov, I. A., Reeburgh, W. S., Spindler, M., Sullivan, C. W., 1992. Ecology of sea ice biota. Polar Biology 12, 417-427.

Huang, W.-Y., Meinschein, W. G., 1976. Sterols as source indicators of organic materials in sediments. Geochimica et Cosmochimica Acta 40, 323-330.

Huang, W.-Y., Meinschein, W., 1979. Sterols as ecological indicators. Geochimica et Cosmochimica Acta 43, 739-745.

Ichinomiya, M., Gomi, Y., Nakamachi, M., Honda, M., Fukuchi, M., Taniguchi, A., 2008. Temporal variations in the abundance and sinking flux of diatoms under fast ice in summer near Syowa Station, East Antarctica. Polar Science 2, 33-40.

Jacobs, S. S., 1991. On the nature and significance of the Antarctic Slope Front. Marine Chemistry 35, 9-24.

Jeffries, M., Weeks, W., Shaw, R., Morris, K., 1993. Structural characteristics of congelation and platelet ice and their role in the development of Antarctic land-fast sea ice. Journal of Glaciology 39, 223-238.

Jennings, A. E., Knudsen, K. L., Hald, M., Hansen, C. V., Andrews, J. T., 2002. A mid-Holocene shift in Arctic sea-ice variability on the East Greenland Shelf. The Holocene 12, 49-58.

Jensen, S., Renberg, L., Reutergardh, L., 1977. Residue analysis of sediment and sewage sludge for organochlorines in the presence of elemental sulfur. Analytical Chemistry 49, 316-318.

Johns, L., Wraige, E. J., Belt, S. T., Lewis, C. A., Massé, G., Robert, J. M., Rowland, S. J., 1999. Identification of a C_{25} highly branched isoprenoid (HBI) diene in Antarctic sediments, Antarctic sea-ice diatoms and cultured diatoms. Organic Geochemistry 30, 1471-1475.

Johnson, G. C., 2008. Quantifying Antarctic bottom water and North Atlantic deep water volumes. Journal of Geophysical Research: Oceans 113, C05027

Jones, R. L., Whatley, R. C., Cronin, T. M., Dowsett, H. J., 1999. Reconstructing late Quaternary deep-water masses in the eastern Arctic Ocean using benthonic Ostracoda. Marine Micropaleontology 37, 251-272.

Justwan, A., Koç, N., Jennings, A. E., 2008. Evolution of the Irminger and East Icelandic Current systems through the Holocene, revealed by diatom-based sea

surface temperature reconstructions. Quaternary Science Reviews 27, 1571-1582.

Kaiser, J., Belt, S. T., Tomczak, M., Brown, T. A., Wasmund, N., Arz, H. W., 2016. C_{25} highly branched isoprenoid alkenes in the Baltic Sea produced by the marine planktonic diatom *Pseudosolenia calcar-avis*. Organic Geochemistry 93, 51-58.

Kennedy, H., Thomas, D. N., Kattner, G., Haas, C., Dieckmann, G. S., 2002. Particulate organic matter in Antarctic summer sea ice: concentration and stable isotopic composition. Marine Ecology Progress Series 238, 1-13.

Killops, S. D., Killops, V. J., 2009. An introduction to organic geochemistry. John Whiley and Sons

Killworth, P. D., 1983. Deep convection in the World Ocean. Reviews of Geophysics 21, 1-26.

Kim, J.-H., Schouten, S., Hopmans, E. C., Donner, B., Sinninghe Damsté, J. S., 2008. Global sediment core-top calibration of the TEX86 paleothermometer in the ocean. Geochimica et Cosmochimica Acta 72, 1154-1173.

Knies, J., 2005. Climate-induced changes in sedimentary regimes for organic matter supply on the continental shelf off northern Norway. Geochimica et Cosmochimica Acta 69, 4631-4647.

Knies, J., Martinez, P., 2009. Organic matter sedimentation in the western Barents Sea region: terrestrial and marine contribution based on isotopic composition and organic nitrogen content. Norwegian Journal of Geology 89, 79-89.

Knies, J., Cabedo-Sanz, P., Belt, S. T., Baranwal, S., Fietz, S., Rosell-Melé, A., 2014. The emergence of modern sea ice cover in the Arctic Ocean. Nature Communications 5, 5608.

Korb, R. E., Whitehouse, M. J., Thorpe, S. E., Gordon, M., 2005. Primary production across the Scotia Sea in relation to the physico-chemical environment. Journal of Marine Systems 57, 231-249.

Kvingedal, B., 2005. Sea-Ice Extent and Variability in the Nordic Seas, 1967—2002, in The Nordic Seas: An Integrated Perspective, ed. Drange Helge, Dokken Trond, Furevik Tore, Gerdes Rüdigerand Wolfgang, B., American Geophysical Union, pp. 39-49.

Levac, E., Vernal, A. D., Blake, W., 2001. Sea-surface conditions in northernmost Baffin Bay during the Holocene: palynological evidence. Journal of Quaternary Science 16, 353-363.

Leventer, A., Domack, E. W., Ishman, S. E., Brachfeld, S., Mcclennen, C. E., Manley, P., 1996. Productivity cycles of 200-300 years in the Antarctic Peninsula region:

understanding linkages among the sun, atmosphere, oceans, sea ice, and biota. Geological Society of America Bulletin 108, 1626-1644.

Leventer, A., Dunbar, R. B., 1996. Factors influencing the distribution of diatoms and other algae in the Ross Sea. Journal of Geophysical Research: Oceans 101, 18489-18500.

Leventer, A., 1998. The fate of Antarctic "Sea Ice Diatoms" and their use as paleoenvironmental indicators., in Antarctic sea ice: Biological Processes, Interactions and Variability, ed Lizotte M. P. and Arrigo K. R., American Geophysical Union, Washington, pp.121-137.

Loeng, H., 1991. Features of the physical oceanographic conditions of the Barents Sea. Polar Research 10, 5-18.

Maiti, K., Carroll, J., Benitez-Nelson, C. R., 2010. Sedimentation and particle dynamics in the seasonal ice zone of the Barents Sea. Journal of Marine Systems 79, 185-198.

Mangoni, O., Saggiomo, M., Modigh, M., Catalano, G., Zingone, A., Saggiomo, V., 2008. The role of platelet ice microalgae in seeding phytoplankton blooms in Terra Nova Bay (Ross Sea, Antarctica): a mesocosm experiment. Polar Biology 32, 311-323.

Massé, G., Rowland, S. J., Sicre, M.-A., Jacob, J., Jansen, E., Belt, S. T., 2008. Abrupt climate changes for Iceland during the last millennium: Evidence from high resolution sea ice reconstructions. Earth and Planetary Science Letters 269, 565-569.

Massé, G., Belt, S. T., Crosta, X., Schmidt, S., Snape, I., Thomas, D. N., Rowland, S. J., 2011. Highly branched isoprenoids as proxies for variable sea ice conditions in the Southern Ocean. Antarctic Science 23, 487-498.

Massom, R., Harris, P., Michael, K. J., Potter, M., 1998. The distribution and formative processes of latent-heat polynyas in East Antarctica. Annals of Glaciology 27, 420-426.

Massom, R., Reid, P., Stammerjohn, S., Raymond, B., Fraser, A., Ushio, S., 2013. Change and variability in East Antarctic sea ice seasonality, 1979/80-2009/10. PloS one 8, e64756.

Matsumoto, G. I., Matsumoto, E., Sasaki, K., Watanuki, K., 1992. Geochemical features of organic matter in sediment cores from Lültzow-Holm Bay, Antarctica., in Organic Matter: Productivity, Accumulation and Preservation in Recent and Ancient Sediments, Whelan, J., and Farrington, J.W., Columbia University Press, New York, pp. 142-176

Matthiessen, J., Turon, J. L., Rochon, A., de Vernal, A., 1997. Organic-walled dinoflagellate cysts: Palynological tracers of sea-surface conditions in middle to high latitude marine environments. Geobios 30, 905-920.

Maykut, G. A., 1978. Energy exchange over young sea ice in the central Arctic. Journal of Geophysical Research: Oceans 83, 3646-3658.

McMinn, A., 1996. Preliminary investigation of the contribution of fast-ice algae to the spring phytoplankton bloom in Ellis Fjord, eastern Antarctica. Polar Biology 16, 301-307.

McMinn, A., 1998. Species succession in fast ice algal communities; a response to UV-B radiation. Korean Journal of Polar Research 8, 47-52.

McMinn, A., Skerratt, J., Trull, T., Ashworth, C., Lizotte, M., 1999. Nutrient stress gradient in the bottom 5 cm of fast ice, McMurdo Sound, Antarctica. Polar biology 21, 220-227.

McMinn, A., Ashworth, C., Ryan, K., 2000. In situ net primary productivity of an Antarctic fast ice bottom algal community. Aquatic Microbial Ecology 21, 177-185.

Medlin, L., 1990. *Berkeleya spp.* from Antarctic waters, including *Berkeleya adeliensis*, sp. nov., a new tube dwelling diatom from the undersurface of sea-ice. Beihefte zur Nova Hedwigia 100, 77-89.

Méheust, M., Stein, R., Fahl, K., Max, L., Riethdorf, J.-R., 2016. High-resolution IP_{25}-based reconstruction of sea-ice variability in the western North Pacific and Bering Sea during the past 18,000 years. Geo-Marine Letters 36, 101-111.

Miles, B. W., Stokes, C. R., Jamieson, S. S., 2016. Pan-ice-sheet glacier terminus change in East Antarctica reveals sensitivity of Wilkes Land to sea-ice changes. Science Advances 2, e1501350.

Moros, M., Emeis, K., Risebrobakken, B., Snowball, I., Kuijpers, A., Mcmanus, J., Jansen, E., 2004. Sea surface temperatures and ice rafting in the Holocene North Atlantic: climate influences on northern Europe and Greenland. Quaternary Science Reviews 23, 2113-2126.

Moros, M., Andrews, J. T., Eberl, D. D., Jansen, E., 2006. Holocene history of drift ice in the northern North Atlantic: Evidence for different spatial and temporal modes. Paleoceanography 21, PA2017.

Mudie, P. J., Rochon, A., 2001. Distribution of dinoflagellate cysts in the Canadian Arctic marine region. Journal of Quaternary Science 16, 603-620.

Müller, J., Massé, G., Stein, R., Belt, S. T., 2009. Variability of sea-ice conditions in the Fram Strait over the past 30,000 years. Nature Geoscience 2, 772-776.

Müller, J., Wagner, A., Fahl, K., Stein, R., Prange, M., Lohmann, G., 2011. Towards quantitative sea ice reconstructions in the northern North Atlantic: A combined biomarker and numerical modelling approach. Earth and Planetary Science Letters 306, 137-148.

Müller, J., Werner, K., Stein, R., Fahl, K., Moros, M., Jansen, E., 2012. Holocene cooling culminates in sea ice oscillations in Fram Strait. Quaternary Science Reviews 47, 1-14.

Müller, J., Stein, R., 2014. High-resolution record of late glacial and deglacial sea ice changes in Fram Strait corroborates ice-ocean interactions during abrupt climate shifts. Earth and Planetary Science Letters 403, 446-455.

Munro, D. R., Dunbar, R. B., Mucciarone, D. A., Arrigo, K. R., Long, M. C., 2010. Stable isotope composition of dissolved inorganic carbon and particulate organic carbon in sea ice from the Ross Sea, Antarctica. Journal of Geophysical Research: Oceans 115, C09005.

Murray, J. W., 2002. Introduction to benthic foraminifera., in Quaternary environmental micropalaeontology, ed. Haslett, S. K., Arnold, Oxford, pp. 5-14.

NASA Goddard Space Flight Center, Ocean Ecology Laboratory, Ocean Biology Processing Group. VIIRS Chlorophyll Data; 2014 Reprocessing. NASA OB.DAAC, Greenbelt, MD, USA. doi: 10.5067/NPP/VIIRS/L3M/CHL/2014.

Navarro-Rodriguez, A., Belt, S. T., Knies, J., Brown, T. A., 2013. Mapping recent sea ice conditions in the Barents Sea using the proxy biomarker IP_{25}: implications for palaeo sea ice reconstructions. Quaternary Science Reviews 79, 26-39.

Navarro-Rodríguez, A. 2014. Reconstruction of recent and palaeo sea ice conditions in the Barents Sea. University of Plymouth (PhD thesis).

Nichols, P. D., Palmisano, A. C., Volkman, J. K., Smith, G. A., White, D. C., 1988. Occurrence of an isoprenoid C_{25} diunsaturated alkene and high neutral lipid content in Antarctic sea-ice diatom communities. Journal of Phycology 24, 90-96.

Nichols, D. S., Nichols, P. D., Sullivan, C. W., 1993. Fatty acid, sterol and hydrocarbon composition of Antarctic sea ice diatom communities during the spring bloom in McMurdo Sound. Antarctic Science 5, 271-278.

Niebauer, H.,Alexander, V., 1985. Oceanographic frontal structure and biological production at an ice edge. Continental Shelf Research 4, 367-388.

Opute, F. I., 1974. Lipid and fatty-acid composition of diatoms. Journal of Experimental Botany 25, 823-835.

Orsi, A. H., Whitworth, T., Nowlin, W. D., 1995. On the meridional extent and fronts of the Antarctic Circumpolar Current. Deep-Sea Research Part I-Oceanographic Research Papers 42, 641-673.

Parkinson, C., Cavalieri, D., 2012. Antarctic sea ice variability and trends, 1979-2010. The Cryosphere 6, 871-880.

Peck, V. L., Allen, C. S., Kender, S., Mcclymont, E. L., Hodgson, D., 2015. Oceanographic variability on the West Antarctic Peninsula during the Holocene and the influence of upper circumpolar deep water. Quaternary Science Reviews 119, 54-65.

Perrette, M., Yool, A., Quartly, G., Popova, E., 2011. Near-ubiquity of ice-edge blooms in the Arctic. Biogeosciences 8, 515-524.

Petty, A., Holland, P., Feltham, D., 2014. Sea ice and the ocean mixed layer over the Antarctic shelf seas. The Cryosphere 8, 761-783.

Pezza, A. B., Rashid, H. A., Simmonds, I., 2012. Climate links and recent extremes in antarctic sea ice, high-latitude cyclones, Southern Annular Mode and ENSO. Climate Dynamics 38, 57-73.

Pfirman, S., Wollenburg, I., Thiede, J., Lange, M. A., 1989. Lithogenic sediment on Arctic pack ice: Potential aeolian flux and contribution to deep sea sediments, in Paleoclimatology and Paleometeorology: Modern and Past Patterns of Global Atmospheric Transport, ed. Leinen, M.and Sarnthein, M., Springer, The Netherlands, Dordrecht, pp. 463-493.

Pike, J., 2013. Interactive comment on "Holocene climate variations in the western Antarctic Peninsula: evidence for sea ice extent predominantly controlled by insolation and ENSO variability changes" by J. Etourneau et al. Climate of the Past Discussions 9, C13-C15.

Pike, J., Swann, G. E. A., Leng, M. J., Snelling, A. M., 2013. Glacial discharge along the west Antarctic Peninsula during the Holocene. Nature Geoscience 6, 199-202.

Poirier, R. K., Cronin, T. M., Briggs Jr, W. M., Lockwood, R., 2012. Central Arctic paleoceanography for the last 50kyr based on ostracode faunal assemblages. Marine Micropaleontology 88, 65-76.

Polyak, L., Alley, R. B., Andrews, J. T., Brigham-Grette, J., Cronin, T. M., Darby, D. A., Dyke, A. S., Fitzpatrick, J. J., Funder, S., Holland, M., Jennings, A. E., Miller, G. H., O'regan, M., Savelle, J., Serreze, M., St. John, K., White, J. W. C., Wolff, E., 2010. History of sea ice in the Arctic. Quaternary Science Reviews 29, 1757-1778.

Reuss, N., Poulsen, L. K., 2002. Evaluation of fatty acids as biomarkers for a natural plankton community. A field study of a spring bloom and a post-bloom period off West Greenland. Marine Biology 141, 423-434.

Riaux-Gobin, C., Poulin, M., Prodon, R., Tréguer, P., 2003. Land-fast ice microalgal and phytoplanktonic communities (Adélie Land, Antarctica) in relation to environmental factors during ice break-up. Antarctic Science 15, 353-364.

Riaux-Gobin, C., Poulin, M., 2004. Possible symbiosis of Berkeleya adeliensis Medlin, Synedropsis fragilis (Manguin) Hasle et al. and Nitzschia lecointei Van Heurck (Bacillariophyta) associated with land-fast ice in Adélie Land, Antarctica. Diatom Research 19, 265-274.

Riaux-Gobin, C., Poulin, M., Dieckmann, G., Labrune, C., Vétion, G., 2011. Spring phytoplankton onset after the ice break-up and sea-ice signature (Adélie Land, East Antarctica). Polar Research 30, 5910

Riaux-Gobin, C., Dieckmann, G. S., Poulin, M., Neveux, J., Labrune, C., Vetion, G., 2013. Environmental conditions, particle flux and sympagic microalgal succession in spring before the sea-ice break-up in Adélie Land, East Antarctica. Polar Research 32, 19675

Riebesell, U., Schloss, I., Smetacek, V., 1991. Aggregation of algae released from melting sea ice-Implications for seeding and sedimentation. Polar biology 11, 239-248.

Rigor, I. G., Wallace, J. M., Colony, R. L., 2002. Response of Sea Ice to the Arctic Oscillation. Journal of Climate 15, 2648-2663.

Risebrobakken, B., Dokken, T., Smedsrud, L. H., Andersson, C., Jansen, E., Moros, M., Ivanova, E. V., 2011. Early Holocene temperature variability in the Nordic Seas: The role of oceanic heat advection versus changes in orbital forcing. Paleoceanography 26, PA4206

Rontani, J.-F., Belt, S. T., Vaultier, F., Brown, T. A., 2011. Visible light induced photo-oxidation of highly branched isoprenoid (HBI) alkenes: Significant dependence on the number and nature of double bonds. Organic Geochemistry 42, 812-822.

Rontani, J. F., Belt, S. T., Vaultier, F., Brown, T. A., Massé, G., 2014. Autoxidative and Photooxidative Reactivity of Highly Branched Isoprenoid (HBI) Alkenes. Lipids 49, 481-494.

Round, F. E., Crawford, R. M., Mann, D. G., 1990. The diatoms: biology & morphology of the genera. Cambridge University Press, Cambridge, U.K.

Rowland, S., Allard, W., Belt, S., Massé, G., Robert, J.-M., Blackburn, S., Frampton, D., Revill, A., Volkman, J., 2001. Factors influencing the distributions of

polyunsaturated terpenoids in the diatom, *Rhizosolenia setigera*. Phytochemistry 58, 717-728.

Rowland, S. J., Robson, J. N., 1990. The widespread occurence of highly branched acyclic C_{20}, C_{25} and C_{30} hydrocarbons in recent sediments and biota-a review. Marine Environmental Research 30, 191-216.

Rüther, D. C., Bjarnadóttir, L. R., Junttila, J., Husum, K., Rasmussen, T. L., Lucchi, R. G., Andreassen, K., 2012. Pattern and timing of the northwestern Barents Sea Ice Sheet deglaciation and indications of episodic Holocene deposition. Boreas 41, 494-512.

Ryan, K. G., Mcminn, A., Hegseth, E. N., Davy, S. K., 2012. The effects of ultraviolet-B radiation on Antarctic sea-ice algae. Journal of phycology 48, 74-84.

Sakshaug, E.,Skjoldal, H. R., 1989. Life at the ice edge. Ambio 18, 60-67.

Sakshaug, E., Johnsen, G. H., Kovacs, K. M., 2009. Ecosystem Barents Sea. Tapir Academic Press, Trondheim, Norway.

Sarnthein, M., Gersonde, R., Niebler, S., Pflaumann, U., Spielhagen, R., Thiede, J., Wefer, G., Weinelt, M., 2003a. Overview of glacial Atlantic Ocean mapping (GLAMAP 2000). Paleoceanography 18, 1030.

Sarnthein, M., Kreveld, S., Erlenkeuser, H., Grootes, P., Kucera, M., Pflaumann, U., Schulz, M., 2003b. Centennial-to-millennial-scale periodicities of Holocene climate and sediment injections off the western Barents shelf, 75˚N. Boreas 32, 447-461.

Schiermeier, Q., 2012. Ice loss shifts Arctic cycles. Nature 489, 185-186.

Schouten, S., Hopmans, E. C., Schefuß, E., Sinninghe Damsté, J. S., 2002. Distributional variations in marine crenarchaeotal membrane lipids: a new tool for reconstructing ancient sea water temperatures? Earth and Planetary Science Letters 204, 265-274.

Scott, D. B., Schell, T., St-Onge, G., Rochon, A.,Blasco, S., 2009. Foraminiferal assemblage changes over the last 15,000 years on the Mackenzie - Beaufort Sea Slope and Amundsen Gulf, Canada: Implications for past sea ice conditions. Paleoceanography 24, PA2219.

Seidenkrantz, M.-S., 2013. Benthic foraminifera as palaeo sea-ice indicators in the subarctic realm-examples from the Labrador Sea-Baffin Bay region. Quaternary Science Reviews 79, 135-144.

Serreze, M. C., Barrett, A. P., Slater, A. G., Steele, M., Zhang, J., Trenberth, K. E., 2007. The large-scale energy budget of the Arctic. Journal of Geophysical Research 112, D11122.

Sinninghe Damsté, J. S., Rijpstra, W. I. C., Schouten, S., Peletier, H., Van Der Maarel, M. J. E. C., Gieskes, W. W. C., 1999a. A C_{25} highly branched isoprenoid alkene and C_{25} and C_{27} *n*-polyenes in the marine diatom *Rhizosolenia setigera*. Organic Geochemistry 30, 95-100.

Sinninghe Damsté, J. S., Schouten, S., Rijpstra, W. I. C., Hopmans, E. C., Peletier, H., Gieskes, W. W. C., Geenevasen, J. A. J., 1999b. Structural identification of the C_{25} highly branched isoprenoid pentaene in the marine diatom *Rhizosolenia setigera*. Organic Geochemistry 30, 1581-1583.

Sinninghe Damsté, J. S., Muyzer, G., Abbas, B., Rampen, S. W., Massé, G., Allard, W. G., Belt, S. T., Robert, J. M., Rowland, S. J., Moldowan, J. M., Barbanti, S. M., Fago, F. J., Denisevich, P., Dahl, J., Trindade, L. A. F., Schouten, S., 2004. The rise of the rhizosolenid diatoms. Science 304, 584-587.

Sinninghe Damsté, S., Rijpstra, W. I. P., Coolen, M. J. L., Schouten, S., Volkman, J. K., 2007. Rapid sulphurisation of highly branched isoprenoid (HBI) alkenes in sulphidic Holocene sediments from Ellis Fjord, Antarctica. Organic Geochemistry 38, 128-139.

Smith, S. L., Smith, W. O., Codispoti, L. A., Wilson, D. L., 1985. Biological observations in the marginal ice zone of the East Greenland Sea. Journal of Marine Research 43, 693-717.

Smith, W. O., Nelson, D. M., 1985. Phytoplankton bloom produced by a receding ice edge in the Ross Sea: spatial coherence with the density field. Science 227, 163-166.

Smith, W. O., Baumann, M. E., Wilson, D. L., Aletsee, L., 1987. Phytoplankton biomass and productivity in the marginal ice zone of the Fram Strait during summer 1984. Journal of Geophysical Research: Oceans 92, 6777-6786.

Solignac, S., Giraudeau, J., de Vernal, A., 2006. Holocene sea surface conditions in the western North Atlantic: Spatial and temporal heterogeneities. Paleoceanography 21, PA2004.

Solignac, S., Grosfjeld, K., Giraudeau, J.,de Vernal, A., 2009. Distribution of recent dinocyst assemblages in the western Barents Sea. Norwegian Journal of Geology 89, 109-119.

Stammerjohn, S., Massom, R., Rind, D.,Martinson, D., 2012. Regions of rapid sea ice change: An inter-hemispheric seasonal comparison. Geophysical Research Letters 39, L06501.

Stein, R., 2008. Arctic Ocean Sediments: Processes, Proxies, and Paleoenvironment. Elsevier, Amsterdam, The Netherlands.

Stein, R., Fahl, K., Schreck, M., Knorr, G., Niessen, F., Forwick, M., Gebhardt, C., Jensen, L., Kaminski, M., Kopf, A., Matthiessen, J., Jokat, W., Lohmann, G., 2016. Evidence for ice-free summers in the late Miocene central Arctic Ocean. Nature Communications 7, 11148

Stockwell, D. A., Kang, S. H., Fryxell, G. A., 1991. Comparisons of diatom biocoenoses with Holocene sediment assemblages in Prydz Bay, Antarctica., in Baron, J. A., Larsen, B., Baldauf, J.G., et al., Proceedings of the Ocean Drilling Program. Science Results 119, 667-673.

Stoynova, V., Shanahan, T. M., Hughen, K. A., de Vernal, A., 2013. Insights into Circum-Arctic sea ice variability from molecular geochemistry. Quaternary Science Reviews 79, 63-73.

Stroeve, J. C., Maslanik, J., Serreze, M. C., Rigor, I., Meier, W.,fowler, C., 2011. Sea ice response to an extreme negative phase of the Arctic Oscillation during winter 2009/2010. Geophysical Research Letters 38, L02502.

Swift, J. H., 1986. The Arctic Waters, in The Nordic Seas, ed. Hurdle, B. G., Springer New York, , pp. 129-154.

Taldenkova, E., Bauch, H., Stepanova, A., Dem'yankov, S., Ovsepyan, A., 2005. Last postglacial environmental evolution of the Laptev Sea shelf as reflected in molluscan, ostracodal, and foraminiferal faunas. Global and Planetary Change 48, 223-251.

Tamura, T., Ohshima, K. I., Nihashi, S., 2008. Mapping of sea ice production for Antarctic coastal polynyas. Geophysical Research Letters 35, L07606

Tanimura, Y., Fukuchi, M., Watanabe, K., Moriwaki, K., 1990. Diatoms in water column and sea-ice in Lützow-Holm Bay, Antarctica, and their preservation in the underlying sediments. Bulletin of the National Science Museum. Series C 16, 15-39.

Thomas, D. N., Kennedy, H., Kattner, G., Gerdes, D., Gough, C., Dieckmann, G. S., 2001. Biogeochemistry of platelet ice: its influence on particle flux under fast ice in the Weddell Sea, Antarctica. Polar Biology 24, 486-496.

Thomas, D. N.,Dieckmann, G. S., 2010. Sea Ice. Whiley Blackwell Publishing, New York.

Tolosa, I., Fiorini, S., Gasser, B., Martín, J., Miquel, J., 2013. Carbon sources in suspended particles and surface sediments from the Beaufort Sea revealed by molecular lipid biomarkers and compound-specific isotope analysis. Biogeosciences 10, 2061-2078

Tortell, P. D., Mills, M. M., Payne, C. D., Maldonado, M. T., Chierici, M., Fransson, A., Alderkamp, A.-C., Arrigo, K. R., 2013. Inorganic C utilization and C isotope

fractionation by pelagic and sea ice algal assemblages along the Antarctic continental shelf. Marine Ecology Progres Series 483, 47-66.

Trull, T., Armand, L., 2001. Insights into Southern Ocean carbon export from the δ 13 C of particles and dissolved inorganic carbon during the SOIREE iron release experiment. Deep Sea Research Part II: Topical Studies in Oceanography 48, 2655-2680.

Tynan, C. T., Ainley, D. G., Stirling, I., 2010. Sea Ice: A Critical Habitat for Polar Marine Mammals and Birds, in Sea Ice, ed. Thomas, D. N.and Dieckmann, G. S., Blackwell Science Ltd., Oxford, pp. 395-423.

Vare, L. L., Massé, G., Gregory, T. R., Smart, C. W., Belt, S. T., 2009. Sea ice variations in the central Canadian Arctic Archipelago during the Holocene. Quaternary Science Reviews 28, 1354-1366.

Vare, L. L., Massé, G., Belt, S. T., 2010. A biomarker-based reconstruction of sea ice conditions for the Barents Sea in recent centuries. The Holocene 20, 637-643.

Vaughan, D. G., Comiso, J. C., Allison, I., Carrasco, J., Kaser, G., Kwok, R., Mote, P., Murray, T., Paul, F., Ren, J., 2013. Observations: Cryosphere, in Climate Change 2013: The Physical Science Basis. Contribution of Working Group I to the Fifth Assessment Report of the Intergovernmental Panel on Climate Change,, ed. Stocker, T. F., Qin, D., Plattner, G.-K., Tignor, M., Allen, S.K., Bosching, J., Nauels, A., Xia, Y., Bex, V., Midgley, P.M., Cambridge University Press, Cambridge, UK, and New York, USA, pp. 317-382.

Venkatesan, M. I., 1988. Organic geochemistry of marine sediments in Antarctic region: Marine lipids in McMurdo Sound. Organic Geochemistry 12, 13-27.

Vinje, T., 1975. Sea ice conditions in the European sector of the marginal seas of the Arctic, 1966-1975. Norsk Polarinst, Arbok, 163-174.

Volkman, J. K., 1986. A review of sterol markers for marine and terrigenous organic matter. Organic Geochemistry 9, 83-99.

Volkman, J. K., Jeffrey, S. W., Nichols, P. D., Rogers, G. I., Garland, C. D., 1989. Fatty acid and lipid composition of 10 species of microalgae used in mariculture. Journal of Experimental Marine Biology and Ecology 128, 219-240.

Volkman, J. K., Barrett, S. M., Dunstan, G. A., 1994. C_{25} and C_{30} highly branched isoprenoid alkenes in laboratory cultures of two marine diatoms. Organic Geochemistry 21, 407-414.

Voronina, E., Polyak, L., De Vernal, A., Peyron, O., 2001. Holocene variations of sea-surface conditions in the southeastern Barents Sea, reconstructed from dinoflagellate cyst assemblages. Journal of Quaternary Science 16, 717-726.

Wang, M., Overland, J. E., 2009. A sea ice free summer Arctic within 30 years? Geophysical Research Letters 36, 2-6.

Whitaker, T., 1982. Primary production of phytoplankton off Signy Island, South Orkneys, the Antarctic. Proceedings of the Royal Society of London. Series B. Biological Sciences 214, 169-189.

Whitworth, T., Orsi, A., Kim, S. J., Nowlin, W., Locarnini, R., 1998. Water masses and mixing near the Antarctic Slope Front., in Ocean, Ice, and Atmosphere: interactions at the Antarctic continental margin, ed. Jacobs., S. S.and Weiss., R. W., American Geophysical Union, Washington, pp. 1-27.

Williams, G., Meijers, A., Poole, A., Mathiot, P., Tamura, T., Klocker, A., 2011. Late winter oceanography off the Sabrina and BANZARE coast (117-128 E), East Antarctica. Deep Sea Research Part II: Topical Studies in Oceanography 58, 1194-1210.

Wisz, M. S., Broennimann, O., Gronkjaer, P., Moller, P. R., Olsen, S. M., Swingedouw, D., Hedeholm, R. B., Nielsen, E. E., Guisan, A., Pellissier, L., 2015. Arctic warming will promote Atlantic-Pacific fish interchange. Nature Climate Change 5, 261-265.

Wraige, E. J., T. Belt, S., A. Lewis, C., A. Cooke, D., Robert, J. M., Massé, G., Rowland, S. J., 1997. Variations in structures and distributions of C_{25} highly branched isoprenoid (HBI) alkenes in cultures of the diatom, *Haslea ostrearia* (Simonsen). Organic Geochemistry 27, 497-505.

Xiao, X., Fahl, K., Stein, R., 2013. Biomarker distributions in surface sediments from the Kara and Laptev seas (Arctic Ocean): indicators for organic-carbon sources and sea-ice coverage. Quaternary Science Reviews 79, 40-52.

Xiao, X., Fahl, K., Müller, J., Stein, R., 2015. Sea-ice distribution in the modern Arctic Ocean: Biomarker records from trans-Arctic Ocean surface sediments. Geochimica et Cosmochimica Acta 155, 16-29.